Universität Bremen

New Insights into Environmental Conditions for the Early Jurassic (Pliensbachian–Toarcian) from Boron, Lithium and Magnesium Isotopes

Dissertation

zur Erlangung des Doktorgrades der
Naturwissenschaften (Dr. rer. nat.)

im Fachbereich Geowissenschaften (FB05)
der Universität Bremen

Vorgelegt von:

TINA KLEIN

Bremen, Deutschland

Mai 2020

marum

Erstgutachter: Prof. Dr. Simone Kasemann (Universität Bremen, Deutschland)

Zweitgutachter: Dr. Claire Rollion-Bard (Institut de physique du globe de Paris, Frankreich)

Promotionskolloquium: 05.06.2020

Versicherung an Eides Statt / *Affirmation in lieu of an oath*

gem. § 5 Abs. 5 der Promotionsordnung vom 18.06.2018 / *according to § 5 (5) of the Doctoral Degree Rules and Regulations of 18 June, 2018*

Ich / I, **Tina Klein, Nedderland 33a, 28355 Bremen, 3106358**

(Vorname / First *Name*, Name / *Name*, Anschrift / *Address*, ggf. Matr.-Nr. / *student ID no., if applicable*)

versichere an Eides Statt durch meine Unterschrift, dass ich die vorliegende Dissertation selbständig und ohne fremde Hilfe angefertigt und alle Stellen, die ich wörtlich dem Sinne nach aus Veröffentlichungen entnommen habe, als solche kenntlich gemacht habe, mich auch keiner anderen als der angegebenen Literatur oder sonstiger Hilfsmittel bedient habe und die zu Prüfungszwecken beigelegte elektronische Version (PDF) der Dissertation mit der abgegebenen gedruckten Version identisch ist. / *With my signature I affirm in lieu of an oath that I prepared the submitted dissertation independently and without illicit assistance from third parties, that I appropriately referenced any text or content from other sources, that I used only literature and resources listed in the dissertation, and that the electronic (PDF) and printed versions of the dissertation are identical.*

Ich versichere an Eides Statt, dass ich die vorgenannten Angaben nach bestem Wissen und Gewissen gemacht habe und dass die Angaben der Wahrheit entsprechen und ich nichts verschwiegen habe. / *I affirm in lieu of an oath that the information provided herein to the best of my knowledge is true and complete.*

Die Strafbarkeit einer falschen eidesstattlichen Versicherung ist mir bekannt, namentlich die Strafandrohung gemäß § 156 StGB bis zu drei Jahren Freiheitsstrafe oder Geldstrafe bei vorsätzlicher Begehung der Tat bzw. gemäß § 161 Abs. 1 StGB bis zu einem Jahr Freiheitsstrafe oder Geldstrafe bei fahrlässiger Begehung. / *I am aware that a false affidavit is a criminal offence which is punishable by law in accordance with § 156 of the German Criminal Code (StGB) with up to three years imprisonment or a fine in case of intention, or in accordance with § 161 (1) of the German Criminal Code with up to one year imprisonment or a fine in case of negligence.*

Bremen, 15.05.2020

Ort / *Place*, Datum / *Date*

Unterschrift / *Signature*

Preface

This dissertation is submitted to achieve the title 'Doctor of Natural Sciences (Dr. rer. nat.)' at the University of Bremen in the Department of Geosciences (FB5) and the research faculty MARUM – Center for Marine Environmental Sciences. This project was part of the research group "TER-SANE – Temperature-related Stressors as a Unifying Principle in Ancient Extinctions", which aimed to resolve the combination of environmental stressors like ocean deoxygenation, ocean acidification, and elevated seawater temperatures as a potential trigger for two past extinction events (Permian–Triassic boundary and Early Jurassic Toarcian Oceanic Anoxic Event). The focus of this project was the investigation of the Early Jurassic event and is subdivided into five chapters:

Chapter 1: This first chapter outlines the background information of this thesis including the motivation and objectives, the different isotope systems used in this study and how to apply them to paleoenvironmental reconstructions, details about the study areas, and a section about the current state of the science of environmental conditions during the Pliensbachian and early Toarcian time interval.

Chapter 2: The second chapter describes all the materials and methods used in this study including the sample collection, sample preparation techniques, laboratory chemical procedures for isotope analyses and further analytical methods, as well as the description of leaching procedure developments. Moreover, a section describes the evaluation of the sample preservation. This chapter is thought to serve as a supplementary material to the manuscripts in chapter 3 and 4.

Chapter 3: This third chapter contains the manuscript "A comparative study on seawater pH changes during the T-OAE (Early Jurassic) with boron isotopes", which is in preparation for submission to *Science* or *Nature Geoscience*. The manuscript examines different archives of carbonates and their usage as seawater pH tracers. Furthermore, it provides the first direct evidence for a seawater pH drop during the Toarcian Oceanic Anoxic Event.

Chapter 4: The fourth chapter contains the manuscript "Enhanced silicate weathering pulses and Lusitanian basin restrictions during the Early Jurassic (Pliensbachian–Toarcian)", which is in preparation for submission to *Geochimica et Chosmochimica Acta*. The manuscript supports already published findings of enhanced continental weathering rates during the T-OAE and Pliensbachian–Toarcian boundary, but is firstly able to unravel the changes in solely silicate weathering as a CO_2 drawdown mechanism. In addition, we are in fact able to outline an evidence of a short-term restriction of the Lusitanian Basin during both investigated events.

Chapter 5: The final chapter summarizes the results of each chapter and gives an outlook for future research.

Note: All images shown in this thesis plus additional data tables with all data generated for this study can be found on the attached CD!

Contents

List of Figures

List of Tables

Abbreviations

AZ	Ammonoid Zone
BdC	Barranco de la Cañada (studied section in Spain)
CIE	Carbon isotope excursion
CL	Cathodoluminescence
IB	Iberian Basin
MC-ICP-MS	Multicollector-inductively coupled plasma-mass spectrometer
LB	Lusitanian Basin
LIP	Large Igneous Province
Ma	Million years
Mya	Million years ago
Pl–To boundary	Pliensbachian-Toarcian boundary
R/FC	Rabaçal/Fonte Coberta (studied section in Portugal)
SEM	Secondary Electron Microprobe
SW	Seawater
SWB	Storm wave base
T-OAE	Toarcian Oceanic Anoxic Event

Abstract

The Early Jurassic (Pliensbachian–Toarcian, $\sim$183 Ma) is characterised by some of the Mesozoics most drastic environmental perturbations. The Pliensbachian–Toarcian boundary (Pl–To) and the early Toarcian Oceanic Anoxic Event (T-OAE) both witnessed a second-order global extinction and severe faunal assemblage changes. The biological crisis for both events is being linked with the emplacement of the Karoo-Ferrar large igneous province (LIP). Rapid intrusive volcanism, together with contact metamorphism, triggered volatile releases of particularly the greenhouse gases carbon dioxide (CO_2) and methane (CH_4) leading to pCO_2 concentrations of 2–4 times higher than pre-industrial levels. This volcanic activity is also recognised in a negative carbon isotope perturbation that can be recorded worldwide. The effects of such elevated atmospheric CO_2 concentrations were manifold: rising temperatures in the atmosphere and seawater, deoxygenation of wide parts of the ocean, a possible ocean acidification event, and drastic changes in the nutrient cycles. The combination of all these stressors is termed as the "deadly quartet" and observed in several mass extinction events during our geological past. Humankind is currently facing the deterioration of its climatic and environmental conditions by even these very stressors. However, the raise in atmorspheric CO_2 concentrations is this time initiated by humans itself by burning fossil fuels and inducing drastic changes in land use. Nonetheless, we do not know how all these stressors will affect our future ecosystem. Therefore, it is of utter importance to investigate past events where the "deadly quartet" occurred and to examine the role of each stressor during the extinction event, to hopefully learn what to probably expect of our future.

One aim of this study is to unravel changes in seawater pH during the T-OAE, as already several indications exist but the direct evidence is lacking so far. With the help of boron isotopes ($\delta^{11}B$) we are not only able to trace such changes, but are also able to compare different archives (inorganic and biogenic carbonates) on their liability as seawater pH recorders. We present high-resolution $\delta^{11}B$ records for two carbonate transects located on opposite margins of the Iberian Massif (Lusitanian and Iberian Basin) and give the first direct evidence for a seawater pH drop during the T-OAE. Because the pH decline is only concise in the inorganic carbonates, while the biogenic carbonates (derived from brachiopods and bivalves) do not show this trend, this leaves the question of the liability of biogenic carbonates as accountable pH recorders.

A second aim is the reconstruction of silicate weathering conditions for the Pl–To boundary and T-OAE. As both events are thought to being triggered by abrupt rises in atmospheric CO_2 from Karoo–Ferrar flood basalt volcanism, this would have implemented Earth's feedback mechanism to draw down the CO_2 amounts with enhanced silicate weathering. Here we present two basins

located around the Iberian Massif that show abrupt changes in the Li isotope signature (δ^7Li) at both events supporting earlier studies findings of elevated continental weathering, whereas we are able to specifically trace the silicate weathering part with our generated Li isotopes. We further suggest that the Lusitanian Basin (Portugal) was probably restricted for a short time at both events owing to abrupt sea level falls and a tectonic event that formed effective barriers to prevent open marine circulation. As no such indications can be found for the Iberian Basin (Spain), we hence suggest that it records open marine conditions, whereas more research with Li isotopes in different basins are recommended to support this idea.

Overall does this thesis contribute important findings to the understanding of the Pliensbachian–Toarcian crisis intervals. A seawater pH drop is now evident with the help of this study, and adds up to confirm the definite occurence of the third stressor of the "deadly quartet", with implications for being the reason for the observed extinction during the T-OAE. However, further research focusing on this part is required to better understand the driving mechanisms of the fauna during this time of extreme changes.

Kurzfassung

Das frühe Jura (Pliensbach–Toarc, vor ~183 Millionen Jahren (Ma)) zeichnet sich durch einige der drastischsten Umweltkatastrophen des Mesozoikums aus. Die Pliensbach–Toarc Grenze (Pl–To) und das im frühen Toarc auftretende Ozeanische Anoxische Event (T-OAE) sind beide von globalem Aussterben und einschneidenden Änderungen der Faunengemeinschaft geprägt. Die biologische Krise beider Events hängt mit dem Auftreten der magmatischen Großprovinz (Large Igneous Province – LIP) Karoo–Ferrar zusammen, bei dem sehr große Mengen an Magma zutage gefördert wurden. Der schnelle, intrusive Vulkanismus des Karoo–Ferrar LIP zusammen mit dem Auftreten von Kontaktmetamorphismus lösten das Entgasen großer Mengen von Treibhausengasen aus, speziell Kohlendioxid (CO_2) und Methan (CH_4). Dies führte zu CO_2 Konzentrationen die 2- bis 4-fach höher liegen als noch vor der industriellen Revolution. Der LIP-Vulkanismus ist außerdem in einer weltweit zu vernehmenden negativen Exkursion in der Kohlenstoff-Isotopie zu erkennen. Die Auswirkungen solch hoher CO_2 Konzentrationen waren vielfältig: Erhöhte Temperaturen in der Atmosphäre sowie im Meereswasser, der Verlust von Sauerstoff von großen Teilen des Ozeans, das Auftreten einer möglichen Ozeanversauerung, sowie gravierende Änderungen im Nährstoffkreislauf. Die Kombination dieser vier genannten Stressfaktoren wird auch "Tödliches Quartett" genannt und dessen Vorkommen konnte schon zusammen mit einigen Massenaussterbeevents unserer geologischen Vergangenheit beobachtet werden. Die Menschheit erfährt momentan dieselben Stressfaktoren, die zur Verschlechterung des Klimas und der Umwelt führen, ebenfalls ausgelöst durch den schnellen Anstieg des Treibhausgases CO_2 in der Atmosphäre. Allerdings sind heute das Verbrennen des fossilen Brennstoffs und massive Änderungen der Landnutzung der Auslöser dafür. Jedoch wissen wir noch nicht, wie sich die ganzen Klimaänderungen in Zukunft auf unser Ökosystem auswirken werden. Daher ist es von größter Wichtigkeit vergangene Events zu erforschen, die mit dem "Tödlichen Quartett" in Verbindung stehen, um herauszufinden, welchen Einfluss jeder Stressfaktor auf das Massenaussterben hatte. Somit können wir hoffentlich Rückschlüsse daraus ziehen, was uns in Zukunft erwarten wird.

Ein Ziel der vorliegenden Studie ist es herauszufinden, ob es Änderungen im pH-Wert des Meereswassers während dem T-OAE gegeben hat, da es bisher noch keinen direkten Nachweis dafür gibt. Mit Hilfe von Bor-Isotopen ($\delta^{11}B$) sind wir nicht nur in der Lage solche Änderungen im pH-Wert des Meereswassers zu entschlüsseln, sondern können auch noch mehrere Archive (anorganische und biogene Karbonate) miteinander vergleichen und somit Rückschlüsse auf deren Zuverlässigkeit als pH-Archive des Meerwassers ziehen. Wir präsentieren hochauflösende $\delta^{11}B$-Profile von zwei karbonatischen Aufschlüssen, die an entgegengesetzten Rändern des Iberischen Massivs liegen (Lusitanisches und Iberisches Becken), und geben den ersten direkten Beweis dafür,

dass es eine Verringerung des Meerwasser-pH-Wertes während des T-OAE gegeben hat. Da diese Verringerung des pH-Wertes nur in den anorganischen Karbonaten aufgezeichnet wurde, lässt dies die Zuverlässigkeit der biogenen Karbonate als pH-Archive anzweifeln.

Ein weiteres Ziel war es, die Verwitterung von Silikaten während der Pl–To Grenze und des T-OAE zu rekonstruieren. Da beide Events vermutlich von einem schnellen Anstieg im atmosphärischen CO_2 Gehalt des Karoo–Ferrar-Vulkanismus ausgelöst wurden, hätte dies den Feedback-Mechanismus der Erde in Gang gesetzt. Dieser bewirkt, dass das überschüssige CO_2 durch die Verwitterung von Silikaten abgebaut wird und die ursprünglichen CO_2 Gehalte wieder erreicht werden. Mit unserer zweiten Studie sind wir in der Lage, abrupte Änderungen in der Li-Isotopie (δ^7Li) an beiden Events nachzuverfolgen, um bereits veröffentliche Ergebnisse zu unterstützen, die erhöhte kontinentale Verwitterungsraten rekonstruieren konnten. Der Unterschied zu diesen Studien ist allerdings, dass unsere generierten Li-Isotope in der Lage sind ausschließlich die silikatische Verwitterung nachzuverfolgen, wofür es bisher noch keine Untersuchungen im frühen Jura gibt. Wir vermuten außerdem, dass das Lusitanische Becken (Portugal) möglicherweise kurzzeitig abgegrenzt vom globalen Meereseinfluss während beider Events gewesen ist. Dies war wahrscheinlich die Folge eines plötzlichen Abfalls des Meereswasserspiegels zusammen mit dem Auftreten eines tektonischen Events, das zur Errichtung von effektiven Barrieren führte und somit den Austausch der globalen Meereszirkulation verhinderte. Da das Iberische Becken (Spanien) eine andere $\delta^{11}B$ Signatur verzeichnet, gehen wir davon aus, dass hier die globale Meeressignatur aufgezeichnet wurde, wobei weitere Studien mit Li-Isotopen in anderen Becken benötigt werden, um diese Theorie zu untermauern.

Allgemein gesehen leistet diese Thesis einen wichtigen Beitrag zum Verständnis der beiden Events im frühen Jura. Wir liefern den Nachweis für einen verringerten Meereswasser pH-Wert, womit ein weiterer Stressfaktor des "Tödlichen Quartetts" nun bewiesen wären. Dies kann nun als Ausgangspunkt für weitere Studien genutzt werden, um die einzelnen Folgen der Stressoren auf die Fauna während des T-OAEs zu untersuchen.

Chapter 1

Introduction

1. Introduction

1.1. Motivation and objectives

Atmospheric CO_2 concentrations have relentlessly increased since the beginning of the industrial revolution from ~280 ppm to about 390 ppm today, owing to mainly anthropogenic fossil fuel burning and changes in land use (IPCC, 2007; Peters et al., 2012). These elevated CO_2 concentrations will lead to higher surface temperatures, which will have drastic effects on our terrestrial ecosystem (e.g. Deutsch et al., 2008; Tewksbury et al., 2008; Wright et al., 2009). But also the marine ecosystem will be influenced, not only by likewise increased seawater temperatures (Munday et al., 2012 and references therein) but also by impacts of the oceans absorption of large parts of atmospheric CO_2 ($> 41\%$; Gruber et al., 2019; Sabine et al., 2004) due to the air–sea equilibrium. Already does this absorption cause an acidification of the surface ocean by an increase of seawater pH by 0.1 units (Caldeira and Wickett, 2003; Wolf-Gladrow et al., 1999), and models predict a further decrease in pH by the year 2300 of about 0.8 units (Caldeira and Wickett, 2003). Another effect of this climate warming on the marine system is the shortage of available oxygen in seawater caused by warmer waters and the increased stratification of the ocean (Bijma et al., 2013; Pörtner et al., 2005).

Hence, the stressors of our modern marine ecosystem are acidification, deoxygenation, warming and changes in nutrient cycling, which are also known as the "deadly quartet" (Bijma et al., 2013; Clapham et al., 2013; Piazza et al., 2019) and already played a major role in several extinction events during our geological past, e.g. the end-Permian (~252 million years ago (Mya)) and end-Triassic (~200 Mya)) extinction events (Brand et al., 2012; Clarkson et al., 2015; Hönisch et al., 2012; Jaraula et al., 2013; Joachimski et al., 2012; Kiessling et al., 2007; Kiessling and Simpson, 2011; Knoll et al., 2007). As our understanding of the final effects of all these combined stressors on the marine ecosystem is still unknown up to date, we can investigate those events in the past and hopefully learn for our future.

The Early Jurassic Pliensbachian–Toarcian times (~180 Mya) were associated with two minor extinction events where high CO_2 levels, climate warming, and ocean deoxygenation occurred (e.g. Benton, 1995; Bodin et al., 2016; Cecca and Macchioni, 2004; Dera and Donnadieu, 2012; Mattioli et al., 2009; McArthur et al., 2008; Percival et al., 2015; Suan et al., 2008). Despite our knowledge about two associated extinction events that occurred during these extreme times — Pliensbachian–Toarcian boundary (183 Mya) and Toarcian Oceanic Anoxic Event (T-OAE, 180 Mya) — still many questions remain unresolved. One question for example is the occurrence of an ocean acidification during both events to add up to the incident of the "deadly quartet" as a possible kill mechanism. Many indications for an acidification already exist for the T-OAE, as for instance a major carbonate production crisis that resulted in the size reduction of marine carbonate producing

organisms (Piazza et al., 2019; Suan et al., 2008), the decrease in the carbonate accumulation rate (Hermoso et al., 2012), and the near disappearance of shallow-water platforms (Trecalli et al., 2012). However, a direct evidence for a drop in seawater pH is lacking so far. Following, the first questions that this study tries to answer are:

1. Is there a change in seawater pH across the T-OAE and Pliensbachian–Toarcian boundary?

2. If there is a decrease in seawater pH, how drastic was it and can it be termed as an ocean acidification event?

3. Which environmental changes lead to the decrease in seawater pH?

4. Which influences do seawater pH changes have on marine calcifiers?

The fourth questions is thought to be addressed together with our research groups paleontologists whom we are working on together on the same transects and who investigate the assemblage changes during the T-OAE event. Also, a further matter of this study is :

5. What are the weathering conditions during the Early Jurassic?

This question aims to unravel changes in silicate weathering. When atmospheric CO_2 concentrations rise Earth's feedback mechanism will be triggered. This means that through the weathering of geologic materials the excess CO_2 will be consumed, which is subsequently transferred to the ocean where is it stored in precipitated carbonate rocks, on the long term leading to a drawdown of the high CO_2 levels and stabilization of Earth's climate. The most important part in this process play silicate minerals as they have the highest consumption capacity of CO_2. Hence, tracing this feedback mechanisms during both Early Jurassic events is likewise of importance and helps us to learn for our future climate.

1.2. Tracing seawater pH with boron isotopes

Dissolved boron occurs as two species in seawater, one being the trigonal boric acid ($B(OH)_3$) and the second being the tetrahedral oriented borate ($B(OH)_4^-$) with relative proportions of 80 and 20 % at pH 8, respectively. The abundance of each species is dependent on the pH as described by this reaction formula (see also Fig. 1):

$$B(OH)_3 + H_2O \leftrightarrow B(OH)_4^- + H^+ \tag{1}$$
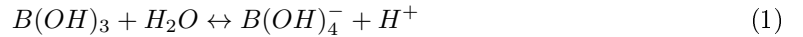
This means that at low pH all dissolved B is present in $B(OH)_3$, whereas at high pH B is present in the $B(OH)_4^-$ species. Owing to stronger boron-oxygen bonds in $B(OH)_3$ this species is enriched in ^{11}B, while $B(OH)_4^-$ is preferentially enriched in ^{10}B (e.g. Zeebe, 2005) with an offset of 26–27 ‰ (Klochko et al., 2006; Nir et al., 2015). Isotopic fractionation between these two species occurs due to coordination-controlled vibration differences as a function of pH, also altering its $\delta^{11}B$ value as both species become enriched in ^{11}B with rising pH and concurrently $B(OH)_4^-$ becoming the dominant aqueous species (Kakihana et al., 1977; Oi et al., 1988; Schwarcz et al., 1969).
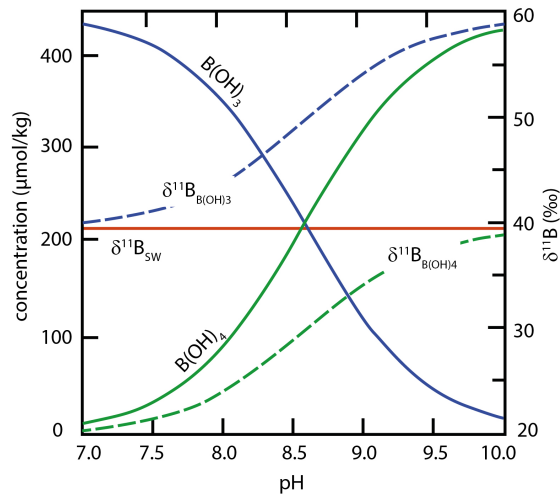
Figure 1. Boron species in modern seawater modified after Xiao et al., 2013. pK_b value from Dickson, 1990 and fractionation factor α from Klochko et al., 2006.

The $\delta^{11}B$ value of today's seawater ($\delta^{11}B_{SW}$) is 39.61 ‰ (Foster et al., 2010) and homogeneous throughout the world ocean (Hemming and Hanson, 1992; Spivack et al., 1987) due to the long residence time of boron in the ocean of 14–20 Ma (Lemarchand et al., 2000, 2002; Spivack et al., 1987) making it a good tracer for long-term changes of at least a few million years in the $\delta^{11}B_{SW}$. The rather heavy $\delta^{11}B_{SW}$ indicates that mechanisms exist that remove the light ^{10}B from the seawater relative to the input from the detritial fraction from the continents with an

δ^{11}B imprint of -15 to -8 ‰ (Ishikawa and Nakamura, 1993). Three sinks of boron in the ocean are recognised: (I) adsorption of boron onto marine clays; this fractionation prefers ^{10}B and is pH dependent, revealing high boron concentrations of 96–132 µg g^{-1} and a δ^{11}B signature of -6 to +2.8 ‰ (Ishikawa and Nakamura, 1993; Palmer et al., 1987), (II) exchange with oceanic crust with δ^{11}B values from -2 to -4 ‰ (Spivack et al., 1987), and (III) the coprecipitation with calcium carbonate revealing δ^{11}B values of modern biogenic and abiogenic marine carbonate between +10 to +30 ‰ (Hemming and Hanson, 1992; Ishikawa and Nakamura, 1993; Vengosh et al., 1991).

The preferential uptake of B(OH)$_4^-$ in calcite was firstly suggested by Hemming and Hanson, 1992 explained by the negatively charged species being more attracted to the positively charged calcite surface than the uncharged B(OH)$_3$ (Palmer et al., 1998; Pearson and Palmer, 2000; Spivack et al., 1993; Xiao et al., 2014). This assumption is used as a basis for many pH reconstruction studies, however recent studies seek to improve our understanding of the B species uptake in carbonates (e.g. Balan et al., 2018; Farmer et al., 2019; Holcomb et al., 2016; Kaczmarek et al., 2016; Mavromatis et al., 2015; Noireaux et al., 2015; Uchikawa et al., 2015). The current findings imply that aragonite seems to only incorporate B(OH)$_4^-$ while calcite may take up a mixture of B(OH)$_3$ and B(OH)$_4^-$. Nevertheless, as it is still a matter of debate how B is incorporated exactly in marine carbonates, pH reconstructions still use the assumption of Hemming and Hanson, 1992 where only B(OH)$_4^-$ is incorporated into the calcite, leading to the following relation:

$$pH = pK_b - log\left[-\frac{\delta^{11}B_{SW} - \delta^{11}B_{borate}}{\delta^{11}B_{SW} - (\alpha_B * \delta^{11}B_{borate}) - 10^3 * (\alpha_B - 1)} \right] \qquad (2)$$

with pK_b being the dissociation constant of B with a given value of 8.597 at 25°C (Dickson, 1990), δ^{11}B$_{SW}$ being the boron isotopic composition of seawater (39.61 ‰, Foster et al., 2010), α_B as the B isotope fractionation factor and δ^{11}B$_{borate}$ as the B isotopic composition of the marine carbonate. A first estimate for the value of α_B was given by Kakihana et al., 1977 with a value of 1.0194 ($\varepsilon_B =$ 19.4 ‰; $\varepsilon_B = (\alpha_B - 1) * 10^3$). By contrast, various subsequent studies found different estimates ranging between 18–30 ‰ depending on the speciation calculation methods. Recent studies, for example, suggested values of 1.025 ± 0.001 (Noireaux et al., 2015), 1.026 ± 0.001 (Nir et al., 2015) and 1.025 ± 0.0005 (Kaczmarek et al., 2016). Nonetheless, in modern studies for pH reconstructions the widely accepted value of 1.0272 ± 0.0006 by Klochko et al., 2006 is still used. Depending on which α_B value is applied the calculated data can alter in the range of 1–2 ‰ (Fig 2). Moreover to mention is a possible small-scale influence of temperature on α_B observed with biotic carbonate precipitation (Farmer et al., 2015; Hönisch et al., 2019; Hönisch et al., 2008; Rae et al., 2011) and inorganic carbonate (Kakihana et al., 1977). As mentioned above, the fractionation of B in calcite is still a matter of debate and in need of clearance. Therefore we apply the α_B from Klochko et al.,

2006 in this study, also because the values fall within the uncertainty from Nir et al., 2015 and for better comparison to other studies.
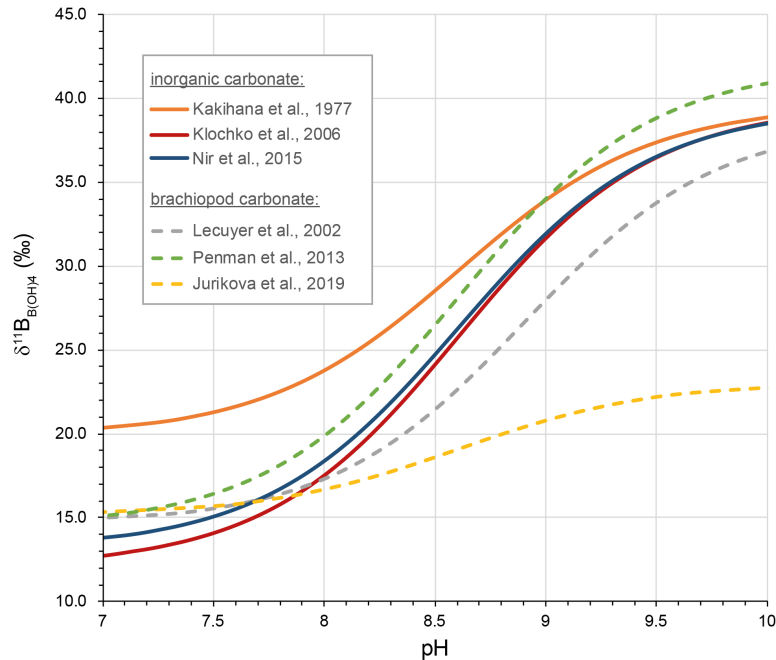
Figure 2. Selected estimated fractionation factors for B (α_B). Applied pK_b value of 8.597 for 25°C (Dickson, 1990) and $\delta^{11}B_{SW} = 39.61$‰ (Foster et al., 2010). For the Penman et al., 2013 calculation a species specific correction factor was used ($a = $ -2.4, for more information see Penman et al., 2013).

Another varying factor in the pH calculation equation is the dissociation constant of boric acid pK_b. Different studies found that pK_b is temperature, pressure and salinity dependant (e.g. Culberson and Pytkowicx, 1968; Dickson, 1990; Hansson, 1973; Roy et al., 1993). Generally spoken, the pK_b increases with decreasing temperature and salinity. As recent studies use the pK_b values from Dickson, 1990 and his results were confirmed by Roy et al., 1993 and are in agreement with the findings from Hansson, 1973, we also apply his values for our reconstructions in this study.

A further matter not yet resolved is the B fractionation during biogenic carbonate precipitation for brachiopods. Fossil brachiopods are often used for isotope analyses as they are regarded to confidently preserve their original chemistry despite post-depositional processes, because their low-magnesium calcite shell is more robust against such influences (e.g. Brand et al., 2012; Brand and Veizer, 1980, 1981; Brand et al., 2003). Only a few studies addressed the potential use of brachiopods as pH tracers up to date (Joachimski et al., 2005; Jurikova et al., 2019; Lécuyer et al., 2002; Penman et al., 2013). Three of those studies investigated the fractionation of B between the brachiopod shell and seawater concluding in different relations of the pH and B incorporation (Fig. 2). What those studies agree on, is the reduced $\delta^{11}B$ sensitivity against pH changes (Jurikova et al., 2019; Penman et al., 2013) compared to the aqueous fractionation in marine carbonates predicted

by Klochko et al., 2006. Also a common finding of both brachiopod studies is the occurrence of vital effects, which leads to an altered δ^{11}B value of the marine organism shell in comparison to the ambient seawater (Jurikova et al., 2019; Penman et al., 2013). Nevertheless, both studies speak for the use of brachiopod derived δ^{11}B as a mean to reconstruct past seawater pH changes, but suggest focusing on a single species or cross-calibrating coeval species.

1.3. Reconstructing paleo-weathering conditions with isotopes

Weathering is an important process to regulate Earth's climate while being influenced by the climate itself. The processes involved in weathering deliver nutrients and solutes to the ocean and have the potential to act as a climate feedback mechanism by stabilizing Earth's climate through the consumption of atmospheric CO_2 and transferring it into the ocean system by forming sedimentary rocks.

The most crucial geological materials that consume CO_2 during chemical weathering are silicate and carbonate minerals, whereas the importance of both on climate stabilization differs. While carbonate minerals are relatively more soluble than silicates, they act as a climate stabilizer on the short term. This is because the dissolution of carbonate and the involved CO_2 consumption is reversible in the oceans by precipitating carbonate and the accompanied return of the greenhouse gas into the ocean–atmosphere system. Nonetheless, carbonate weathering also is a strong buffer to ocean acidity by adding alkalinity in the form of bicarbonate and carbonate ions.

On the other hand, weathering of silicate minerals also adds alkalinity through bicarbonate but on a lesser extend. Moreover, it can act as a net sink for CO_2 and help balancing Earth's climate on the long term, especially by weathering Ca and Mg silicates (France-Lanord and Derry, 1997). Silicate weathering is also more complex as carbonate weathering, because carbonates simply dissolve completely (congruent weathering) while silicate weathering involves the formation of a new secondary clay mineral (incongruent weathering), which is an important process for forming soils.

To reconstruct paleo-weathering conditions several isotopic systems can be used as a tracer and different systems should also be combined to verify ones theory. In the following the three different isotopic systems of Sr, Li and Mg are explained as tracers for continental weathering processes.

1.3.1. Strontium isotopes

The element strontium (Sr) has four isotopes 84 (0.56%), 86 (9.87%), 87 (7.04%) and 88 (82.53%) with each relative abundances (Faure, 1986). The ^{87}Sr isotope is the product of radioactive decay of ^{87}Rb and thus the proportions vary according to the time passed. Sr can be used as a tracer for global weathering because of its long residence time in the oceans (1–5 Ma, McArthur et al., 2012; Palmer and Edmond, 1989). It enters the oceans through weathering of silicate and carbonate minerals as well as submarine hydrothermal alteration. The major sink for Sr is the precipitation of marine carbonates, whilst this process does not involve isotopic fractionation and records the Sr signal of the time the rock was formed (Edmond, 1992). Today's ^{87}Sr/^{86}Sr composition of the seawater is 0.70917 and varied greatly over the geological timescale (Palmer and Edmond, 1989).

Simply spoken, as each input source of Sr has a distinct lower (hydrothermal alteration) and higher (continental river flux) Sr isotopic composition, the variations should be the result of differing input rates of each process (Palmer and Edmond, 1992). However, Raymo and Ruddiman, 1992 already stated that this simplified view of increasing $^{87}Sr/^{86}Sr$ in the oceans is unlikely to generally correlate with increased silicate weathering rates due to higher atmospheric CO_2 concentrations. This is because of the differing abundances of Ca and Mg in the silicates and accordingly their varying amounts of CO_2 consumption (Dessert et al., 2003). While granitic silicates generate a high $^{87}Sr/^{86}Sr$ they have rather low Ca and Mg contents, in contrast to mafic silicates that show low $^{87}Sr/^{86}Sr$ ratios but high Ca and Mg abundances and hence have the ability to act as a stronger CO_2 sink than granitic silicates. This effect can be observed since the Eocene as marine $^{87}Sr/^{86}Sr$ ratios were constantly increasing, which is almost certainly the result of different rock types that have been weathered and does not speak for elevated CO_2 consumption (Derry, 2009).

Modern day Sr river input dominates the ocean budget by contributing two-third of the total Sr content in the oceans in contrast to one-third from hydrothermal systems. The river $^{87}Sr/^{86}Sr$ is greatly influenced by the so called "memory effect", which describes the weathering of old marine carbonates and the release of their ancient Sr isotopic composition of the past oceans that have been relatively more radiogenic.

Note that already a number of studies exist that tried to explain the oscillations of the $^{87}Sr/^{86}Sr$ seawater signature during Pliensbachian–Toarican times (see section 1.5) in terms of continental weathering. None of those studies were able to explain the steep decrease in Sr isotopic signature at the Pl–To boundary as well the distinct rise to more radiogenic values during the T-OAE (Fig. 19). Sr isotopes are not unambiguous in their interpretation when it comes to differ between carbonate and silicate weathering rates, as explained above. Because the $^{87}Sr/^{86}Sr$ isotopic signature of this study retraces the already published seawater signal, this study will only use the generated Sr isotopes in terms of stratigraphy and evaluation of the preservation. Continental weathering reconstructions will thus be conducted with Mg and Li isotopes.

1.3.2. Magnesium isotopes

Magnesium (Mg) has three stable isotopes (24, 25, 26) with typical relative abundances of 78.99%, 10.00% and 11.01%, respectively (Berglund and Wieser, 2011). As the mass difference between ^{24}Mg and ^{26}Mg is relatively large with over 8%, significant mass fractionation in numerous geological processes can be observed. With its long residence time in seawater of over 10 Ma (Li, 1982) it exceeds the ocean mixing time of 1–2 kya (Garrison, 2006) and thus is homogeneously distributed in the oceans. In today's seawater $\delta^{26}Mg$ compositions of -0.83 ± 0.09‰ are reported (Foster et al., 2010; Ling et al., 2011) with average Mg contents of 53 mmol/l (Foster et al., 2010; Tipper et al., 2006). The main sinks of Mg are hydrothermal circulation at mid-ocean ridges, the precipitation

of dolomite, as well as ion-exchange reactions with clays (Elderfield and Schultz, 1996). The main sources of Mg into the oceans are rivers (Tipper et al., 2006).

The fractionation of Mg isotopes occurs during the formation of carbonate minerals, which prefer to incorporate the light Mg isotope with weaker Mg bonding strength, and during the formation of silicate minerals, which take up the heavier Mg isotopes (Schauble, 2011). But also the vegetation has the potential to fractionate Mg isotopes as they are highly enriched in Mg and preferentially take up the light Mg and thus deplete the surface waters (Anderson et al., 1983; Bi et al., 2007; Black et al., 2006). On the other hand, the decay of plants thus may drive the isotopic composition of surface waters to lighter values. Typical δ^{26}Mg values of silicates range between -0.77 to -0.09 ‰ and hence are virtually uniform, indicating a limitation of Mg isotopic compositions at high temperatures (e.g. Chakrabarti and Jacobsen, 2010; Liu et al., 2010; Teng et al., 2010a). In contrast, carbonate minerals show a wide variety of δ^{26}Mg between -5.6 to -1 ‰ (e.g. Fantle and Higgins, 2014; Gao et al., 2018; Li et al., 2012; Wang et al., 2017). The Mg isotopic content of rivers is consequently controlled by the formation and weathering of these terrestrial components and explains the high δ^{26}Mg diversity in modern river waters of in mean -1.09 ‰ with a range of $\pm$ 2.5 ‰ (Tipper et al., 2006).

Another important process during incongruent silicate rock weathering is the formation of secondary (clay) minerals. Clays usually prefer the incorporation of the heavy Mg isotopes into their crystal lattice (Tipper et al., 2006; Tipper et al., 2010), but also light Mg isotopes can be adsorbed on the surface of the mineral (Opfergelt et al., 2014; Wimpenny et al., 2014). During weathering the light Mg isotopes are washed out by fluids and leave the weathering products (such as soil and clay minerals) with heavy Mg isotopic compositions (e.g. Brenot et al., 2008; Gao, 2016; Liu et al., 2014; Teng et al., 2010b; Tipper et al., 2006).

The fractionation of Mg isotopes into calcite minerals is also complex and not yet fully resolved as it depends on several factors like temperature, calcite growth rate, the aqueous Mg concentration, pH, mineralogy, the precipitation process and the Mg content in the calcite (Galy et al., 2002; Immenhauser et al., 2010; Li et al., 2012; Saenger and Wang, 2014; Wang et al., 2019). For instance, the temperature effect on Mg fractionation is found to be negligible at temperatures between 4– 45°C with rather small temperature sensitivities of 0.011 ‰ /°C (Li et al., 2012) and 0.009 ‰ /°C (Wang et al., 2013). Moreover, mineralogy also plays a role as the Mg isotope fractionation in in calcites is larger than in aragonites with a general increasing fractionation as follows: aragonite < dolomite < magnesite < calcite (Wang et al., 2013). Precipitation rates influence the Mg isotope fractionation likewise to that effect that fractionation is smaller at faster rates (Immenhauser et al., 2010; Mavromatis et al., 2013), and larger fractionation has been observed in calcites with lower Mg contents (Wang et al., 2019). Lastly, effects from aqueous Mg concentration, pH and the precipitation process have been suggested by Saenger and Wang, 2014 but no empirical studies

exist up to date to evaluate the specific fractionation processes in greater detail.

1.3.3. Lithium isotopes

Lithium (Li) has two stable isotopes, [6]Li and [7]Li, with typical relative abundances of 7.52%, 92.48%, respectively (Berglund and Wieser, 2011). As the relative mass difference between both isotopes is large the fractionation at low-temperature processes has a wide span, making it a good tracer for those processes in a geological context. The seawater δ^7Li amounts to 31.0 ± 0.5‰ (Broecker and Peng, 1982) and is globally evenly distributed, owing to the long residence time of Li in seawater of about 1.2 Ma (Stoffynegli and Mackenzie, 1984) exceeding the rates of ocean mixing. The main sinks for Li in the oceans is the incorporation into clays and the subsequent integration into marine sediments, which makes up 70% of the Li removal, and the low-temperature alteration of oceanic crust, which also involves the formation of clays (Chan et al., 1992; Chan et al., 2006; James et al., 1999; Seyfried et al., 1998; Verney-Carron et al., 2011; Vigier et al., 2008). During formation of clay minerals Li isotopes fractionate and [6]Li is preferentially incorporated into the mineral lattice as well as adsorbed onto the clay mineral surface (e.g. Pistiner and Henderson, 2003; Vigier et al., 2008; Williams and Hervig, 2005; Wimpenny et al., 2015; Wunder et al., 2010, 2007, 2006), explaining the relatively light Li isotope composition of those phases and the heavy δ^7Li of seawater.

The main sources of Li into the ocean are continental river runoff with its signature of low-temperature chemical weathering processes, and hydrothermal activity high-temperature processes at the mid-ocean ridge (Elderfield and Schultz, 1996; Gaillardet et al., 2003; Huh et al., 1998; Lui-Heung et al., 1994). Both sources contribution to the Li seawater budget is nearly equal but the Li isotopic composition is very distinct with a mean of ~ 8.3‰ for hydrothermal fluxes (Elderfield and Schultz, 1996; Lui-Heung et al., 1994; Rudnick and Gao, 2003; Tomascak et al., 2008) and 23.5‰ for the mean river runoff (Huh et al., 1998). The reason for the large isotopic offset between the two sources is the isotopic fractionation of Li during chemical weathering. The fractionation on the continents occurs according to the fractionation in seawater. During chemical weathering of silicate minerals secondary (clay) minerals are formed (incongruent weathering), leading to a high δ^7Li river signature with low Li concentrations. However, during congruent weathering, and thus only primary silicate mineral dissolution, low δ^7Li and high Li element concentrations can be observed in the rivers (Dellinger et al., 2015; Kisakurek et al., 2005; Liu et al., 2015; Misra and Froelich, 2012; Pogge von Strandmann et al., 2010, 2013).

A major advantage of using Li isotopes for the reconstruction of chemical weathering in comparison to other isotope systems like strontium, magnesium, calcium and osmium is that Li isotopes are almost exclusively fractionated and drained in rivers by the weathering of silicates (silicate weathering contributes more than 95%) (Dellinger et al., 2015; Huh et al., 2001; Kisakurek et al.,

2005; Millot et al., 2010). While being transported in rivers, only a small portion of Li ($\sim$20%) is available in the dissolved load, while the majority is transported in suspended phases (e.g. Dellinger et al., 2015; Gaillardet et al., 2003; Palmer and Edmond, 1992). A fractionation also occurs between these two phases with an offset of about 2‰, the bedload being mostly heavier than the suspended sediments, whereas there is a dependence on the secondary mineralogy (Kisakurek et al., 2005; Millot et al., 2010; Pogge von Strandmann et al., 2006; Wimpenny et al., 2010).

While clay minerals have high Li contents as they are easily incorporated into the crystal structure, carbonate minerals have rather low Li concentrations (Burton and Vigier, 2012) controlled by the concentration of available Li in the precipitation solution (Hathrone and James, 2006; Marriott et al., 2004a,b; Misra and Froelich, 2009, 2012; Rollion-Bard et al., 2009). However, there are several factors that affect the incorporation of elemental and isotopic Li into inorganic calcite minerals. On the one hand, elemental Li concentrations are higher at low temperatures and there is also a positive correlation for salinity, Li isotopes on the other hand are not fractionated by these two influences (Marriott et al., 2004a). Moreover, Li concentrations are also affected by the calcite growth rates and pH, revealing higher concentrations with higher growth rates and less elemental Li with higher pH (Füger et al., 2019), whereas no studies exist that show the same behaviour for Li isotopes. Albeit, Li isotopes show an isotopic offset when it comes to different mineralogies as calcites reveal an offset of -2 to -6‰ to the water they precipitated from, in contrast to aragonites that showed a larger offset ($\sim$-11 to -10‰) (Marriott et al., 2004a,b; Pogge von Strandmann et al., 2019). Nevertheless, several studies support the use of inorganic calcites as archives for past Li isotope ratios in seawater, although great care should be taken with the leaching methods and the quantification of a possible influence of diagenesis on the primary δ^7Li composition (e.g. Marriott et al., 2004a; Pogge von Strandmann et al., 2013, 2019).

1.4. Study Areas
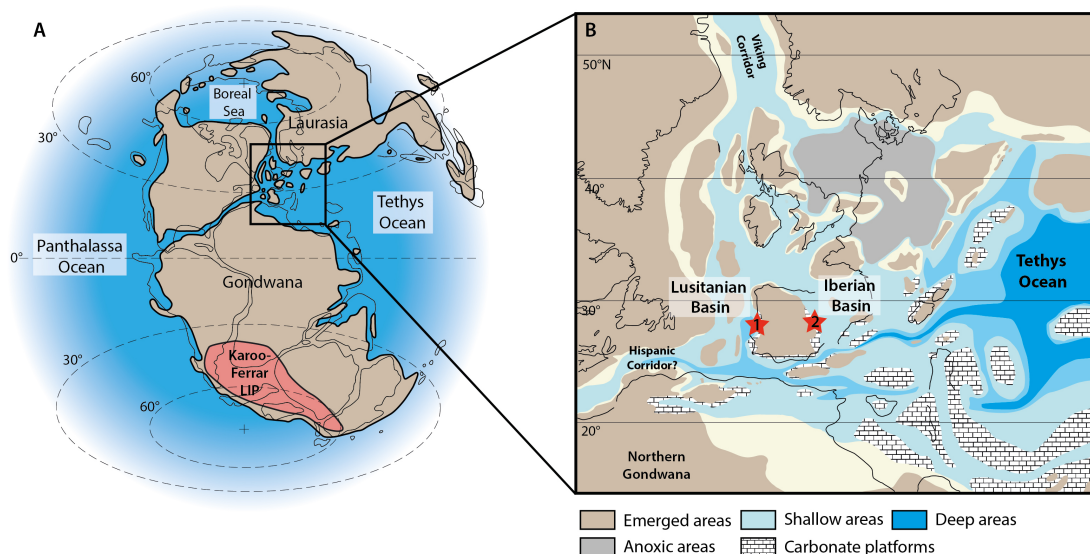
Figure 3. Paleogeography and study area location maps. (A) Global paleogeography during the Early Jurassic, modified after Dera et al., 2011 and Korte et al., 2015. Red area depicts the suggested expansion of the Karoo–Ferrar Large Igneous Province (LIP). (B) Detailed reconstructed map of the NW Tethys area, showing that mainly the northern part of this area suffered anoxia during the T-OAE (modified after Bassoullet and Baudin, 1994; Ruebsam et al., 2018). Stars mark the locations of the studied areas – (1) Rabaçal/Fonte Coberta (Lusitanian Basin) and (2) Barranco de la Cañada (Iberian Basin). *[High-resolution image on attached CD]*

1.4.1. Rabaçal/Fonte Coberta - Lusitanian Basin (Portugal)

The origin of the Peri-Tethyan Lusitanian Basin is related to the opening of the Atlantic Ocean during the Mesozoic (e.g. Alves et al., 2009; Rasmussen et al., 1998; Wilson et al., 1989). It comprises of a small, shallow (less than 160–200 m depth; Bjerrum et al., 2001) and narrow north–south elongated basin that was limited to the east by the Iberian Massif, to the north by shallow seas and to the west by emerged horst blocks. To the south it was open to the epicontinental basins of the NW tethyan realm (Bassoulet et al., 1993) (Fig. 11). Located in the Lusitanian Basin are the Rabaçal (40 °03'08.0"N 8 °27'30.5"W) and Fonte Coberta (40 °03'36.5"N 8 °27'33.4"W) composite sections, situated 1 km south of the small village Fonte Coberta and about 2.5 km north of the village Rabaçal. This section represents a former homoclinal northeast dipping outer/mid-ramp environment during the Early Jurassic with a paleo-waterdepth of 80–120 m (Gahr, 2005; Silva et al., 2015). The depositional environment is thought to have remained below storm-wave base throughout the studied time interval (Gahr, 2005). The biozonation in this succession is well defined through ammonites, nannofossils and dinoflagellate cysts (Comas-Rengifo et al., 2013; Correia et al., 2018; Ferreira et al., 2015; Mouterde et al., 1964-1965).

The studied part of this section encompasses 73 m from which 17 m covers the Pliensbachian (*margaritatus* and *spinatum* AZ — for an overview of the biostragigraphy see Fig. 4) as well as 55 m of the early to middle Toarcian (*polymorphum*, *levisoni* and *bifrons* AZ)(see Fig. 9). Lithologically the studied section covers the Lemede Formation (Pliensbachian) and the São Gião Formation (Toarcian), which can be subdivided into the following members (Fig. 9, 12) (e.g. Duarte et al., 2018 and references therein):

Lemede Formation. This formation spans across the *margaritatus* and *spinatum* AZ and consists of centimetre scale marl and decimetre scale bioturbated limestone alternations (Duarte, 2007).

Marly limestone with Leptaena fauna (MLLF) member (mb). Resembling the base of the São Gião Formation this member is dominated by marls. It comprises an alternation of bioturbated grayish decimetre marls with centimetric fossiliferous micrites to biomicrites/wackestones. At the top of this member a thick limestone bed occurres (at ~6 m height in the lithological log, Fig. 9) which serves as a reference level in the whole Lusitanian basin, with exception of the southern sectors.

Thin nodular limestone (TNL) mb. Commencing about the *polymorphum-levisoni* AZ boundary and thus marking the onset of the TOAE, the TNL mb is identified by a striking change in sedimentology that can be followed throughout the Lusitanian Basin: few cm-thin marlstones alternated with brownish claystone and micritic to microsparitic limestones. The succession appears nodular and has a typical total thickness of about 7 m. This striking sedimentological change is referred to as storm flow conditions and/or distal turbidite currents probably caused by tectonic activity of the Berlenga-Farilhões block.

Marls and marly limestones with Hildaites and Hildoceras (MMLHH) mb. Returning to decimetre to metre-thick marl and marly limestone alternations the MMLHH mb spans from the middle *levisoni* AZ up to the upper *bifrons* AZ.

Remarkably, the typical black shale depositions, which are characteristic for the T-OAE and can be found throughout the globe, are not developed in this section. This is due to the oxygenated state of this area during the anoxic event. In fact, there is no evidence for low-oxygen conditions in the Rabaçal/Fonte Coberta region as total organic carbon levels are rather low (Duarte et al., 2005) and bioturbation traces during the crisis speak for oxygenated bottom conditions (Piazza et al., 2019).

Age of base	Stage	Spain (Submediterranean Province)		Portugal (Mediterranean Province)		Age of base
		Zone	Subzone	Zone	Subzone	
	middle Toarcian	bifrons	bifrons	bifrons	bifrons	
180.39			sublevisoni		sublevisoni	**180.39**
	early Toarcian	serpentinum	falciferum	levisoni	falciferum	
182.92			elegantulum		levisoni	**182.92**
		tenuicostatum	semicelatum II	polymorphum	semicelatum II	
183.72			paltum		mirabile	**183.72**
	late Pliensbachian	emaciatum	elisa	spinatum	hawskerense	
184.55			solare		apyrenum	
		algovianum	levidorsatum			**185.12**
			meneghenii			
			accuratum	margaritatus	gibbosus	
186.15			bertrandi			
			ragazzonii			
		lavinianum	cornacaldense		subnodosus	
188.29					stokesi	**188.29**

Figure 4. Ammonite Biostratigraphy Zones for submediterranean (Spain; BdC section) and mediterranean Provinces (Portugal; R/FC section) (Page, 2003). Ages given in million years (Ma) according to Geological Time Scale 2016 (Ogg et al., 2016).

1.4.2. Barranco de la Cañada - Iberian Basin (Spain)

The Barranco de la Cañada section is located in the former Iberian Basin (Fig. 11), which in turn is situated in the Iberian Range, representing a moderately deformed intraplate chain (Celtiberian Chain) that was formed by a NW trending folded and thrusted belt (Vicente et al., 2009). During the Early Jurassic sedimentation was dominated by shallow carbonate platforms and transgressive hemipelagic alternations of limestone and marls deposited in an intracontinental basin during a post-rift episode (Gómez and Fernández-López, 2006; Gómez and Goy, 2005). The outcrop is situated ~5 km west of the village Albarracín (40°23'53.4"N 1°30'07.4"W). Its complete succession of the upper Pliensbachian up to the middle Toarcian make it a good example to investigate the T-OAE. The studied interval spans in total 48 m, from which 15 m cover the Pliensbachian (Barahona Formation) and 33 m belong to the Toarcian (Turmiel Formation), reaching up to the *bifrons* ammonoid zone (AZ) (Fig. 9). Facies, ammonite zones and fossil paragenesis were described in detail by Gahr, 2002. The succession represents a former gently sloped homoclinal mid-ramp environment (e.g. Comas-Rengifo et al., 1996; Gahr, 2002) with a paleo-water depth of about

40–70 m. Compared to the Rabaçal/Fonte Coberta section the here described outcrop was slightly shallower and less influenced by tectonic activity, but both sections were most of the time below storm wave base (e.g. Duarte and Soares, 1993; Kullberg et al., 2001).

The lithology in this section is an alternation of marls and limestones. The Pliensbachian *margaritatus* and lower *spinatum* AZ are dominated by metre-thick limestones with frequently occurring biomicrites. Up to the Pl–To boundary and the *tenuicostatum* AZ limestones (biomicrites) occur in decimetre-thick layers alternated with marly limestones and calcareous marls. The whole *tenuicostatum* AZ (corresponding to the *polymorphum* AZ in the Lusitanian Basin) is dominated by marls with a few centimetre-thick marly limestone layers. The subsequent *serpentium* AZ (corresponding to the *levisoni* AZ in the Lusitantian Basin) as well as the *bifrons* AZ are an alternation of centimetre-tick limestones varying in their clay contents and marls (Gahr, 2002).

Matching the findings in the Lusitanian Basin this area of the Iberian Basin seemed to be oxygenated during the T-OAE crisis interval, based on the occurrence of plenty of fossils throughout the event (Gahr, 2002; Piazza et al., 2020).

1.5. State of the Science: Environmental conditions during late Pliensbachian–early Toarcian times

The Early Jurassic (Pliensbachian–Toarcian, ~183 Ma) is characterised by some of the Mesozoics most drastic environmental perturbations. The Pliensbachian–Toarcian boundary (Pl–To) and the early Toarcian both witnessed a second-order global extinction impacting ~5 % of marine families and up to ~13 % of terrestrial families during the Toarcian (Benton, 1995). Also, severe assemblage changes of pelagic and benthic organisms can be observed (Cecca and Macchioni, 2004; Danise et al., 2019; Gómez et al., 2008; Mattioli et al., 2009; Palliani and Riding, 2003; Piazza et al., 2019, 2020; Wignall and Bond, 2008). The crisis interval during the early Toarcian spread over the boreal ammonite *tenuicostatum–falciferum* AZ and coincided with the onset of deposits of laminated organic-rich black shales that can be found worldwide and record an event of globally widespread anoxic conditions of the oceans (T-OAE, Jenkyns, 1988; Jenkyns, 2010).

The biological crisis during the T-OAE as well as during the Pl–To boundary is being linked with the emplacement of the Karoo–Ferrar large igneous province (LIP), which occurred during the breakup of Gondwana and appears in South Africa across Antarctica and southestern Australasia including Tasmania (Fig. 11) (e.g. Aarnes et al., 2011; Burgess et al., 2015; Elliot and Fleming, 2008; Elliot, 2013; Pálfy and Smith, 2000; Percival et al., 2015; Svensen et al., 2012). Several phases of LIP extrusion were recognised spreading over several million years from the early to mid-Toarcian stage with each phase lasting several 10–100 kya (Percival et al., 2015). Volumetrically the Karoo–Ferrar LIP is one of the biggest flood bastalts during the Phanerozoic (Rampino and Stothers, 1988) with nowadays more than two million cubic kilometres outcropping igneous rocks (Pankhurst et al., 2000). Rapid intrusive magmatism together with contact metamorphism triggered volatile releases of especially the greenhouse gases CO_2 and methane (CH_4) leading to recently calibrated pCO_2 concentrations of 2–4 times higher than pre-industrial levels (Dera and Donnadieu, 2012; Ullmann et al., 2020), which then in turn drove the environmental change and lead to the biotic crisis and extinction (Svensen et al., 2012). This volcanogenic CO_2 has an isotopically light carbon imprint ($\delta^{13}C$ ~-7‰ Hesselbo et al., 2007), which is thought to be the cause of the globally recognised negative carbon-isotope excursion (CIE) during the T-OAE with an evidenced drop of ~3–9‰, depending on the material analysed (e.g. Danise et al., 2019; Hesselbo et al., 2000; Izumi et al., 2012; Kemp et al., 2005; Littler et al., 2010; Suan et al., 2011). Two more causes debated for the cause of the CIE are first, the input of thermogenic CO_2 released during the interaction of Karoo–Ferrar magma and organic-rich sediments or second, the release of methane from the dissociation of marine clathrates ($\delta^{13}C$ ~-60‰; e.g. Hesselbo et al., 2000; Kemp et al., 2011; McElwain et al., 2005; Pálfy and Smith, 2000; Svensen et al., 2012, 2007). As the CIE is observed globally in many diverse materials, like wood, carbonate and marine organic matter, it stands to reason that

both the atmosphere and the ocean systems were perturbed. Therefore the CIE serves as a better marker for the onset of the T-OAE than the commencing deposition of the black shales (e.g. Bodin et al., 2016; Hesselbo et al., 2007; Reolid et al., 2014; Röhl et al., 2001; Suan et al., 2011; Them et al., 2017; Xu et al., 2017). Furthermore, during the Pl–To boundary a smaller negative CIE with a magnitude of ∼-2 ‰ was recognised (Hesselbo et al., 2007; Littler et al., 2010; Percival et al., 2016). The duration of the CIE and OAE has recently been calibrated to be between ∼300 and 900 kyr (Boulila et al., 2014; Huang and Hesselbo, 2014; Ikeda and Hori, 2014; Pittet et al., 2014; Suan et al., 2008), whereas the Pl–To boundary event was astronomically calibrated to a shorter duration of ∼60 kyr (e.g. Huang and Hesselbo, 2014; Pittet et al., 2014).

A further environmental perturbation triggered by elevated CO_2 gas amounts is the rise in atmospheric temperatures, which have been modelled with a rise of about 3°C and 5°C for the tropical and midlatitude areas, respectively (Dera and Donnadieu, 2012; Pálfy and Smith, 2000). The high latitudes are more impacted by atmopsheric heating of about 10°C due to the reductions in the ice shield and albedo. Concurrently to atmospheric heating, the seawater temperatures were also affected by warming, which can be directly reconstructed with $\delta^{18}O$ isotopes derived from brachiopod shells and belemnites. While the latest Pliensbachian *spinatum* AZ was dominated by a rather cold climate with seawater temperatures around 11–16°C (Bailey et al., 2003; Dera and Donnadieu, 2012; Dera et al., 2011; Rosales et al., 2004; Suan et al., 2010) and probable existing continental ice masses (Suan et al., 2010), the Pl–To boundary experienced an abrupt rise in the seawater temperature by ∼4–5°C (Suan et al., 2008) with a subsequent decrease to low sea-surface temperatures and cold and wet climate with accelerated physical weathering prior to the T-OAE (Bailey et al., 2003; Lézin et al., 2013; Rosales et al., 2004; Suan et al., 2010). Ongoing, during the T-OAE and hence the CIE a seawater temperature rise of about 3–7°C was recorded (Bailey et al., 2003; McArthur et al., 2000; Suan et al., 2010, 2008; Ullmann et al., 2020) with a maximum temperature of 26°C (Rosales et al., 2004; Ullmann et al., 2020). After the T-OAE the early Toarcian climate was dominated by greenhouse conditions (Dera et al., 2011) as is also evident for the middle Toarcian *bifrons* AZ (Bailey et al., 2003; Dera et al., 2011; Gómez and Arias, 2010; Gómez and Goy, 2011; Léonide et al., 2012).

The theory behind entering the state of widespread oxygen-depleted oceans is that elevated CO_2 amounts in the atmosphere lead to warmer global temperatures accompanied by an enhanced hydrological cycle and higher continental weathering rates, which would have raised the nutrient fluxes into the oceans (Brazier et al., 2015; Cohen et al., 2004; Fu et al., 2017; Hermoso and Pellenard, 2014). This condition subsequently enhanced primary productivity and resulted in the anoxic conditions through the oxidation of the elevated extent of organic matter in more restricted settings (Jenkyns, 2010). This enhanced carbon burial is also conspicuous in the carbon isotope curve predating the T-OAE and negative CIE through a broad positive excursion with a magnitude

of $\sim +3$ ‰ (Hesselbo et al., 2007; Huang and Hesselbo, 2014; Jenkyns, 1988; Suan et al., 2008).

According to this theory the investigation of continental weathering rates during the T-OAE has been of special interest as it played an important role in leading to the anoxic conditions of the oceans, and also helped to terminate the state of elevated CO_2 as the process of chemical weathering consumes this greenhouse gas. Strontium isotopes ($^{87}Sr/^{86}Sr$) can be used as a mean to reconstruct changes in continental weathering and were the first tries to unravel the history of continental weathering during the T-OAE. Sr isotope data were firstly published for the T-OAE by Jones et al., 1994, who investigated belemnites and oysters from three different sections in the UK. They firstly detected the strontium isotope excursion where values drop to more unradiogenic values across the Sinemurian–Pliensbachian intervals, the curve becoming steeper from the *margaritatus* AZ on with a slow increase across the Pliensbachian–Toarcian boundary (Fig. 19). A study by Jones and Jenkyns, 2001 suggested that this decrease to more unradiogenic Sr values might be the result of increased hydrothermal activity. Ongoing in the strontium-isotope curve is the most remarkable jump to pre-excursion $^{87}Sr/^{86}Sr$ ratios starting at the *exaratum* subzone (equals the *elegantulum* subzone) and reaching into the overlying *falciferum* subzone and hence crossing the T-OAE (see Fig. 19, red box). This sudden increase has also been recorded by McArthur et al., 2000 from belemnites collected at the Yorkshire coast. Both publications interpreted this rapid increase as a result from condensed intervals or hiatuses in the sedimentological log, and not as a result of higher continental weathering rates, as such a rapid shift seemed unlikely considering the long residence time of Sr in the ocean (~ 1 Ma; McArthur et al., 2012). In an effort to explain the sharp increase in Sr isotopic composition during the T-OAE Waltham and Gröcke, 2006 tried to model these data. Unfortunately, they were not able to recreate the abrupt increase of seawater $^{87}Sr/^{86}Sr$ and stated three different possible drivers for the abrupt Sr isotopic change: an increase of the strontium flux from the continents by weathering, a change in continental weathered minerals with more radiogenic $^{87}Sr/^{86}Sr$ or increased hydrothermal venting. In the end they concluded that a minor climatic event could have also lead to the shift instead of a postulated major event. Hence, up to date there is no clear explanation for neither this Sr-isotope excursion during the late Pliensbachian nor the sharp shift to more radiogenic values during the T-OAE. Also interestingly to mention, compared to other OAEs like those during the Cretaceous, which also record Sr-isotope excursions, the Toarcian OAE occurs at the end of the excursion, while for the Early Aptian and Cenomanian-Turonian OAEs they appear at the the respective onsets of the OAEs (Jones and Jenkyns, 2001).

Luckily, there are more isotope systems that can serve as tracers for continental weathering changes. An early study from Yorkshire (UK; Cohen et al., 2004) suggested on the base of more radiogenic $^{187}Os/^{188}Os$ isotopes an increase of 4–8 times in magnitude of continental weathering rates during the T-OAE. However, these data stand in contrast to more recent studies with

^{187}Os/^{188}Os conducted in two different realms: the eastern margin of the Panthalassa Ocean (Them et al., 2017) and NW Tethys (Percival et al., 2016) (Fig. 14). Both recent studies record a similar magnitude in the Os isotope excursion during the T-OAE speaking for a global event of $\sim$3 times increased weathering rates relative to the conditions prior to the T-OAE (Percival et al., 2016; Them et al., 2017). The more radiogenic Os isotopes recorded by Cohen et al., 2004 are most probably the cause of a basinal restriction and regional influences (McArthur et al., 2008; Waltham and Gröcke, 2006). Moreover, Percival et al., 2016 recorded likewise more radiogenic ^{187}Os/^{188}Os and thus $\sim$2 times elevated weathering rates for the Pl-To boundary. More assumptions about increased weathering rates derive from a negative $\delta^{44/40}$Ca isotope excursion with a suggested increasing factor of 5 for the Pl–To boundary event as well as the T-OAE (Brazier et al., 2015) (Fig. 14). This study speculated that two processes played together in leaving the seawater enriched in the light ^{40}Ca isotope and explaining the negative Ca isotope excursion: (I) increased riverine fluxes and thus weathering rates together with (II) ocean acidification associated with decreased carbonate burial due to the massive input of CO_2.

Another approach for continental weathering reconstructions was performed by Hermoso and Pellenard, 2014. Their study used relative clay mineral (kaolinite) occurrences as an equivalent for weathering intensities. With their findings they demonstrated decreased weathering rates as relative proportions of kaolinite were diminished during the late Pliensbachian (prior to the Pl-To boundary), emphasising the theory of a cooling and arid climate with the probable occurrence of ice sheets during this interval (Bailey et al., 2003; Chandler et al., 1992; Dera and Donnadieu, 2012; Dera et al., 2011; Suan et al., 2010). Ongoing, the kaolinite contents revealed a cold and dry climate for the early Toarcian (prior to the T-OAE), warmer conditions for the T-OAE interval with enhanced kaolinite supply and thus elevated weathering conditions, and finally warm and humid climate conditions for the time interval after the T-OAE (Hermoso and Pellenard, 2014). Furthermore, they hypothesised that the short kaolinite enrichment episode discovered at the beginning of the CIE ceased very quickly due to the rapid removal of the greenhouse gasses in the atmosphere.

Higher greenhouse gas concentrations in the ocean–atmosphere system are also to blame for a carbonate production crisis during the T-OAE and Pl–To events as evident in the size reduction in marine carbonate producing organisms (*Schizosphaerella*, Mattioli and Pittet, 2002; Suan et al., 2008; and solely for the T-OAE for brachiopods by Piazza et al., 2019). Accordingly, a decrease in carbonate accumulation in the basinal depositional environment (Mattioli et al., 2004, 2009) and the near disappearance of shallow-water platforms was induced (Dromart et al., 1996; Trecalli et al., 2012). Not only were higher temperatures a trigger for this carbonate production crisis, but also a probable ocean acidification event catalysed by the massive CO_2 injections in the marine system (Beerling and Brentnall, 2007; Hermoso et al., 2009; Kemp et al., 2005). Hints for a reduced

seawater pH level are recorded by the characteristic diminished total carbonate content during the T-OAE caused by reduced seawater carbonate saturation (Hermoso et al., 2012; Suan et al., 2008) possibly also affecting the especially selective extinction against marine calcifying organisms like corals and unbuffered organisms (Kiessling and Simpson, 2011) as well as buffered organisms like bivalves as shown by Trecalli et al., 2012. Hence, direct evidence for an acidification event during the T-OAE is not given up do date and will be delivered with this study (see chapter 3).

References

Aarnes, I., H. Svensen, S. Polteau, and S. Planke (2011). "Contact metamorphic de-volatilization of shales in the Karoo Basin, South Africa, and the effects of multiple sill intrusions". *Chemical Geology* 281.3-4, pp. 181–194. DOI: 10.1016/j.chemgeo.2010.12.007.

Alves, T. M., C. Moita, T. Cunha, M. Ullnaess, R. Myklebust, J. H. Monteiro, and G. Manuppella (2009). "Diachronous evolution of Late Jurassic-Cretaceous continental rifting in the northeast Atlantic (west Iberian margin)". *Tectonics* 28.4. DOI: 10.1029/2008TC002337.

Anderson, J. M., J. Proctor, and H. W. Vallack (1983). "Ecological Studies in Four Contrasting Lowland Rain Forests in Gunung Mulu National Park, Sarawak: III. Decomposition Processes and Nutrient Losses from Leaf Litter". *The Journal of Ecology* 71.2, p. 503. DOI: 10.2307/2259731.

Bailey, T. R., Y. Rosenthal, J. M. McArthur, B. van de Schootbrugge, and M. F. Thirlwall (2003). "Paleoceanographic changes of the Late Pliensbachian–Early Toarcian interval: A possible link to the genesis of an Oceanic Anoxic Event". *Earth and Planetary Science Letters* 212.3-4, pp. 307–320. DOI: 10.1016/S0012-821X(03)00278-4.

Balan, E., J. Noireaux, V. Mavromatis, G. D. Saldi, V. Montouillout, M. Blanchard, F. Pietrucci, C. Gervais, J. R. Rustad, J. Schott, and J. Gaillardet (2018). "Theoretical isotopic fractionation between structural boron in carbonates and aqueous boric acid and borate ion". *Geochimica et Cosmochimica Acta* 222, pp. 117–129. DOI: 10.1016/j.gca.2017.10.017.

Bassoulet, J. P., S. Elmi, A. Poisson, F. Cecca, Y. Bellion, R. Guiraud, and F. Baudin (1993). "Middle Toarcian (184-182 Ma)". *Atlas Tethys Paleoenvironmental Maps*. Ed. by J. Dercourt, L. E. Ricou, and B. Vrielynck. Gauthier-Villars, Paris, pp. 63–80.

Bassoullet, J.-P. and F. Baudin (1994). "Le toarcien inférieur: Une période de crise dans les bassins et sur les plate-formes carbonatées de l'Europe du Nord-Ouest et de la Téthys". *Geobios* 27, pp. 645–654. DOI: 10.1016/S0016-6995(94)80227-0.

Beerling, D. J. and S. J. Brentnall (2007). "Numerical evaluation of mechanisms driving Early Jurassic changes in global carbon cycling". *Geology* 35.3, p. 247. DOI: 10.1130/G23416A.1.

Benton, M. J. (1995). "Diversification and extinction in the history of life". *Science (New York, N.Y.)* 268.5207, pp. 52–58. DOI: 10.1126/science.7701342.

Berglund, M. and M. E. Wieser (2011). "Isotopic compositions of the elements 2009: IUPAC Technical Report". *Pure Application Chemistry* 83, pp. 397–410.

Bi, E. B. B., N. Vigier, A. Poszwa, and A. Bernot (2007). "Compared Mg isotope compositions of plants, rocks and waters". *Geochimica et Cosmochimica Acta* 71.A106.

Bijma, J., H.-O. Portner, C. Yesson, and A. D. Rogers (2013). "Climate change and the oceans–what does the future hold?" *Marine pollution bulletin* 74.2, pp. 495–505. DOI: 10.1016/j.marpolbul.2013.07.022.

Bjerrum, C. J., F. Surlyk, J. H. Callomon, and R. L. Slingerland (2001). "Numerical paleoceanographic study of the Early Jurassic Transcontinental Laurasian Seaway". *Paleoceanography* 16.4, pp. 390–404. DOI: 10.1029/2000PA000512.

Black, J. R., Q.-z. Yin, and W. H. Casey (2006). "An experimental study of magnesium-isotope fractionation in chlorophyll-a photosynthesis". *Geochimica et Cosmochimica Acta* 70.16, pp. 4072–4079. DOI: 10.1016/j.gca.2006.06.010.

Bodin, S., F.-N. Krencker, T. Kothe, R. Hoffmann, E. Mattioli, U. Heimhofer, and L. Kabiri (2016). "Perturbation of the carbon cycle during the late Pliensbachian – early Toarcian: New insight from high-resolution carbon isotope records in Morocco". *Journal of African Earth Sciences* 116, pp. 89–104. DOI: 10.1016/j.jafrearsci.2015.12.018.

Boulila, S., B. Galbrun, E. Huret, L. A. Hinnov, I. Rouget, S. Gardin, and A. Bartolini (2014). "Astronomical calibration of the Toarcian Stage: Implications for sequence stratigraphy and duration of the early Toarcian OAE". *Earth and Planetary Science Letters* 386, pp. 98–111. DOI: 10.1016/j.epsl.2013.10.047.

Brand, U., G. Jiang, K. Azmy, J. Bishop, and I. P. Montañez (2012). "Diagenetic evaluation of a Pennsylvanian carbonate succession (Bird Spring Formation, Arrow Canyon,

Nevada, U.S.A.) — 1: Brachiopod and whole rock comparison". *Chemical Geology* 308-309, pp. 26–39. DOI: 10.1016/j.chemgeo.2012.03.017.

Brand, U. and J. Veizer (1980). "Chemical Diagenesis of a Multicomponent Carbonate System–1: Trace Elements". *SEPM Journal of Sedimentary Research* Vol. 50. DOI: 10.1306/212F7BB7-2B24-11D7-8648000102C1865D.

– (1981). "Chemical Diagenesis of a Multicomponent Carbonate System 2: Stable Isotopes". *Journal of Sedimentary Petrology* 51.3, pp. 987–997.

Brand, U., A. Logan, N. Hiller, and J. Richardson (2003). "Geochemistry of modern brachiopods: Applications and implications for oceanography and paleoceanography". *Chemical Geology* 198.3-4, pp. 305–334. DOI: 10.1016/S0009-2541(03)00032-9.

Brazier, J.-M., G. Suan, T. Tacail, L. Simon, J. E. Martin, E. Mattioli, and V. Balter (2015). "Calcium isotope evidence for dramatic increase of continental weathering during the Toarcian oceanic anoxic event (Early Jurassic)". *Earth and Planetary Science Letters* 411, pp. 164–176. DOI: 10.1016/j.epsl.2014.11.028.

Brenot, A., C. Cloquet, N. Vigier, J. Carignan, and C. France-Lanord (2008). "Magnesium isotope systematics of the lithologically varied Moselle river basin, France". *Geochimica et Cosmochimica Acta* 72.20, pp. 5070–5089. DOI: 10.1016/j.gca.2008.07.027.

Broecker, W. S. and T. H. Peng (1982). *Tracers in the Sea*. Palisades, New York: Eldigio Pr.

Burgess, S. D., S. A. Bowring, T. H. Fleming, and D. H. Elliot (2015). "High-precision geochronology links the Ferrar large igneous province with early-Jurassic ocean anoxia and biotic crisis". *Earth and Planetary Science Letters* 415, pp. 90–99. DOI: 10.1016/j.epsl.2015.01.037.

Burton, K. W. and N. Vigier (2012). "Lithium isotopes as tracers in marine and terrestrial environments". *Handbook of Environmental Isotope Geochemistry*. Ed. by M. Baskaran. Berlin, Heidelberg: Springer Berlin Heidelberg, pp. 41–59.

Caldeira, K. and M. E. Wickett (2003). "Oceanography: anthropogenic carbon and ocean pH". *Nature* 425.6956, p. 365. DOI: 10.1038/425365a.

Cecca, F. and F. Macchioni (2004). "The two Early Toarcian (Early Jurassic) extinction events in ammonoids". *Lethaia* 37.1, pp. 35–56. DOI: 10.1080/00241160310008257.

Chakrabarti, R. and S. B. Jacobsen (2010). "The isotopic composition of magnesium in the inner Solar System". *Earth and Planetary Science Letters* 293.3-4, pp. 349–358. DOI: 10.1016/j.epsl.2010.03.001.

Chan, L., J. Edmond, G. Thompson, and K. Gillis (1992). "Lithium isotopic composition of submarine basalts: Implications for the lithium cycle in the oceans". *Earth and Planetary Science Letters* 108.1-3, pp. 151–160. DOI: 10.1016/0012-821X(92)90067-6.

Chan, L.-H., W. P. Leeman, and T. Plank (2006). "Lithium isotopic composition of marine sediments". *Geochemistry, Geophysics, Geosystems* 7.6, pp. 1–25. DOI: 10.1029/2005GC001202.

Chandler, M. A., D. Rind, and R. Ruedy (1992). "Pangaean climate during the Early Jurassic: GCM simulations and the sedimentary record of paleoclimate". *Geological Society of America Bulletin* 104.5, p. 543. DOI: 10.1130/0016-7606(1992)104{\textless}0543:PCDTEJ{\textgreater}2.3.CO;2.

Clapham, M. E., M. L. Fraiser, P. J. Marenco, and S.-z. Shen (2013). "Taxonomic composition and environmental distribution of post-extinction rhynchonelliform brachiopod faunas: Constraints on short-term survival and the role of anoxia in the end-Permian mass extinction". *Palaeogeography, Palaeoclimatology, Palaeoecology* 374, pp. 284–292. DOI: 10.1016/j.palaeo.2013.02.002.

Clarkson, M. O., S. A. Kasemann, R. A. Wood, T. M. Lenton, S. J. Daines, S. Richoz, F. Ohnemueller, A. Meixner, S. W. Poulton, and E. T. Tipper (2015). "Ocean acidification and the Permo-Triassic mass extinction". *Science (New York, N.Y.)* 348.6231, pp. 229–232. DOI: 10.1126/science.aaa0193.

Cohen, A. S., A. L. Coe, S. M. Harding, and L. Schwark (2004). "Osmium isotope evidence for the regulation of atmospheric CO_2 by continental weathering". *Geology* 32.2, p. 157. DOI: 10.1130/G20158.1.

Comas-Rengifo, M. J., J. J. Gómez, A. Goy, C. F. Arias, J. Bernad, F. García Joral, and Herrero, C., Martínez, G., Perilli, N. (1996). "The Toarcian in the Rambla del Salto (Sierra Palomera) section". *International Subcommission on Jurassic Stratigraphy, 1st Toarcian and 4th Aalenian working groups meeting*. Ed. by Universidad Complutense de Madrid. Madrid, pp. 27–48.

Comas-Rengifo, M. J., L. V. Duarte, F. García Joral, and A. Goy (2013). "Los braquiópodos del Toarciense Inferior (Jurásico) en el área de Rabaçal-Condeixa (Portugal): distribución estratigráfica y paleobiogeografía". *Comunicações geológicas* 100.Esp. I, pp. 37–42.

Correia, V. F., J. B. Riding, L. V. Duarte, P. Fernandes, and Z. Pereira (2018). "The Early Jurassic palynostratigraphy of the Lusitanian Basin, western Portugal". *Geobios* 51.6, pp. 537–557. DOI: 10.1016/j.geobios.2018.03.001.

Culberson, C. and R. M. Pytkowicx (1968). "Effect of pressure on carbonic acid, boric acid, and the pH in seawater". *Limnology and Oceanography* 13.3, pp. 403–417. DOI: 10.4319/lo.1968.13.3.0403.

Danise, S., M.-E. Clémence, G. D. Price, D. P. Murphy, J. J. Gómez, and R. J. Twitchett (2019). "Stratigraphic and environmental control on marine benthic community change through the early Toarcian extinction event (Iberian Range, Spain)". *Palaeogeography, Palaeoclimatology, Palaeoecology* 524, pp. 183–200. DOI: 10.1016/j.palaeo.2019.03.039.

Dellinger, M., J. Gaillardet, J. Bouchez, D. Calmels, P. Louvat, A. Dosseto, C. Gorge, L. Alanoca, and L. Maurice (2015). "Riverine Li isotope fractionation in the Amazon River basin controlled by the weathering regimes". *Geochimica et Cosmochimica Acta* 164, pp. 71–93. DOI: 10.1016/j.gca.2015.04.042.

Dera, G. and Y. Donnadieu (2012). "Modeling evidences for global warming, Arctic seawater freshening, and sluggish oceanic circulation during the Early Toarcian anoxic event". *Paleoceanography* 27.2, pp. 1–15. DOI: 10.1029/2012PA002283.

Dera, G., P. Neige, J.-L. Dommergues, and A. Brayard (2011). "Ammonite paleobiogeography during the Pliensbachian–Toarcian crisis (Early Jurassic) reflecting paleoclimate, eustasy, and extinctions". *Global and Planetary Change* 78.3-4, pp. 92–105. DOI: 10.1016/j.gloplacha.2011.05.009.

Derry, L. A. (2009). "Weathering and Climate". *Encyclopedia of Paleoclimatology and Ancient Environments*. Ed. by V. Gornitz. Encyclopedia of Earth Sciences Series. Dordrecht: Springer Netherlands, pp. 981–986.

Dessert, C., B. Dupré, J. Gaillardet, L. M. François, and C. J. Allègre (2003). "Basalt weathering laws and the impact of basalt weathering on the global carbon cycle". *Chemical Geology* 202.3-4, pp. 257–273. DOI: 10.1016/j.chemgeo.2002.10.001.

Deutsch, C. A., J. J. Tewksbury, R. B. Huey, K. S. Sheldon, C. K. Ghalambor, D. C. Haak, and P. R. Martin (2008). "Impacts of climate warming on terrestrial ectotherms across latitude". *Proceedings of the National Academy of Sciences of the United States of America* 105.18, pp. 6668–6672. DOI: 10.1073/pnas.0709472105.

Dickson, A. G. (1990). "Thermodynamics of the dissociation of boric acid in synthetic seawater from 273.15 to 318.15 K". *Deep Sea Research Part A. Oceanographic Research Papers* 37.5, pp. 755–766. DOI: 10.1016/0198-0149(90)90004-F.

Dromart, G., P. Allemand, J.-P. Garcia, and C. Robin (1996). "Cyclic fluctuation of carbonate production through the Jurassic along a Burgundy-Ardèche cross-section, eastern France". *Bulletin de la Societe Geologique de France* 167, pp. 423–433.

Duarte, L. V. (2007). "Lithostratigraphy, sequence stratigraphy and depositional setting of the Pliensbachian and Toarcian series in the Lusitanian Basin, Portugal". *Ciências da Terra (UNL)* 16, pp. 17–23.

Duarte, L. V., M. J. Comas-Rengifo, F. García Joral, A. Goy, O. Miguez-Salas, and F. J. Rodríguez-Tovar (2018). "Sedimentological and macroinvertebrate record across the Lower Toarcian in the Rabacal area - Stop 2.2". *Field Trip Guidebook: The Toarcian Oceanic Anoxic Event in the Western Iberian Margin and its context within the Lower Jurassic evolution of the Lusitanian Basin*. Ed. by L. V. Duarte and R. L. Silva. Portugal, pp. 71–82.

Duarte, L. V., R. Rodrigues, L. C. Oliveira, and F. Silva, eds. (2005). *XIV Semana de*

Geoquímica and VIII Congresso de Geoquímica dos Países de Lingua Portuguesa. 1st ed. Aveiro (Portugal).

Duarte, L. V. and A. F. Soares (1993). "Eventos de natureza tempestíticae turbidítica no toarciano inferior da Bacia Lusitaniana(sector norte)". *Cadernos de Geografía* 12, pp. 89–95.

Edmond, J. M. (1992). "Himalayan tectonics, weathering processes, and the strontium isotope record in marine limestones". *Science (New York, N.Y.)* 258.5088, pp. 1594–1597. DOI: 10.1126/science.258.5088.1594.

Elderfield, H. and A. Schultz (1996). "Mid-Ocean Ridge Hydrothermal Fluxes and the Chemical Composition of the Ocean". *Annu. Rev. Earth Planet. Sci.* 24.1, pp. 191–224. DOI: 10.1146/annurev.earth.24.1.191.

Elliot, D. H. and T. H. Fleming (2008). "Physical volcanology and geological relationships of the Jurassic Ferrar Large Igneous Province, Antarctica". *Journal of Volcanology and Geothermal Research* 172.1-2, pp. 20–37. DOI: 10.1016/j.jvolgeores.2006.02.016.

Elliot, D. H. (2013). "The geological and tectonic evolution of the Transantarctic Mountains: A review". *Geological Society, London, Special Publications* 381.1, pp. 7–35. DOI: 10.1144/SP381.14.

Fantle, M. S. and J. Higgins (2014). "The effects of diagenesis and dolomitization on Ca and Mg isotopes in marine platform carbonates: Implications for the geochemical cycles of Ca and Mg". *Geochimica et Cosmochimica Acta* 142, pp. 458–481. DOI: 10.1016/j.gca.2014.07.025.

Farmer, J. R., O. Branson, J. Uchikawa, D. E. Penman, B. Hönisch, and R. E. Zeebe (2019). "Boric acid and borate incorporation in inorganic calcite inferred from B/Ca, boron isotopes and surface kinetic modeling". *Geochimica et Cosmochimica Acta* 244, pp. 229–247. DOI: 10.1016/j.gca.2018.10.008.

Farmer, J. R., B. Hönisch, L. F. Robinson, and T. M. Hill (2015). "Effects of seawater-pH and biomineralization on the boron isotopic composition of deep-sea bamboo corals". *Geochimica et Cosmochimica Acta* 155, pp. 86–106. DOI: 10.1016/j.gca.2015.01.018.

Faure, G. (1986). *Principles of Isotope Geology*. Smith and Wyllie intermediate geology series. New York: Wiley.

Ferreira, J., E. Mattioli, B. Pittet, M. Cachão, and J. E. Spangenberg (2015). "Palaeoecological insights on Toarcian and lower Aalenian calcareous nannofossils from the Lusitanian Basin (Portugal)". *Palaeogeography, Palaeoclimatology, Palaeoecology* 436, pp. 245–262. DOI: 10.1016/j.palaeo.2015.07.012.

Foster, G. L., P. A. E. Pogge von Strandmann, and J. W. B. Rae (2010). "Boron and magnesium isotopic composition of seawater". *Geochemistry, Geophysics, Geosystems* 11.8, n/a–n/a. DOI: 10.1029/2010GC003201.

France-Lanord, C. and L. A. Derry (1997). "Organic carbon burial forcing of the carbon cycle from Himalayan erosion". *Nature* 390.6655, pp. 65–67. DOI: 10.1038/36324.

Fu, X., J. Wang, S. Zeng, X. Feng, D. Wang, and C. Song (2017). "Continental weathering and palaeoclimatic changes through the onset of the Early Toarcian oceanic anoxic event in the Qiangtang Basin, eastern Tethys". *Palaeogeography, Palaeoclimatology, Palaeoecology* 487, pp. 241–250. DOI: 10.1016/j.palaeo.2017.09.005.

Füger, A., F. Konrad, A. Leis, M. Dietzel, and V. Mavromatis (2019). "Effect of growth rate and pH on lithium incorporation in calcite". *Geochimica et Cosmochimica Acta* 248, pp. 14–24. DOI: 10.1016/j.gca.2018.12.040.

Gahr, M. E. (2002). "Palökologie des Makrobenthos aus dem Unter-Toarc SW-Europas: Dissertation". *Beringeria* 31.

– (2005). "Response of Lower Toarcian (Lower Jurassic) macrobenthos of the Iberian Peninsula to sea level changes and mass extinction". *Journal of Iberian Geology* 31.2, pp. 197–215.

Gaillardet, J., J. Viers, and B. Dupré (2003). "Trace Elements in River Waters". *Treatise on Geochemistry*. Ed. by H. D. Holland and K. K. Turekian. Elsevier, pp. 225–272.

Galy, A., M. Bar-Matthews, L. Halicz, and R. O'Nions (2002). "Mg isotopic composition of carbonate: Insight from speleothem formation". *Earth and Planetary Science Letters* 201.1, pp. 105–115. DOI: 10.1016/S0012-821X(02)00675-1.

Gao, T. (2016). *High-precision measurement of Mg isotopes and their geochemical behaviors during continental weathering.* Beijing: China University of Geosciences (in Chinese with English abstract).

Gao, T., S. Ke, S.-J. Wang, F. Li, C. Liu, J. Lei, C. Liao, and F. Wu (2018). "Contrasting Mg isotopic compositions between Fe-Mn nodules and surrounding soils: Accumulation of light Mg isotopes by Mg-depleted clay minerals and Fe oxides". *Geochimica et Cosmochimica Acta* 237, pp. 205–222. DOI: 10.1016/j.gca.2018.06.028.

Garrison, T. (2006). *Oceanography: An invitation to marine science.* 6. edition. Brook and Cole Publishers.

Gómez, J. J. and C. Arias (2010). "Rapid warming and ostracods mass extinction at the Lower Toarcian (Jurassic) of central Spain". *Marine Micropaleontology* 74.3-4, pp. 119–135. DOI: 10.1016/j.marmicro.2010.02.001.

Gómez, J. J. and S. R. Fernández-López (2006). "The Iberian Middle Jurassic carbonate-platform system: Synthesis of the palaeogeographic elements of its eastern margin (Spain)". *Palaeogeography, Palaeoclimatology, Palaeoecology* 236.3-4, pp. 190–205. DOI: 10.1016/j.palaeo.2005.11.008.

Gómez, J. J., A. Goy, and M. L. Canales (2008). "Seawater temperature and carbon isotope variations in belemnites linked to mass extinction during the Toarcian (Early Jurassic) in Central and Northern Spain. Comparison with other European sections". *Palaeogeography, Palaeoclimatology, Palaeoecology* 258.1-2, pp. 28–58. DOI: 10.1016/j.palaeo.2007.11.005.

Gómez, J. J. and A. Goy (2005). "Late Triassic and Early Jurassic palaeogeographic evolution and depositional cycles of the Western Tethys Iberian platform system (Eastern Spain)". *Palaeogeography, Palaeoclimatology, Palaeoecology* 222.1-2, pp. 77–94. DOI: 10.1016/j.palaeo.2005.03.010.

– (2011). "Warming-driven mass extinction in the Early Toarcian (Early Jurassic) of northern and central Spain. Correlation with other time-equivalent European sections". *Palaeogeography, Palaeoclimatology, Palaeoecology* 306.3-4, pp. 176–195. DOI: 10.1016/j.palaeo.2011.04.018.

Gruber, C., Y. Harlavan, D. Pousty, D. Winkler, and J. Ganor (2019). "Enhanced chemical weathering of albite under seawater conditions and its potential effect on the Sr ocean budget". *Geochimica et Cosmochimica Acta* 261, pp. 20–34. DOI: 10.1016/j.gca.2019.06.049.

Hansson, I. (1973). "A new set of acidity constants for carbonic acid and boric acid in sea water". *Deep Sea Research and Oceanographic Abstracts* 20.5, pp. 461–478. DOI: 10.1016/0011-7471(73)90100-9.

Hathrone, E. and R. James (2006). "Temporal record of lithium in seawater: A tracer for silicate weathering?" *Earth and Planetary Science Letters* 246.3-4, pp. 393–406. DOI: 10.1016/j.epsl.2006.04.020.

Hemming, N. G. and G. N. Hanson (1992). "Boron isotopic composition and concentration in modern marine carbonates". *Geochimica et Cosmochimica Acta* 56.1, pp. 537–543. DOI: 10.1016/0016-7037(92)90151-8.

Hermoso, M., F. Minoletti, L. Le Callonnec, H. C. Jenkyns, S. P. Hesselbo, R. E. M. Rickaby, M. Renard, M. de Rafélis, and L. Emmanuel (2009). "Global and local forcing of Early Toarcian seawater chemistry: A comparative study of different paleoceanographic settings (Paris and Lusitanian basins)". *Paleoceanography* 24.4, p. 307. DOI: 10.1029/2009PA001764.

Hermoso, M., F. Minoletti, R. E. Rickaby, S. P. Hesselbo, F. Baudin, and H. C. Jenkyns (2012). "Dynamics of a stepped carbon-isotope excursion: Ultra high-resolution study of Early Toarcian environmental change". *Earth and Planetary Science Letters* 319-320, pp. 45–54. DOI: 10.1016/j.epsl.2011.12.021.

Hermoso, M. and P. Pellenard (2014). "Continental weathering and climatic changes inferred from clay mineralogy and paired carbon isotopes across the early to middle Toarcian in the Paris Basin". *Palaeogeography, Palaeoclimatology, Palaeoecology* 399, pp. 385–393. DOI: 10.1016/j.palaeo.2014.02.007.

Hesselbo, Grocke, Jenkyns, Bjerrum, Farrimond, B. H. S. Morgans, and Green (2000). "Massive dissociation of gas hydrate during a Jurassic oceanic anoxic event". *Na-*

ture 406.6794, pp. 392–395. DOI: 10.1038/35019044..

Hesselbo, S. P., H. C. Jenkyns, L. V. Duarte, and L. C. Oliveira (2007). "Carbon-isotope record of the Early Jurassic (Toarcian) Oceanic Anoxic Event from fossil wood and marine carbonate (Lusitanian Basin, Portugal)". *Earth and Planetary Science Letters* 253.3-4, pp. 455–470. DOI: 10.1016/j.epsl.2006.11.009.

Holcomb, M., T. M. DeCarlo, G. A. Gaetani, and M. McCulloch (2016). "Factors affecting B/Ca ratios in synthetic aragonite". *Chemical Geology* 437, pp. 67–76. DOI: 10.1016/j.chemgeo.2016.05.007.

Hönisch, B., S. M. Eggins, L. L. Haynes, K. A. Allen, K. D. Holland, and K. Lorbacher (2019). "Boron Proxies in Paleoceanography and Paleoclimatology". *Analytical Methods in Earth and Environmental Sciences Series*. Ed. by Wiley-Blackwell, p. 264.

Hönisch, B. et al. (2012). "The geological record of ocean acidification". *Science (New York, N.Y.)* 335.6072, pp. 1058–1063. DOI: 10.1126/science.1208277.

Hönisch, B., T. Bickert, and N. G. Hemming (2008). "Modern and Pleistocene boron isotope composition of the benthic foraminifer *Cibicidoides wuellerstorfi*". *Earth and Planetary Science Letters* 272.1-2, pp. 309–318. DOI: 10.1016/j.epsl.2008.04.047.

Huang, C. and S. P. Hesselbo (2014). "Pacing of the Toarcian Oceanic Anoxic Event (Early Jurassic) from astronomical correlation of marine sections". *Gondwana Research* 25.4, pp. 1348–1356. DOI: 10.1016/j.gr.2013.06.023.

Huh, Y., L.-H. Chan, and J. M. Edmond (2001). "Lithium isotopes as a probe of weathering processes: Orinoco River". *Earth and Planetary Science Letters* 194.1-2, pp. 189–199. DOI: 10.1016/S0012-821X(01)00523-4.

Huh, Y., L.-H. Chan, L. Zhang, and J. M. Edmond (1998). "Lithium and its isotopes in major world rivers: Implications for weathering and the oceanic budget". *Geochimica et Cosmochimica Acta* 62.12, pp. 2039–2051. DOI: 10.1016/S0016-7037(98)00126-4.

Ikeda, M. and R. S. Hori (2014). "Effects of Karoo–Ferrar volcanism and astronomical cycles on the Toarcian Oceanic Anoxic Events (Early Jurassic)". *Palaeogeog-* *raphy, Palaeoclimatology, Palaeoecology* 410, pp. 134–142. DOI: 10.1016/j.palaeo.2014.05.026.

Immenhauser, A., D. Buhl, D. Richter, A. Niedermayr, D. Riechelmann, M. Dietzel, and U. Schulte (2010). "Magnesium-isotope fractionation during low-Mg calcite precipitation in a limestone cave − Field study and experiments". *Geochimica et Cosmochimica Acta* 74.15, pp. 4346–4364. DOI: 10.1016/j.gca.2010.05.006.

IPCC (2007). "Summary for policymakers". *Climate Change 2007: The Physical Science Basis*. Ed. by S. Solomon, D. Qin, M. Manning, Chen. Z., M. Marquis, K. B. Averyt, M. Tignor, and H. L. Miller. Cambridge: Cambridge University Press.

Ishikawa, T. and E. Nakamura (1993). "Boron isotope systematics of marine sediments". *Earth and Planetary Science Letters* 117.3-4, pp. 567–580. DOI: 10.1016/0012-821X(93)90103-G.

Izumi, K., T. Miyaji, and K. Tanabe (2012). "Early Toarcian (Early Jurassic) oceanic anoxic event recorded in the shelf deposits in the northwestern Panthalassa: Evidence from the Nishinakayama Formation in the Toyora area, west Japan". *Palaeogeography, Palaeoclimatology, Palaeoecology* 315-316, pp. 100–108. DOI: 10.1016/j.palaeo.2011.11.016.

James, R. H., M. D. Rudnicki, and M. R. Palmer (1999). "The alkali element and boron geochemistry of the Escanaba Trough sediment-hosted hydrothermal system". *Earth and Planetary Science Letters* 171.1, pp. 157–169. DOI: 10.1016/S0012-821X(99)00140-5.

Jaraula, C. M., K. Grice, R. J. Twitchett, M. E. Böttcher, P. LeMetayer, A. G. Dastidar, and L. F. Opazo (2013). "Elevated pCO2 leading to Late Triassic extinction, persistent photic zone euxinia, and rising sea levels". *Geology* 41.9, pp. 955–958. DOI: 10.1130/G34183.1.

Jenkyns, H. C. (1988). "The early Toarcian (Jurassic) anoxic event; stratigraphic, sedimentary and geochemical evidence". *American Journal of Science* 288.2, pp. 101–151. DOI: 10.2475/ajs.288.2.101.

Jenkyns, H. C. (2010). "Geochemistry of oceanic anoxic events". *Geochemistry, Geophysics, Geosystems* 11.3, pp. 1–30. DOI: 10.1029/2009GC002788.

Joachimski, M. M., X. Lai, S. Shen, H. Jiang, G. Luo, B. Chen, J. Chen, and Y. Sun (2012). "Climate warming in the latest Permian and the Permian-Triassic mass extinction". *Global and Planetary Change* 40.3, pp. 195–198. DOI: 10.1130/G32707.1.

Joachimski, M. M., L. Simon, R. van Geldern, and C. Lécuyer (2005). "Boron isotope geochemistry of Paleozoic brachiopod calcite: Implications for a secular change in the boron isotope geochemistry of seawater over the Phanerozoic". *Geochimica et Cosmochimica Acta* 69.16, pp. 4035–4044. DOI: 10.1016/j.gca.2004.11.017.

Jones, C. E. and H. C. Jenkyns (2001). "Seawater strontium isotopes, oceanic anoxic events, and seafloor hydrothermal activity in the Jurassic and Cretaceous". *American Journal of Science* 301, pp. 112–149.

Jones, C. E., H. C. Jenkyns, and S. P. Hesselbo (1994). "Strontium isotopes in Early Jurassic seawater". *Geochimica et Cosmochimica Acta* 58.4, pp. 1285–1301.

Jurikova, H., V. Liebetrau, M. Gutjahr, C. Rollion-Bard, M. Y. Hu, S. Krause, D. Henkel, C. Hiebenthal, M. Schmidt, J. Laudien, and A. Eisenhauer (2019). "Boron isotope systematics of cultured brachiopods: Response to acidification, vital effects and implications for palaeo-pH reconstruction". *Geochimica et Cosmochimica Acta* 248, pp. 370–386. DOI: 10.1016/j.gca.2019.01.015.

Kaczmarek, K., G. Nehrke, S. Misra, J. Bijma, and H. Elderfield (2016). "Investigating the effects of growth rate and temperature on the B/Ca ratio and $\delta^{11}B$ during inorganic calcite formation". *Chemical Geology* 421, pp. 81–92. DOI: 10.1016/j.chemgeo.2015.12.002.

Kakihana, H., M. Kotaka, S. Satoh, M. Nomura, and M. Okamoto (1977). "Fundamental Studies on the Ion-Exchange Separation of Boron Isotopes". *Bulletin of the Chemical Society of Japan* 50.1, pp. 158–163. DOI: 10.1246/bcsj.50.158.

Kemp, D. B., A. L. Coe, A. S. Cohen, and L. Schwark (2005). "Astronomical pacing of methane release in the Early Jurassic period". *Nature* 437.7057, pp. 396–399. DOI: 10.1038/nature04037.

Kemp, D. B., A. L. Coe, A. S. Cohen, and G. P. Weedon (2011). "Astronomical forcing and chronology of the early Toarcian (Early Jurassic) oceanic anoxic event in Yorkshire, UK". *Paleoceanography* 26.4, p. 633. DOI: 10.1029/2011PA002122.

Kiessling, W., M. Aberhan, B. Brenneis, and P. J. Wagner (2007). "Extinction trajectories of benthic organisms across the Triassic–Jurassic boundary". *Palaeogeography, Palaeoclimatology, Palaeoecology* 244.1-4, pp. 201–222. DOI: 10.1016/j.palaeo.2006.06.029.

Kiessling, W. and C. Simpson (2011). "On the potential for ocean acidification to be a general cause of ancient reef crises". *Global Change Biology* 17.1, pp. 56–67. DOI: 10.1111/j.1365-2486.2010.02204.x.

Kisakurek, B., R. H. James, and N. B. Harris (2005). "Li and δ^7Li in Himalayan rivers: Proxies for silicate weathering?" *Earth and Planetary Science Letters* 237.3-4, pp. 387–401. DOI: 10.1016/j.epsl.2005.07.019.

Klochko, K., A. J. Kaufman, W. Yao, R. H. Byrne, and J. A. Tossell (2006). "Experimental measurement of boron isotope fractionation in seawater". *Earth and Planetary Science Letters* 248.1-2, pp. 276–285. DOI: 10.1016/j.epsl.2006.05.034.

Knoll, A. H., R. K. Bambach, J. L. Payne, S. Pruss, and W. W. Fischer (2007). "Paleophysiology and end-Permian mass extinction". *Earth and Planetary Science Letters* 256.3-4, pp. 295–313. DOI: 10.1016/j.epsl.2007.02.018.

Korte, C., S. P. Hesselbo, C. V. Ullmann, G. Dietl, M. Ruhl, G. Schweigert, and N. Thibault (2015). "Jurassic climate mode governed by ocean gateway". *Nature communications* 6, p. 10015. DOI: 10.1038/ncomms10015.

Kullberg, J., F. Olóriz, B. Marques, P. Caetano, and R. Rocha (2001). "Flatpebble conglomerates: A local marker for Early Jurassic seismicity related to synrift tectonics in the Sesimbra area (Lusitanian Basin, Portugal)". *Sedimentary Geology* 139.1, pp. 49–70. DOI: 10.1016/S0037-0738(00)00160-3.

Lécuyer, C., P. Grandjean, B. Reynard, F. Albarède, and P. Telouk (2002). "$^{11}B/^{10}B$ analysis of geological materials by ICP–MS Plasma 54: Application to the boron fractionation between brachiopod calcite and seawater". *Chemical Geology* 186.1-2,

pp. 45–55. DOI: 10.1016/S0009-2541(01)00425-9.

Lemarchand, D., J. Gaillardet, E. Lewin, and C. J. Allègre (2000). "The influence of rivers on marine boron isotopes and implications for reconstructing past ocean pH". *Nature* 408.6815, pp. 951–954. DOI: 10.1038/35050058.

Lemarchand, D., J. Gaillardet, É. Lewin, and C. Allègre (2002). "Boron isotope systematics in large rivers: Implications for the marine boron budget and paleo-pH reconstruction over the Cenozoic". *Chemical Geology* 190.1-4, pp. 123–140. DOI: 10.1016/S0009-2541(02)00114-6.

Léonide, P., M. Floquet, C. Durlet, F. Baudin, B. Pittet, and C. Lécuyer (2012). "Drowning of a carbonate platform as a precursor stage of the Early Toarcian global anoxic event (Southern Provence sub-Basin, Southeast France)". *Sedimentology* 59.1, pp. 156–184. DOI: 10.1111/j.1365-3091.2010.01221.x.

Lézin, C., B. Andreu, P. Pellenard, J.-L. Bouchez, L. Emmanuel, P. Fauré, and P. Landrein (2013). "Geochemical disturbance and paleoenvironmental changes during the Early Toarcian in NW Europe". *Chemical Geology* 341, pp. 1–15. DOI: 10.1016/j.chemgeo.2013.01.003.

Li, W., S. Chakraborty, B. L. Beard, C. S. Romanek, and C. M. Johnson (2012). "Magnesium isotope fractionation during precipitation of inorganic calcite under laboratory conditions". *Earth and Planetary Science Letters* 333-334, pp. 304–316. DOI: 10.1016/j.epsl.2012.04.010.

Li, Y.-H. (1982). "A brief discussion on the mean oceanic residence time of elements". *Geochimica et Cosmochimica Acta* 46.12, pp. 2671–2675. DOI: 10.1016/0016-7037(82)90386-6.

Ling, M.-X., F. Sedaghatpour, F.-Z. Teng, P. D. Hays, J. Strauss, and W. Sun (2011). "Homogeneous magnesium isotopic composition of seawater: An excellent geostandard for Mg isotope analysis". *Rapid communications in mass spectrometry : RCM* 25.19, pp. 2828–2836. DOI: 10.1002/rcm.5172.

Littler, K., S. P. Hesselbo, and H. C. Jenkyns (2010). "A carbon-isotope perturbation at the Pliensbachian–Toarcian boundary: Evidence from the Lias Group, NE England".

Geological Magazine 147.02, p. 181. DOI: 10.1017/S0016756809990458.

Liu, S.-A., F.-Z. Teng, Y. He, S. Ke, and S. Li (2010). "Investigation of magnesium isotope fractionation during granite differentiation: Implication for Mg isotopic composition of the continental crust". *Earth and Planetary Science Letters* 297.3-4, pp. 646–654. DOI: 10.1016/j.epsl.2010.07.019.

Liu, X.-M., F.-Z. Teng, R. L. Rudnick, W. F. McDonough, and M. L. Cummings (2014). "Massive magnesium depletion and isotope fractionation in weathered basalts". *Geochimica et Cosmochimica Acta* 135, pp. 336–349. DOI: 10.1016/j.gca.2014.03.028.

Liu, X.-M., C. Wanner, R. L. Rudnick, and W. F. McDonough (2015). "Processes controlling δ^7Li in rivers illuminated by study of streams and groundwaters draining basalts". *Earth and Planetary Science Letters* 409, pp. 212–224. DOI: 10.1016/j.epsl.2014.10.032.

Lui-Heung, C., J. M. Gieskes, Y. Chen-Feng, and J. M. Edmond (1994). "Lithium isotope geochemistry of sediments and hydrothermal fluids of the Guaymas Basin, Gulf of California". *Geochimica et Cosmochimica Acta* 58.20, pp. 4443–4454. DOI: 10.1016/0016-7037(94)90346-8.

Marriott, C. S., G. M. Henderson, N. S. Belshaw, and A. W. Tudhope (2004a). "Temperature dependence of δ^7Li, δ^{44}Ca and Li/Ca during growth of calcium carbonate". *Earth and Planetary Science Letters* 222.2, pp. 615–624. DOI: 10.1016/j.epsl.2004.02.031.

Marriott, C. S., G. M. Henderson, R. Crompton, M. Staubwasser, and S. Shaw (2004b). "Effect of mineralogy, salinity, and temperature on Li/Ca and Li isotope composition of calcium carbonate". *Chemical Geology* 212.1-2, pp. 5–15. DOI: 10.1016/j.chemgeo.2004.08.002.

Mattioli, E. and B. Pittet (2002). "Contribution of calcareous nannoplankton to carbonate deposition: A new approach applied to the Lower Jurassic of central Italy". *Marine Micropaleontology* 45.2, pp. 175–190. DOI: 10.1016/S0377-8398(02)00039-7.

Mattioli, E., B. Pittet, R. Palliani, H.-J. Röhl, A. Schmid-Röhl, and E. Morettini (2004). "Phytoplankton evidence for the timing and

correlation of palaeoceanographical changes during the early Toarcian oceanic anoxic event (Early Jurassic)". *Journal of the Geological Society* 161.4, pp. 685–693. DOI: 10.1144/0016-764903-074.

Mattioli, E., B. Pittet, L. Petitpierre, and S. Mailliot (2009). "Dramatic decrease of pelagic carbonate production by nanno-plankton across the Early Toarcian anoxic event (T-OAE)". *Global and Planetary Change* 65.3-4, pp. 134–145. DOI: 10.1016/j.gloplacha.2008.10.018.

Mavromatis, V., Q. Gautier, O. Bosc, and J. Schott (2013). "Kinetics of Mg partition and Mg stable isotope fractionation during its incorporation in calcite". *Geochimica et Cosmochimica Acta* 114, pp. 188–203. DOI: 10.1016/j.gca.2013.03.024.

Mavromatis, V., V. Montouillout, J. Noireaux, J. Gaillardet, and J. Schott (2015). "Characterization of boron incorporation and speciation in calcite and aragonite from co-precipitation experiments under controlled pH, temperature and precipitation rate". *Geochimica et Cosmochimica Acta* 150, pp. 299–313. DOI: 10.1016/j.gca.2014.10.024.

McArthur, J. M., T. J. Algeo, B. van de Schootbrugge, Q. Li, and R. J. Howarth (2008). "Basinal restriction, black shales, Re-Os dating, and the Early Toarcian (Jurassic) oceanic anoxic event". *Paleoceanography* 23.4, n/a–n/a. DOI: 10.1029/2008PA001607.

McArthur, J. M., D. Donovan, M. F. Thirlwall, B. W. Fouke, and D. Mattey (2000). "Strontium isotope profile of the early Toarcian (Jurassic) oceanic anoxic event, the duration of ammonite biozones, and belemnite palaeotemperatures". *Earth and Planetary Science Letters* 179.2, pp. 269–285. DOI: 10.1016/S0012-821X(00)00111-4.

McArthur, J. M., R. J. Howarth, and G. A. Shields (2012). "Strontium Isotope Stratigraphy". *The Geologic Time Scale*. Ed. by F. M. Gradstein, J. Ogg, M. Schmitz, and G. Ogg. Elsevier, pp. 127–144. DOI: 10.1016/B978-0-444-59425-9.00007-X.

McElwain, J. C., J. Wade-Murphy, and S. P. Hesselbo (2005). "Changes in carbon dioxide during an oceanic anoxic event linked to intrusion into Gondwana coals". *Nature*

435.7041, pp. 479–482. DOI: 10.1038/nature03618.

Millot, R., N. Vigier, and J. Gaillardet (2010). "Behaviour of lithium and its isotopes during weathering in the Mackenzie Basin, Canada". *Geochimica et Cosmochimica Acta* 74.14, pp. 3897–3912. DOI: 10.1016/j.gca.2010.04.025.

Misra, S. and P. N. Froelich (2009). "Measurement of lithium isotope ratios by quadrupole-ICP-MS: Application to seawater and natural carbonates". *Journal of Analytical Atomic Spectrometry* 24.11, p. 1524. DOI: 10.1039/B907122A.

– (2012). "Lithium isotope history of Cenozoic seawater: Changes in silicate weathering and reverse weathering". *Science (New York, N.Y.)* 335.6070, pp. 818–823. DOI: 10.1126/science.1214697.

Mouterde, R., C. Ruget, and F. Moitinho de Almeida (1964-1965). "Coupe du Lias au Sud de Condeixa". *Comunicações dos Serviços Geológicas de Portugal* 48, pp. 61–91.

Munday, P. L., M. I. McCormick, and G. E. Nilsson (2012). "Impact of global warming and rising CO_2 levels on coral reef fishes: what hope for the future?" *The Journal of experimental biology* 215.Pt 22, pp. 3865–3873. DOI: 10.1242/jeb.074765.

Nir, O., A. Vengosh, J. S. Harkness, G. S. Dwyer, and O. Lahav (2015). "Direct measurement of the boron isotope fractionation factor: Reducing the uncertainty in reconstructing ocean paleo-pH". *Earth and Planetary Science Letters* 414, pp. 1–5. DOI: 10.1016/j.epsl.2015.01.006.

Noireaux, J., V. Mavromatis, J. Gaillardet, J. Schott, V. Montouillout, P. Louvat, C. Rollion-Bard, and D. R. Neuville (2015). "Crystallographic control on the boron isotope paleo-pH proxy". *Earth and Planetary Science Letters* 430, pp. 398–407. DOI: 10.1016/j.epsl.2015.07.063.

Ogg, J. G., F. M. Gradstein, and G. Ogg (2016). *A concise geologic time scale 2016*. Amsterdam, Netherlands: Elsevier. URL: http://search.ebscohost.com/login.aspx?direct=true&scope=site&db=nlebk&AN=1218972.

Oi, T., T. Tsukamoto, H. Akai, H. Kakihana, and M. Hosoe (1988). "Boron isotope separation by ion-exchange chromatog-

raphy using an anion-exchange resin in halide forms". *Journal of Chromatography A* 450.3, pp. 343–352. DOI: 10.1016/S0021-9673(01)83589-5.

Opfergelt, S., K. W. Burton, R. B. Georg, A. J. West, R. A. Guicharnaud, B. Sigfusson, C. Siebert, S. R. Gislason, and A. N. Halliday (2014). "Magnesium retention on the soil exchange complex controlling Mg isotope variations in soils, soil solutions and vegetation in volcanic soils, Iceland". *Geochimica et Cosmochimica Acta* 125, pp. 110–130. DOI: 10.1016/j.gca.2013.09.036.

Page, K. (2003). "The Lower Jurassic of Europe: its subdivision and correlation". *Geological Survey of Denmark and Greenland* 1, pp. 23–59.

Pálfy, J. and P. L. Smith (2000). "Synchrony between Early Jurassic extinction, oceanic anoxic event, and the Karoo-Ferrar flood basalt volcanism". *Geology* 28.8, p. 747. DOI: 10.1130/0091-7613(2000)28{\textless}747:SBEJEO{\textgreater}2.0.CO;2.

Palliani, R. B. and J. B. Riding (2003). "Biostratigraphy, provincialism and evolution of European early Jurassic (Pliensbachian to early Toarcian) dinoflagellate cysts". *Palynology* 27.1, pp. 179–214. DOI: 10.1080/01916122.2003.9989586.

Palmer, M. R. and J. M. Edmond (1989). "The strontium isotope budget of the modern ocean". *Earth and Planetary Science Letters* 92.1, pp. 11–26. DOI: 10.1016/0012-821X(89)90017-4.

Palmer, M. R., A. J. Spivack, and J. M. Edmond (1987). "Temperature and pH controls over isotopic fractionation during adsorption of boron on marine clay". *Geochimica et Cosmochimica Acta* 51.9, pp. 2319–2323. DOI: 10.1016/0016-7037(87)90285-7.

Palmer, M. and J. Edmond (1992). "Controls over the strontium isotope composition of river water". *Geochimica et Cosmochimica Acta* 56.5, pp. 2099–2111. DOI: 10.1016/0016-7037(92)90332-D.

Palmer, Pearson, and Cobb (1998). "Reconstructing past ocean pH-depth profiles". *Science (New York, N.Y.)* 282.5393, pp. 1468–1471. DOI: 10.1126/science.282.5393.1468.

Pankhurst, R. J., T. R. Riley, C. M. Fanning, and S. P. Kelley (2000). "Episodic Silicic Volcanism in Patagonia and the Antarctic Peninsula: Chronology of Magmatism Associated with the Break-up of Gondwana". *Journal of Petrology* 41.5, pp. 605–625. DOI: 10.1093/petrology/41.5.605.

Pearson, P. N. and M. R. Palmer (2000). "Atmospheric carbon dioxide concentrations over the past 60 million years". *Nature* 406.6797, pp. 695–699. DOI: 10.1038/35021000.

Penman, D. E., B. Hönisch, E. T. Rasbury, N. G. Hemming, and H. J. Spero (2013). "Boron, carbon, and oxygen isotopic composition of brachiopod shells: Intra-shell variability, controls, and potential as a paleo-pH recorder". *Chemical Geology* 340, pp. 32–39. DOI: 10.1016/j.chemgeo.2012.11.016.

Percival, L., A. S. Cohen, M. K. Davies, A. J. Dickson, S. P. Hesselbo, H. C. Jenkyns, M. J. Leng, T. A. Mather, M. S. Storm, and W. Xu (2016). "Osmium isotope evidence for two pulses of increased continental weathering linked to Early Jurassic volcanism and climate change". *Geology* 44.9, pp. 759–762. DOI: 10.1130/G37997.1.

Percival, L., M. Witt, T. A. Mather, M. Hermoso, H. C. Jenkyns, S. P. Hesselbo, A. H. Al-Suwaidi, M. S. Storm, W. Xu, and M. Ruhl (2015). "Globally enhanced mercury deposition during the end-Pliensbachian extinction and Toarcian OAE: A link to the Karoo–Ferrar Large Igneous Province". *Earth and Planetary Science Letters* 428, pp. 267–280. DOI: 10.1016/j.epsl.2015.06.064.

Peters, G. P., G. Marland, C. Le Quéré, T. Boden, J. G. Canadell, and M. R. Raupach (2012). "Rapid growth in CO2 emissions after the 2008–2009 global financial crisis". *Nature Climate Change* 2.1, pp. 2–4. DOI: 10.1038/nclimate1332.

Piazza, V., L. V. Duarte, J. Renaudie, and M. Aberhan (2019). "Reductions in body size of benthic macroinvertebrates as a precursor of the early Toarcian (Early Jurassic) extinction event in the Lusitanian Basin, Portugal". *Paleobiology* 45.02, pp. 296–316. DOI: 10.1017/pab.2019.11.

Piazza, V., C. V. Ullmann, and M. Aberhan (2020). "Temperature-related body size change of marine benthic macroinvertebrates across the Early Toarcian Anoxic Event". *Scientific Reports* 10.4675, pp. 1–13. DOI: 10.1038/s41598-020-61393-5.

Pistiner, J. S. and G. M. Henderson (2003). "Lithium-isotope fractionation during continental weathering processes". *Earth and Planetary Science Letters* 214.1-2, pp. 327–339. DOI: 10.1016/S0012-821X(03)00348-0.

Pittet, B., G. Suan, F. Lenoir, L. V. Duarte, and E. Mattioli (2014). "Carbon isotope evidence for sedimentary discontinuities in the lower Toarcian of the Lusitanian Basin (Portugal): Sea level change at the onset of the Oceanic Anoxic Event". *Sedimentary Geology* 303, pp. 1–14. DOI: 10.1016/j.sedgeo.2014.01.001.

Pogge von Strandmann, P. A. E., K. W. Burton, R. H. James, P. van Calsteren, and S. R. Gislason (2010). "Assessing the role of climate on uranium and lithium isotope behaviour in rivers draining a basaltic terrain". *Chemical Geology* 270.1-4, pp. 227–239. DOI: 10.1016/j.chemgeo.2009.12.002.

Pogge von Strandmann, P. A. E., H. C. Jenkyns, and R. G. Woodfine (2013). "Lithium isotope evidence for enhanced weathering during Oceanic Anoxic Event 2". *Nature Geoscience* 6.8, pp. 668–672. DOI: 10.1038/NGEO1875.

Pogge von Strandmann, P. A., K. W. Burton, R. H. James, P. van Calsteren, S. R. Gíslason, and F. Mokadem (2006). "Riverine behaviour of uranium and lithium isotopes in an actively glaciated basaltic terrain". *Earth and Planetary Science Letters* 251.1-2, pp. 134–147. DOI: 10.1016/j.epsl.2006.09.001.

Pogge von Strandmann, P. A., W. T. Fraser, S. J. Hammond, G. Tarbuck, I. G. Wood, E. H. Oelkers, and M. J. Murphy (2019). "Experimental determination of Li isotope behaviour during basalt weathering". *Chemical Geology*. DOI: 10.1016/j.chemgeo.2019.04.020.

Pörtner, H. O., M. Langenbuch, and B. Michaelidis (2005). "Synergistic effects of temperature extremes, hypoxia, and increases in CO 2 on marine animals: From Earth history to global change". *Journal of Geophysical Research* 110.C9. DOI: 10.1029/2004JC002561.

Rae, J. W., G. L. Foster, D. N. Schmidt, and T. Elliott (2011). "Boron isotopes and B/Ca in benthic foraminifera: Proxies for the deep ocean carbonate system". *Earth and Planetary Science Letters* 302.3-4, pp. 403–413. DOI: 10.1016/j.epsl.2010.12.034.

Rampino, M. R. and R. B. Stothers (1988). "Flood basalt volcanism during the past 250 million years". *Science (New York, N.Y.)* 241.4866, pp. 663–668. DOI: 10.1126/science.241.4866.663.

Rasmussen, E. S., S. Lomholt, C. Andersen, and O. V. Vejbæk (1998). "Aspects of the structural evolution of the Lusitanian Basin in Portugal and the shelf and slope area offshore Portugal". *Tectonophysics* 300.1-4, pp. 199–225. DOI: 10.1016/S0040-1951(98)00241-8.

Raymo, M. E. and W. F. Ruddiman (1992). "Tectonic forcing of late Cenozoic climate". *Nature* 359.6391, pp. 117–122. DOI: 10.1038/359117a0.

Reolid, M., M. Emanuela, L. M. Nieto, and F. J. Rodríguez-Tovar (2014). "The Early Toarcian Oceanic Anoxic Event in the External Subbetic (Southiberian Palaeomargin, Westernmost Tethys): Geochemistry, nannofossils and ichnology". *Palaeogeography, Palaeoclimatology, Palaeoecology* 411, pp. 79–94. DOI: 10.1016/j.palaeo.2014.06.023.

Röhl, H.-J., A. Schmid-Röhl, W. Oschmann, A. Frimmel, and L. Schwark (2001). "The Posidonia Shale (Lower Toarcian) of SW-Germany: An oxygen-depleted ecosystem controlled by sea level and palaeoclimate". *Palaeogeography, Palaeoclimatology, Palaeoecology* 165.1-2, pp. 27–52. DOI: 10.1016/S0031-0182(00)00152-8.

Rollion-Bard, C., N. Vigier, A. Meibom, D. Blamart, S. Reynaud, R. Rodolfo-Metalpa, S. Martin, and J.-P. Gattuso (2009). "Effect of environmental conditions and skeletal ultrastructure on the Li isotopic composition of scleractinian corals". *Earth and Planetary Science Letters* 286.1-2, pp. 63–70. DOI: 10.1016/j.epsl.2009.06.015.

Rosales, I., S. Quesada, and S. Robles (2004). "Paleotemperature variations of Early Jurassic seawater recorded in geochemical trends of belemnites from the Basque–Cantabrian basin, northern Spain". *Palaeogeography, Palaeoclimatology, Palaeoecology* 203.3-4, pp. 253–275. DOI: 10.1016/S0031-0182(03)00686-2.

Roy, R. N., L. N. Roy, M. Lawson, K. M. Vogel, C. Porter Moore, W. Davis, and F. J.

Millero (1993). "Thermodynamics of the dissociation of boric acid in seawater at S = 35 from 0 to 55°C". *Marine Chemistry* 44.2-4, pp. 243–248. DOI: 10.1016/0304-4203(93) 90206-4.

Rudnick, R. L. and S. Gao (2003). "Composition of the Continental Crust". *Treatise on Geochemistry*. Ed. by H. D. Holland and K. K. Turekian. Elsevier, pp. 1–64.

Ruebsam, W., T. Müller, J. Kovács, J. Pálfy, and L. Schwark (2018). "Environmental response to the early Toarcian carbon cycle and climate perturbations in the northeastern part of the West Tethys shelf". *Gondwana Research* 59, pp. 144–158. DOI: 10. 1016/j.gr.2018.03.013.

Sabine, C. L., R. A. Feely, N. Gruber, R. M. Key, K. Lee, J. L. Bullister, R. Wanninkhof, C. S. Wong, D. W. R. Wallace, B. Tilbrook, F. J. Millero, T.-H. Peng, A. Kozyr, T. Ono, and A. F. Rios (2004). "The oceanic sink for anthropogenic CO2". *Science (New York, N.Y.)* 305.5682, pp. 367–371. DOI: 10.1126/science.1097403.

Saenger, C. and Z. Wang (2014). "Magnesium isotope fractionation in biogenic and abiogenic carbonates: Implications for paleoenvironmental proxies". *Quaternary Science Reviews* 90, pp. 1–21. DOI: 10.1016/j.quascirev.2014.01.014.

Schauble, E. A. (2011). "First-principles estimates of equilibrium magnesium isotope fractionation in silicate, oxide, carbonate and hexaaquamagnesium^{2+} crystals". *Geochimica et Cosmochimica Acta* 75.3, pp. 844–869. DOI: 10.1016/j.gca.2010. 09.044.

Schwarcz, H. P., E. K. Agyei, and C. C. McMullen (1969). "Boron isotopic fractionation during clay adsorption from sea-water". *Earth and Planetary Science Letters* 6.1, pp. 1–5. DOI: 10.1016/0012-821X(69) 90084-3.

Seyfried, W. E., X. Chen, and L.-H. Chan (1998). "Trace Element Mobility and Lithium Isotope Exchange During Hydrothermal Alteration of Seafloor Weathered Basalt: An Experimental Study at 350C, 500 Bars". *Geochimica et Cosmochimica Acta* 62.6, pp. 949–960. DOI: 10.1016/S0016-7037(98)00045-3.

Silva, R. L., L. V. Duarte, and M. J. Comas-Rengifo (2015). "Facies and Carbon Isotope Chemostratigraphy of Lower Jurassic Carbonate Deposits, Lusitanian Basin (Portugal)". *Chemostratigraphy*. Elsevier, pp. 341–371. DOI: 10.1016/B978-0-12-419968-2.00013-3.

Spivack, A. J., M. R. Palmer, and J. M. Edmond (1987). "The sedimentary cycle of the boron isotopes". *Geochimica et Cosmochimica Acta* 51.7, pp. 1939–1949. DOI: 10.1016/0016-7037(87)90183-9.

Spivack, A. J., C.-F. You, and H. J. Smith (1993). "Foraminiferal boron isotope ratios as a proxy for surface ocean pH over the past 21 Myr". *Nature* 363.6425, pp. 149–151. DOI: 10.1038/363149a0.

Stoffynegli, P. and F. T. Mackenzie (1984). "Mass balance of dissolved lithium in the oceans". *Geochimica et Cosmochimica Acta* 48.4, pp. 859–872. DOI: 10.1016/0016-7037(84)90107-8.

Suan, G., E. Mattioli, B. Pittet, C. Lécuyer, B. Suchéras-Marx, L. V. Duarte, M. Philippe, L. Reggiani, and F. Martineau (2010). "Secular environmental precursors to Early Toarcian (Jurassic) extreme climate changes". *Earth and Planetary Science Letters* 290.3-4, pp. 448–458. DOI: 10.1016/j.epsl. 2009.12.047.

Suan, G., E. Mattioli, B. Pittet, S. Mailliot, and C. Lécuyer (2008). "Evidence for major environmental perturbation prior to and during the Toarcian (Early Jurassic) oceanic anoxic event from the Lusitanian Basin, Portugal". *Paleoceanography* 23.1. DOI: 10.1029/2007PA001459.

Suan, G., B. L. Nikitenko, M. A. Rogov, F. Baudin, J. E. Spangenberg, V. G. Knyazev, L. A. Glinskikh, A. A. Goryacheva, T. Adatte, J. B. Riding, K. B. Föllmi, B. Pittet, E. Mattioli, and C. Lécuyer (2011). "Polar record of Early Jurassic massive carbon injection". *Earth and Planetary Science Letters* 312.1-2, pp. 102–113. DOI: 10.1016/j. epsl.2011.09.050.

Svensen, H., F. Corfu, S. Polteau, Ø. Hammer, and S. Planke (2012). "Rapid magma emplacement in the Karoo Large Igneous Province". *Earth and Planetary Science Letters* 325-326, pp. 1–9. DOI: 10.1016/j. epsl.2012.01.015.

Svensen, H., S. Planke, L. Chevallier, A. Malthe-Sørenssen, F. Corfu, and B. Jamtveit (2007). "Hydrothermal venting of

greenhouse gases triggering Early Jurassic global warming". *Earth and Planetary Science Letters* 256.3-4, pp. 554–566. DOI: 10.1016/j.epsl.2007.02.013.

Teng, F.-Z., W.-Y. Li, S. Ke, B. Marty, N. Dauphas, S. Huang, F.-Y. Wu, and A. Pourmand (2010a). "Magnesium isotopic composition of the Earth and chondrites". *Geochimica et Cosmochimica Acta* 74.14, pp. 4150–4166. DOI: 10.1016/j.gca.2010.04.019.

Teng, F.-Z., W.-Y. Li, R. L. Rudnick, and L. R. Gardner (2010b). "Contrasting lithium and magnesium isotope fractionation during continental weathering". *Earth and Planetary Science Letters* 300.1-2, pp. 63–71. DOI: 10.1016/j.epsl.2010.09.036.

Tewksbury, J. J., R. B. Huey, and C. A. Deutsch (2008). "Ecology. Putting the heat on tropical animals". *Science* 320.5881, pp. 1296–1297. DOI: 10.1126/science.1159328.

Them, T. R., B. C. Gill, A. H. Caruthers, D. R. Gröcke, E. T. Tulsky, R. C. Martindale, T. P. Poulton, and P. L. Smith (2017). "High-resolution carbon isotope records of the Toarcian Oceanic Anoxic Event (Early Jurassic) from North America and implications for the global drivers of the Toarcian carbon cycle". *Earth and Planetary Science Letters* 459, pp. 118–126. DOI: 10.1016/j.epsl.2016.11.021.

Tipper, E. T., A. Galy, J. Gaillardet, M. Bickle, H. Elderfield, and E. Carder (2006). "The magnesium isotope budget of the modern ocean: Constraints from riverine magnesium isotope ratios". *Earth and Planetary Science Letters* 250.1-2, pp. 241–253. DOI: 10.1016/j.epsl.2006.07.037.

Tipper, E. T., J. Gaillardet, P. Louvat, F. Capmas, and A. F. White (2010). "Mg isotope constraints on soil pore-fluid chemistry: Evidence from Santa Cruz, California". *Geochimica et Cosmochimica Acta* 74.14, pp. 3883–3896. DOI: 10.1016/j.gca.2010.04.021.

Tomascak, P. B., C. H. Langmuir, P. J. Le Roux, and S. B. Shirey (2008). "Lithium isotopes in global mid-ocean ridge basalts". *Geochimica et Cosmochimica Acta* 72.6, pp. 1626–1637. DOI: 10.1016/j.gca.2007.12.021.

Trecalli, A., J. Spangenberg, T. Adatte, K. B. Föllmi, and M. Parente (2012). "Carbonate platform evidence of ocean acidification at the onset of the early Toarcian oceanic anoxic event". *Earth and Planetary Science Letters* 357-358, pp. 214–225. DOI: 10.1016/j.epsl.2012.09.043.

Uchikawa, J., D. E. Penman, J. C. Zachos, and R. E. Zeebe (2015). "Experimental evidence for kinetic effects on B/Ca in synthetic calcite: Implications for potential $B(OH)_4$ and $B(OH)_3$ incorporation". *Geochimica et Cosmochimica Acta* 150, pp. 171–191. DOI: 10.1016/j.gca.2014.11.022.

Ullmann, C. V., R. Boyle, L. V. Duarte, S. P. Hesselbo, S. A. Kasemann, T. Klein, T. M. Lenton, V. Piazza, and M. Aberhan (2020). "Warm afterglow from the Toarcian Oceanic Anoxic Event drives the success of deep-adapted brachiopods". *Scientific reports* 10.6549. DOI: 10.1038/s41598-020-63487-6.

Vengosh, A., Y. Kolodny, A. Starinsky, A. R. Chivas, and M. T. McCulloch (1991). "Coprecipitation and isotopic fractionation of boron in modern biogenic carbonates". *Geochimica et Cosmochimica Acta* 55.10, pp. 2901–2910. DOI: 10.1016/0016-7037(91)90455-E.

Verney-Carron, A., N. Vigier, and R. Millot (2011). "Experimental determination of the role of diffusion on Li isotope fractionation during basaltic glass weathering". *Geochimica et Cosmochimica Acta* 75.12, pp. 3452–3468. DOI: 10.1016/j.gca.2011.03.019.

Vicente, G. de, R. Vegas, A. Muñoz-Martín, J. D. van Wees, A. Casas-Sáinz, A. Sopeña, Y. Sánchez-Moya, A. Arche, J. López-Gómez, A. Olaiz, and J. Fernández-Lozano (2009). "Oblique strain partitioning and transpression on an inverted rift: The Castilian Branch of the Iberian Chain". *Tectonophysics* 470.3-4, pp. 224–242. DOI: 10.1016/j.tecto.2008.11.003.

Vigier, N., A. Decarreau, R. Millot, J. Carignan, S. Petit, and C. France-Lanord (2008). "Quantifying Li isotope fractionation during smectite formation and implications for the Li cycle". *Geochimica et Cosmochimica Acta* 72.3, pp. 780–792. DOI: 10.1016/j.gca.2007.11.011.

Waltham, D. and D. R. Gröcke (2006). "Non-uniqueness and interpretation of the sea-

water ^{87}Sr/^{86}Sr curve". *Geochimica et Cosmochimica Acta* 70.2, pp. 384–394. DOI: 10.1016/j.gca.2005.09.014.

Wang, W., T. Qin, C. Zhou, S. Huang, Z. Wu, and F. Huang (2017). "Concentration effect on equilibrium fractionation of Mg-Ca isotopes in carbonate minerals: Insights from first-principles calculations". *Geochimica et Cosmochimica Acta* 208, pp. 185–197. DOI: 10.1016/j.gca.2017.03.023.

Wang, W., C. Zhou, Y. Liu, Z. Wu, and F. Huang (2019). "Equilibrium Mg isotope fractionation among aqueous Mg^{2+}, carbonates, brucite and lizardite: Insights from first-principles molecular dynamics simulations". *Geochimica et Cosmochimica Acta* 250, pp. 117–129. DOI: 10.1016/j.gca.2019.01.042.

Wang, Z., P. Hu, G. Gaetani, C. Liu, C. Saenger, A. Cohen, and S. Hart (2013). "Experimental calibration of Mg isotope fractionation between aragonite and seawater". *Geochimica et Cosmochimica Acta* 102, pp. 113–123. DOI: 10.1016/j.gca.2012.10.022.

Wignall, P. B. and D. P. Bond (2008). "The end-Triassic and Early Jurassic mass extinction records in the British Isles". *Proceedings of the Geologists' Association* 119.1, pp. 73–84. DOI: 10.1016/S0016-7878(08)80259-3.

Williams, L. B. and R. L. Hervig (2005). "Lithium and boron isotopes in illite-smectite: The importance of crystal size". *Geochimica et Cosmochimica Acta* 69.24, pp. 5705–5716. DOI: 10.1016/j.gca.2005.08.005.

Wilson, R. C. L., R. N. Hiscott, M. G. Willis, and F. M. Gradstein (1989). "The Lusitanian Basin of west-central Portugal: Mesozoic and Tertiary tectonic, stratigraphic and subsidence history". *Extensional Tectonics and Stratigraphy of the North Atlantic Margins AAPG Memoir*. Ed. by Tankard, A. J., Balkwill, H. R., pp. 341–361.

Wimpenny, J., C. A. Colla, P. Yu, Q.-z. Yin, J. R. Rustad, and W. H. Casey (2015). "Lithium isotope fractionation during uptake by gibbsite". *Geochimica et Cosmochimica Acta* 168, pp. 133–150. DOI: 10.1016/j.gca.2015.07.011.

Wimpenny, J., R. H. James, K. W. Burton, A. Gannoun, F. Mokadem, and S. R. Gíslason (2010). "Glacial effects on weathering processes: New insights from the elemental and lithium isotopic composition of West Greenland rivers". *Earth and Planetary Science Letters* 290.3-4, pp. 427–437. DOI: 10.1016/j.epsl.2009.12.042.

Wimpenny, J., Q.-z. Yin, D. Tollstrup, L.-W. Xie, and J. Sun (2014). "Using Mg isotope ratios to trace Cenozoic weathering changes: A case study from the Chinese Loess Plateau". *Chemical Geology* 376, pp. 31–43. DOI: 10.1016/j.chemgeo.2014.03.008.

Wolf-Gladrow, D. A., U. F. L. Riebesell, S. Burkhardt, and J. Bijma (1999). "Direct effects of CO_2 concentration on growth and isotopic composition of marine plankton". *Tellus B* 51.2, pp. 461–476. DOI: 10.1034/j.1600-0889.1999.00023.x.

Wright, S. J., H. C. Muller-Landau, and J. Schipper (2009). "The future of tropical species on a warmer planet". *Conservation biology : the journal of the Society for Conservation Biology* 23.6, pp. 1418–1426. DOI: 10.1111/j.1523-1739.2009.01337.x.

Wunder, B., F. Deschamps, A. Watenphul, S. Guillot, A. Meixner, R. L. Romer, and R. Wirth (2010). "The effect of chrysotile nanotubes on the serpentine-fluid Li-isotopic fractionation". *Contributions to Mineralogy and Petrology* 159.6, pp. 781–790. DOI: 10.1007/s00410-009-0454-x.

Wunder, B., A. Meixner, R. L. Romer, A. Feenstra, G. Schettler, and W. Heinrich (2007). "Lithium isotope fractionation between Li-bearing staurolite, Li-mica and aqueous fluids: An experimental study". *Chemical Geology* 238.3-4, pp. 277–290. DOI: 10.1016/j.chemgeo.2006.12.001.

Wunder, B., A. Meixner, R. L. Romer, and W. Heinrich (2006). "Temperature-dependent isotopic fractionation of lithium between clinopyroxene and high-pressure hydrous fluids". *Contributions to Mineralogy and Petrology* 151.1, pp. 112–120. DOI: 10.1007/s00410-005-0049-0.

Xiao, J., Z. d. Jin, Y. k. Xiao, and M. y. He (2014). "Controlling factors of the δ^{11}B-pH proxy and its research direction". *Environmental Earth Sciences* 71.4, pp. 1641–1650. DOI: 10.1007/s12665-013-2568-8.

Xiao, J., Y. k. Xiao, Z. d. Jin, M. y. He, and C. q. Liu (2013). "Boron isotope varia-

tions and its geochemical application in nature". *Australian Journal of Earth Sciences* 60.4, pp. 431–447. DOI: 10.1080/08120099.2013.813585.

Xu, W., M. Ruhl, H. C. Jenkyns, S. P. Hesselbo, J. B. Riding, D. Selby, B. D. A. Naafs, J. W. H. Weijers, R. D. Pancost, E. W. Tegelaar, and E. F. Idiz (2017). "Carbon sequestration in an expanded lake system during the Toarcian oceanic anoxic event". *Nature Geoscience* 10.2, pp. 129–134. DOI: 10.1038/ngeo2871.

Zeebe, R. E. (2005). "Stable boron isotope fractionation between dissolved $B(OH)_3$ and $B(OH)_4$". *Geochimica et Cosmochimica Acta* 69.11, pp. 2753–2766. DOI: 10.1016/j.gca.2004.12.011.

Chapter 2

Materials, Methods and Sample Preservation

Manuscript in preparation as supplementary materials to manuscripts from chapter 3 and 4

Contributions to this manuscript:

I, Tina Klein, the first author of this manuscript, have contributed to this manuscript (supplementary material) the following:

- Sample collection at both sections R/FC and BdC together with researchers from our research group TERSANE (DFG, FOR 2332) and Friedrich Lucassen from my working group

- Sample preparation of all micritic carbonates (as described in section 2.3)

- Development of an age model for the Pliensbachian at the section BdC

- All isotope analyses (Sr, B, Mg, Li) that are stated in this thesis have been prepared and conducted by myself

- Development and refinement of leaching procedures for each isotope system on micritic carbonates together with my supervisors and co-authors Anette Meixner and Prof. Simone Kasemann

- Preparation and conduction of cathodoluminescence images on micritic carbonates

- Preparation of micritic carbonates for SEM images (I attended the measurements that have been performed by the SEM operator in the working group petrology of the ocean crust, FB5, University of Bremen)

- Preparation of micritic carbonates for XRD measurements (measurements have been conducted by the central laboratory for crystallography and applied material sciences at the University of Bremen)

- Interpretation of the sample condition, together with my supervisors and co-authors (see section 2.7)

- The preparation of the fossil material (extraction of convenient shell parts) was conducted by C.V. Ullmann (co-author)

- Preparation of this manuscript/ supplementary material

2. Materials, Methods and Sample Preservation

2.1. Sample collection

Marine carbonates and biogenic material from shallow water environments were collected from two different locations in the western Tethys — in Rabaçal/Fonte Coberta (Portugal; 40°03'08.0"N 8°27'30.5"W) representing the Lusitanian Basin and Barranco de la Cañada (Spain; 40°23'53.4"N 1°30'07.4"W) for the Iberian Basin (see section 1.4). Both sections are about 600 km located apart from each other. For this study 20 carbonate samples and 5 brachiopod samples for the Lusitanian Basin as well as 25 carbonate samples, 33 brachiopod, and 24 bivalve samples for the Iberian Basin were collected. The fossiliferous material (brachiopods and bivalves) was collected in collaboration with palaeontologists from our research group TERSANE (DFG, FOR 2332) and their preservation evaluation, as well as oxygen and carbon isotopes, are published in Ullmann et al., 2020. Sampling intervals amount to 0.1–11 m covering the upper Pliensbachian from the *margaritatus* AZ up to the middle Toarcian *bifrons* AZ, comprising the Pl–To boundary and the T-OAE crisis interval.

2.2. Age model

The age model for this study is based on the latest findings on the biozonations published by Comas-Rengifo et al., 2013, Correia et al., 2018, and Ferreira et al., 2015 for Rabaçal/Fonte Coberta, and for the Barranco de la Cañada section by Gahr, 2002, 2005, as well as observations in the field. The absolute ages for the ammonite zones (AZ) are defined by the Geological Time Scale 2016 (Ogg et al., 2016) and given in Fig. 4. The lower boundary of the *spinatum* AZ for BdC is based on Sr isotopes generated for this study and calibrated on the $^{87}Sr/^{86}Sr$ seawater curve from McArthur et al., 2000. The age model was established with the assumption that sedimentation rates were constant throughout the studied interval.

2.3. Sample preparation

Based on visual and optical examinations micritic carbonate samples were preselected for further analyses. Every sample with a micritic matrix and no obvious secondary alteration signs, such as colour changes, lack of structural cohesion or powdery appearance, were selected. For this study, 20 micritic samples for the Lusitanian and 25 samples from the Iberian Basin were chosen for further diagenetic screening. Five badly preserved carbonate samples from the Obón section (Spain; 40°54'59.3"N 0°43'19.9"W; described by Val et al., 2017) were picked for a comparative study.

The micritic carbonates were cut into thin slices with a diamond saw (research group petrology

of the ocean crust, University of Bremen). Ongoing, each slice was examined under a binocular microscope and carefully broken into small pieces with a preparation needle. During this sampling it was crucial to ensure to only pick the pristine micritic matrix, avoiding any fossils, veins, late stage secondary alteration or dolomitization, fractures, pervasive recrystallization, any spar or microspar, as well as areas where original sedimentary features (e.g. burrow traces, finely detailed sedimentary lamination) were preserved. Subsequently, the chips were manually pestled with an agate mortar, while it was crucial to grind them not too finely to avert reaming any clay minerals. The powdered sample material was used for any further trace element and isotope analyses.

Although great care was taken during the sampling, it was not possible for all carbonate samples to only sample the matrix. For several samples the shell material was so densly packed that a sampling around it was impossible. The shell material included in the sampling for the Barranco de la Cañada section comprised mostly of shell material, a sampling of other fragments was still especially avoided. The affected micritic carbonate samples are declared as "mixed samples" in Table 6 in the appendix.

For SEM and CL imaging small pieces of the carbonate were chipped from each sample and embedded in epoxy resin (EpoxyCure Epoxy Resin 20-8130-032 by Buehler). Next, they were lapped with siliciumcarbid cloths starting with a grain size of 400 going down to 5000 µm. Then the epoxy mounts were polished with aluminium oxide emulsion down to a grain size of 0.05 µm. Both steps were conducted in the processing labs of University of Bremen (Geo building, research group geodynamics of the polar regions).

2.3.1. Fossil preparation

For all fossil shells the surface was cleaned from sediments and altered rinds and for brachiopods calcite of the primary shell layer was removed if present using a preparation needle, scalpel or hand-held drill with diamond coated drill bit. For most fossil samples, shell material was extracted as sheaths of multiple shell layers with a preparation needle. Where this was not possible due to the dense nature of the material (mostly for Gryphaea), samples were taken with a scalpel or hand-held drill using a diamond coated drill bit of approx. 1 mm diameter. Sample sizes ranged from 0.9 to 14 mg (typically 1–3 mg) for fossils.

2.4. Sample purification for isotope analyses

In total 20 well preserved micritic carbonate rock samples covering the upper Pliensbachian to the middle Toarcian were picked for the Lusitanian and Iberian Basin, respectively, for further boron (B), lithium (Li), strontium (Sr) and magnesium (Mg) isotope analyses. Additionally, 22 brachiopod and 13 bivalve shell materials from the Iberian range section were analysed for their B isotope ratios, as well as 33 brachiopods for their Sr isotope composition. For the Lusitanian Basin 5 brachiopod samples were analysed for their $\delta^{11}B$ composition.

All sample preparations for isotope analyses were conducted in the Isotope Geochemistry Clean Laboratory at MARUM — Center for Marine Environmental Sciences, University of Bremen, Germany. This section describes the sample purification techniques applied in this study, which is performed right after each dissolution method described in section 2.6. For each isotope system a distinct ion exchange chromatography procedure was applied to separate the aiming isotopes from their sample matrix. The same procedures were conducted for the micrites and fossil shell material.

2.4.1. Strontium isotopes

The chromatographic Sr procedure is modified after Pin and Bassin, 1992 and shown in detail in Appendix C, Figure 22. Previously, dissolved sample powder (procedure described in section 2.6.3) containing 300 ng Sr for one measurement were dried and redissolved in 2 M HNO_3. Subsequently, $\sim$70 µl of Triskem Sr spec resin (mesh size 50–100 µm) were loaded on the columns and first washed with ultrapure water (Milli-Q) and 2 M HNO_3. In a next step the sample material was added in 100 µl steps. Unwanted elements were removed from the resin by washing the resin with in total 1200 µl 2 M HNO_3. The eluate was disposed and the Sr fraction was collected by rinsing the column with 200 µl 0.05 M HNO_3. Before drying the Sr fraction at 80–100°C two drops of 0.1 M H_3PO_4 were added. After drying two steps were applied to remove any potential organic matter from the Sr fraction: first, 70 µl of concentrated HNO_3 (65 %) were added and the sample dried at 80–100°C, and secondly it was treated with 40 µl of H_2O_2 and dried at 100°C. Finally, the columns were cleaned and the resin discarded.

2.4.2. Boron isotopes

The B purification of micritic carbonates and fossil shell materials was performed with a cation exchange in PP BIORAD Bio-Spin columns with 1 ml of BIORAD resin AG 50WX8 (200–400 mesh size). The procedure is described in detail in Appendix C, Figure 23. For this separation a specific distilled HCl ($< 70\,^{\circ}C$) was used to ensure that the B contamination was kept as low as possible. For B separations it is also important to add mannitol to the sample solution to prevent any B loss during the evaporation process (1 µg B : 40 µg mannitol) (Nakamura et al., 1992).

The powdered sample material was digested as described in section 2.6.4 and for the separation again dissolved in 0.02 M HCl. Each sequence consists of 14 columns from which 11 were available for sample material, while the remaining three columns were loaded each with two standard materials (NIST SRM 951 and bottom seawater from SuSu Knolls) and one procedual blank in order to validate the separation procedure. The resin was cleaned with 6.2 M HCl and subsequently conditioned with 0.02 M HCl. From now Savillex beakers were placed under the columns to collect the main B fraction. The sample solution was placed on the resin and eluted by various steps with 0.02 M HCl. The "tail" fraction was collected after the main fraction to check for any B loss by adding 2 ml 0.02 M HCl. Evaporation of the main and tail fractions was done below 67 °C. During this step it was crucial to prevent the sample from falling dry for too long as this might lead to loss of B. After drying the samples were thus also immediately dissolved in 2 % HNO_3 as a preparation for the concentration check on the MC-ICP-MS and the subsequent measurement. For B loss determinations the tail fractions were dissolved in 0.5 ml 2 % HNO_3.

2.4.3. Lithium isotopes

Li isotopes were separated from their matrix using the two-step column separation procedure modified after Moriguti and Nakamura, 1998. The first separation was conducted with PP-BIORAD columns loaded with 1.4 ml BIORAD resin AG 50WX8 (200–400 mesh size; volume in 6 N HCl), and for the second separation the same resin was used, but only 1 ml contained in PE-BIORAD Bio-spin columns. For each sequence 14 columns were available, from which 3 were blocked for standards (L-SVEC/ NIST SRM 8485 and in-house standard bottom seawater from SuSu Knolls) plus a procedural blank. Li isotopes fractionate during the ion exchange chromatography and thus the "head" and "tail" fractions (fractions before and after the Li main fraction, respectively) were collected and checked for Li loss.

The powdered sample material was dissolved as described in section 2.6.5 and redissolved for the first Li separation in 2 ml 0.15 M HCl (detailed procedure description in Appendix C, Figure 24). After precleaning and conditioning the columns, the sample solution was loaded on the resin and the head fraction was collected with the following 2 ml of 0.15 M HCl. Following, the Li main fraction was sampled by eluting the resin with in total 28 ml of 0.15 M HCl and the tail fraction was collected with the subsequent 2 ml. All fractions were evaporated at 90 °C. After drying the sample was redissolved in 1 ml 0.15 M HCl for the second separation procedure. Differing from the first Li separation the collection of the head, main and tail Li fraction is done with 0.5 M HCl in 50 % ethanol. During each elution step with this acid it was crucial to load the resin continuously after each liquid passed the column to ensure the continuity of the molarity. Evaporation of each Li fraction was done as during the first Li separation. After drying, all Li fractions were dissolved in 2 % HNO_3. Head and tail fractions were checked for Li loss during the separation and the main

fraction was analysed for its Li concentration for the subsequent measurement on MC-ICP-MS. Here it was also important to check the sodium (Na) concentration (should range below 1 V), as this element would interfere with the Li isotopes during the measurement.

2.4.4. Magnesium isotopes

Isotopes of the element Mg were extracted from the sample matrix through ion exchange chromatography with PE BIORAD Bio-spin columns filled with BIORAD resin AG50WX8 (200–400 mesh size) after the method from Strelow, 1960; Strelow et al., 1965. The steps taken during the separation are listed in Appendix C, Figure 26. Similar to the B and Li separation, the Mg sequence also has 14 available columns from which 3 are blocked for two standards (in-house standard bottom seawater SuSu Knolls and GSJ-JCp-1) and one for a procedural blank. According to the Li procedure here the "head" and "tail" fractions were checked for any Mg loss during the separation.

As a first step for the Mg separation every already clean Savillex-beaker to be used is again pre-cleaned over night with 1 ml at 120 °C on the hotplate with closed lids to keep the contamination as minimal as possible. Further, the sample material is redissolved in 0.5 ml 0.8 M HCl, after being digested as described in section 2.6.6. After the cleaning and conditioning steps of the columns the sample is loaded on the resin, while already collecting for the head fraction. The rest of the head fraction is eluted with in total 8.5 ml 0.8 M HCl. The main Mg fraction is eluted with 13 x 1 ml 0.8 M HCl, while the tail fraction is sampled with 2 ml of the same acid. All fraction solutions were evaporated at 90 °C. If there was no visible residue, any organic material was removed by adding 15 µl of H_2O_2 in the hot beaker and dried at 90 °C. When all fractions dried off they were redissolved in 2 % HNO_3, head an tail fractions were checked for Mg loss. Main fractions were analysed for their Mg concentrations as well as any calcium and sodium impurities due to interferences of these elements during measurement.

2.5. Analytical methods

2.5.1. Optical and element concentration analyses

Secondary Electron Microscopy (SEM) images (backscatter and secondary electron images as well as element mappings) were taken with a field emission electron microscope SUPRA 40 (Zeiss) coupled with an EDX detector XFlash 6|30 (Bruker). Cathodoluminescence (CL) images were taken with the same epoxy mounts as for the SEM images. The CL equipment used was the Technosyn Cold Cathode Luminescence Model 8200 Mk II, both CL and SEM devices are located within the research group petrology of the ocean crust, Department of Geosciences, University of Bremen. Additional SEM images were taken with a Tescan Vega 3 XMU coupled with an Oxford EDX detector at the Zentrum für Marine Tropenforschung (ZMT, Geolaboratory, Bremen, Germany).

In a first try for trace element measurements, 40 mg of the powdered sample were dissolved in 1 ml of 0.5 M HCl. 1 ml of this aliquot was extracted and diluted with 2 ml 0.5 M HCl and passed for trace element analysis with ICP-OES. The results made clear that during the dissolution process of the samples also the detritial fraction was affected, thus not representing solely the trace element concentrations of the matrix. For this reason, the method for preparing the samples for trace element analyses were adjusted, so that the carbonate was leached with 0.1 M HCl dissolving only 25 % instead of 100 % of the carbonate fraction. Accordingly, 100 mg of the sample material were leached for 2 hours in 5 ml of 0.1 M HCl. 4 ml of the aliquot were extracted and mannitol was added for the boron fraction (see section 2.6.4). The samples were dried $< 70°C$ and afterwards 3 ml of 0.5 M HCl were added and analysed again for their trace element concentrations. High purity certified multi element standards were used for element-specific instrumental calibration. Results of the trace element measurements can be found in the Appendix B. Each trace element analyses were conducted with ICP-OES, for the samples from R/FC at the inorganic geochemistry laboratory, University of Bremen with an Agilant 720 and the majority of the BdC samples were analysed at the Alfred-Wegener Insitute (AWI, Bremerhaven, Germany). Measurements for R/FC have a 2rsd of 3% determined through 3 times repeated measurements of two international standard materials during the sequence. For BdC repeated measurements of a standard solution during the sequence also yielded a 2rsd of 3%. Li and B trace element concentrations for BdC were measured with ICP-MS (Neptune Plus, Thermo Fisher) and repeated measurements of the international standards NIST 8545 and NIST 951 over the period of 3 years yielded a 2rsd of 4% for Li (n=36) and 9% for B (n=108), respectively.

Half-quantitative x-ray diffraction pattern analyses were performed with an X'Pert Pro multipurpose diffractometer in the Department of Geosciences, University of Bremen (Central Laboratory

for Crystallography and Applied Material Sciences, ZEKAM). The XRD analysis results are listed in Table 1.

2.5.2. Isotope analyses

Most isotope ratios reported in this study are given in δ-notation (‰) relative to their certified international reference materials. The δ-notation is universally described for each element X as follows:

$$\delta^a\mathrm{X} = \left(\frac{\left(\frac{^a\mathrm{X}}{^b\mathrm{X}}\right)_{sample}}{\left(\frac{^a\mathrm{X}}{^b\mathrm{X}}\right)_{standard}} - 1 \right) * 1000 \tag{3}$$

with a and b being the isotopes of the element.

Boron (B), lithium (Li) , strontium (Sr) and magnesium (Mg) isotope ratios were determined in the Isotope Geochemistry laboratory at MARUM - Center for Marine Environmental Sciences (University of Bremen, Germany). Dissolution methods and sample purification procedures for each isotope system are described in section 2.6.

Carbon and Oxygen Isotopes

Carbon and oxygen isotopes were analysed with a Thermo Finnigan MAT 252 gas isotope mass spectrometer with Kiel III automated carbonate preparation at MARUM, University of Bremen, Germany. Results are given in Appendix A and Fig. 7 relative to the Vienna Peedee Belemnite (VPDB) standard. The analytical reproducibility of δ^{13}C and δ^{18}O of the house standard (Solnhofer limestone) are better than $\pm$ 0.04‰ and $\pm$ 0.05‰ (2sd) for each respectively.

Strontium Isotopes

Sr isotope measurements were performed using a ThermoFisher Scientific Triton Plus thermal ionization mass spectrometer (TIMS) in the dynamic multicollection mode. The purified Sr fraction was dissolved in 0.1 M H_3PO_4 and loaded on a single degassed rhenium filament, which was previously covered with a tantalum emitter. The instrumental precision was controlled with the replicate analyses of the international standard NIST SRM 987, which yielded a ^{87}Sr/^{86}Sr mean value of 0.710250 $\pm$ 0.000011 (2sd, n=13) over a period of 3 years and is in accordance with published values (0.710238 $\pm$ 0.000008, Brand, 2004; 0.71024 $\pm$ 0.002%, Gruber et al., 2019). The long term external reproducibility of our laboratory is $\pm$ 0.000015 (2sd). The instrumental mass fractionation was corrected using ^{88}Sr/^{86}Sr = 8.375.

Boron, Lithium and Magnesium Isotopes

B, Li and Mg isotopes were analysed with a ThermoFisher Scientific Neptune Plus Multicollector-inductively coupled plasma-mass spectrometer (MC-ICP-MS) using a stable introduction system (SIS) and a high-efficiency x-cone. All isotope ratios were measured using the standard-sample-bracketing method with the respective international reference materials NIST SRM 951, NIST SRM 8545 (L-SVEC) and a Mg ICP Standard (Alfa Aesar Magnesium plasma standard solution, Specpure) as the bracketing standard. Each sample was analysed at least three times in blocks and 2% HNO_3 was used for baseline corrections and at a time measured before and after each standard and sample. Isotope ratios are reported in per mill (‰) with the delta notation relative to the certified reference materials (see equation 5). To control and verify the chemical purification and dissolution procedures in this study, each series contained an international reference material which underwent the same separation and dissolution methods as the sample materials.

B isotope ratios $^{11}B/^{10}B$ were concurrently analysed on the Faraday cups L3 and H3 with typical ^{11}B intensities of the standard NIST SRM 951 (100 ppb) of around $1.5\,V$ and baseline intensities around $7\,mV$. Procedural blanks were mostly below 1% (two sequences ranged between $2–7\%$) and thus not affecting the sample composition. The leakage of B during the purification was below 0.2%. $\delta^{11}B$ of the NIST 951 reference material was -0.1 ± 0.1 ‰ (2se, n=37; over a period of 3 years), the long-term reproducibility 2sd of the laboratory is ± 0.5 ‰. Repeated measurements of the in-house standard bottom seawater from SuSu Knolls (BSW) yielded $\delta^{11}B$ vaules of 39.7 ± 0.4 ‰ (2sd, n=28), which are in agreement with published data (39.61 ± 0.04 ‰; Foster et al., 2010). For verifying the precision and accuracy of the method the certified standards GSJ-JCt-1 and GSJ-JCp-1 were also analysed. Average $\delta^{11}B$ values for JCt-1 are 16.3 ± 0.2 ‰ (2sd, n=2) and JCp-1 24.5 ± 0.1 ‰ (2sd, n=1), which are both according to published values (e.g. Farmer et al., 2016; Foster et al., 2013; Wang et al., 2010).

The Li isotopes ^{6}Li and ^{7}Li were simultaneously measured on the Faraday cups L4 and H4. Intensities for ^{7}Li in the bracketing standard (25 ppb) were typically around $1.5\,V$ and baseline intensities in average around $11\,mV$. Li loss during the separation was less than 0.01% and procedural blanks were below 0.01% and thus not affecting the sample isotopic composition. The reproducibility of NIST SRM 8545 for the three years of this project was $\delta^{7}Li = -0.1 \pm 0.3$ ‰ (2sd, n=14), whereas the long-term reproducibility 2sd of the laboratory is ± 0.5 ‰. To control the accuracy and precision of the method the in-house standard bottom seawater from SuSu Knolls (BSW) was also repeatedly measured and yielded a value of $\delta^{7}Li = 30.5 \pm 0.4$ ‰ (2sd, n=7), which is within analytical uncertainty in agreement with published literature values (31.1 ± 0.3 ‰ (2sd); see e.g. Huang et al., 2010; Pogge von Strandmann et al., 2019a; Wimpenny et al., 2010).

Differing from B and Li isotope ratios, Mg isotopes are reported relative to the international reference material DSM-3 and not the bracketing standard. The conversion from the Mg delta ICP Standard values to those equivalent on the DSM-3 scale is expressed as follows (Young and Galy, 2004):

$$\delta^x \mathrm{Mg}^{\mathrm{sample}}_{\mathrm{DSM3}} = \delta^x \mathrm{Mg}^{\mathrm{sample}}_{\mathrm{MgICP}} + \delta^x \mathrm{Mg}^{\mathrm{MgICP}}_{\mathrm{DSM3}} + 0.001 * \delta^x \mathrm{Mg}^{\mathrm{sample}}_{\mathrm{MgICP}} * \delta^x \mathrm{Mg}^{\mathrm{MgICP}}_{\mathrm{DSM3}} \tag{4}$$

with x referring to either to the isotope 25 or 26. To control each single Mg measurement sequence the international reference materials DSM-3 and Cambridge-1 (Cam-1) were additionally analysed.

Mg isotopes with masses 24, 25 and 26 were each counted on the Faraday cups L3, center cup and H3. Typical intensities of the bracketing standard (200 ppb) on the mass $^{25}\mathrm{Mg}$ were ranging around $1.7\,\mathrm{V}$ with baseline intensities around $0.8\,\mathrm{mV}$. The instrumental precision is validated through the repeated measurement of the international reference materials Cam-I and DSM-3. Measured $\delta^{26}\mathrm{Mg}$ isotopes over the three years of this project yield Cam-I values in accordance to published data (-2.61 ± 0.06 ‰ (2sd, n=8); compare with -2.62 ± 0.04 ‰ from Pogge von Strandmann et al., 2011; Tipper et al., 2006; Tipper et al., 2010). For DSM-3 a precision of 0.03 ‰ was achieved with a $\delta^{26}\mathrm{Mg}$ of 0.00 ‰ (2sd, n=8), which is validated by published data (0.01 ± 0.14 ‰; Tipper et al., 2006). The external reproducibility was secured through repeated preparation and measurements of the in-house seawater standard (SuSu Knolls) that yielded a value of -0.85 ± 0.05 ‰ (2se, n=13) and GSJ-JCp-1 -2.00 ± 0.19 ‰ (2se, n=6), also in agreement with published values of -0.83 ± 0.09 ‰ (Foster et al., 2010; Ling et al., 2011), and -1.96 ± 0.05 ‰ (Teng, 2017), respectively. Also, procedural blanks confirmed that no contamination of the sample material occurred ($<0.1\,\%$) and Mg loss during the separation was also negligible ($<0.1\,\%$).

2.6. Leaching procedure development for isotope analyses

Clay minerals and other detritial components of the carbonate rock can contaminate the sample solution by detritial mineral dissolution. So far, the techniques applied by Ohnemueller et al., 2014 and Clarkson et al., 2015 avoided any detectable contamination by the detritial fraction. However, the carbonate rocks used in their studies contained less clay and detritus amounts, making it crucial to refine the digestion techniques for each isotopic system in this study. This section describes the leaching experiments undertaken for each isotope system to achieve the best true matrix isotopic results. The sample material worked with for the digestion experiments was the powdered micrite material from the Rabaçal/Fonte Coberta section.

If not stated otherwise, all sample preparation steps were conducted in the clean laboratories of the Isotope Geochemistry research group, MARUM at University of Bremen, Germany.

2.6.1. Fossil material

The well preserved brachiopod and bivalve shell material was prepared for the isotope chromatography through several steps. First, sufficient shell material was weighed out and subsequently cleaned thrice with ultrapure water and ethanol. Afterwards the shells were dissolved in sufficient volume of 1 M HCl and reacted for at most 24 h until the reaction ceased. In a final step the aliquot was centrifuged and pipetted for isotope column separation.

2.6.2. Determination of the detritial fraction

The mineralogical composition of the detritus was determined with X-Ray Diffraction pattern analysis (see section 2.5.1, for results Table 1). The majority of the detritial fraction comprises typical detritial minerals found in carbonates: quartz, biotite and to a minor content clay minerals. The mean clay mineral content in the carbonate rocks is 4 %.

To determine the weight percentage of the detritus 100 mg of powdered sample material was dissolved with 0.5 M HCl, so that the whole carbonate fraction was in solution. This fraction was removed and the residue washed with ultrapure water 3–5 times. Afterwards, the residue was evaporated at 90 °C in the drying oven and after cooling down weighted out. Results are noted in Appendix B, Table 6, 5.

2.6.3. Strontium isotopes

For the Sr digestion experiments 4 samples from the Rabaçal/Fonte Coberta section were chosen, each distinct in their content of detritus and stratigraphical position (pre-, post- and T-OAE crisis interval).

Sample	Calc	low-Mg calc	Qz	Msc/Biot	Chl Group	Serp Group	Kaolin Group	Amph	Spha	Orth	Py	Rut
P1	81		9	6					1			
P4	45	23	13	5	3					6	3	
P7	74		17	12		2				7		
P9	76		8	4		6		5				
P10	69	14	9	4		4						
P12	71	20	4	4		1						
P15	87		8	3			2					
P16	75		14	5	5							1
P17	72		11	4			9	4				
P18	79		13	6			3					

Table 1. Results of mineralogical composition derived from half quantitative analyses with XRD. Abbreviations stand for Calc – Calcite, Qz – Quartz, Msc/Biot – Muscovite/Biotite, Chl – Chlorite, Serp – Serpentine, Amph – Amphiboles, Spha – Sphalerite, Orth – Orthoclase, Py – Pyrite, Rut – Rutile

After weighing 50 mg for each digestion experiment from each sample, the powdered material was washed (only for batch 4 and 5, see Table 2). Therefore, ultrapure water was added to the sample ($\sim$5 ml) and left standing for 24 hours, while carefully pivoted repeatedly during the whole timespan. Afterwards, the water was removed and either discarded or prepared for Sr purification (section 2.4). Subsequently, the distinct acid for each dissolution experiment was added to the sample. When calculating the amount of the acid to dissolve the carbonate fraction the detritus had to be subtracted from the total volume. Every acid was reacted with the sample as long as it took with the help of an ultrasonic bath until the reaction ceased (which could take up to 4 hours).

Different dissolution methods were tested (see Table 2), partially according to methods found in literature. Some authors state that attacking detrital minerals, and thus nontarget minerals, by acid leaching poses a danger for the real $^{87}Sr/^{86}Sr$ of the matrix (e.g. Brand, 2004; DePaolo et al., 1983; McArthur et al., 1993a; Montañez et al., 1996; Ohde and Elderfield, 1992). Preleachings are advised to minimise the contamination of the detrital fraction (Bailey et al., 2000). However, Denison et al., 1994 and Brand, 2004 agreed that without preleaching only a content of more than 30 % of detritus impacts the matrix $^{87}Sr/^{86}Sr$.

To test the sequential dissolution method for whole rocks described by Bailey et al., 2000, we carried out different procedures of sequential leachings (batch 2–5, see Table 2) where different amounts of the carbonate were dissolved with varying acids and analysed for their Sr isotopic composition. Testing the influence of the detrital fraction on the matrix Sr signal was done with batch 1, but

could also be determined with all digestion runs. Run 1 was the very first try in leaching only 25 % of the carbonate fraction with a relatively weak acid. Run 2–6 include dissolution of the whole carbonate fraction with different molarities ranging from 0.5 M HCl to 2.5 M HCl. Ongoing, to determine the Sr isotopic composition of the detritus in run 6 two strong acids were mixed, after all of the carbonate fraction was removed and reacted for 24 h at room temperature.

Batch no.	Run no.	Acid	Carbonate dissolved (%)	Remarks
1	1	0.1 M HCl	25	
	2	0.5 M HCl	100	
	3	0.6 M HCl	100	
	4	1.0 M HCl	100	
	5	2.0 M HCl	100	
	6	2.5 M HCl	100	
	7	6 M HCl + 6 M HNO$_3$	/	on detritus (residue) of no. 4, reacted for 24 h at room temperature
2	8	0.5 M HCl	50	
	9	0.5 M HCl	30	on carbonate residue of no. 8
3	10	1.0 M HCl	50	
	11	1.0 M HCl	30	on carbonate residue of no. 10
4	12	/	/	water from washing fraction
	13	0.1 M HCl	40	
	14	0.5 M HCl	30	only on samples P1 & P7
	15	1.0 M HCl	30	only on samples P13 & P18
5	16	/	/	water from washing fraction
	17	1.0 M C$_2$H$_4$O$_2$	40	
	18	0.5 M HCl	30	only on samples P1 & P7
	19	1.0 M HCl	30	only on samples P13 & P18

Table 2. Summary of the different dissolution steps for digestion procedure development for Sr isotopes on micritic carbonate rocks
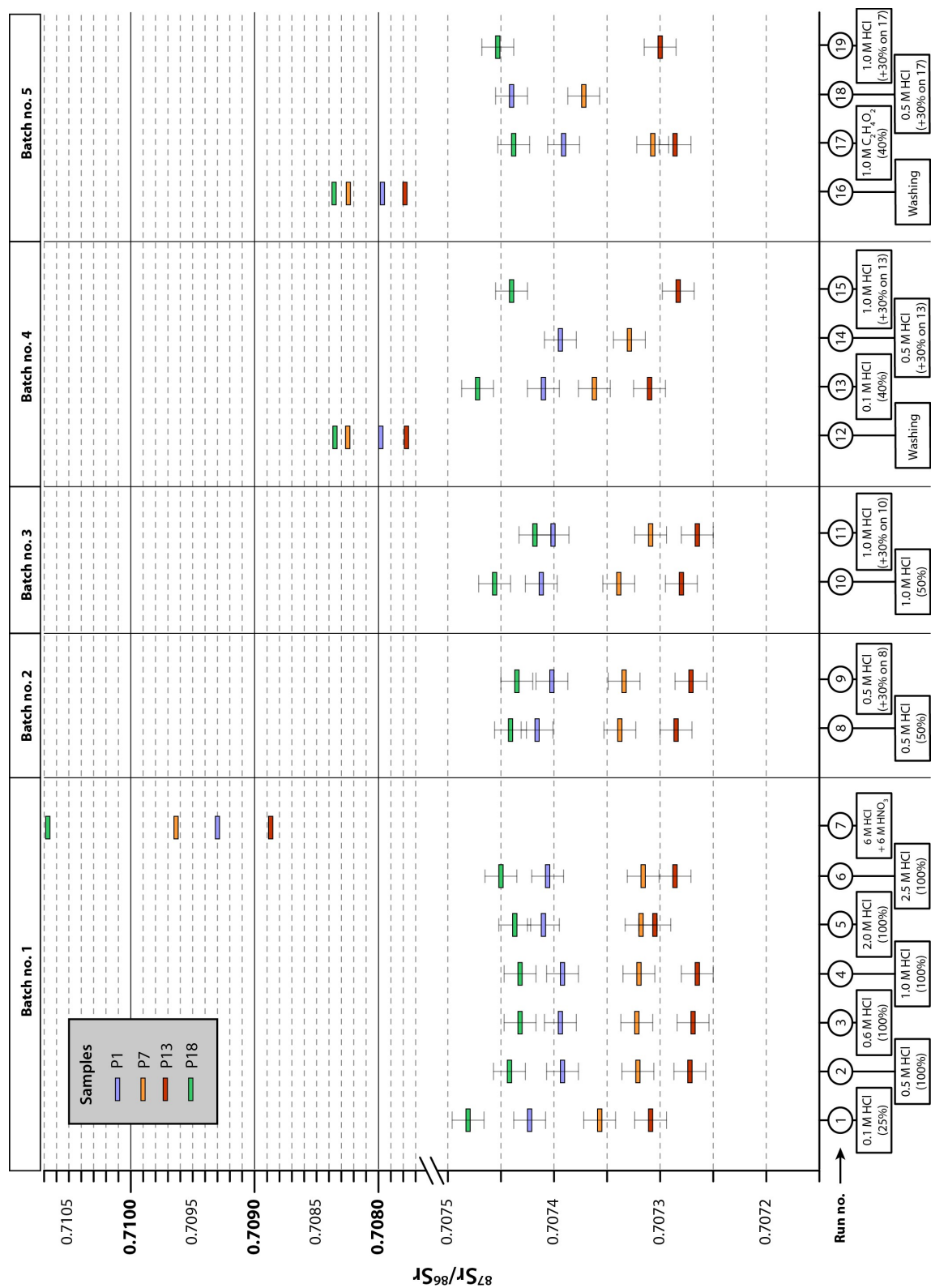
Figure 5. Plot of Sr isotopic results for all dissolution experiments. For explanation of run and batch numbers see Table 2. Below each run number the used acid and the amount of dissolved carbonate are depicted.

The $^{87}Sr/^{86}Sr$ isotopic composition of the detritus in this study is as expected much more radiogenic than the matrix signal (detritus: 0.708–0.710; matrix: 0.707 | see Figure 5). Run 1 demonstrates that leaching of only 25 % of the carbonate fraction still bears the influence of the detrital fraction with $^{87}Sr/^{86}Sr$ values being more radiogenic than those with 100 % dissolved carbonate. With our samples containing up to 22 % detritus and the $^{87}Sr/^{86}Sr$ of the sequential leachings of batch 2 and 3 show that the preleachings still contain a minor imprint of contaminant Sr, as there is a slight trend to more unradiogenic values for the second leachings, although they overlap in their analytical errors (run 9 and 11). These second leaching results plus the results from run 2–6, where the total carbonate fraction was dissolved, confirm the findings of Denison et al., 1994 and Brand, 2004 that a detrital content of at least $\leq 22\,\%$ does not influence the matrix Sr signal when 80–100 % of the carbonate is dissolved.

Following the suggested sequential leaching procedure of Bailey et al., 2000 with preleaching 40 % of the sample to remove the main fraction of the contaminant Sr and subsequently dissolving the following 30 % of the carbonate for Sr analyses is performed in batch 4 and 5. First, the sample was washed in ultrapure water for 24 hours, which removes the water-soluble Sr from ion-exchange sites as seen in the more radiogenic $^{87}Sr/^{86}Sr$ signature of the washing fraction. Secondly, 40 % of the carbonate were dissolved with 0.1 M HCl and 1 M acetic acid, respectively. The results show that at least for batch 4 the preleachtes are slightly more radiogenic than the following 30 % dissolved carbonate fraction representing the matrix signal, thus containing contaminant Sr from ion-exchange sites from the detritus. However, batch 5 reveals lower $^{87}Sr/^{86}Sr$ for the preleachates than the matrix, speaking for using an preleaching acid that was too mild to remove all the contaminant Sr. Comparing the Sr signals from the sequential leachates that are thought to represent the matrix (run 9, 10, 14, 15) with those of the total carbonate dissolution (run 2–6) speaks against the necessity of a preleaching as suggested by the aforementioned authors, as all fractions exhibit the same $^{87}Sr/^{86}Sr$ signature.

Conclusion

Comparing the $^{87}Sr/^{86}Sr$ from the matrix leachates with those of the 100 % carbonate dissolutions from run 2–6 implies that a preleaching is not necessary to remove the unwanted Sr from nontarget minerals, as the 100 % digestions are the most unradiogenic and thus closer to the real seawater Sr signal. Dissolving at least 80 % of the carbonate is adequate to overprint the signal of the detrital minerals, whereas a medium strong acid should be used (at least 0.5 M HCl). Dissolving the whole carbonate fraction is not advised as there is still the possibility that the noncarbonate residuum could be attacked during this process and the detrital Sr signature could impurify the matrix signal, although this was not observed in this study. Washing the sample material with ultrapure water prior to leaching is a step that is additionally applied, because it already removes

a part of the contaminant Sr. Although this step not coercively necessary as a comparison between the washed and leached fractions (run 14, 15) and the unwashed dissolved fractions (run 2–6) demonstrates.

With these findings, the Sr isotopes of this study were for simplifying matters prepared with the same method as the boron isotopes (see section 2.6.4) by dissolving 80 % of the carbonate fraction with 1 M HCl, and thus partitioned from the same aliquot for Sr isotope purification.
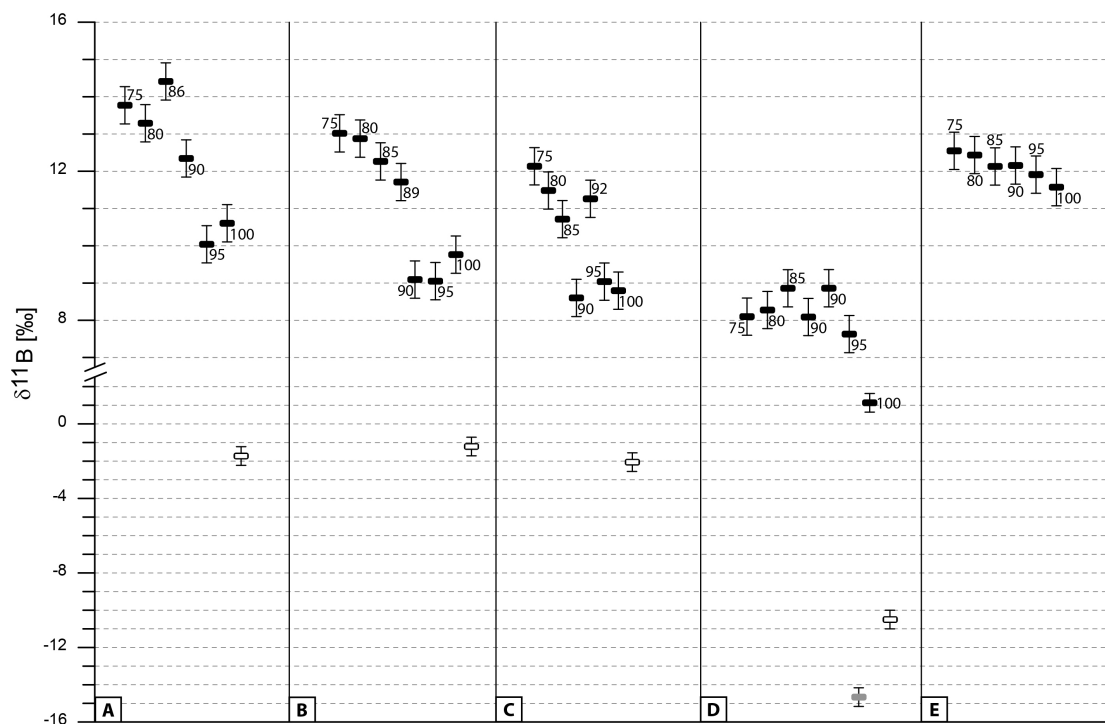
2.6.4. Boron isotopes

Figure 6. Results of the $\delta^{11}B$ dissolution experiments. Leaching was done with 1 M HCl with different amounts of dissolved carbonate (noted at each data point). Three samples with different detritus amounts and two standard materials were picked for the experiment: A = P7 (22 % detritus), B = P8 (16 % detritus), C = P11 (10 % detritus), D = KH (standard, 13 % detritus), E = IAEA-B7 (standard, 0.2 % detritus). Black filled symbols are carbonate fractions, white and grey filled the detrital fraction. The detritus $\delta^{11}B$ was determined by treating the sample 24 hours with 6 M HCl at 68°C (white symbols) and at room temperature (grey symbol). For interpretation see text.

The boron digestion methods described in Clarkson et al., 2015 and Ohnemueller et al., 2014 dissolve 50 % of the carbonate fraction with 1 M HCl for 24 hours. However, their sample material contained much less detritus than the sample material used in this study. For our sample material with in mean 14 % detritus leaving the sample for that long in contact with the reagent acid makes it far more prone to contamination by the detrital fraction. Consequently, we have to refine this method and adjust it to micritic carbonate sample material with higher detritus contents.

Besides using three different samples with differing detritus contents, two standard sample materials were additionally used for the dissolution experiments. The standards IAEA-B7 and KH were picked for this purpose because both are limestones and KH additionally has a detritial amount of about 13 % (B7 is relatively pure with 0.2 % detritus) and thus well resembles our processed sample material.

For the dissolution tests, sample powder containing 250 ng B were weighed and subsequently treated with ultrapure water for washing purposes for 24 hours with occasional pivoting. Afterwards, the fluid was removed with centrifuge and pipette. For the dissolution 1 M HCl was used, since it was already proven as the best acid for leaching B isotopes on carbonates (Clarkson et al., 2015; Ohnemueller et al., 2014). For the digestion a special distilled HCl acid was used (once subboiled $< 67\,°C$) to keep the B contamination as low as possible. The acid was added to the sample according to the varying amounts of carbonate to be leached (75–100 % carbonate). Accelerated with an ultrasonic bath the end of the dissolution reaction was bided (max. 4 hours) and the fluid extracted with centrifuge and pipette. A mannitol complex ($1\,\mu g$ B : $40\,\mu g$ mannitol) was added to the solution prior to evaporation below $67\,°C$ and subsequent B isotope purification and measurement.
The B isotope ratio of the detritus was determined on all samples and the KH standard on the runs where the total carbonate was dissolved. 2 ml of 6 M HCl was added to the residuum plus mannitol and placed with lid for 24 hours on a hotplate at $68\,°C$. For the KH standard a second run on the detritus was done with the same steps as previously described, but reacted at room temperature. Subsequent B purification and measurements were performed as described in section 2.4, 2.5.2. The results of the δ^{11}B dissolution experiments are summarised in Figure 6.

The B isotope ratio for the detritus reveals, as expected, relative much lighter δ^{11}B of about -1 to -2 ‰ (Figure 6). Such light B isotope signatures are due to the preferential uptake of the ^{10}B isotope by adsorption onto clays (Palmer et al., 1987; Schwarcz et al., 1969). The difference between the two different digestion methods for the KH detritus is due to the temperature the reaction was accelerated with. At $68\,°C$ the reaction of the acid with the detritus is more aggressive and dissolves more B from the detritial minerals. Furthermore, as evident in the plot of the different dissolution steps for δ^{11}B, there is a clear trend towards lighter B isotope ratios the more carbonate is dissolved. This trend is due to the rising influence of the contaminant B from the detritus on the matrix signal. The trend is also visible in the standard materials, for B7 with only minor detritus content the trend is mitigated. It appears that the true matrix δ^{11}B is reflected by dissolving 75–80 % of the carbonate through the stabilisation of the B signal (Fig. 6) .

Conclusion

The final method, with which the micritic sample material in this study was dissolved to gain the true matrix signal, is by leaching 80 % of the carbonate fraction with 1 M HCl. Prior to the digestion, washing of the sample powder with ultrapure water is mandatory, as it removes the water-soluble B from ion-exchange sites as evidenced by the Sr dissolution experiments.

2.6.5. Lithium isotopes

Avoiding the dilution of Li from the silicate minerals is critical during acid dilution of carbonates, as they contain much higher Li concentrations and lower δ^7Li than the carbonate fraction and could thus easily contaminate the carbonate Li signal (Bastian et al., 2018; Pogge von Strandmann et al., 2013). The Li isotopic imprint of the detrital fraction is characteristically light, because the ^{6}Li isotope is preferentially incorporated by secondary clay minerals (Burton and Vigier, 2012). The carbonate leaching procedure of this study is based on the findings of Pogge von Strandmann et al., 2013, Bastian et al., 2018 and Macedo de Paula-Santos et al., 2017. Pogge von Strandmann et al., 2013 showed that the Al/Ca ratio in carbonates must be >0.8 mmol/mol, before the carbonate Li isotope signature is contaminated by Li derived from clays, supported by the study of Bastian et al., 2018 who suggested an Al/Ca ratio below 2 mmol/mol. Moreover, all studies found that weak acids should be used during the leaching since stronger acids increase the content of contaminant Li. Macedo de Paula-Santos et al., 2017 also varied the amount of leached carbonate between 20 and 50 %, finding that dissolving only 20 % yields the heavier δ^7Li and hence less contaminated signature. The studies by Macedo de Paula-Santos et al., 2017 and Pogge von Strandmann et al., 2013 obtained the best results by leaching the micritic carbonate in 0.1 M HCl for 1 hour.

In an effort to refine the above described leaching methods and gaining the δ^7Li that is closest to the matrix signal, we carried out leaching experiments by varying the amount of leached carbonate (30 %, 25 %, 22.5 %, 20 %). According to Pogge von Strandmann et al., 2013 we dissolved our carbonate samples with 0.1 M HCl, but for 2 hours. We decided for the extra hour of leaching as 1 hour did not always seem to be sufficient for the neutralisation reaction of acid and carbonate to finalise. Differences in the δ^7Li of the 1 hour and 2 hour leachings were not observed, as best seen in the leaching experiments for Mg (see section 2.6.6). As the leaching procedures and behaviour for both elements during leaching are equal, an impact from the detrital fraction would drive the δ^{26}Mg and likewise the δ^7Li isotopic signature to lighter values (Opfergelt et al., 2014; Pogge von Strandmann et al., 2013; Wimpenny et al., 2014). As this process can not be observed during the Mg leaching experiments, the same must be true for Li. The results of the Li leaching experiments are found in Table 3. For the experiments 3 samples with differing detrital contents were chosen, and also for a better evaluation and comparison of the gained data the KH standard material,

because it resembles with its 13 % detritus well our sample material. To determine which isotopic imprint any contaminant Li holds, the detritus was leached with 6 M HCl for 24 hours at 90°C.

sample	leached fraction δ^7Li (‰)				
	30%	25%	22.5%	20%	detritus
P7	14.9	13.8	13.1	13.2	-2.9
P8	14.4	14.8	14.1	12.7	-2.9
P11	16.2	17.6	16.4	15.3	-3.3
KH	12.6	12.4	10.9	8.3	-11.0

Table 3. Results of δ^7Li leaching experiments in varying the amount of dissolved carbonate. Each sample has different detritus contents: P7 = 22 %, P8 = 16 %, P11 = 10 %, KH = 13 %.

The difficulty with leaching Li on carbonates is always to find the right amount of leached carbonate that represents the matrix signal and thus heaviest δ^7Li, while not leaching too much to affect the detritus or too less and not leaching enough to properly represent the matrix. It can be seen from Table 3 that the more carbonate is leached the heavier the δ^7Li becomes. There are small differences in the δ^7Li between the 25 and 30 % dissolved carbonate step, the isotopic value becoming only slightly heavier, indicating equilibrium with the matrix signal. However, sample P11 reveals a lighter value by dissolving the maximum amount of carbonate contradicting the trends observed in the other samples. The observed trend is probably due to the influence of the detritial contaminant Li, as too much of the carbonate is leached, also affecting the detritus. We therefore decided to continue our Li experiments by leaching 25 % of the carbonate fraction, since it represents the most stable and unaffected matrix signature.

Conclusion

The final method with which the micritic sample material in this study was dissolved to gain the true δ^7Li matrix signal is by leaching 25 % of the carbonate fraction with 0.1 M HCl. Prior to the digestion, washing of the sample powder with ultrapure water is mandatory.

2.6.6. Magnesium isotopes

As Li and Mg have a similar ion radius they also behave similarly during secondary mineral formation and carbonate leaching. The Mg isotopes fractionate during secondary mineral formation taking up the heavy isotopes and thus enrich the residuum in the light ^{24}Mg isotope (Tipper et al., 2006; Tipper et al., 2010), meaning that the detritus in carbonates should have a heavy isotopic imprint. As the light isotope is also attached at clay minerals by adsorption, like with Li leaching,

it is also easily affected during the digestion of the carbonate material. For this reason, the same carbonate leaching method as performed for Li isotopes was preferred. To test if any differences in the Mg isotope values are produced in comparison with other leaching methods, we also performed the Mg leaching methods from Pogge von Strandmann et al., 2012 and Macedo de Paula-Santos et al., 2017, who reacted their samples with 0.2 N HCl for 2 hours and 0.1 N HCl for 1 hour, respectively. The results of the leaching experiments are given in Table 4 and reveal that every leaching method leads within uncertainty to the same δ^{26}Mg value. These results lead to the conclusion that all three methods can be used for Mg leaching on our carbonates. For simplicity and better comparison in this study we use the same method as described for Li leaching.

sample	δ^{26}**Mg**$_{DSM3}$ (‰)		
	leaching 1	leaching 2	leaching 3
P7	-3.46	-3.41	-3.44
P11	-3.58	-3.61	-3.57
P19	-3.57	-3.51	-3.57
KH	-3.85	-3.84	-3.85

Table 4. Mg isotopic results of the leaching experiments performed on 3 carbonate samples and one standard reference material KH, also with differing detritial contents. Leaching 1 refers to the leaching procedure done in this study as described for Li isotopes (see section 2.6.5, leaching for 2 hours with 0.1 M HCl). For comparatative reasons, two different leaching methods described in the literature were performed to validate our method. Leaching 2 refers to the method described by Macedo de Paula-Santos et al., 2017 who treated the sample for 1 hour with 0.1 M HCl. Leaching 3 refers to Pogge von Strandmann et al., 2012 who treated their samples for 1 hour with 0.2 M HCl.

2.7. Evaluation of the sample preservation

Marine carbonate rocks are widely used for paleoenvironmental reconstructions as they are thought to reflect the chemistry of the ambient seawater during its time of deposition. However, diagenesis may influence and alter the original chemistry of the carbonate. In the case of carbonate sediments, it is important to note that they experienced some kind of post-depositional diagenetic alteration during the conversion from unlithified carbonate mud into carbonate rocks (Bathurst, 1971; Higgins et al., 2018; Swart and Eberli, 2005). The magnitude of alteration is dependent on a few factors of the diagenetic environment: (I) the stability of the mineralogy, (II) the chemical composition of the diagenetic fluid, (III) the mechanism of solute transport (diffusion vs. advection), (IV) pressure and temperature during the burial history (e.g. Ahm et al., 2018; Banner, 1995; Banner and Hanson, 1990; Brand et al., 2012; Brand and Veizer, 1980, 1981). To quantify the degree of the alteration and overprint of the initial chemistry of the carbonate, it is thus crucial to test the preservation of the rock with different methods as stated in the literature (Brand et al., 2011 and references therein). For this study the already successfully applied methods by Kasemann et al., 2010, Ohnemueller et al., 2014 and Clarkson et al., 2015 were used. In the following the single methods for the investigation for any crucial diagenetic alteration of the initially selected carbonate rocks are described.

2.7.1. Optical tests of the microstructure

Cathodoluminescence (CL) images is one mean to assess the degree of diagenetic alteration in micritic carbonates. The luminescence of carbonates is caused by several factors, the main factor being the presence of trace elements (Machel, 1985 and references therein). Important activators in calcites are manganese (Mn) and iron (Fe) is amongst the most important quenchers. The amount of each element determines the color of the crystals luminescence. Colors observed in carbonates are usually red, orange and yellow. However, Machel, 1985 and Machel et al., 1991 demonstrated that only relying on the intensity of the color as an indicator for high Mn or Fe contents is not possible. Thus, using CL as an only mean in the chemical interpretation of diagenesis is neglected, which is why a set of several tests is applied in this study. CL images are nonetheless used for qualitative petrography as for detecting growth zones, discontinuities and peculiar cementation fabrics (e.g. Dickson, 1983; Walkden and Berry, 1984). All of our selected carbonate samples showed no such patterns and the luminescence was according to their trace element concentrations of Mn and Fe, ranging from yellowish to reddish implying an incorporation during recrystallization (Appendix A, Fig. 21).

Scanning electron microscopy (SEM) is generally used as a screening test to asses the microstructure of carbonate rocks (e.g. Brand et al., 2012, 2011). The images showed no signs of alteration

and no dolomitization of the matrix was observed. EDX measurements yielded the typical minerals incorporated in carbonates (e.g. quartz, biotite, feldspar, clay minerals)(Appendix A, Fig. 20 — images for all samples can be found on this thesis attached compact disc).

2.7.2. Mineralogical, elemental and isotopic tests

Clay minerals, and other detrital components of the carbonate rock, can contaminate the sample solution by detritial mineral dissolution. So far, the techniques applied by Ohnemueller et al., 2014 and Clarkson et al., 2015 avoided any detectable contamination by the detritial fraction. However, to test for any detritial contamination of the sample solution, not only the trace element compositions of characteristic elements (e.g. Al, Si, Ba), but also XRD analyses were performed to determine the amount and varieties of the clay minerals and detritial components. The mineralogical composition of the detritus was determined with X-Ray Diffraction pattern analysis (see section 2.5.1, for results Table 1). The majority of the detritial fraction comprises typical detritial minerals found in carbonates: quartz, biotite and to a minor content clay minerals. The mean content of clay minerals in the carbonate rocks is 4 %.

Furthermore, trace element concentrations were performed for assessing the diagenetic overprint. If a limestone is exposed to meteoric waters during post-depositional processes and is dissolved and recrystallized, elements like Fe and Mn usually become enriched, whereas strontium (Sr) and sodium (Na) are lost as those waters contain less or more of those elements, respectively (Brand and Veizer, 1980; Denison et al., 1994; Pingitore, 1978). In particular, Sr and Mn are often used in studies for diagenetic effects because they have opposing trends. A study by Denison et al., 1994 proposed the use of static limits for whole rocks, deeming samples with the elemental concentrations of Sr > 900 ppm and Mn < 300 ppm as well preserved. However, this method ignores the natural variations due to spatial and temporal differences (Brand et al., 2012). For this reason, this study concentrates not only on the absolute trace element values but the ratios of Mn/Sr together with δ^{13}C, δ^{18}O and ^{87}Sr/^{86}Sr isotopic values, which are often used as an indicator for diagenetic alteration (Jacobsen and Kaufman, 1999). Also, conspicuous values in the amounts of any trace elements (e.g. B, Al, Sr, Mn, K, Fe) are used in this study as hints for a probable poor preservation.

In the mineralogical and isotopic tests conspicuous patterns were detected for samples S8, S10, S20, S21, S22 for the BdC section. Sample S8 has also an apparent high Mn/Sr ratio of $\sim$2 and striking different isotopic values for ^{87}Sr/^{86}Sr, δ^{11}B, δ^{18}O, also true for some of the other four mentioned samples (Fig. 9, Table 5, 6). All five samples were deemed diagenetically overprinted and neglected for any further environmental interpretation. Also, any statistically significant correlation between boron and elemental concentrations (Al, Ba, Ca, Fe, Mg, Mn, P, S, Si, Sr) was tested but not found, as well as the correlation between δ^{13}C, δ^{18}O and δ^{11}B (see Fig. 7).

Preservation of the original $\delta^{13}C$ and $\delta^{18}O$ seawater signal

The alteration of the initial carbonate chemistry by early marine diagenesis is dependent inter alia on the abundance of an element in the carbonate and the amount added to it by the diagenetic fluid. $\delta^{13}C$ isotopes are thus amongst the most robust isotopes due to the high carbon concentrations in the carbonate rocks relative to the highest amount that could be added by diagenetic fluids (Banner and Hanson, 1990; Derry, 2010). Owing to the high abundance of oxygen in water $\delta^{18}O$ isotopes are in contrast the less stable isotope system in carbonates (Ahm et al., 2018). Accordingly, during meteoric diagenesis both $\delta^{13}C$ and $\delta^{18}O$ isotopes become lighter the greater the influence of the diagenetic fluid, as it is usually depleted in ^{18}O and ^{13}C (Vogel, 1959). Generally, potential primary isotope signals are thought to be preserved with $\delta^{18}O > -4‰$ and $\delta^{13}C > +1‰$ (Banner, 1995; Brand and Veizer, 1981), whereas these limitations ignore, among other things, spatial and temporal variations due to differences in local conditions (Brand et al., 2012). Hence, it is once more important to combine different screening tests to separate unaltered from altered material.

The comparison of our generated $\delta^{13}C_{micrite}$ and $\delta^{18}O_{micrite}$ isotopes with already published values for each basin is displayed in Appendix A, Figure 18 (BdC) and 17 (R/FC). The $\delta^{13}C$ for the R/FC section are well aligned with published data for the Lusitanian basin, even though the CIE does not reach negative values. This could be owing to the shallower water depth at the R/FC section representing the mid-/outer ramp environment, compared to the Peniche section, which represents the basin facies and shows the most negative values for the CIE. For the BdC section the published $\delta^{13}C$ and $\delta^{18}O$ values show a wide scatter (Danise et al., 2019), with our generated data lying amidst the published data. Luckily, fossil carbon and oxygen isotopes also exist for the BdC and R/FC sections published by Ullmann et al., 2020. Brachiopods and bivalves are thought to be the best sample material for isotope analyses because their low-Mg-calcite is more resistant against diagenetic alteration (e.g. Al-Aasm and Veizer, 1982; Angiolini et al., 2010; Brand et al., 2012; Brand and Veizer, 1980; Brand, 2004; Mii and Grossman, 1994). Ullmann et al., 2020 deemed the brachiopod and bivalves from the BdC and R/FC as well preserved. Our $\delta^{13}C_{micrite}$ are very close to the fossil values for both sections, speaking for a likewise good preservation. The $\delta^{18}O_{micrite}$ data in contrast are lighter as the $\delta^{18}O_{fossil}$ data, indicating a diagenetic overprint. The previously mentioned samples S8, S10, S20, S21, S22 already conspicuous in trace element contents also reveal a rather negative $\delta^{18}O_{micrite}$ imprint with values lower than -4‰, also speaking for its diagenetic altered nature on these samples.

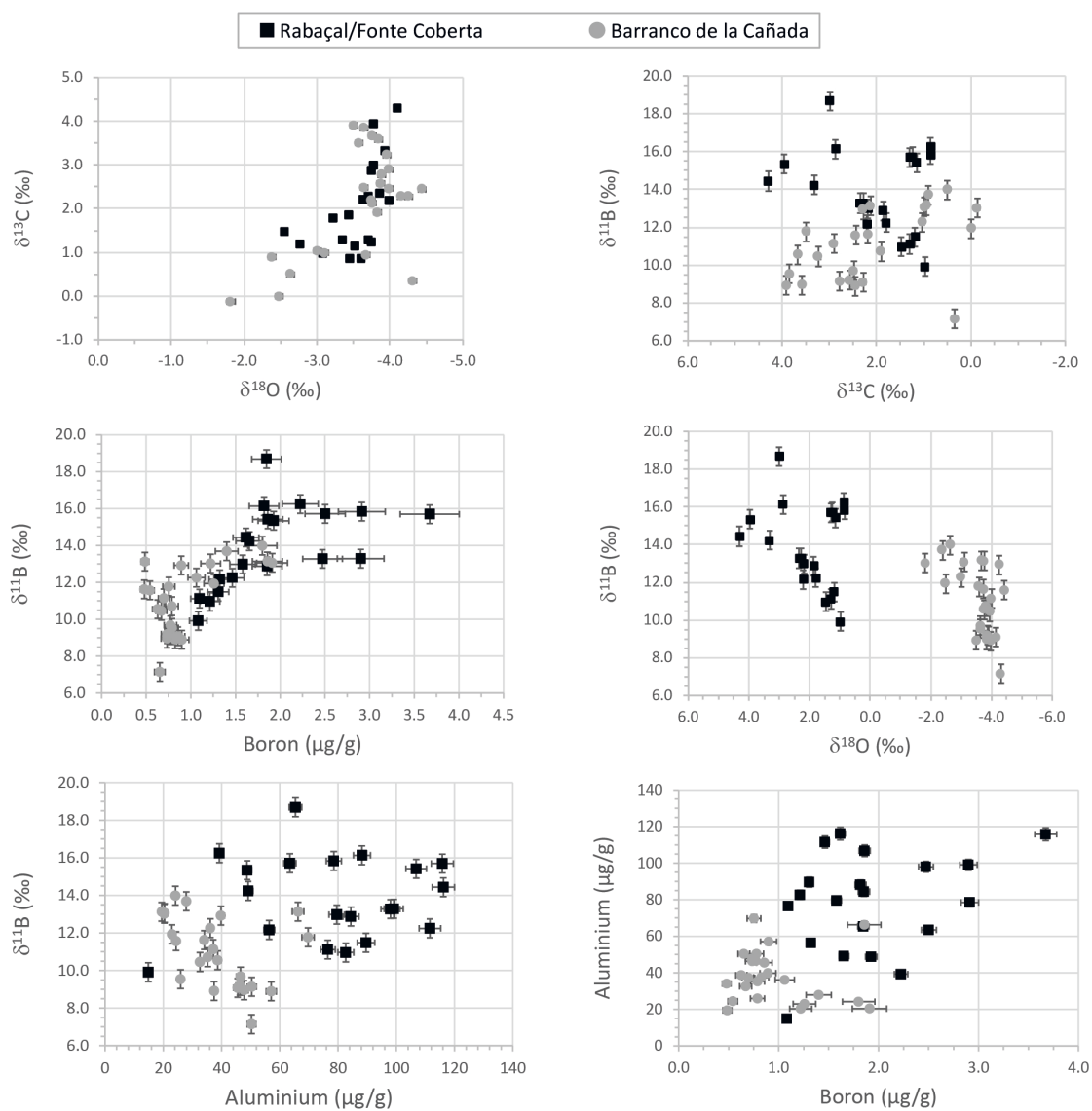**Figure 7.** Isotope and elemental plots for R/FC and BdC sections. Cross-plots of δ^{11}B, δ^{13}C and δ^{18}O isotope data (2sd) and boron and aluminium concentrations (with 2rsd) for micritic carbonates of both sections in this study. No significant correlation can be observed. *[High-resolution image on attached CD]*

Preservation of the original $^{87}Sr/^{86}Sr$ seawater signal

The Sr digestion experiments helped to clarify which method can be best used to exclude the biggest influence of the nontarget minerals on the $^{87}Sr/^{86}Sr$ of the matrix (section 2.6.3). Nonetheless, our micritic carbonate values are more radiogenic than the published seawater Sr values derived from belemnites for the Early Jurassic (McArthur et al., 2000) for both, the BdC and R/FC section (Fig. 19). This is a phenomenon observed by many studies on carbonates (e.g. Brand et al., 2012; Brand, 2004; Denison et al., 1994) deriving from diagenetic equilibration. The amount on how much the matrix $^{87}Sr/^{86}Sr$ deviates from the seawater Sr signatures is thought to be dependant on three factors of the diagenetic fluid: (1) how much Sr was imported; (2) the isotopic composition of the imported Sr; and (3) the pore volume of the rock (Denison et al., 1994). Hence, though influenced by diagenetic fluids a whole rock can preserve the original seawater signature, if the diagenetic $^{87}Sr/^{86}Sr$ is comparable with that of the host limestone. However, both our sample sets from BdC and R/FC are more radiogenic than the seawater Sr signal (McArthur et al., 2000) (Fig. 19) implying not to bear the original $^{87}Sr/^{86}Sr$ seawater signal, although the trends in the Sr curve are still preserved. The micrites from BdC show less a deviation from the seawater Sr curve than the R/FC. Additionally to the micrites we were also able to generate Sr isotopes on well preserved fossil brachiopod and bivalve shell material for the BdC section. The fit between the belemnite Sr values from McArthur et al., 2000 and our newly generated brachiopod and bivalve data is well within the range and plotting on the published data (Fig. 19).

2.7.3. Conclusion

Five samples from the BdC sections that were firstly chosen for further isotope analyses were found diagenetically altered: S8, S10, S20, S21, S22, S23. All five samples were noticeably divergent from the trace element contents of the additional samples, and they all also had $\delta^{18}O$ values below -4 ‰. They furthermore showed a distinct different $\delta^{11}B$ and $^{87}Sr/^{86}Sr$ isotopic composition, making it more clear that these samples should be neglected for further isotope analyses and interpretation approaches.

2.8. Preservation of the original δ^{11}B, δ^{7}Li and δ^{26}Mg seawater signatures

The preservation of each sample was carefully checked by several methods (as discussed above) and did not reveal major impacts on the initial isotopic composition of the carbonate rock. However, as the degree of alteration is dependent on several factors, one isotope system can be strongly influenced by diagenesis, whereas other isotopic systems are unaffected. The preservation of the original δ^{11}B, δ^{7}Li and δ^{26}Mg can hence be additionally ensured by analysing multiple sections of the same period for their isotopic signature (Pogge von Strandmann et al., 2019b).
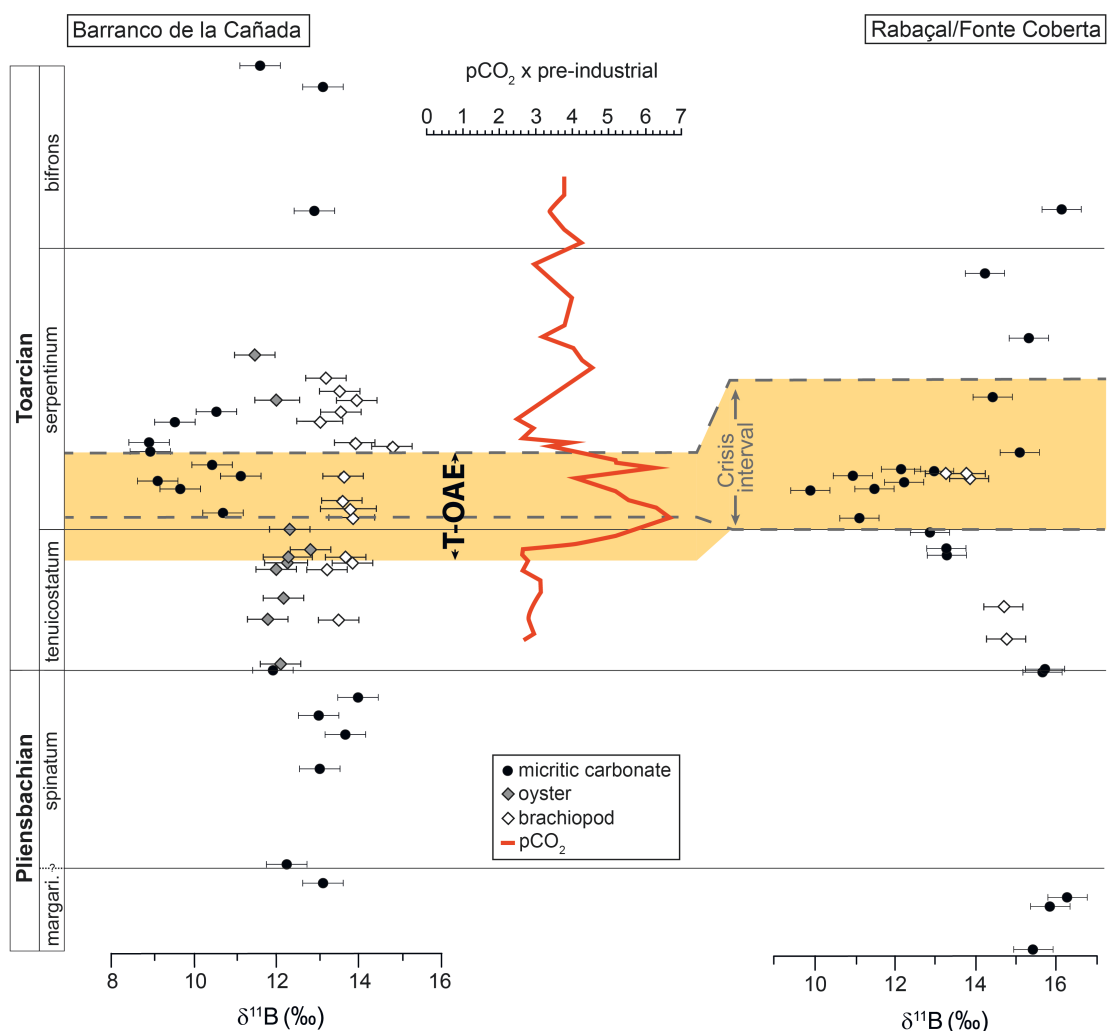
2.8.1. Boron isotope signal

Figure 8. Atmospheric CO_2 concentration reconstruction for the T-OAE from Ullmann et al., 2020 plotted with B isotopes from this study. *[High-resolution image on attached CD]*

Our δ^{11}B isotopes generated for R/FC and BdC show the same trends in decreasing B values during the T-OAE. Besides the change in seawater pH this drop could also be influenced by a few other factors, which are discussed in the following paragraphs.

Temperature

Temperature reconstructions with δ^{18}O isotopes from low-Mg calcite brachiopods for the BdC section revealed a rise in seawater temperatures of 3.5 ± 0.3 °C during the T-OAE (Ullmann et al., 2020). As the dissociation constant of boric acid (pK_b) decreases with increasing temperature (Dickson, 1990) the given seawater warming at the site of precipitation could lead to an increase in the boron isotopic composition in the marine carbonates, even if the seawater pH was stable at this time. The reconstructed rise in seawater temperature would equal an increase in δ^{11}B of about 0.45 ‰ at a given pH of 8. Since this would be a rather minor increase, and the oxygen isotopes at the BdC section increase concordantly with the decrease in the δ^{11}B signal, the influence of the ambient seawater temperature on the boron isotope signal is unlikely.

Salinity

Accordingly to temperature changes, alterations in salinity also affect the pK_b value (Dickson, 1990). To produce a significant negative shift in δ^{11}B composition of marine carbonates a drastic decrease in salinity is necessary (e.g. from 35 psu to 25 psu). However, models reconstructing the sea surface salinity changes during the T-OAE show that the areas around the Bdc and R/FC were not affected by salinity fluctuations (Dera and Donnadieu, 2012). What is more, both of our study areas represent shallow water environments that should be farther away from freshwater inputs. Thus, an effect of salinity on our boron composition of the marine carbonates is probably not given.

Water-Depth

As the depth in the water column increases, the temperature and hence δ^{11}B composition decreases accordingly. Remarkably, the absolute δ^{11}B values at the BdC site is generally $\sim$2 ‰ lower than at the R/FC site, although the boron isotope excursions during the T-OAE crisis interval have a similar magnitude. Given the greater paleo-depth at R/FC of about 80–120 m (Gahr, 2002, 2005) compared to the depth of 40–70 m at BdC, lower temperatures and δ^{11}B values are rather expected at the R/FC. Thus, the different water depths can not be accounted for the offset in the general δ^{11}B signature at both sites.

Atmospheric CO_2 concentrations

Rapid inputs of CO_2 and CH_4 into the atmosphere derived from Karoo–Ferrar intrusive volcanism

and the dissociation of marine clathrates at the onset of the T-OAE (Burgess et al., 2015; Elliot, 2013; McElwain et al., 2005; Percival et al., 2015; Svensen et al., 2012) have already been suggested to be a cause for a possible seawater acidification (Beerling and Brentnall, 2007; Hermoso et al., 2009; Kemp et al., 2005). Climate models from Dera and Donnadieu, 2012 estimated a rise in atmospheric CO_2 concentrations of about 2–4 times higher than pre-industrial levels, which has been confirmed by the current study from Ullmann et al., 2020, based on models from $\delta^{18}O$ isotopes from brachiopod and bivalve shell material. Fig. 8 shows the direct correlation between the reconstructed rise in CO_2 with the concurrent decline in $\delta^{11}B$ for both studied sections, emphasizing the authenticity of a seawater signal for our boron isotope data.

Conclusion

Effects from salinity and water temperature associated with depth can mainly be ruled out as drivers for the negative $\delta^{11}B$ excursion seen in both sections. The rapid rise is atmospheric CO_2 and a subsequent drop in seawater pH it thus the most likely driver. The offset in absolute values in both basins must be the effect of regional differences we were not able to decipher.

2.8.2. Lithium and Magnesium isotope signal

For this study, the two sections R/FC (Portugal) and BdC (Spain) display the same δ^7Li values prior and after the T-OAE, although during the OAE interval both sections reveal a different signature, which could be due to regional differences. Furthermore, comparing the trends of the δ^7Li signature to already published Ca, Sr, and Os isotopes (Fig. 14) the simultaneous changes in isotopy during the T-OAE and Pl–To boundary support the idea of a primary seawater signal preserved in the carbonate rocks (for further information see discussion in chapter 4).

The Mg isotopes for both sections have a likewise light isotopic signature with rather negative values (-3.98‰ − -3.59‰) with a slight offset between the two sections of 0.39‰. Generally, carbonate rocks have a relatively wide span of $\delta^{26}Mg$ signatures (-5.6 to -1‰, e.g. Fantle and Higgins, 2014; Gao et al., 2018; Li et al., 2012; Wang et al., 2017) as many low-temperature processes fractionate the Mg isotopes during the incorporation into the calcite. Our generated $\delta^{26}Mg$ values thus fall within the reasonable range of up to date published values of carbonate rocks. Diagenetic overprint may shift the $\delta^{26}Mg$ to more negative and even more positive values (Fantle and Higgins, 2014), however the lack of variability in both sections over the investigated time span ($> \sim7Ma$) is conspicuous. If diagenesis would have influenced the primary signal of both sections a uniform shift in $\delta^{26}Mg$ in the same direction affecting the whole transect is rather unlikely. Also, the difference in absolute $\delta^{26}Mg$ values at both sections is small and probably owing

to regional differences as they record different basins in the northwestern Tethys. To conclude, the Li and Mg isotope signals recorded here for the two basins record a true seawater signal.

2.9. Calculation of seawater pH with boron isotopes

Dissolved boron occurs as two species in seawater, one being the trigonal boric acid $(B(OH)_3)$ and the second being the tetrahedral oriented borate $(B(OH)_4^-)$ with relative proportions of 80 and 20% at pH 8, respectively. The abundance of each species is dependent on the pH meaning that at low pH all dissolved B is present in $B(OH)_3$ whereas at high pH B is present in the $B(OH)_4^-$ species. Owing to stronger boron-oxygen bonds in $B(OH)_3$ this species is enriched in ^{11}B whereas $B(OH)_4^-$ is preferentially enriched in ^{10}B (e.g. Zeebe, 2005) with an offset of 26–27 ‰ (Klochko et al., 2006; Nir et al., 2015). Isotopic fractionation between these two species occurs due to coordination-controlled vibration differences as a function of pH, also altering its $\delta^{11}B$ value as both species become enriched in ^{11}B with rising pH and concurrently $B(OH)_4^-$ becoming the dominant aqueous species (Kakihana et al., 1977; Oi et al., 1988; Schwarcz et al., 1969).

Using boron isotopes incorporated into marine calcites as a mean to reconstruct seawater pH is based on the assumption that the calcite preferentially takes up $B(OH)_4^-$, which was firstly suggested by Hemming and Hanson, 1992. The negatively charged species is thought to being more attracted to the positively charged calcite surface as the uncharged $B(OH)_3$ (Palmer et al., 1998; Pearson and Palmer, 2000; Spivack et al., 1993; Xiao et al., 2014). However, recent studies imply that aragonite seems to only incorporate borate while calcite may take up a mixture of boric acid and borate (Noireaux et al., 2015). Nevertheless, as it is still a matter of debate how B is incorporated exactly in inorganic marine carbonates, pH reconstructions still use the assumption of Hemming and Hanson, 1992 that only borate is incorporated into the calcite, leading to the pH–$\delta^{11}B$ relation shown in equation 2. A few important variables are to be solved to calculate past seawater pH. First, the B isotope fractionation factor, where a first estimate for the value of α_B was given by Kakihana et al., 1977 with a value of 1.0194 ($\varepsilon_B = 19.4$ ‰; $\varepsilon_B = (\alpha_B - 1) * 10^3$). However, various subsequent studies found different estimates ranging between 18–30 ‰ depending on the speciation calculation methods. For example suggested recent studies values of 1.025 ± 0.001 (Noireaux et al., 2015), 1.026 ± 0.001 (Nir et al., 2015) and 1.025 ± 0.0005 (Kaczmarek et al., 2016). However, in modern studies for pH reconstructions the widely accepted value of 1.0272 ± 0.0006 by Klochko et al., 2006 is still used. Depending on which α_B value is applied the calculated data can alter in the range of 1–2 ‰ (Fig. 2). Moreover to mention is a possible small-scale influence of temperature on α_B observed with biotic carbonate precipitation (Farmer et al., 2015; Hönisch et al., 2019; Hönisch et al., 2008; Rae et al., 2011) and inorganic carbonate (Kakihana et al., 1977). As mentioned above, the fractionation of B into calcites is still a matter of debate and in need of clearance. Therefore we apply the α_B from Klochko et al., 2006 in this study, also because the values fall within the uncertainty from Nir et al., 2015 and for better comparison to other studies.

Another varying factor in the pH calculation equation is the dissociation constant of boric acid pK_b. Different studies found that pK_b is temperature, pressure and salinity dependant (e.g. Culberson and Pytkowicx, 1968; Dickson, 1990; Hansson, 1973; Roy et al., 1993). Generally spoken, the pK_b increases with decreasing temperature and salinity. As recent studies use the pK_b values from Dickson, 1990 and his results were confirmed by Roy et al., 1993 and are in line with the findings from Hansson, 1973, we also apply his values for our reconstructions in this study.

A further important prerequisite is the δ^{11}B isotopic composition of the seawater (δ^{11}B$_{SW}$) during the time of deposition. Today's δ^{11}B$_{SW}$ is 39.61 ‰ (Foster et al., 2010) and globally homogenous, though many studies have shown that this value during ancient time can be highly variable (Clarkson et al., 2015; Henehan et al., 2019; Joachimski et al., 2005; Kasemann et al., 2010; Paris et al., 2010) due to the long residence time of B in seawater. Here we test different values for δ^{11}B$_{SW}$ to find the best fit of reconstructed pH values with our recorded δ^{11}B isotopes on micrites and brachiopods (Fig. 10).

First, the δ^{11}B$_{SW}$ during the Early Jurassic can not exceed a value of 36 ‰ as a lot of our recorded values would then not be able to calculate for a pH value. Using this value for pH calculation would mean that we record a major drop of 0.8–0.9 for the T-OAE. However, if we lower the δ^{11}B$_{SW}$ value to as much as 33 ‰ we would get a rather moderate drop of 0.4–0.5. This uncertainty in pH calculations is included in our models.

Second, Jurikova et al., 2019 assumed that the δ^{11}B recorded in brachiopod shells does probably not reflect the δ^{11}B$_{SW}$ composition, but a mixture of the internal calcifying fluid and that of the ambient seawater. If we go one step further and assume that they only record the internal fluid with their secondary shell, which would support the stability of our δ^{11}B$_{brachiopod}$ data, we would then also be able to make suggestions about the pH drop observed in the micrites. Modern brachiopods have an internal fluid pH of 7.8, which is thought to be a remnant of their time of evolution (Jurikova et al., 2019). Calculating the equivalent δ^{11}B of their internal fluid would thus be ∼35 ‰ (when applying the B fractionation from Penman et al., 2013, which has the best fit). Since the micrites prior and after the T-OAE record the same δ^{11}B signature as the brachiopods, this would imply that the same δ^{11}B$_{SW}$ prevailed during this time. Adjusting this value to our pH reconstructions results in a scenario where a drop of 0.6 in both basins was recorded (Fig. 10). Nevertheless, this would only be the case if brachiopods exclusively record the δ^{11}B of their internal fluid and not a mixture with the ambient seawater, which would further complicate calculations. To clarify this matter, further research on brachiopods and the source of their δ^{11}B records is needed.

References

Al-Aasm, I. and J. Veizer (1982). "Chemical Stabilization of Low-Mg Calcite: An Example of Brachiopods". *SEPM Journal of Sedimentary Research* Vol. 52. DOI: 10.1306/212F80E4-2B24-11D7-8648000102C1865D.

Ahm, A.-S. C., C. J. Bjerrum, C. L. Blättler, P. K. Swart, and J. A. Higgins (2018). "Quantifying early marine diagenesis in shallow-water carbonate sediments". *Geochimica et Cosmochimica Acta* 236, pp. 140–159. DOI: 10.1016/j.gca.2018.02.042.

Angiolini, L., A. Checconi, M. Gaetani, and R. Rettori (2010). "The latest Permian mass extinction in the Alborz Mountains (North Iran)". *Geological Journal* 45.2-3, pp. 216–229. DOI: 10.1002/gj.1203.

Bailey, T. R., J. M. McArthur, H. Prince, and M. F. Thirlwall (2000). "Dissolution methods for strontium isotope stratigraphy: Whole rock analysis". *Chemical Geology* 167.3-4, pp. 313–319. DOI: 10.1016/S0009-2541(99)00235-1.

Banner, J. L. (1995). "Application of the trace element and isotope geochemistry of strontium to studies of carbonate diagenesis". *Sedimentology* 42.5, pp. 805–824. DOI: 10.1111/j.1365-3091.1995.tb00410.x.

Banner, J. L. and G. N. Hanson (1990). "Calculation of simultaneous isotopic and trace element variations during water-rock interaction with applications to carbonate diagenesis". *Geochimica et Cosmochimica Acta* 54.11, pp. 3123–3137. DOI: 10.1016/0016-7037(90)90128-8.

Bastian, L., N. Vigier, S. Reynaud, M.-E. Kerros, M. Revel, and G. Bayon (2018). "Lithium Isotope Composition of Marine Biogenic Carbonates and Related Reference Materials". *Geostandards and Geoanalytical Research* 42.3, pp. 403–415. DOI: 10.1111/ggr.12218.

Bathurst, R. (1971). *Carbonate sediments and their diagenesis*. Vol. 12. Developments in sedimentology. Amsterdam: Elsevier. URL: http://www.sciencedirect.com/science/book/9780444408914.

Beerling, D. J. and S. J. Brentnall (2007). "Numerical evaluation of mechanisms driving Early Jurassic changes in global carbon cycling". *Geology* 35.3, p. 247. DOI: 10.1130/G23416A.1.

Brand, U., G. Jiang, K. Azmy, J. Bishop, and I. P. Montañez (2012). "Diagenetic evaluation of a Pennsylvanian carbonate succession (Bird Spring Formation, Arrow Canyon, Nevada, U.S.A.) — 1: Brachiopod and whole rock comparison". *Chemical Geology* 308-309, pp. 26–39. DOI: 10.1016/j.chemgeo.2012.03.017.

Brand, U., A. Logan, M. A. Bitner, E. Griesshaber, K. Azmy, and D. Buhl (2011). "What is the ideal proxy of Palaeozoic seawater chemistry?" *Memoirs of the Association of Australasian Palaeontologists* 41, pp. 9–24.

Brand, U. and J. Veizer (1980). "Chemical Diagenesis of a Multicomponent Carbonate System–1: Trace Elements". *SEPM Journal of Sedimentary Research* Vol. 50. DOI: 10.1306/212F7BB7-2B24-11D7-8648000102C1865D.

– (1981). "Chemical Diagenesis of a Multicomponent Carbonate System 2: Stable Isotopes". *Journal of Sedimentary Petrology* 51.3, pp. 987–997.

Brand, U. (2004). "Carbon, oxygen and strontium isotopes in Paleozoic carbonate components: An evaluation of original seawater-chemistry proxies". *Chemical Geology* 204.1-2, pp. 23–44. DOI: 10.1016/j.chemgeo.2003.10.013.

Burgess, S. D., S. A. Bowring, T. H. Fleming, and D. H. Elliot (2015). "High-precision geochronology links the Ferrar large igneous province with early-Jurassic ocean anoxia and biotic crisis". *Earth and Planetary Science Letters* 415, pp. 90–99. DOI: 10.1016/j.epsl.2015.01.037.

Burton, K. W. and N. Vigier (2012). "Lithium isotopes as tracers in marine and terrestrial environments". *Handbook of Environmental Isotope Geochemistry*. Ed. by M. Baskaran. Berlin, Heidelberg: Springer Berlin Heidelberg, pp. 41–59.

Clarkson, M. O., S. A. Kasemann, R. A. Wood, T. M. Lenton, S. J. Daines, S. Richoz, F. Ohnemueller, A. Meixner, S. W. Poulton, and E. T. Tipper (2015). "Ocean acidification and the Permo-Triassic mass extinction". *Science (New York, N.Y.)* 348.6231, pp. 229–232. DOI: 10.1126/science.aaa0193.

Comas-Rengifo, M. J., L. V. Duarte, F. García Joral, and A. Goy (2013). "Los braquiópo-

dos del Toarciense Inferior (Jurásico) en el área de Rabaçal-Condeixa (Portugal): distribución estratigráfica y paleobiogeografía". *Comunicações geológicas* 100.Esp. I, pp. 37–42.

Correia, V. F., J. B. Riding, L. V. Duarte, P. Fernandes, and Z. Pereira (2018). "The Early Jurassic palynostratigraphy of the Lusitanian Basin, western Portugal". *Geobios* 51.6, pp. 537–557. DOI: 10.1016/j.geobios.2018.03.001.

Culberson, C. and R. M. Pytkowicx (1968). "Effect of pressure on carbonic acid, boric acid, and the pH in seawater". *Limnology and Oceanography* 13.3, pp. 403–417. DOI: 10.4319/lo.1968.13.3.0403.

Danise, S., M.-E. Clémence, G. D. Price, D. P. Murphy, J. J. Gómez, and R. J. Twitchett (2019). "Stratigraphic and environmental control on marine benthic community change through the early Toarcian extinction event (Iberian Range, Spain)". *Palaeogeography, Palaeoclimatology, Palaeoecology* 524, pp. 183–200. DOI: 10.1016/j.palaeo.2019.03.039.

Denison, R. E., R. B. Koepnick, A. Fletcher, M. W. Howell, and W. S. Callaway (1994). "Criteria for the retention of original seawater $^{87}Sr/^{86}Sr$ in ancient shelf limestones". *Chemical Geology* 112.1-2, pp. 131–143. DOI: 10.1016/0009-2541(94)90110-4.

DePaolo, D. J., F. T. Kyte, B. D. Marshall, J. R. O'Neil, and J. Smit (1983). "Rb-Sr, Sm-Nd, K-Ca, O, and H isotopic study of Cretaceous-Tertiary boundary sediments, Caravaca, Spain: Evidence for an oceanic impact site". *Earth and Planetary Science Letters* 64.3, pp. 356–373. DOI: 10.1016/0012-821X(83)90096-1.

Dera, G. and Y. Donnadieu (2012). "Modeling evidences for global warming, Arctic seawater freshening, and sluggish oceanic circulation during the Early Toarcian anoxic event". *Paleoceanography* 27.2, pp. 1–15. DOI: 10.1029/2012PA002283.

Derry, L. A. (2010). "A burial diagenesis origin for the Ediacaran Shuram–Wonoka carbon isotope anomaly". *Earth and Planetary Science Letters* 294.1-2, pp. 152–162. DOI: 10.1016/j.epsl.2010.03.022.

Dickson, A. G. (1990). "Thermodynamics of the dissociation of boric acid in synthetic seawater from 273.15 to 318.15 K". *Deep Sea Research Part A. Oceanographic Research Papers* 37.5, pp. 755–766. DOI: 10.1016/0198-0149(90)90004-F.

Dickson, J. (1983). "Graphical modelling of crystal aggregates and its relevance to cement diagnosis". *Royal Society of London, Pilosphical Transactions* A309, pp. 465–502.

Elliot, D. H. (2013). "The geological and tectonic evolution of the Transantarctic Mountains: A review". *Geological Society, London, Special Publications* 381.1, pp. 7–35. DOI: 10.1144/SP381.14.

Fantle, M. S. and J. Higgins (2014). "The effects of diagenesis and dolomitization on Ca and Mg isotopes in marine platform carbonates: Implications for the geochemical cycles of Ca and Mg". *Geochimica et Cosmochimica Acta* 142, pp. 458–481. DOI: 10.1016/j.gca.2014.07.025.

Farmer, J. R., B. Hönisch, L. F. Robinson, and T. M. Hill (2015). "Effects of seawater-pH and biomineralization on the boron isotopic composition of deep-sea bamboo corals". *Geochimica et Cosmochimica Acta* 155, pp. 86–106. DOI: 10.1016/j.gca.2015.01.018.

Farmer, J. R., B. Hönisch, and J. Uchikawa (2016). "Single laboratory comparison of MC-ICP-MS and N-TIMS boron isotope analyses in marine carbonates". *Chemical Geology* 447, pp. 173–182. DOI: 10.1016/j.chemgeo.2016.11.008.

Ferreira, J., E. Mattioli, B. Pittet, M. Cachão, and J. E. Spangenberg (2015). "Palaeoecological insights on Toarcian and lower Aalenian calcareous nannofossils from the Lusitanian Basin (Portugal)". *Palaeogeography, Palaeoclimatology, Palaeoecology* 436, pp. 245–262. DOI: 10.1016/j.palaeo.2015.07.012.

Foster, G. L., P. A. E. Pogge von Strandmann, and J. W. B. Rae (2010). "Boron and magnesium isotopic composition of seawater". *Geochemistry, Geophysics, Geosystems* 11.8, n/a–n/a. DOI: 10.1029/2010GC003201.

Foster, G. L., B. Hönisch, G. Paris, G. S. Dwyer, J. W. Rae, T. Elliott, J. Gaillardet, N. G. Hemming, P. Louvat, and A. Vengosh (2013). "Interlaboratory comparison of boron isotope analyses of boric acid, seawater and marine $CaCO_3$ by MC-ICPMS and NTIMS". *Chemical Geology* 358, pp. 1–14. DOI: 10.1016/j.chemgeo.2013.08.027.

Gahr, M. E. (2002). "Palökologie des Makrobenthos aus dem Unter-Toarc SW-Europas: Dissertation". *Beringeria* 31.

– (2005). "Response of Lower Toarcian (Lower Jurassic) macrobenthos of the Iberian Peninsula to sea level changes and mass extinction". *Journal of Iberian Geology* 31.2, pp. 197–215.

Gao, T., S. Ke, S.-J. Wang, F. Li, C. Liu, J. Lei, C. Liao, and F. Wu (2018). "Contrasting Mg isotopic compositions between Fe-Mn nodules and surrounding soils: Accumulation of light Mg isotopes by Mg-depleted clay minerals and Fe oxides". *Geochimica et Cosmochimica Acta* 237, pp. 205–222. DOI: 10.1016/j.gca.2018.06.028.

Gruber, C., Y. Harlavan, D. Pousty, D. Winkler, and J. Ganor (2019). "Enhanced chemical weathering of albite under seawater conditions and its potential effect on the Sr ocean budget". *Geochimica et Cosmochimica Acta* 261, pp. 20–34. DOI: 10.1016/j.gca.2019.06.049.

Hansson, I. (1973). "A new set of acidity constants for carbonic acid and boric acid in sea water". *Deep Sea Research and Oceanographic Abstracts* 20.5, pp. 461–478. DOI: 10.1016/0011-7471(73)90100-9.

Hemming, N. G. and G. N. Hanson (1992). "Boron isotopic composition and concentration in modern marine carbonates". *Geochimica et Cosmochimica Acta* 56.1, pp. 537–543. DOI: 10.1016/0016-7037(92)90151-8.

Henehan, M. J., A. Ridgwell, E. Thomas, S. Zhang, L. Alegret, D. N. Schmidt, J. W. B. Rae, J. D. Witts, N. H. Landman, S. E. Greene, B. T. Huber, J. R. Super, N. J. Planavsky, and P. M. Hull (2019). "Rapid ocean acidification and protracted Earth system recovery followed the end-Cretaceous Chicxulub impact". *Proceedings of the National Academy of Sciences of the United States of America* 116.45, pp. 22500–22504. DOI: 10.1073/pnas.1905989116.

Hermoso, M., F. Minoletti, L. Le Callonnec, H. C. Jenkyns, S. P. Hesselbo, R. E. M. Rickaby, M. Renard, M. de Rafélis, and L. Emmanuel (2009). "Global and local forcing of Early Toarcian seawater chemistry: A comparative study of different paleoceanographic settings (Paris and Lusitanian basins)". *Paleoceanography* 24.4, p. 307. DOI: 10.1029/2009PA001764.

Higgins, J. A., C. L. Blättler, E. A. Lundstrom, D. P. Santiago-Ramos, A. A. Akhtar, A.-S. Crüger Ahm, O. Bialik, C. Holmden, H. Bradbury, S. T. Murray, and P. K. Swart (2018). "Mineralogy, early marine diagenesis, and the chemistry of shallow-water carbonate sediments". *Geochimica et Cosmochimica Acta* 220, pp. 512–534. DOI: 10.1016/j.gca.2017.09.046.

Hönisch, B., S. M. Eggins, L. L. Haynes, K. A. Allen, K. D. Holland, and K. Lorbacher (2019). "Boron Proxies in Paleoceanography and Paleoclimatology". *Analytical Methods in Earth and Environmental Sciences Series*. Ed. by Wiley-Blackwell, p. 264.

Hönisch, B., T. Bickert, and N. G. Hemming (2008). "Modern and Pleistocene boron isotope composition of the benthic foraminifer *Cibicidoides wuellerstorfi*". *Earth and Planetary Science Letters* 272.1-2, pp. 309–318. DOI: 10.1016/j.epsl.2008.04.047.

Huang, K.-F., C.-F. You, Y.-H. Liu, R.-M. Wang, P.-Y. Lin, and C.-H. Chung (2010). "Low-memory, small sample size, accurate and high-precision determinations of lithium isotopic ratios in natural materials by MC-ICP-MS". *Journal of Analytical Atomic Spectrometry* 25.7, p. 1019. DOI: 10.1039/B926327F.

Jacobsen, S. B. and A. J. Kaufman (1999). "The Sr, C and O isotopic evolution of Neoproterozoic seawater". *Chemical Geology* 161.1-3, pp. 37–57. DOI: 10.1016/S0009-2541(99)00080-7.

Joachimski, M. M., L. Simon, R. van Geldern, and C. Lécuyer (2005). "Boron isotope geochemistry of Paleozoic brachiopod calcite: Implications for a secular change in the boron isotope geochemistry of seawater over the Phanerozoic". *Geochimica et Cosmochimica Acta* 69.16, pp. 4035–4044. DOI: 10.1016/j.gca.2004.11.017.

Jurikova, H., V. Liebetrau, M. Gutjahr, C. Rollion-Bard, M. Y. Hu, S. Krause, D. Henkel, C. Hiebenthal, M. Schmidt, J. Laudien, and A. Eisenhauer (2019). "Boron isotope systematics of cultured brachiopods: Response to acidification, vital effects and implications for palaeo-pH reconstruction". *Geochimica et Cosmochimica Acta* 248,

pp. 370–386. DOI: 10.1016/j.gca.2019.01.015.

Kaczmarek, K., G. Nehrke, S. Misra, J. Bijma, and H. Elderfield (2016). "Investigating the effects of growth rate and temperature on the B/Ca ratio and δ^{11}B during inorganic calcite formation". *Chemical Geology* 421, pp. 81–92. DOI: 10.1016/j.chemgeo.2015.12.002.

Kakihana, H., M. Kotaka, S. Satoh, M. Nomura, and M. Okamoto (1977). "Fundamental Studies on the Ion-Exchange Separation of Boron Isotopes". *Bulletin of the Chemical Society of Japan* 50.1, pp. 158–163. DOI: 10.1246/bcsj.50.158.

Kasemann, S. A., A. R. Prave, A. E. Fallick, C. J. Hawkesworth, and K.-H. Hoffmann (2010). "Neoproterozoic ice ages, boron isotopes, and ocean acidification : Implications for a snowball Earth". *Geology* 38.9, pp. 775–778. DOI: 10.1130/G30851.1.

Kemp, D. B., A. L. Coe, A. S. Cohen, and L. Schwark (2005). "Astronomical pacing of methane release in the Early Jurassic period". *Nature* 437.7057, pp. 396–399. DOI: 10.1038/nature04037.

Klochko, K., A. J. Kaufman, W. Yao, R. H. Byrne, and J. A. Tossell (2006). "Experimental measurement of boron isotope fractionation in seawater". *Earth and Planetary Science Letters* 248.1-2, pp. 276–285. DOI: 10.1016/j.epsl.2006.05.034.

Li, W., S. Chakraborty, B. L. Beard, C. S. Romanek, and C. M. Johnson (2012). "Magnesium isotope fractionation during precipitation of inorganic calcite under laboratory conditions". *Earth and Planetary Science Letters* 333-334, pp. 304–316. DOI: 10.1016/j.epsl.2012.04.010.

Ling, M.-X., F. Sedaghatpour, F.-Z. Teng, P. D. Hays, J. Strauss, and W. Sun (2011). "Homogeneous magnesium isotopic composition of seawater: An excellent geostandard for Mg isotope analysis". *Rapid communications in mass spectrometry : RCM* 25.19, pp. 2828–2836. DOI: 10.1002/rcm.5172.

Macedo de Paula-Santos, G., M. Babinski, F. Wilckens, and A. Meixner (2017). "The Li and Mg isotope record of the carbonate rocks of the Bambuí Goup, Sao Francisco Basin, Brazil (Dissertation)". Sao Paulo.

Machel, H. G. (1985). "Cathodoluminescence in Calcite and Dolomite and Its Chemical Interpretation". *Geoscience Canada* 12.4, pp. 139–147.

Machel, H. G., R. A. Mason, A. N. Mariano, and A. Mucci (1991). "Causes and emission of luminescence in calcite and dolomite". *Luminescence Microscopy and Spectroccopy: Qualitative and Quantitative Applications.* Ed. by C. E. Barker and O. C. Kopp. Tulsa: Society for Sedimentary Geology, pp. 9–25.

McArthur, J. M., D. Donovan, M. F. Thirlwall, B. W. Fouke, and D. Mattey (2000). "Strontium isotope profile of the early Toarcian (Jurassic) oceanic anoxic event, the duration of ammonite biozones, and belemnite palaeotemperatures". *Earth and Planetary Science Letters* 179.2, pp. 269–285. DOI: 10.1016/S0012-821X(00)00111-4.

McArthur, J. M., M. F. Thirlwall, M. Chen, A. S. Gale, and W. J. Kennedy (1993a). "Strontium isotope stratigraphy in the Late Cretaceous: Numerical calibration of the Sr isotope curve and intercontinental correlation for the campanian". *Paleoceanography* 8.6, pp. 859–873. DOI: 10.1029/93PA02324.

McElwain, J. C., J. Wade-Murphy, and S. P. Hesselbo (2005). "Changes in carbon dioxide during an oceanic anoxic event linked to intrusion into Gondwana coals". *Nature* 435.7041, pp. 479–482. DOI: 10.1038/nature03618.

Mii, H.-S. and E. L. Grossman (1994). "Late Pennsylvanian seasonality reflected in the ^{18}O and elemental composition of a brachiopod shell". *Geology* 22.7, p. 661. DOI: 10.1130/0091-7613(1994)022{\textless}0661:LPSRIT{\textgreater}2.3.CO;2.

Montañez, I. P., J. L. Banner, D. A. Osleger, L. E. Borg, and P. J. Bosserman (1996). "Integrated Sr isotope variations and sea-level history of Middle to Upper Cambrian platform carbonates: Implications for the evolution of Cambrian seawater ^{87}Sr/^{86}Sr". *Geology* 24.10, p. 917. DOI: 10.1130/0091-7613(1996)024{\textless}0917:ISIVAS{\textgreater}2.3.CO;2.

Moriguti, T. and E. Nakamura (1998). "High-yield lithium separation and the precise isotopic analysis for natural rock and aqueous samples". *Chemical Geology* 145.1-2, pp. 91–104. DOI: 10.1016/S0009-2541(97)00163-0.

Nakamura, E., T. Ishikawa, and Birck, J-L., Allègre, C.J. (1992). "Precise boron isotopic

analysis of natural rock samples using a boron-mannitol complex". *Chemical Geology* 94, pp. 193–204.

Nir, O., A. Vengosh, J. S. Harkness, G. S. Dwyer, and O. Lahav (2015). "Direct measurement of the boron isotope fractionation factor: Reducing the uncertainty in reconstructing ocean paleo-pH". *Earth and Planetary Science Letters* 414, pp. 1–5. DOI: 10.1016/j.epsl.2015.01.006.

Noireaux, J., V. Mavromatis, J. Gaillardet, J. Schott, V. Montouillout, P. Louvat, C. Rollion-Bard, and D. R. Neuville (2015). "Crystallographic control on the boron isotope paleo-pH proxy". *Earth and Planetary Science Letters* 430, pp. 398–407. DOI: 10.1016/j.epsl.2015.07.063.

Ogg, J. G., F. M. Gradstein, and G. Ogg (2016). *A concise geologic time scale 2016*. Amsterdam, Netherlands: Elsevier. URL: http://search.ebscohost.com/login.aspx?direct=true&scope=site&db=nlebk&AN=1218972.

Ohde, S. and H. Elderfield (1992). "Strontium isotope stratigraphy of Kita-daito-jima Atoll, North Philippine Sea: Implications for Neogene sea-level change and tectonic history". *Earth and Planetary Science Letters* 113.4, pp. 473–486. DOI: 10.1016/0012-821X(92)90125-F.

Ohnemueller, F., A. R. Prave, A. E. Fallick, and S. A. Kasemann (2014). "Ocean acidification in the aftermath of the Marinoan glaciation". *Geology* 42.12, pp. 1103–1106. DOI: 10.1130/G35937.1.

Oi, T., T. Tsukamoto, H. Akai, H. Kakihana, and M. Hosoe (1988). "Boron isotope separation by ion-exchange chromatography using an anion-exchange resin in halide forms". *Journal of Chromatography A* 450.3, pp. 343–352. DOI: 10.1016/S0021-9673(01)83589-5.

Opfergelt, S., K. W. Burton, R. B. Georg, A. J. West, R. A. Guicharnaud, B. Sigfusson, C. Siebert, S. R. Gislason, and A. N. Halliday (2014). "Magnesium retention on the soil exchange complex controlling Mg isotope variations in soils, soil solutions and vegetation in volcanic soils, Iceland". *Geochimica et Cosmochimica Acta* 125, pp. 110–130. DOI: 10.1016/j.gca.2013.09.036.

Palmer, M. R., A. J. Spivack, and J. M. Edmond (1987). "Temperature and pH controls over isotopic fractionation during adsorption of boron on marine clay". *Geochimica et Cosmochimica Acta* 51.9, pp. 2319–2323. DOI: 10.1016/0016-7037(87)90285-7.

Palmer, Pearson, and Cobb (1998). "Reconstructing past ocean pH-depth profiles". *Science (New York, N.Y.)* 282.5393, pp. 1468–1471. DOI: 10.1126/science.282.5393.1468.

Paris, G., A. Bartolini, Y. Donnadieu, V. Beaumont, and J. Gaillardet (2010). "Investigating boron isotopes in a middle Jurassic micritic sequence: Primary vs. diagenetic signal". *Chemical Geology* 275.3-4, pp. 117–126. DOI: 10.1016/j.chemgeo.2010.03.013.

Pearson, P. N. and M. R. Palmer (2000). "Atmospheric carbon dioxide concentrations over the past 60 million years". *Nature* 406.6797, pp. 695–699. DOI: 10.1038/35021000.

Penman, D. E., B. Hönisch, E. T. Rasbury, N. G. Hemming, and H. J. Spero (2013). "Boron, carbon, and oxygen isotopic composition of brachiopod shells: Intra-shell variability, controls, and potential as a paleo-pH recorder". *Chemical Geology* 340, pp. 32–39. DOI: 10.1016/j.chemgeo.2012.11.016.

Percival, L., M. Witt, T. A. Mather, M. Hermoso, H. C. Jenkyns, S. P. Hesselbo, A. H. Al-Suwaidi, M. S. Storm, W. Xu, and M. Ruhl (2015). "Globally enhanced mercury deposition during the end-Pliensbachian extinction and Toarcian OAE: A link to the Karoo–Ferrar Large Igneous Province". *Earth and Planetary Science Letters* 428, pp. 267–280. DOI: 10.1016/j.epsl.2015.06.064.

Pin, C. and C. Bassin (1992). "Evaluation of a strontium-specific extraction chromatographic method for isotopic analysis in geological materials". *Analytica Chimica Acta* 269.2, pp. 249–255. DOI: 10.1016/0003-2670(92)85409-Y.

Pingitore, N. E. (1978). "The behavior of Zn2+ and Mn2+ during carbonate diagenesis: Theory and applications". *Journal of Sedimentary Petrology* 48.3, pp. 799–814.

Pogge von Strandmann, P. A. E., H. C. Jenkyns, and R. G. Woodfine (2013). "Lithium isotope evidence for enhanced weathering during Oceanic Anoxic Event 2".

Nature Geoscience 6.8, pp. 668–672. DOI: 10.1038/NGEO1875.

Pogge von Strandmann, P. A., T. Elliott, H. R. Marschall, C. Coath, Y.-J. Lai, A. B. Jeffcoate, and D. A. Ionov (2011). "Variations of Li and Mg isotope ratios in bulk chondrites and mantle xenoliths". *Geochimica et Cosmochimica Acta* 75.18, pp. 5247–5268. DOI: 10.1016/j.gca.2011.06.026.

Pogge von Strandmann, P. A., W. T. Fraser, S. J. Hammond, G. Tarbuck, I. G. Wood, E. H. Oelkers, and M. J. Murphy (2019a). "Experimental determination of Li isotope behaviour during basalt weathering". *Chemical Geology*. DOI: 10.1016/j.chemgeo.2019.04.020.

Pogge von Strandmann, P. A., S. Opfergelt, Y.-J. Lai, B. Sigfússon, S. R. Gislason, and K. W. Burton (2012). "Lithium, magnesium and silicon isotope behaviour accompanying weathering in a basaltic soil and pore water profile in Iceland". *Earth and Planetary Science Letters* 339-340, pp. 11–23. DOI: 10.1016/j.epsl.2012.05.035.

Pogge von Strandmann, P. A., D. N. Schmidt, N. J. Planavsky, G. Wei, C. L. Todd, and K.-H. Baumann (2019b). "Assessing bulk carbonates as archives for seawater Li isotope ratios". *Chemical Geology* 530, p. 119338. DOI: 10.1016/j.chemgeo.2019.119338.

Rae, J. W., G. L. Foster, D. N. Schmidt, and T. Elliott (2011). "Boron isotopes and B/Ca in benthic foraminifera: Proxies for the deep ocean carbonate system". *Earth and Planetary Science Letters* 302.3-4, pp. 403–413. DOI: 10.1016/j.epsl.2010.12.034.

Roy, R. N., L. N. Roy, M. Lawson, K. M. Vogel, C. Porter Moore, W. Davis, and F. J. Millero (1993). "Thermodynamics of the dissociation of boric acid in seawater at S = 35 from 0 to 55°C". *Marine Chemistry* 44.2-4, pp. 243–248. DOI: 10.1016/0304-4203(93)90206-4.

Schwarcz, H. P., E. K. Agyei, and C. C. McMullen (1969). "Boron isotopic fractionation during clay adsorption from sea-water". *Earth and Planetary Science Letters* 6.1, pp. 1–5. DOI: 10.1016/0012-821X(69)90084-3.

Spivack, A. J., C.-F. You, and H. J. Smith (1993). "Foraminiferal boron isotope ratios as a proxy for surface ocean pH over the past 21 Myr". *Nature* 363.6425, pp. 149–151. DOI: 10.1038/363149a0.

Strelow, F. W. E. (1960). "An Ion Exchange Selectivity Scale of Cations Based on Equilibrium Distribution Coefficients". *Analytical Chemistry* 32.9, pp. 1185–1188. DOI: 10.1021/ac60165a042.

Strelow, F. W. E., R. Rethemeyer, and C. J. C. Bothma (1965). "Ion Exchange Selectivity Scales for Cations in Nitric Acid and Sulfuric Acid Media with a Sulfonated Polystyrene Resin". *Analytical Chemistry* 37.1, pp. 106–111. DOI: 10.1021/ac60220a027.

Svensen, H., F. Corfu, S. Polteau, Ø. Hammer, and S. Planke (2012). "Rapid magma emplacement in the Karoo Large Igneous Province". *Earth and Planetary Science Letters* 325-326, pp. 1–9. DOI: 10.1016/j.epsl.2012.01.015.

Swart, P. K. and G. Eberli (2005). "The nature of the δ^{13}C of periplatform sediments: Implications for stratigraphy and the global carbon cycle". *Sedimentary Geology* 175.1-4, pp. 115–129. DOI: 10.1016/j.sedgeo.2004.12.029.

Teng, F.-Z. (2017). "Magnesium Isotope Geochemistry". *Reviews in Mineralogy and Geochemistry* 82.1, pp. 219–287. DOI: 10.2138/rmg.2017.82.7.

Tipper, E. T., A. Galy, J. Gaillardet, M. Bickle, H. Elderfield, and E. Carder (2006). "The magnesium isotope budget of the modern ocean: Constraints from riverine magnesium isotope ratios". *Earth and Planetary Science Letters* 250.1-2, pp. 241–253. DOI: 10.1016/j.epsl.2006.07.037.

Tipper, E. T., J. Gaillardet, P. Louvat, F. Capmas, and A. F. White (2010). "Mg isotope constraints on soil pore-fluid chemistry: Evidence from Santa Cruz, California". *Geochimica et Cosmochimica Acta* 74.14, pp. 3883–3896. DOI: 10.1016/j.gca.2010.04.021.

Ullmann, C. V., R. Boyle, L. V. Duarte, S. P. Hesselbo, S. A. Kasemann, T. Klein, T. M. Lenton, V. Piazza, and M. Aberhan (2020). "Warm afterglow from the Toarcian Oceanic Anoxic Event drives the success of deep-adapted brachiopods". *Scientific reports* 10.6549. DOI: 10.1038/s41598-020-63487-6.

Val, J., B. Bádenas, M. Aurell, and I. Rosales (2017). "Cyclostratigraphy and

chemostratigraphy of a bioclastic storm-dominated carbonate ramp (late Pliensbachian, Iberian Basin)". *Sedimentary Geology* 355, pp. 93–113. DOI: 10.1016/j.sedgeo.2017.04.007.

Vogel, J. C. (1959). "Über den Isotopengehalt des Kohlenstoffs in Süsswasser Kalkablagerungen". *Geochimica et Cosmochimica Acta* 16, pp. 236–245.

Walkden, G. M. and J. R. Berry (1984). "Syntaxial overgrowth in muddy crinoidal limestones: cathodoluminescence sheds new light on an old problem". *Sedimentology* 31, pp. 251–267.

Wang, B.-S., C.-F. You, K.-F. Huang, S.-F. Wu, S. K. Aggarwal, C.-H. Chung, and P.-Y. Lin (2010). "Direct separation of boron from Na- and Ca-rich matrices by sublimation for stable isotope measurement by MC-ICP-MS". *Talanta* 82.4, pp. 1378–1384. DOI: 10.1016/j.talanta.2010.07.010.

Wang, W., T. Qin, C. Zhou, S. Huang, Z. Wu, and F. Huang (2017). "Concentration effect on equilibrium fractionation of Mg-Ca isotopes in carbonate minerals: Insights from first-principles calculations". *Geochimica et Cosmochimica Acta* 208, pp. 185–197. DOI: 10.1016/j.gca.2017.03.023.

Wimpenny, J., R. H. James, K. W. Burton, A. Gannoun, F. Mokadem, and S. R. Gíslason (2010). "Glacial effects on weathering processes: New insights from the elemental and lithium isotopic composition of West Greenland rivers". *Earth and Planetary Science Letters* 290.3-4, pp. 427–437. DOI: 10.1016/j.epsl.2009.12.042.

Wimpenny, J., Q.-z. Yin, D. Tollstrup, L.-W. Xie, and J. Sun (2014). "Using Mg isotope ratios to trace Cenozoic weathering changes: A case study from the Chinese Loess Plateau". *Chemical Geology* 376, pp. 31–43. DOI: 10.1016/j.chemgeo.2014.03.008.

Xiao, J., Z. d. Jin, Y. k. Xiao, and M. y. He (2014). "Controlling factors of the δ^{11}B-pH proxy and its research direction". *Environmental Earth Sciences* 71.4, pp. 1641–1650. DOI: 10.1007/s12665-013-2568-8.

Young, E. D. and A. Galy (2004). "The Isotope Geochemistry and Cosmochemistry of Magnesium". *Reviews in Mineralogy and Geochemistry* 55.1, pp. 197–230. DOI: 10.2138/gsrmg.55.1.197.

Zeebe, R. E. (2005). "Stable boron isotope fractionation between dissolved $B(OH)_3$ and $B(OH)_4$". *Geochimica et Cosmochimica Acta* 69.11, pp. 2753–2766. DOI: 10.1016/j.gca.2004.12.011.

Chapter 3

A comparative study on seawater pH changes during the T-OAE (Early Jurassic) with boron isotopes

T. Klein[1], A. Meixner[1], C.V. Ullmann[2], L.V. Duarte[3], S.A. Kasemann[1], R.A. Wood[4]

[1] University of Bremen, MARUM – Center for Marine Environmental Sciences and Faculty of Geosciences, 28359 Bremen, Germany

[2] University of Exeter, Global Systems Institute, College of Life and Environment, Exeter EX4 4QE, United Kingdom

[3] MARE & University of Coimbra, 3030-790 Coimbra, Portugal

[4] School of Geosciences, University of Edinburgh, West Mains Road, Edinburgh EH9 3FE, United Kingdom

Contributions to this manuscript:

I, Tina Klein, the first author of this manuscript, have contributed to this manuscript the following:

- Sample preparation of all micritic carbonates (see chapter 4, section 2.3)

- Boron isotope preparation and measurements on all micritc carbonates and fossil shell materials (the shell material was provided by the co-author Clemens V. Ullmann)

- Interpretation of the boron isotopic data partially together with co-authors

- Preparation of this manuscript

3. A comparative study on seawater pH changes during the T-OAE (Early Jurassic) with boron isotopes

3.1. Abstract

Reconstructing past seawater pH changes with boron isotopes (δ^{11}B) on different archives has been the focus of several studies for many years, with brachiopods being regarded as a good archive. We present high-resolution δ^{11}B records for two carbonate transects located on opposite margins of the Iberian Massif during the Toarcian Oceanic Anoxic Event (T-OAE), a time interval where ocean acidification triggered by a rapid and massive CO_2 injection is suggested. We compare δ^{11}B generated on inorganic micritic carbonates with biogenic carbonate shell material from brachiopods and bivalves, as well as give the first direct evidence for a seawater pH drop during the T-OAE. Because the pH decline is only concise in the micritic carbonates this leaves the question of the liability of biogenic carbonates as pH recorders.

3.2. Introduction

The Toarcian Oceanic Anoxic Event (T-OAE, $\sim$183 Ma; Early Jurassic) records an episode that is not only characterized by widespread anoxic conditions of the oceans (Jenkyns, 2010), but also a second-order extinction event and severe assemblage changes of pelagic and benthic organisms (e.g. Benton, 1995; Danise et al., 2019; Piazza et al., 2019). The environmental and biological crisis is linked to pulses of rapid intrusive volcanism and contact metamorphism of the Karoo–Ferrar large igneous province (Burgess et al., 2015; Elliot, 2013; Percival et al., 2015) that lead to pCO$_2$ concentrations of at least 2–4 times higher than pre-industrial levels (Dera and Donnadieu, 2012; Ullmann et al., 2020). The rise in volcanogenic CO_2, together with the release of methane from the dissociation of marine clathrates (McElwain et al., 2005; Svensen et al., 2012), is also noticed in the globally recognised negative carbon isotope excursion (CIE) during the T-OAE with an evidenced drop of $\sim$3–9‰ (e.g. Danise et al., 2019; Kemp et al., 2005; Suan et al., 2011) and a recently calibrated duration of 300–900 kyr (Boulila et al., 2014; Percival et al., 2016). Hence, global elevated atmospheric temperatures of $\sim$5°C for the mid-latitudes (Dera and Donnadieu, 2012) and 3–7°C for seawater temperatures (Suan et al., 2010; Ullmann et al., 2020) were the result. Another suggested effect of a rapid input of CO_2 in the atmosphere–ocean system at the onset of the T-OAE is a consequential ocean acidification event, which has been assumed for quite some time (Beerling and Brentnall, 2007; Hermoso et al., 2009; Kemp et al., 2005). Indications exist in the form of a carbonate production crisis that is evidenced by the size reduction in marine calcifying organisms (Mattioli and Pittet, 2002; Suan et al., 2008), a decrease in the carbonate accumulation rate and thus reduced seawater carbonate saturation (Hermoso et al., 2012; Mattioli et al., 2004, 2009; Suan

et al., 2008), and the near disappearance of shallow-water platforms (Dromart et al., 1996; Trecalli et al., 2012). Moreover, the extinction was especially selective against marine calcifying organisms like corals, bivalves and unbuffered organisms (Kiessling and Simpson, 2011; Trecalli et al., 2012). With this study we deliver (1) the direct evidence for a seawater pH drop during the T-OAE, (2) show that brachiopods do not act as a good archive for reconstructions of pH changes and (3) present the first data set yet available for boron isotopes on fossil bivalves.

3.3. Materials and Methods

To test for a possible seawater pH drop during the T-OAE we generated two boron isotope (δ^{11}B) profiles on marine micritic carbonates from shallow water environments for two sections: Rabaçal/Fonte Coberta (R/FC) in Portugal, and Barranco de la Cañada (BdC) in Spain, each located in the former Lusitanian (LB) and Iberian Basin (IB) in the NW Tethys, respectively (Fig. 9, supplement/ see section 1.4). Additionally, shell material from well preserved rhynchonellid brachiopods and bivalves (oyster: *Gryphaea*)(from Ullmann et al., 2020) was analysed for their boron isotopic composition in order to assess their application as proxies for past seawater pH changes. For both successions the biozonation is well defined so that the ammonite stratigraphy together with the distinct carbon isotope (δ^{13}C) and ^{87}Sr/^{86}Sr isotope curves are used for age model constraints (supplement/see chapter 2, section 2.2).

3.4. Results

Sampling intervals reached from the latest Pliensbachian *margaritatus* ammonoid zone (AZ) to the mid-Toarcian *bifrons* AZ and analysed δ^{13}C$_{micrite}$ isotopes retrace the CIE characteristic for the T-OAE (Fig. 9). Values for R/FC range between 0.85 and 4.30 ‰ , for BdC between -0.13 and 3.91 ‰ and plot well with the published data for the corresponding brachiopod and oyster δ^{13}C as well as published bulk rock data for each basin (for discussion see supplement/ section 2.7.2). The analogous δ^{11}B$_{micrite}$ values show similar values for pre- and post-boron isotope excursion (BIE) times at both sections with in mean 15.38 $\pm$ 0.7 ‰ (1sd, n=8) for R/FC and 12.88 $\pm$ 0.7 ‰ (1sd, n=10) for BdC (Fig. 9), the offset between both basins probably being a cause of regional differences. A gradual decrease during the T-OAE can be observed with a reduction of 5.5 ‰ for R/FC and 3.7 ‰ for BdC, indicating a decline in seawater pH for both basins. Minimum δ^{11}B$_{micrite}$ values are 9.92 and 9.14 ‰ for R/FC and BdC respectively. In contrast, the δ^{11}B$_{brachiopod}$ show a different signature with rather stable boron isotopes of in mean 13.7 $\pm$ 0.4 ‰ (1sd, n=22) for BdC and 14.1 $\pm$ 0.7 ‰ (1sd, n=5) for R/FC even during the T-OAE. For the oysters we see a similar pattern with only a slight offset from the brachiopods and mean δ^{11}B of 12.3 $\pm$ 0.4 ‰ (1sd, n=13).

3.5. Discussion

For the reconstruction of seawater pH the δ^{11}B–pH relationship has often been applied (e.g. Clark-son et al., 2015; Sosdian et al., 2018), whereas the fractionation factor of B (α_B) into marine calcites is still a matter of debate (see supplement/ section 1.2). The widely accepted empirical value from Klochko et al., 2006 is still used in modern studies and hence also applied in this study for better comparison. Calculating the past seawater pH with our generated δ^{11}B$_{micrite}$ data (20°C and 35 psu) reveals a drop of 0.4–0.6 in the pH value during the T-OAE interval for R/FC and BdC, respectively, and strongly depending on the pH reconstruction scenarios (see supplement/ chapter 2, section 2.9; Fig. 10). Relying on which pH value was present prior to the T-OAE, such a drop could be accounted for an acidification event. As the Early Jurassic δ^{11}B composition of the seawater is not known, but mandatory for absolute pH calculations, we are only able to constrain the relative drop in seawater pH in this study.

   The onset of the decline in δ^{11}B is latest during the *polymorphum* AZ, and thus prior to the defined boundary of the T-OAE as shown for R/FC, commencing concurrently with the abrupt rise in atmospheric CO_2 concentrations (Fig. 8). For BdC a timing for the onset cannot be resolved due to the lack of proper sample material. However, a concordant gradual decline in seawater pH during the T-OAE interval for both basins is observed, while the ending of the pH decline is decoupled with R/FC returning earlier to pre-T-OAE conditions than BdC. While both sections are located around the Iberian Massif, they are still situated on opposite margins (Fig. 9), which could nonetheless lead to differences in weathering intensities, bathymetries, sedimentation rates, and water temperatures. As influences of water-depth and temperature can be ruled out in this case (see supplement/ section 2.7), and sedimentation rates were comparable in both basins (Gahr, 2005) varying weathering intensities coupled with basin restrictions can be accounted for a possible mechanism. Through the intensification of continental weathering, ocean alkalinity is elevated and enables the buffering of a lowered seawater pH (e.g. Hönisch et al., 2012; Kasemann et al., 2014). Several studies already suggested an enhanced discharge from the continents during the T-OAE, with varying magnitudes of 3 times stronger weathering rates from the eastern margin of the Panthalassa Ocean (Them et al., 2017) and the northern parts of the NW Tethys (Percival et al., 2016), whereas 5 times stronger fluxes were reconstructed for the LB (Brazier et al., 2015). Corresponding data sets are up to date lacking for the IB, however as different rates for weathering fluxes throughout the NW Tethys region exist, lower fluxes than reported in the LB can also be assumed for the IB affecting the relatively longer recovery time for the seawater pH level, which is nonetheless in accordance with the long duration of the raised CO_2 levels (9). Therefore, the higher reconstructed weathering rates for the LB, together with a probable basin restriction (for further discussion see section 4.5.4) could be a driver for the observed faster seawater pH recovery.
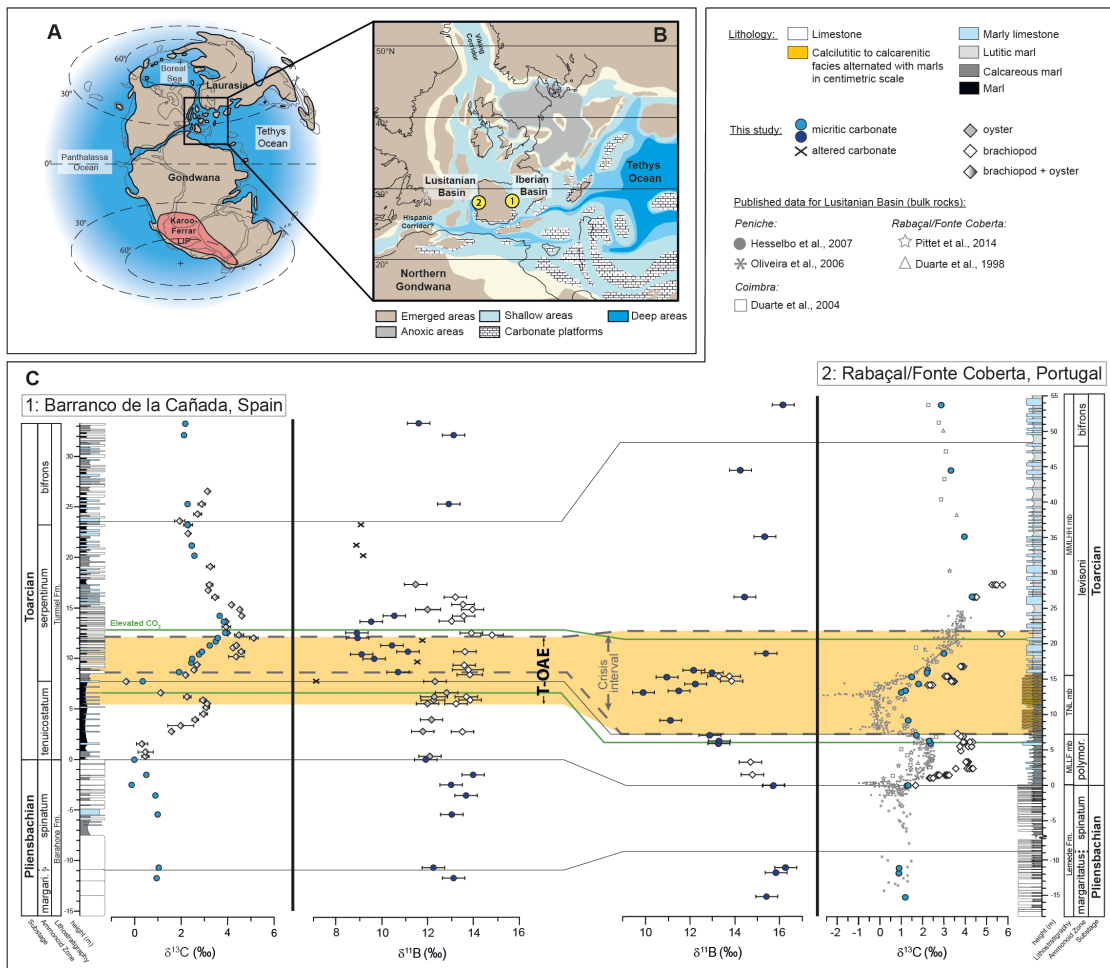
Figure 9. (A) Paleogeographic reconstruction for the Early Jurassic (∼180 Ma) (modified after Dera et al., 2011; Korte et al., 2015) showing the position of the NW Tethys realm (B) Enlarged section of the NW Tethys showing the locations of the two sampled sections on the Iberian Massif, Barranco de la Cañada (BdC) (1) and Rabaçal /Fonte Coberta (R/FC) (2) (modified after Bassoulet et al., 1993; Ruebsam et al., 2018) (C) Generated boron and carbon isotope data for both sections with long-term external reproducibility (2sd) of ± 0.5 ‰ for δ^{11}B, for δ^{13}C ± 0.03 ‰ for R/FC and ± 0.04 ‰ for BdC samples are plotted. Brachiopod and oyster carbon isotope data, the T-OAE interval (orange colored area), the crisis interval (dashed line), and the interval of elevated CO_2 (green lines) as published by Piazza et al., 2019, 2020; Ullmann et al., 2020. For better comparability of the CIE at R/FC reported data for the Lusitanian Basin are plotted from literature by Duarte, 1998; Duarte et al., 2004; Hesselbo et al., 2007; Oliveira et al., 2006; Pittet et al., 2014. δ^{11}B values for the altered carbonates are depicted as crosses but were not taken into account for interpretation (for further information see supplement/ chapter 2, section 2.7). Lithological log from BdC modified after Gahr, 2002 and for R/FC after Duarte, 1995; Paredes et al., 2016. *[High-resolution image on attached CD]*

An additional fact is that at both sections the seawater pH drops not only fall in line with elevated CO_2 concentrations, but also the defined crisis intervals (Ullmann et al., 2020) (Fig. 8), which mark the inception of the extinction horizon and severe assemblage changes with the solely occurrence of the opportunistic brachiopod *Soaresirhynchia* (Piazza et al., 2019; Ullmann et al.,

2020). This finding indicates that the drop in seawater pH might be accounted for a kill mechanism, together with global warming, ocean deoxygenation and changes in nutrient cycling termed as the "deadly quartet" (Bijma et al., 2013; Piazza et al., 2019). This term describes the coupling of those four stressors, which usually occurred during past mass extinction events (Jenkyns, 2010), and was also suggested for the T-OAE (see above).

A further matter not yet resolved is the B fractionation during biogenic carbonate precipitation for brachiopods and bivalves. Fossil brachiopods are often used for isotope analyses as they are regarded to confidently preserve their original chemistry in their secondary shell layer despite post-depositional processes, owing to the robustness of their low-magnesium calcite shell against such influences (e.g. Brand et al., 2012; Brand and Veizer, 1980, 1981; Brand et al., 2003). Rhynchonellid brachiopods are the favoured brachiopod order for geochemical analyses because their secondary shell material is in equilibrium with the ambient seawater, and furthermore the geochemical signature is not altered by vital effects (Brand et al., 2013; Ullmann et al., 2017). Only a few studies addressed the potential use of brachiopods as pH tracers up to date (Joachimski et al., 2005; Jurikova et al., 2019; Lécuyer et al., 2002; Penman et al., 2013), however none of them included rhynchonellid brachiopods. Three of those studies investigated the fractionation of B between the brachiopod shell and seawater, with each study concluding in different relations of the pH and B incorporation (Fig. 10). However, what those studies agree on is the reduced δ^{11}B sensitivity against pH changes in brachiopods (Jurikova et al., 2019; Penman et al., 2013) compared to the empirical aqueous fractionation in marine carbonates predicted by Klochko et al., 2006, and that they reveal vital effects by altering the incorporated ambient seawater δ^{11}B signature into their shell (Jurikova et al., 2019; Penman et al., 2013). Despite all the uncertainties, the studies speak for the use of brachiopod derived δ^{11}B as a mean to reconstruct past seawater pH changes, but suggest focusing on a single species or cross-calibrating coeval species.

Although we were not able to stick to a single species of brachiopods for our study, as the assemblage changes were too severe at both sections, we nevertheless only used rhynchonellid brachiopods to ensure the best possible results. Interestingly, our data set of δ^{11}B$_{brachipod}$ stands in stark contrast to the BIE visible in the micrites, since they do not record this event (Fig. 9). Nevertheless, the δ^{11}B$_{brachipod}$ data have a scatter of about 2 ‰, which could reflect the seawater pH drop in terms of their reduced sensitivity (Fig. 10). On the other hand, Jurikova et al., 2019 suggested that the secondary layer reflects a mixed signal of the internal calcifying fluid and that of the ambient seawater. Yet, what speaks against it is that the δ^{11}B$_{brachipod}$ values fall into the same range as the δ^{11}B$_{micrite}$ prior and after the T-OAE interval. Also, if an alteration by the internal fluid would be given lower δ^{11}B values would be expected as pH measurements of the fluid on modern species revealed low values of 7.8 (Jurikova et al., 2019), assuming past brachiopods precipitated their shell at the same level or below that of seawater pH. But, if we consider recording
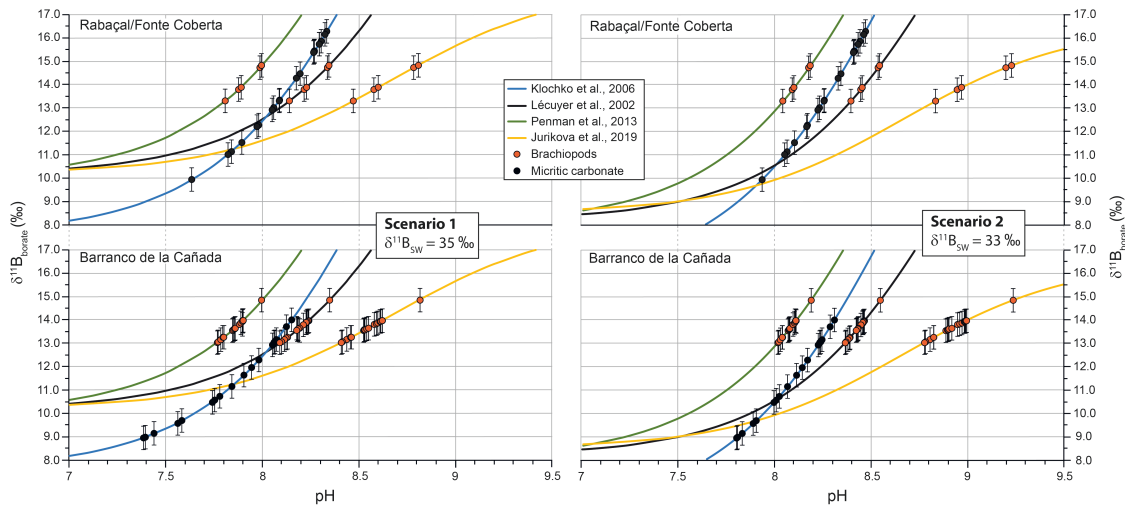
Figure 10. Two scenarios for a seawater pH reconstruction with biogenic and abiogenic carbonate B fractionation approaches. Curves and generated data are plotted for varying $\delta^{11}B_{SW}$, 20°C and 35 psu, imitating two possible scenarios for the Early Jurassic ocean conditions (for details see supplement/ chapter 2, section 2.9). The three different brachiopod fractionation curves for boron including the analysed $\delta^{11}B$ data from this study are displayed. For comparison the empirical fractionation curve for marine carbonates including the micritic $\delta^{11}B$ data is plotted. The curve from Penman et al., 2013 includes a species specific offset that was calculated for a different brachiopod species than used in this study, but owing to the absence of a calculated offset for our species and only for comparison matters we plotted our data on their curve. *[High-resolution image on attached CD]*

the internal fluid $\delta^{11}B$ this would mean that we need to adjust our $\delta^{11}B_{micrite}$ pH reconstructions (supplement/ chapter 2, section 2.9; Fig. 10).

Besides, when comparing the different fractionation curves with our generated boron data in micrites and brachiopods (Fig. 10) the very alkaline reconstructed seawater pH of above 9 for the curve of Jurikova et al., 2019 is very unlikely and does not speak for the uniformity of their curve and the application of such on pH reconstructions. In contrast, the curves from Penman et al., 2013 and Lécuyer et al., 2002 plot closer to the empirical carbonate curve from Klochko et al., 2006, still both curves show a minor drop in pH by contrast to the study from Jurikova et al., 2019.

For bivalves up to date no study on the incorporation of boron into their shell in relation to the ambient seawater pH exists. A recent study from Sutton et al., 2018 reported the first $\delta^{11}B$ data available for the modern oyster species *C. virginica* with a value of 16.03‰ at a seawater pH of 8.2, and hence not falling on the pH curve from Klochko et al., 2006. Our firstly reported $\delta^{11}B$ on fossil oysters show a mean value of 12.3‰ and thus heavier isotopic composition as the according micrites. Lacking appropriate data during the T-OAE interval, we are unfortunately not able to assess if oysters were able to record the change in seawater pH as evident in the micrites. Nonetheless, as our $\delta^{11}B_{oyster}$ values are still not in accordance with the micrite values, they also fall below the empirical pH curve from Klochko et al., 2006. Thus, our findings indicate that the

incorporation of boron into the bivalve shell is likewise more complex and in need of clearance.

3.6. Conclusions

The T-OAE was a time of extreme environmental perturbations with a massive input of volcanogenic CO_2 that lead to a seawater pH drop as evidenced with $\delta^{11}B$ isotopes on marine carbonates for two basins. The magnitude of the pH drop is matter of current models and will clarify if we can speak of an acidification event. Despite this, the BIE is not recorded in brachiopod or bivalve shells, stressing the point for more research in this area.

3.7. Acknowledgements

References

Bassoulet, J. P., S. Elmi, A. Poisson, F. Cecca, Y. Bellion, R. Guiraud, and F. Baudin (1993). "Middle Toarcian (184-182 Ma)". *Atlas Tethys Paleoenvironmental Maps*. Ed. by J. Dercourt, L. E. Ricou, and B. Vrielynck. Gauthier-Villars, Paris, pp. 63–80.

Beerling, D. J. and S. J. Brentnall (2007). "Numerical evaluation of mechanisms driving Early Jurassic changes in global carbon cycling". *Geology* 35.3, p. 247. DOI: 10.1130/G23416A.1.

Benton, M. J. (1995). "Diversification and extinction in the history of life". *Science (New York, N.Y.)* 268.5207, pp. 52–58. DOI: 10.1126/science.7701342.

Bijma, J., H.-O. Portner, C. Yesson, and A. D. Rogers (2013). "Climate change and the oceans–what does the future hold?" *Marine pollution bulletin* 74.2, pp. 495–505. DOI: 10.1016/j.marpolbul.2013.07.022.

Boulila, S., B. Galbrun, E. Huret, L. A. Hinnov, I. Rouget, S. Gardin, and A. Bartolini (2014). "Astronomical calibration of the Toarcian Stage: Implications for sequence stratigraphy and duration of the early Toarcian OAE". *Earth and Planetary Science Letters* 386, pp. 98–111. DOI: 10.1016/j.epsl.2013.10.047.

Brand, U., G. Jiang, K. Azmy, J. Bishop, and I. P. Montañez (2012). "Diagenetic evaluation of a Pennsylvanian carbonate succession (Bird Spring Formation, Arrow Canyon, Nevada, U.S.A.) — 1: Brachiopod and whole rock comparison". *Chemical Geology* 308-309, pp. 26–39. DOI: 10.1016/j.chemgeo.2012.03.017.

Brand, U. and J. Veizer (1980). "Chemical Diagenesis of a Multicomponent Carbonate System–1: Trace Elements". *SEPM Journal of Sedimentary Research* Vol. 50. DOI: 10.1306/212F7BB7-2B24-11D7-8648000102C1865D.

— (1981). "Chemical Diagenesis of a Multicomponent Carbonate System 2: Stable Isotopes". *Journal of Sedimentary Petrology* 51.3, pp. 987–997.

Brand, U., K. Azmy, M. A. Bitner, A. Logan, M. Zuschin, R. Came, and E. Ruggiero (2013). "Oxygen isotopes and $MgCO_3$ in brachiopod calcite and a new paleotemperature equation". *Chemical Geology* 359,

pp. 23–31. DOI: 10.1016/j.chemgeo.2013.09.014.

Brand, U., A. Logan, N. Hiller, and J. Richardson (2003). "Geochemistry of modern brachiopods: Applications and implications for oceanography and paleoceanography". *Chemical Geology* 198.3-4, pp. 305–334. DOI: 10.1016/S0009-2541(03)00032-9.

Brazier, J.-M., G. Suan, T. Tacail, L. Simon, J. E. Martin, E. Mattioli, and V. Balter (2015). "Calcium isotope evidence for dramatic increase of continental weathering during the Toarcian oceanic anoxic event (Early Jurassic)". *Earth and Planetary Science Letters* 411, pp. 164–176. DOI: 10.1016/j.epsl.2014.11.028.

Burgess, S. D., S. A. Bowring, T. H. Fleming, and D. H. Elliot (2015). "High-precision geochronology links the Ferrar large igneous province with early-Jurassic ocean anoxia and biotic crisis". *Earth and Planetary Science Letters* 415, pp. 90–99. DOI: 10.1016/j.epsl.2015.01.037.

Clarkson, M. O., S. A. Kasemann, R. A. Wood, T. M. Lenton, S. J. Daines, S. Richoz, F. Ohnemueller, A. Meixner, S. W. Poulton, and E. T. Tipper (2015). "Ocean acidification and the Permo-Triassic mass extinction". *Science (New York, N.Y.)* 348.6231, pp. 229–232. DOI: 10.1126/science.aaa0193.

Danise, S., M.-E. Clémence, G. D. Price, D. P. Murphy, J. J. Gómez, and R. J. Twitchett (2019). "Stratigraphic and environmental control on marine benthic community change through the early Toarcian extinction event (Iberian Range, Spain)". *Palaeogeography, Palaeoclimatology, Palaeoecology* 524, pp. 183–200. DOI: 10.1016/j.palaeo.2019.03.039.

Dera, G. and Y. Donnadieu (2012). "Modeling evidences for global warming, Arctic seawater freshening, and sluggish oceanic circulation during the Early Toarcian anoxic event". *Paleoceanography* 27.2, pp. 1–15. DOI: 10.1029/2012PA002283.

Dera, G., P. Neige, J.-L. Dommergues, and A. Brayard (2011). "Ammonite paleobiogeography during the Pliensbachian–Toarcian crisis (Early Jurassic) reflecting paleoclimate, eustasy, and extinctions". *Global and Plan-*

etary Change 78.3-4, pp. 92–105. DOI: `10.1016/j.gloplacha.2011.05.009`.

Dromart, G., P. Allemand, J.-P. Garcia, and C. Robin (1996). "Cyclic fluctuation of carbonate production through the Jurassic along a Burgundy-Ardèche cross-section, eastern France". *Bulletin de la Societe Geologique de France* 167, pp. 423–433.

Duarte, L. V. (1995). *O Toarciano da Bacia Lusitaniana. Estratigrafia e evolução sedimentogénica: Ph.D. thesis*. Coimbra, Portugal.

– (1998). "Clay minerals and geochemical evolution in the Toarcian Lower Aalenian of the Lusitanian Basin". *Cuadernos de Geologa Iberica* 24, pp. 69–98.

Duarte, L. V., N. Perilli, R. Dino, R. Rodrigues, and R. Paredes (2004). "Lower to middle Toarcian from the Coimbra region (Lusitanian Basin, Portugal): Sequence stratigraphy, calcareous nannofossils and stable-isotope evolution". *Rivista Italiana di Paleontologia e Stratigrafia* 110.1, pp. 115–127.

Elliot, D. H. (2013). "The geological and tectonic evolution of the Transantarctic Mountains: A review". *Geological Society, London, Special Publications* 381.1, pp. 7–35. DOI: `10.1144/SP381.14`.

Gahr, M. E. (2002). "Palökologie des Makrobenthos aus dem Unter-Toarc SW-Europas: Dissertation". *Beringeria* 31.

– (2005). "Response of Lower Toarcian (Lower Jurassic) macrobenthos of the Iberian Peninsula to sea level changes and mass extinction". *Journal of Iberian Geology* 31.2, pp. 197–215.

Hermoso, M., F. Minoletti, L. Le Callonnec, H. C. Jenkyns, S. P. Hesselbo, R. E. M. Rickaby, M. Renard, M. de Rafélis, and L. Emmanuel (2009). "Global and local forcing of Early Toarcian seawater chemistry: A comparative study of different paleoceanographic settings (Paris and Lusitanian basins)". *Paleoceanography* 24.4, p. 307. DOI: `10.1029/2009PA001764`.

Hermoso, M., F. Minoletti, R. E. Rickaby, S. P. Hesselbo, F. Baudin, and H. C. Jenkyns (2012). "Dynamics of a stepped carbon-isotope excursion: Ultra high-resolution study of Early Toarcian environmental change". *Earth and Planetary Science Let-*

ters 319-320, pp. 45–54. DOI: `10.1016/j.epsl.2011.12.021`.

Hesselbo, S. P., H. C. Jenkyns, L. V. Duarte, and L. C. Oliveira (2007). "Carbon-isotope record of the Early Jurassic (Toarcian) Oceanic Anoxic Event from fossil wood and marine carbonate (Lusitanian Basin, Portugal)". *Earth and Planetary Science Letters* 253.3-4, pp. 455–470. DOI: `10.1016/j.epsl.2006.11.009`.

Hönisch, B. et al. (2012). "The geological record of ocean acidification". *Science (New York, N.Y.)* 335.6072, pp. 1058–1063. DOI: `10.1126/science.1208277`.

Jenkyns, H. C. (2010). "Geochemistry of oceanic anoxic events". *Geochemistry, Geophysics, Geosystems* 11.3, pp. 1–30. DOI: `10.1029/2009GC002788`.

Joachimski, M. M., L. Simon, R. van Geldern, and C. Lécuyer (2005). "Boron isotope geochemistry of Paleozoic brachiopod calcite: Implications for a secular change in the boron isotope geochemistry of seawater over the Phanerozoic". *Geochimica et Cosmochimica Acta* 69.16, pp. 4035–4044. DOI: `10.1016/j.gca.2004.11.017`.

Jurikova, H., V. Liebetrau, M. Gutjahr, C. Rollion-Bard, M. Y. Hu, S. Krause, D. Henkel, C. Hiebenthal, M. Schmidt, J. Laudien, and A. Eisenhauer (2019). "Boron isotope systematics of cultured brachiopods: Response to acidification, vital effects and implications for palaeo-pH reconstruction". *Geochimica et Cosmochimica Acta* 248, pp. 370–386. DOI: `10.1016/j.gca.2019.01.015`.

Kasemann, S. A., P. A. Pogge von Strandmann, A. R. Prave, A. E. Fallick, T. Elliott, and K.-H. Hoffmann (2014). "Continental weathering following a Cryogenian glaciation: Evidence from calcium and magnesium isotopes". *Earth and Planetary Science Letters* 396, pp. 66–77. DOI: `10.1016/j.epsl.2014.03.048`.

Kemp, D. B., A. L. Coe, A. S. Cohen, and L. Schwark (2005). "Astronomical pacing of methane release in the Early Jurassic period". *Nature* 437.7057, pp. 396–399. DOI: `10.1038/nature04037`.

Kiessling, W. and C. Simpson (2011). "On the potential for ocean acidification to be a general cause of ancient reef crises". *Global*

Change Biology 17.1, pp. 56–67. DOI: 10 . 1111/j.1365-2486.2010.02204.x.

Klochko, K., A. J. Kaufman, W. Yao, R. H. Byrne, and J. A. Tossell (2006). "Experimental measurement of boron isotope fractionation in seawater". *Earth and Planetary Science Letters* 248.1-2, pp. 276–285. DOI: 10.1016/j.epsl.2006.05.034.

Korte, C., S. P. Hesselbo, C. V. Ullmann, G. Dietl, M. Ruhl, G. Schweigert, and N. Thibault (2015). "Jurassic climate mode governed by ocean gateway". *Nature communications* 6, p. 10015. DOI: 10 . 1038 / ncomms10015.

Lécuyer, C., P. Grandjean, B. Reynard, F. Albarède, and P. Telouk (2002). "^{11}B/^{10}B analysis of geological materials by ICP–MS Plasma 54: Application to the boron fractionation between brachiopod calcite and seawater". *Chemical Geology* 186.1-2, pp. 45–55. DOI: 10.1016/S0009-2541(01) 00425-9.

Mattioli, E. and B. Pittet (2002). "Contribution of calcareous nannoplankton to carbonate deposition: A new approach applied to the Lower Jurassic of central Italy". *Marine Micropaleontology* 45.2, pp. 175–190. DOI: 10.1016/S0377-8398(02)00039-7.

Mattioli, E., B. Pittet, R. Palliani, H.-J. Röhl, A. Schmid-Röhl, and E. Morettini (2004). "Phytoplankton evidence for the timing and correlation of palaeoceanographical changes during the early Toarcian oceanic anoxic event (Early Jurassic)". *Journal of the Geological Society* 161.4, pp. 685–693. DOI: 10 . 1144/0016-764903-074.

Mattioli, E., B. Pittet, L. Petitpierre, and S. Mailliot (2009). "Dramatic decrease of pelagic carbonate production by nannoplankton across the Early Toarcian anoxic event (T-OAE)". *Global and Planetary Change* 65.3-4, pp. 134–145. DOI: 10.1016/ j.gloplacha.2008.10.018.

McElwain, J. C., J. Wade-Murphy, and S. P. Hesselbo (2005). "Changes in carbon dioxide during an oceanic anoxic event linked to intrusion into Gondwana coals". *Nature* 435.7041, pp. 479–482. DOI: 10 . 1038 / nature03618.

Oliveira, L. C., R. Rodrigues, L. V. Duarte, and V. B. Lemos (2006). "Oil generation potential assessment and paleoenvironmental interpretation based on biomarkers and stable carbon isotopes of the Pliensbachian — lower Toarcian (Lower Jurassic) of the Peniche region (Lusitanian Basin, Portugal)". *B. Geoci. Petrobras* 14.2, pp. 207–234.

Paredes, R., M. J. Comas-Rengifo, and L. V. Duarte (2016). "Passagem Pliensbaquiano-Toarciano: a diversidade de macroinvertebrados antes da extinção". *O Jurássico da região de Penela: novos avanços no conhecimento estratigráfico*. Ed. by L. V. Duarte and S. Sêco, pp. 30–40.

Penman, D. E., B. Hönisch, E. T. Rasbury, N. G. Hemming, and H. J. Spero (2013). "Boron, carbon, and oxygen isotopic composition of brachiopod shells: Intra-shell variability, controls, and potential as a paleo-pH recorder". *Chemical Geology* 340, pp. 32–39. DOI: 10.1016/j.chemgeo.2012.11.016.

Percival, L., A. S. Cohen, M. K. Davies, A. J. Dickson, S. P. Hesselbo, H. C. Jenkyns, M. J. Leng, T. A. Mather, M. S. Storm, and W. Xu (2016). "Osmium isotope evidence for two pulses of increased continental weathering linked to Early Jurassic volcanism and climate change". *Geology* 44.9, pp. 759–762. DOI: 10.1130/G37997.1.

Percival, L., M. Witt, T. A. Mather, M. Hermoso, H. C. Jenkyns, S. P. Hesselbo, A. H. Al-Suwaidi, M. S. Storm, W. Xu, and M. Ruhl (2015). "Globally enhanced mercury deposition during the end-Pliensbachian extinction and Toarcian OAE: A link to the Karoo–Ferrar Large Igneous Province". *Earth and Planetary Science Letters* 428, pp. 267–280. DOI: 10.1016/j.epsl.2015. 06.064.

Piazza, V., L. V. Duarte, J. Renaudie, and M. Aberhan (2019). "Reductions in body size of benthic macroinvertebrates as a precursor of the early Toarcian (Early Jurassic) extinction event in the Lusitanian Basin, Portugal". *Paleobiology* 45.02, pp. 296–316. DOI: 10.1017/pab.2019.11.

Piazza, V., C. V. Ullmann, and M. Aberhan (2020). "Temperature-related body size change of marine benthic macroinvertebrates across the Early Toarcian Anoxic Event". *Scientific Reports* 10.4675, pp. 1–13. DOI: 10.1038/s41598-020-61393-5.

Pittet, B., G. Suan, F. Lenoir, L. V. Duarte, and E. Mattioli (2014). "Carbon isotope evidence for sedimentary discontinuities in the lower Toarcian of the Lusitanian Basin (Por-

tugal): Sea level change at the onset of the Oceanic Anoxic Event". *Sedimentary Geology* 303, pp. 1–14. DOI: 10.1016/j.sedgeo.2014.01.001.

Ruebsam, W., T. Müller, J. Kovács, J. Pálfy, and L. Schwark (2018). "Environmental response to the early Toarcian carbon cycle and climate perturbations in the northeastern part of the West Tethys shelf". *Gondwana Research* 59, pp. 144–158. DOI: 10.1016/j.gr.2018.03.013.

Sosdian, S. M., R. Greenop, M. P. Hain, G. L. Foster, P. N. Pearson, and C. H. Lear (2018). "Constraining the evolution of Neogene ocean carbonate chemistry using the boron isotope pH proxy". *Earth and Planetary Science Letters* 498, pp. 362–376. DOI: 10.1016/j.epsl.2018.06.017.

Suan, G., E. Mattioli, B. Pittet, C. Lécuyer, B. Suchéras-Marx, L. V. Duarte, M. Philippe, L. Reggiani, and F. Martineau (2010). "Secular environmental precursors to Early Toarcian (Jurassic) extreme climate changes". *Earth and Planetary Science Letters* 290.3-4, pp. 448–458. DOI: 10.1016/j.epsl.2009.12.047.

Suan, G., E. Mattioli, B. Pittet, S. Mailliot, and C. Lécuyer (2008). "Evidence for major environmental perturbation prior to and during the Toarcian (Early Jurassic) oceanic anoxic event from the Lusitanian Basin, Portugal". *Paleoceanography* 23.1. DOI: 10.1029/2007PA001459.

Suan, G., B. L. Nikitenko, M. A. Rogov, F. Baudin, J. E. Spangenberg, V. G. Knyazev, L. A. Glinskikh, A. A. Goryacheva, T. Adatte, J. B. Riding, K. B. Föllmi, B. Pittet, E. Mattioli, and C. Lécuyer (2011). "Polar record of Early Jurassic massive carbon injection". *Earth and Planetary Science Letters* 312.1-2, pp. 102–113. DOI: 10.1016/j.epsl.2011.09.050.

Sutton, J. N., Y.-W. Liu, J. B. Ries, M. Guillermic, E. Ponzevera, and R. A. Eagle (2018). "δ^{11}B as monitor of calcification site pH in divergent marine calcifying organisms". *Biogeosciences* 15, pp. 1447–1467. DOI: 10.5194/bg-15-1447-2018.

Svensen, H., F. Corfu, S. Polteau, Ø. Hammer, and S. Planke (2012). "Rapid magma emplacement in the Karoo Large Igneous Province". *Earth and Planetary Science Letters* 325-326, pp. 1–9. DOI: 10.1016/j.epsl.2012.01.015.

Them, T. R., B. C. Gill, A. H. Caruthers, D. R. Gröcke, E. T. Tulsky, R. C. Martindale, T. P. Poulton, and P. L. Smith (2017). "High-resolution carbon isotope records of the Toarcian Oceanic Anoxic Event (Early Jurassic) from North America and implications for the global drivers of the Toarcian carbon cycle". *Earth and Planetary Science Letters* 459, pp. 118–126. DOI: 10.1016/j.epsl.2016.11.021.

Trecalli, A., J. Spangenberg, T. Adatte, K. B. Föllmi, and M. Parente (2012). "Carbonate platform evidence of ocean acidification at the onset of the early Toarcian oceanic anoxic event". *Earth and Planetary Science Letters* 357-358, pp. 214–225. DOI: 10.1016/j.epsl.2012.09.043.

Ullmann, C. V., R. Boyle, L. V. Duarte, S. P. Hesselbo, S. A. Kasemann, T. Klein, T. M. Lenton, V. Piazza, and M. Aberhan (2020). "Warm afterglow from the Toarcian Oceanic Anoxic Event drives the success of deep-adapted brachiopods". *Scientific reports* 10.6549. DOI: 10.1038/s41598-020-63487-6.

Ullmann, C. V., R. Frei, C. Korte, and C. Lüter (2017). "Element/Ca, C and O isotope ratios in modern brachiopods: Species-specific signals of biomineralization". *Chemical Geology* 460, pp. 15–24. DOI: 10.1016/j.chemgeo.2017.03.034.

Chapter 4

Enhanced silicate weathering pulses and Lusitanian basin restrictions during the Early Jurassic (Pliensbachian–Toarcian)

T. Klein[1], A. Meixner[1], L.V. Duarte[2], S.A. Kasemann[1], R.A. Wood[3]

[1] University of Bremen, MARUM – Center for Marine Environmental Sciences and Faculty of Geosciences, 28359 Bremen, Germany

[2] MARE & University of Coimbra, 3030-790 Coimbra, Portugal

[3] School of Geosciences, University of Edinburgh, West Mains Road, Edinburgh EH9 3FE, United Kingdom

Contributions to this manuscript:

I, Tina Klein, the first author of this manuscript, have contributed to this manuscript the following:

- Sample preparation of all micritic carbonates (see chapter 2, section 2.3)

- All lithium and magnesium isotope measurements presented

- Interpretation of data and development of hypotheses

- Preparation of this manuscript

4. Enhanced silicate weathering pulses and Lusitanian basin restrictions during the Early Jurassic (Pliensbachian–Toarcian)

4.1. Abstract

The Pliensbachian–Toarcian boundary and Toarcian Oceanic Anoxic Event (T-OAE) are thought to being triggered by abrupt rises in atmospheric CO_2 from Karoo–Ferrar flood basalt volcanism, which would have implemented Earth's feedback mechanism to draw down the CO_2 amounts with enhanced silicate weathering. Here we present two basins located around the Iberian Massif that show abrupt changes in the δ^7Li isotope signature at both events, supporting earlier studies findings of elevated continental weathering, whereas we are able to specifically trace the silicate weathering part with Li isotopes. We further suggest that the Lusitanian Basin (Portugal) was probably restricted for a short time at both events owing to abrupt sea level falls and a tectonic event that formed effective barriers to prevent open marine circulation. Hence, the Iberian Basin (Spain) is thought to record open marine conditions, whereas more research with Li isotopes in sections within the tethyan or even other realms are recommended to support this idea.

4.2. Introduction

The Early Jurassic Toarcian Oceanic Anoxic Event (T-OAE, $\sim$183 Mya; Jenkyns, 1988; Jenkyns, 2010) is a globally recognised event of widespread anoxic conditions of the oceans that occurred concurrently with the Karoo–Ferrar large igneous province (e.g. Aarnes et al., 2011; Burgess et al., 2015; Elliot and Fleming, 2008; Elliot, 2013; Pálfy and Smith, 2000; Percival et al., 2015; Svensen et al., 2012), and subsequently most likely triggered a biotic crisis (Cecca and Macchioni, 2004; Danise et al., 2019; Gómez et al., 2008; Mattioli et al., 2009; Palliani and Riding, 2003; Piazza et al., 2019; Wignall and Bond, 2008). The cause for the crisis were elevated atmospheric pCO_2 concentrations in the order of 2–4 times higher than pre-industrial levels (Dera and Donnadieu, 2012; Ullmann et al., 2020) that derived from Karoo–Ferrars rapid intrusive magmatism, and together with contact metamorphism, also raised the greenhouse gas concentrations of methane (Svensen et al., 2012). This volcanogenic CO_2 has a distinct isotopically light carbon imprint and can be globally recognised as a negative carbon isotope excursion (CIE) during the T-OAE with an evidenced drop of $\sim$3–9 ‰, depending on the material analysed (e.g. Danise et al., 2019; Hesselbo et al., 2000; Izumi et al., 2012; Kemp et al., 2005; Littler et al., 2010; Suan et al., 2011). The duration of the CIE and OAE has been calibrated between $\sim$300–900 kya (Boulila et al., 2014; Huang et al., 2014; Ikeda and Hori, 2014; Pittet et al., 2014; Suan et al., 2008). The

following environmental perturbation triggered by those high CO_2 amounts were manifold. The latest Pliensbachian *spinatum* ammonoid zone (AZ) was dominated by rather cold climate with seawater temperatures around 11–16°C (Bailey et al., 2003; Dera and Donnadieu, 2012; Dera et al., 2011; Rosales et al., 2004; Suan et al., 2010) and probable existing continental ice masses (Suan et al., 2010). The subsequent Pliensbachian–Toarcian boundary (Pl–To) experienced an abrupt rise in seawater temperatures (also linked to the activity of Karoo–Ferrar) by ∼4–5°C (Suan et al., 2008) with a subsequent decrease to lower sea-surface temperatures, with cold and dry climate conditions and accelerated physical weathering prior to the T-OAE (Bailey et al., 2003; Hermoso and Pellenard, 2014; Lézin et al., 2013; Rosales et al., 2004; Suan et al., 2010). Ongoing, during the T-OAE, and hence the CIE, a rise in seawater temperature of about 3–7°C was recorded (Bailey et al., 2003; McArthur et al., 2000; Suan et al., 2010, 2008; Ullmann et al., 2020), together with a rise in atmospheric temperatures of about 3–5°C for the tropical and midlatitude areas (Dera and Donnadieu, 2012; Pálfy and Smith, 2000) and thus warm and humid climate conditions (Hermoso and Pellenard, 2014). After the T-OAE the early and middle Toarcian climates were dominated by greenhouse conditions (Bailey et al., 2003; Dera et al., 2011; Gómez and Arias, 2010; Gómez and Goy, 2011; Léonide et al., 2012).

Another effect of elevated CO_2 concentrations were higher continental weathering rates, which are thought to be the trigger for entering the state of a widespread anoxic ocean. The higher weathering rates would have raised the nutrient fluxes into the oceans (Brazier et al., 2015; Cohen et al., 2004; Fu et al., 2017; Hermoso and Pellenard, 2014), which enhanced the primary productivity, and through the resulting oxidation of the huge amounts of organic matter, anoxia in more restricted settings of the global ocean was induced (Jenkyns, 2010). On the other hand, continental weathering (especially silicate weathering) consumes CO_2 and helps to stabilize Earth's climate. Reconstructing the rates and regimes of continental weathering during the T-OAE has thus been of special interest. Several studies already exist that looked into this matter finding ∼3 times increased weathering rates for the T-OAE interval from $^{187}Os/^{188}Os$ isotopes (Percival et al., 2016; Them et al., 2017a) and about 2 times elevated weathering rates for the Pl–To boundary (Percival et al., 2016). A study with $\delta^{44/40}Ca$ isotopes in contrast found an increase of a factor of 5 for the continental weathering rates for both events (Brazier et al., 2015).

As the yet available studies on continental weathering during the T-OAE concentrated on the absolute weathering rates, we aim to unravel the changes in the different weathering regimes and hence the changes in silicate and carbonate weathering. As weathering of both geologic materials includes the consumption of CO_2, carbonate weathering only acts as a short term climate stabilizer, as the dissolution of carbonate in the oceans by lowered pH levels leads to the return of the greenhouse gas into the ocean–atmosphere system. Nevertheless, carbonate weathering also is a strong buffer to ocean acidity by adding alkalinity in the form of bicarbonate and carbonate ions

(Berner, 2003). By contrast, silicate weathering acts as a net sink for CO_2 and helps balancing Earth's climate on the long term, especially by weathering Ca and Mg silicates (France-Lanord and Derry, 1997). Silicate weathering is also more complex as carbonate weathering as carbonates simply dissolve completely (congruent weathering) while silicate weathering involves the formation of a new secondary clay mineral (incongruent weathering), which is an important process for forming soils. Because both weathering processes are differently crucial for the drawdown of atmospheric CO_2, the rates of each weathering process are of utter importance for the efficiency of Earth's climate stabilization. With this study we present new high-resolution lithium (Li) and magnesium (Mg) isotopes from two different locations in the western Tethys during the T-OAE and Pl–To boundary that help to understand the changing mechanisms of weathering during times of elevated CO_2 concentrations.

4.2.1. Isotopic variations during continental weathering – from continental sources to marine sinks

Magnesium isotopes

Magnesium (Mg) has three stable isotopes (24, 25, 26) with typical relative abundances of 78.99%, 10.00% and 11.01%, respectively (Berglund and Wieser, 2011). As the mass difference between ^{24}Mg and ^{26}Mg is relatively large with over 8%, significant mass fractionation in numerous geological processes can be observed. With its long residence time in seawater of over 10 Ma (Li, 1982) it exceeds the ocean mixing time of 1–2 kya (Garrison, 2006), and thus is homogeneously distributed in the oceans with a current seawater $\delta^{26}Mg$ composition of -0.83 ± 0.09‰ (Foster et al., 2010; Ling et al., 2011). The main sinks of Mg are hydrothermal circulation at mid-ocean ridges, the precipitation of dolomite, as well as ion-exchange reactions with clays (Elderfield and Schultz, 1996), while the main sources of Mg into the oceans are continental rivers (Tipper et al., 2006).

The fractionation of Mg isotopes occurs during the formation of carbonate minerals, which prefer to incorporate the light Mg isotope with weaker Mg bonding strength. However, the specifics of the fractionation are not yet fully resolved, since it depends on several factors like temperature, calcite growth rate, aqueous Mg concentration, pH, mineralogy, the precipitation process and Mg content in the calcite (Galy et al., 2002; Immenhauser et al., 2010; Li et al., 2012; Saenger and Wang, 2014; Wang et al., 2019). This explains the wide variety of $\delta^{26}Mg$ in carbonate minerals between -5.6 to -1‰ (e.g. Fantle and Higgins, 2014; Gao et al., 2018; Li et al., 2012; Wang et al., 2017). Silicate minerals also fractionate the Mg isotopes by preferentially incorporating the heavier Mg isotopes (Schauble, 2011). Typical $\delta^{26}Mg$ values of silicates range between -0.77 to -0.09‰ and hence are virtually uniform, indicating a limitation of Mg isotopic compositions at high temperatures (e.g. Chakrabarti and Jacobsen, 2010; Liu et al., 2010; Teng et al., 2010a).

Another Mg fractionation process occurs during the weathering of silicate rocks, where secondary clay minerals are formed (incongruent weathering). This process usually prefers the incorporation of the heavy Mg isotopes into their crystal lattice (Tipper et al., 2006; Tipper et al., 2010). This practically means that during the weathering process the light Mg isotope is washed out by fluids and leaves the weathering products, such as soil and clay minerals, with a heavy Mg isotopic composition (e.g. Brenot et al., 2008; Gao, 2016; Liu et al., 2014; Teng et al., 2010b; Tipper et al., 2006). The Mg isotopic content of rivers is thus controlled by the formation and weathering of carbonates and silicates, whereas the vegetation might also play a role (Anderson et al., 1983; Bi et al., 2007; Black et al., 2006), explaining the high diversity of δ^{26}Mg in modern river waters of in mean -1.09 ‰ with a range of ± 2.5 ‰ (Tipper et al., 2006).

Lithium isotopes

Lithium (Li) has two stable isotopes, ^{6}Li and ^{7}Li, with typical relative abundances of 7.52%, 92.48%, respectively (Berglund and Wieser, 2011). As the relative mass difference between both isotopes is large, the fractionation at low-temperature processes has a wide span making it a good tracer for those processes in a geological context. Especially the reconstruction of chemical weathering on continents is a major advantage of Li isotopes, because unlike other isotope systems as strontium, magnesium, calcium and osmium, Li is almost exclusively fractionated and drained in rivers by the weathering of silicates (silicate weathering contributes more than 95%) (Dellinger et al., 2015; Huh et al., 2001; Kisakurek et al., 2005; Millot et al., 2010).

The seawater δ^7Li amounts to 31.0 ± 0.5 ‰ (Broecker and Peng, 1982) and is globally evenly distributed, owing to the long residence time of Li in seawater of about 1.2 Ma (Stoffynegli and Mackenzie, 1984) exceeding the rates of ocean mixing. The main sinks for Li in the oceans is the incorporation into clays and the subsequent integration into marine sediments, which makes up 70% of the Li removal. Another sink is the low-temperature alteration of oceanic crust, which also involves the formation of clays (Chan et al., 1992; Chan et al., 2006; James et al., 1999; Seyfried et al., 1998; Verney-Carron et al., 2011; Vigier et al., 2008). During formation of clay minerals Li isotopes fractionate and ^{6}Li is preferentially incorporated into the mineral lattice, as well as adsorbed onto the clay mineral surface (e.g. Pistiner and Henderson, 2003; Vigier et al., 2008; Williams and Hervig, 2005; Wimpenny et al., 2015; Wunder et al., 2010, 2007, 2006), explaining the relatively light Li isotope composition of those phases and the heavy δ^7Li of seawater.

The main sources of Li into the ocean are continental river runoff, with its signature of low-temperature chemical weathering processes, and hydrothermal activity high-temperature processes at the mid-ocean ridge (Elderfield and Schultz, 1996; Gaillardet et al., 2003; Huh et al., 1998; Lui-Heung et al., 1994). Both sources contribution to the Li seawater budget is nearly equal, but the

Li isotopic composition is very distinct with a mean of $\sim$8.3 ‰ for hydrothermal fluxes (Elderfield and Schultz, 1996; Lui-Heung et al., 1994; Rudnick and Gao, 2003; Tomascak et al., 2008) and 23.5 ‰ for the mean river runoff (Huh et al., 1998). The reason for the large isotopic offset between the two sources is the isotopic fractionation of Li during terrestrial chemical weathering. The fractionation on the continents occurs according to the fractionation during clay mineral formation in seawater. As secondary (clay) minerals are formed during silicate mineral weathering (incongruent weathering), this leads to a high δ^7Li river signature with low Li concentrations. However, during congruent weathering, and thus only primary silicate mineral dissolution, low δ^7Li and high Li element concentrations can be observed in the rivers (Dellinger et al., 2015; Kisakurek et al., 2005; Liu et al., 2015; Misra and Froelich, 2012; Pogge von Strandmann et al., 2010, 2013). The ability to differentiate between congruent and incongruent weathering gives us the opportunity to track changes in the intensity of silicate weathering and hence the feedback of Earth's environment to elevated CO_2 concentrations.
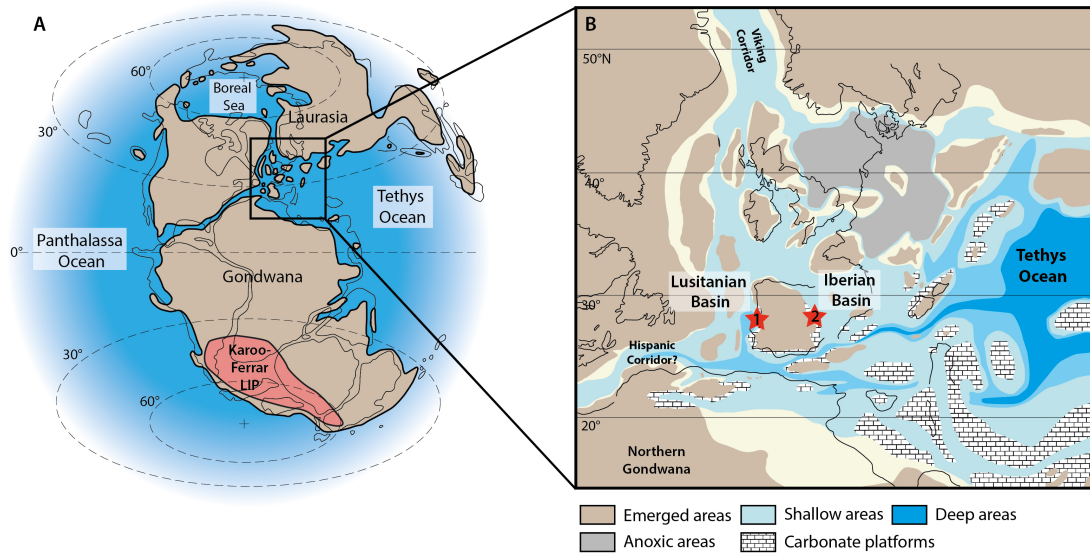
4.3. Materials and Methods

Figure 11. Paleogeography and study area location maps. (A) Global paleogeography during the Early Jurassic, modified after Dera et al., 2011 and Korte et al., 2015. Red area depicts the suggested expansion of the Karoo–Ferrar Large Igneous Province (LIP). (B) Detailed reconstructed map of the NW Tethys area, showing that mainly the northern part of this area suffered anoxia during the T-OAE (modified after Bassoullet and Baudin, 1994; Ruebsam et al., 2018). Stars mark the locations of the studied areas – (1) Rabaçal/Fonte Coberta (Lusitanian Basin) and (2) Barranco de la Cañada (Iberian Basin). *[High-resolution image on attached CD]*

4.3.1. Study areas

Marine micritic carbonates from shallow water environments were collected from two different locations in the western Tethys – in Rabaçal/Fonte Coberta (R/FC, Portugal, 40°03'08.0"N 8°27'30.5"W) representing the Lusitanian Basin and Barranco de la Cañada (BdC, Spain, 40°23'53.4"N 1°30'07.4"W) for the Iberian Basin (Fig. 1; also see supplement/ section 1.4). For this study 20 carbonate samples for the Lusitanian Basin as well as 25 carbonate samples for the Iberian Basin were collected and checked for their preservation (see supplement/ section 2.7). Sampling intervals amount to 0.1–11 m, covering the upper Pliensbachian from the *margaritatus* AZ up to the middle Toarcian *bifrons* AZ, comprising the Pliensbachian–Toarcian boundary and the T-OAE crisis interval.

The age model for this study is based on the latest findings on the biozonations published by Comas-Rengifo et al., 2013, Correia et al., 2018 and Ferreira et al., 2015 for Rabaçal/Fonte Coberta, and for the Barranco de la Cañada section by Gahr, 2002 and Gahr, 2005, as well as additional observations in the field. The absolute ages for the AZ are defined by the Geological Time Scale 2016 (Ogg et al., 2016). The lower boundary of the *spinatum* AZ for BdC is based on Sr isotopes

generated for this study and calibrated on the ^{87}Sr/^{86}Sr seawater curve from McArthur et al., 2000.

4.3.2. Sample preparation

After passing the sample scrutiny for diagenetic overprints (see supplement/ section 2.7), the 20 samples from R/FC and remaining 20 samples from BdC were prepared for further isotope analyses. First, the micritic carbonates were cut into thin slices with a diamond saw (research group petrology of the ocean crust, University of Bremen). Ongoing, each slice was examined under a binocular microscope and carefully broken into small pieces with a preparation needle. During this sampling it was crucial to ensure to only pick the pristine micritic matrix, avoiding any fossils, veins, late stage secondary alteration or dolomitization, fractures, pervasive recrystallization, any spar or microspar as well as areas where original sedimentary features (e.g. burrow traces, finenely detailed sedimentary lamination) were preserved. Subsequently, the chips were manually pestled not too finely with an agate mortar to avert reaming any clay minerals. The powdered sample material was used for any further isotope analyses.

4.3.3. Isotope ratio measurement

All sample preparations for isotope analyses were conducted in the Isotope Geochemistry clean laboratory at MARUM – Center for Marine Environmental Sciences, University of Bremen, Germany. The powdered sample material was leached as described below (section 4.3.4.) prior to ion exchange column chromatography. All isotope measurements were operated with a ThermoFisher Scientific Neptune Plus MC-ICP-MS with a stable introduction system (SIS) and high-efficiency x-cone. Isotope ratios are reported in per mill (‰) with the delta-notation relative to the certified reference materials:

$$\delta^a X = \left(\frac{\left(\frac{^a X}{^b X} \right)_{sample}}{\left(\frac{^a X}{^b X} \right)_{standard}} - 1 \right) * 1000 \tag{5}$$

with a and b being the isotopes of each element.

Li isotopes were separated from their matrix using the two-step column separation procedure with BIORAD resin AG 50WX8 modified after Moriguti and Nakamura, 1998. Head and tail fractions of each separation were checked for Li loss and its purity with MC-ICP-MS. The standard-sample-bracketing method with international reference material NIST SRM 8545 (L-SVEC) was applied. The reproducibility of NIST SRM 8545 for the three years of this project was δ^7Li = -0.1 ± 0.3 ‰ (2sd, n=14), whereas the long-term reproducibility 2sd of the laboratory is ± 0.5 ‰. To control the accuracy and precision of the method the in-house standard bottom seawater from SuSu Knolls (BSW) was also repeatedly measured and yielded a value of δ^7Li = 30.5 ± 0.4 ‰ (2sd, n=7), which

is within analytical uncertainty in agreement with published literature values (31.1 ± 0.3 ‰ (2sd); see e.g. Huang et al., 2010; Pogge von Strandmann et al., 2019; Wimpenny et al., 2010).

Isotopes of the element Mg were extracted from the sample matrix through ion exchange chromatography with BIORAD resin AG50WX8 and 0.8 M HCl following the procedure described by (Strelow, 1960; Strelow et al., 1965). Head and tail fractions of the separation were likewise checked for Mg loss with MC-ICP-MS. Each series also contained an international reference standard, which underwent the same preparation and leaching methods as the sample materials. Measured δ^{26}Mg values were normed to the DSM-3 scale as described by Young and Galy, 2004. Repeated measurements of the international standard CAM1 yielded a δ^{26}Mg$_{DSM3}$ value of -2.61 ± 0.06 ‰ (2sd, n=8), for DSM-3 0.00 ± 0.03 ‰ (2sd, n=8), repeated measurements and preparations for the in-house seawater standard (SuSu Knolls) yield -0.85 ± 0.05 ‰ (2se, n=13) and for GSJ-JCp-1 -2.00 ± 0.19 ‰ (2se, n=6), all in agreement with published values -2.623 ± 0.03 ‰ (Teng, 2017), 0.01 ± 0.14 ‰ (Tipper et al., 2006), $-0.83. \pm 0.09$ ‰ (Foster et al., 2010; Ling et al., 2011), and -1.96 ± 0.05 ‰ (Teng, 2017), respectively.

4.3.4. Leaching procedure

Clay minerals and other detritial components of the carbonate rock can contaminate the sample solution by detritial mineral dissolution. So far, the techniques applied by Ohnemueller et al., 2014 and Clarkson et al., 2015 avoided any detectable contamination by the detritial fraction. However, the carbonate rocks used in their studies contained less clay and detritus amounts, making it crucial to refine the leaching techniques for each isotopic system in this study. This section describes the leaching experiments undertaken for each isotope system to achieve the best true matrix isotopic results.

Lithium isotopes

Avoiding the dilution of Li from the clay minerals is critical during acid dilution of carbonates, as they contain much higher Li concentrations and lower δ^7Li than the carbonate fraction and could thus easily contaminate the carbonate Li signal (Bastian et al., 2018; Pogge von Strandmann et al., 2013). The Li isotopic imprint of the detritial fraction is characteristically light, because as the ^{6}Li isotope is preferentially incorporated by secondary clay minerals (Burton and Vigier, 2012). The carbonate leaching procedure of this study is based on the findings of Pogge von Strandmann et al., 2013, Bastian et al., 2018 and Macedo de Paula-Santos et al., 2017. Best results in these studies were gained by leaching the micritic carbonate in 0.1M HCl for 1 hour.

In an effort to refine the above described leaching methods and gaining the δ^7Li that is closest to the matrix signal, we carried out leaching experiments by varying the amount of leached carbonate

(30%, 25%, 22.5%, 20% — results and detailed discussion can be found in the supplement/ section 2.6.5. Our experiments showed that the micritic carbonates are best leached for 2 hours with 0.1M HCl by dissolving 25% of the carbonate fraction to gain the true δ^7Li matrix signal.

Magnesium isotopes

As Li and Mg have a similar ion radius they also behave similarly during secondary mineral formation and carbonate leaching. The Mg isotopes fractionate during secondary mineral formation taking up the heavy isotopes and thus enrich the residuum in the light ^{24}Mg isotope (Tipper et al., 2006; Tipper et al., 2010), meaning that the detritus in carbonates should have a heavy isotopic imprint. As it is also attached at clay minerals by adsorption like Li it is likewise easily affected during the digestion of the carbonate material. For this reason, the same carbonate leaching method as performed for Li isotopes was preferred. Results of our carried out leaching experiments showed no differences for our micritic carbonates between the different leaching methods in other publications (see supplement/ section 2.6.6), hence for simplicity and better comparison of both isotopic systems the same leaching method as described for Li was applied.

4.3.5. Sample preservation

Marine carbonate rocks are widely used for paleoenvironmental reconstructions with Li and Mg isotope as they are thought to reflect the chemistry of the ambient seawater during its time of deposition (Higgins and Schrag, 2012; Pogge von Strandmann et al., 2019). However, diagenesis may influence and alter the original chemistry of the carbonate, which is why it is crucial to scrutinize the miciritc carbonates for any diagenetic overprints. The detailed results and interpretation for the different tests conducted in the course of this study are listed in the supplementary material/ section 2.7.

4.4. Results

Striking are the shifts to more positive δ^7Li values of about 2.4 ‰ at the Pl–To boundary and 5.7 ‰ during the Toarcian OAE to values of 19-20 ‰ (Fig. 12). However, this abrupt rise in δ^7Li is only distinct at the R/FC section. Although the pre- and post-T-OAE δ^7Li values at both sections lie in the same range, the absolute values differ during the OAE with BdC signature showing even a minor decrease in the Li isotopes simultaneously with the decrease seen in R/FC.

Mg isotopes show only little variation at both sections over the studied interval with mean δ^{26}Mg values of -3.59 $\pm$ 0.09 ‰ (1sd) for R/FC and -3.98 $\pm$ 0.15 ‰ (1sd) at BdC (Fig. 12).

4.5. Discussion

4.5.1. Implications for the seawater isotopic composition during the Early Jurassic

Mg isotopes derived from marine carbonates are fractionated by a number of low-temperature processes, making it difficult to make any assumptions about the δ^{26}Mg composition of seawater. Relative changes in the isotopic composition of the carbonates may though speak for a change in the seawater composition, and hence the continental river fluxes as the main source of Mg (and thus continental weathering rates), when all other fractionating processes can be excluded as a possible driver. Both sections in this study record stable δ^{26}Mg values for the late Pliensbachian–early Toarcian with a minor offset in the absolute values between both basins, which might be owing to differences in regional circumstances. The stability of both Mg records suggests no changes in any of the drivers that might influence the δ^{26}Mg of the carbonate rock and hence also the seawater signature over the whole studied interval.

Li isotopes on the contrary are relatively unaffected by a lot of low-temperature processes, and as the possible overprint of diagenesis probably has no effect on the Li isotopic composition of the studied rocks (see section 2.8.2), they have the potential to carry the original δ^7Li seawater (δ^7Li$_{SW}$) signature (Pogge von Strandmann et al., 2019). Correcting our Li data for the calcite isotopic fractionation of ∼6 ‰, which is the current highest value published (Pogge von Strandmann et al., 2019) we gain a δ^7Li$_{SW}$ between 20.3–22.0 ‰ for the whole studied interval (acting on the assumption of mean measured δ^7Li values for the late Pliensbachian of 16.0 ‰ and 14.3 ‰ for pre- and post-T-OAE). Compared to nowadays δ^7Li$_{SW}$ of ∼31 ‰ (Broecker and Peng, 1982; Pogge von Strandmann et al., 2019), to published values from the Late Cretaceous (94 Ma) of ∼26–27 ‰, and to reconstructed values from the Late Jurassic (155–148 Ma) of ∼29–32 ‰ (Ullmann et al., 2013), our generated values for the Early Jurassic are rather more comparable to the minimum values

recorded during the Paleogene of $\sim$22 ‰ (Lechler et al., 2015; Misra and Froelich, 2012; Pogge von Strandmann et al., 2013). Given the higher Li isotope composition of seawater during the Late Jurassic compared to the Early Jurassic ($\sim$180 Ma) the $\delta^7 \text{Li}_{SW}$ composition was not constant during the whole Jurassic epoch and required a major rise in $\delta^7 \text{Li}_{SW}$ of $\sim$9–12 ‰, and from here even a minor decrease to reach the Late Cretaceous level. To resolve these $\delta^7 \text{Li}_{SW}$ changes more studies covering the Jurassic time interval are needed.

Also, minor oscillations seemed to already appear during the studied interval of the Early Jurassic. Mean $\delta^7 \text{Li}$ values prior to the Pl–To boundary are $\sim$16 ‰, whereas subsequently pre- and post-T-OAE values reveal a mean value of $\sim$14 ‰, suggesting a drop in the $\delta^7 \text{Li}_{SW}$ in the Toarcian that persisted at least until the mid-Toarcian.

4.5.2. Observed $\delta^7 \text{Li}$ trends in R/FC and BdC

Variations in the seawater $\delta^7 \text{Li}$ signature are a result of the varying fluxes of the main Li sources, being hydrothermal activity and continental rivers. Strictly speaking, a positive excursion as observed for the Pl–To boundary and T-OAE interval in R/FC could mean either a decrease in hydrothermal fluxes, an increase in riverine fluxes, or, if river fluxes stayed stable, a change in congruency and thus changes in the fluvial $\delta^7 \text{Li}$, or even a combination of all these three factors. Li element concentrations also vary with the change in congruency, but the Li concentrations derived from marine carbonates can not be used as tracers because too many factor influence the incorporation into the calcite mineral (see above). The possible influence of hydrothermal activity is discussed in the section below, but seen as rather unlikely. As no information about the river fluxes during the studied intervals exist we consider them for now stable until box model efforts can be conducted and help to answer this question. In the following we will focus on the changes in the different silicate weathering congruencies, in terms of congruent and incongruent weathering, and the possible mechanisms behind it.

The $\delta^7 \text{Li}$ record from R/FC reveals two major increases at the Pl–To boundary of about 2.4 ‰ and shortly after the onset of the T-OAE of about 5.7 ‰ (Fig. 12, 13). Those shifts go along with two eruption pulses from the Karoo–Ferrar LIP volcanism, which are also recognised as a perturbation in the carbon isotope record (e.g. Aarnes et al., 2011; Burgess et al., 2015; Elliot and Fleming, 2008; Elliot, 2013; Pálfy and Smith, 2000; Percival et al., 2015; Svensen et al., 2012). This

---

Figure 12 _(following page)_. Generated $\delta^{13}\text{C}$, $\delta^7 \text{Li}$ and $\delta^{26}\text{Mg}$ isotopes for BdC and R/FC sections. Brachiopod and oyster carbon isotope data, the T-OAE interval (orange colored area), the crisis interval (dashed line), and the interval of elevated CO_2 (red lines) as published by Piazza et al., 2019, 2020; Ullmann et al., 2020. For better comparability of the CIE at R/FC, published data for the Lusitanian Basin are plotted from literature by Duarte, 1998; Duarte et al., 2004; Hesselbo et al., 2007; Oliveira et al., 2006; Pittet et al., 2014. Lithological log from BdC modified after Gahr, 2002 and for R/FC after Duarte, 1995 and Paredes et al., 2016. _[High-resolution image on attached CD]_
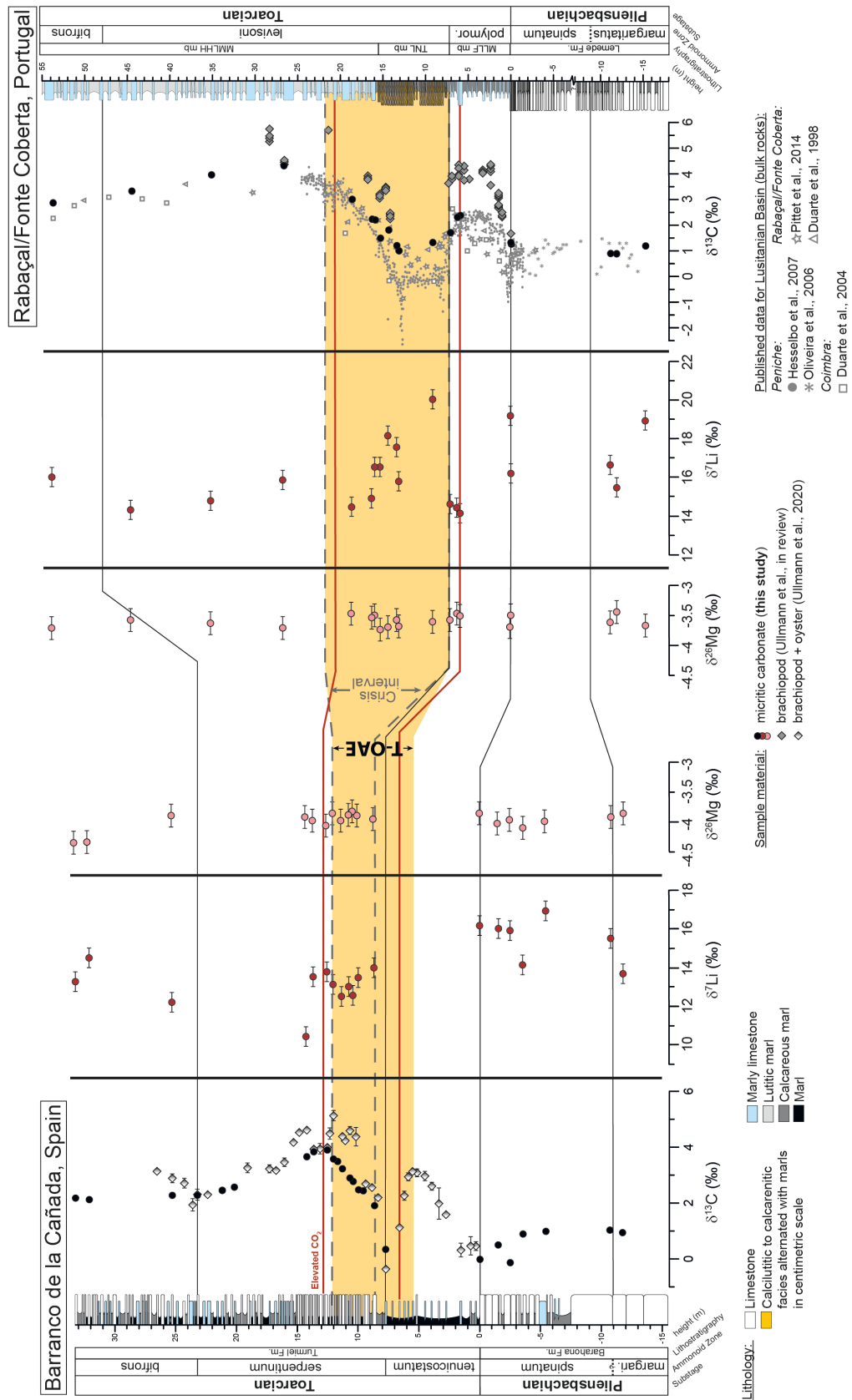
volcanism is thought to being the cause for higher atmospheric CO_2 concentrations, which in turn
fueled Earth's climate feedback mechanism of enhanced silicate weathering. Two recent studies,
investigating two OAE events during the Cretaceous period, already showed the importance of
silicate weathering to sequester CO_2 on the long term (Lechler et al., 2015; Pogge von Strandmann
et al., 2013). The two abrupt shifts to positive δ^7Li values recognised in this study for the Early
Jurassic period suggests a change in weathering congruency with a higher fractionation of Li iso-
topes away from primary silicate mineral dissolution and congruent weathering, to the domination
of secondary clay mineral formation that take up the ^{6}Li isotope (incongruent weathering). These
short-term shifts had an approximate duration of $\sim$150 kyrs for the T-OAE and $\sim$7 kyrs for the
Pl–To boundary. Subsequently, the δ^7Li values become lighter implying a regime change to more
congruent weathering.

However, die Li isotope record from BdC shows a different pattern. If we assume that the same
δ^7Li values prevailed at BdC as for R/FC during *tenuicostatum/polymorphum* AZ (as we were not
able to recover well preserved sample material from this interval) then instead of following the
rise in δ^7Li during the T-OAE, as observed in R/FC, a decrease is recorded (Fig. 12, 13). Also,
increased δ^7Li values are not observed during the Pl–To boundary for the BdC section, although
this is probably owing to the lack of sufficient sample material covering this event. A decrease in
δ^7Li rather speaks for primary mineral dissolution and congruent weathering. The trend observed
here also does not show as a sharp shift in δ^7Li as seen in R/FC, which could, however, be due
to the lack of a sample at the horizon where the minimum δ^{13}C value occurred. Nevertheless,
the maximum drop in δ^7Li observed for BdC is 1.7 ‰, and values subsequently recover to record
heavier values until they reach the same isotopic signature as for R/FC at the end phase of the
OAE.

4.5.3. Constraints from multi-isotope excursions

In terms of hydrothermal activity, the radiogenic isotope Sr is often used to determine the hy-
drothermal fluxes as they are more sensitive against such changes (Pogge von Strandmann et al.,
2013) and would show more unradiogenic signature with higher activity. However, for the Sr iso-
topes a gradual decrease in the isotopic signature was observed starting in the Sinemurian and
stretching into the Pliensbachian, reaching its minimum values close to the Pl–To boundary (Jones
et al., 1994; McArthur et al., 2000)(Fig. 14). This decrease was probably the result of increased
hydrothermal activity (Jones and Jenkyns, 2001), and the influence of this process ceased dur-
ing the Toarcian as Sr isotopes gradually became more radiogenic (Fig. 14). Short-term abrupt
changes in hydrothermal fluxes are not recorded in the Sr-isotope-curve at both events and are thus
a rather unlikely driver for the observed positive δ^7Li shift, although a minor contribution might
be possible at the Pl–To boundary, when Sr isotopes became more radiogenic and hydrothermal

activity decreased. However, Sr isotopes would not be able to record such short-term events, as this isotopic system is generally well buffered due to its long residence time in the ocean. Os, on the other hand, has also radiogenic isotopes that behave comparably to Sr, but have a much shorter residence time, and hence are able to record such short-term fluctuations (Peucker-Ehrenbrink and Ravizza, 2000). Three studies in total exist that concentrated on $^{187}Os/^{188}Os$ isotopes during the Pliensbachian–Toarcian. An early study from the NE Tethys region (Cleveland Basin) suggested an increase of 4–8 times in magnitude of continental weathering rates during the T-OAE (Cohen et al., 2004). However, the global extend of this signal was questioned, first by the restriction of the depositional basin and the condensation of the section (McArthur et al., 2008), and second by two recent additional Os isotope studies focussing on two basins that were probably connected to the open ocean. To investigate the global scope of enhanced weathering rates each study covered a different realm in the Pliensbachian–Toarcian: the northern Tethys (Cardigan Bay Basin, Wales; Percival et al., 2016) and the Panthalassa Ocean (Western Canada Sedimentary Basin; Them et al., 2017a) (Fig. 14). Remarkably, both studies found $\sim$3 times increased continental weathering rates during the Early Toarcian, based on an increase in the Os isotope values (more radiogenic), although the absolute values differ, which could be a result of regional differences. Also, the Pl–To boundary event is likewise calculated to a $\sim$2 times increased flux from the continents (Percival et al., 2016).

More assumptions about increased weathering rates derive from a negative $\delta^{44/40}Ca$ isotope excursion with a suggested increase by a factor of 5 for the Pl–To boundary event as well as the T-OAE (Brazier et al., 2015). This study speculated that two processes played together in leaving the seawater enriched in the light ^{40}Ca isotope and explaining the negative Ca isotope excursion: the increased riverine fluxes, and thus weathering rates, together with ocean acidification associated with decreased carbonate burial due to the massive input of CO_2 in the ocean–atmosphere system.

$\delta^{26}Mg$ isotopes generated in this study show no variations at the Pl–To boundary or T-OAE events, contrasting the signatures of the other isotopic systems (Fig. 14). This observation is probably due to the well buffered state of Mg in seawater as a result of the residence time, that compared to all the other isotopic systems reported here is tremendously long (Li, 1982). Such short-term fluctuations, as recorded for the late Pliensbachian and early Toarcian, can for all these reasons not be captured with Mg isotopes.

The onset of isotopic excursions in each study is also coincidental with the onset of our generated δ^7Li isotopes for both basins (Fig. 14), strongly supporting an alike effect of increased continental weathering on this isotopic system (for a detailed discussion of the δ^7Li signals see below). Further, a model published by Ullmann et al., 2020, based on reconstructions of sea water temperatures and atmospheric CO_2 contents, also assumed a peak in silicate weathering that perfectly falls into line with the peaks observed in Li and Ca isotopes (Fig. 14). Moreover, Li isotopes can also be
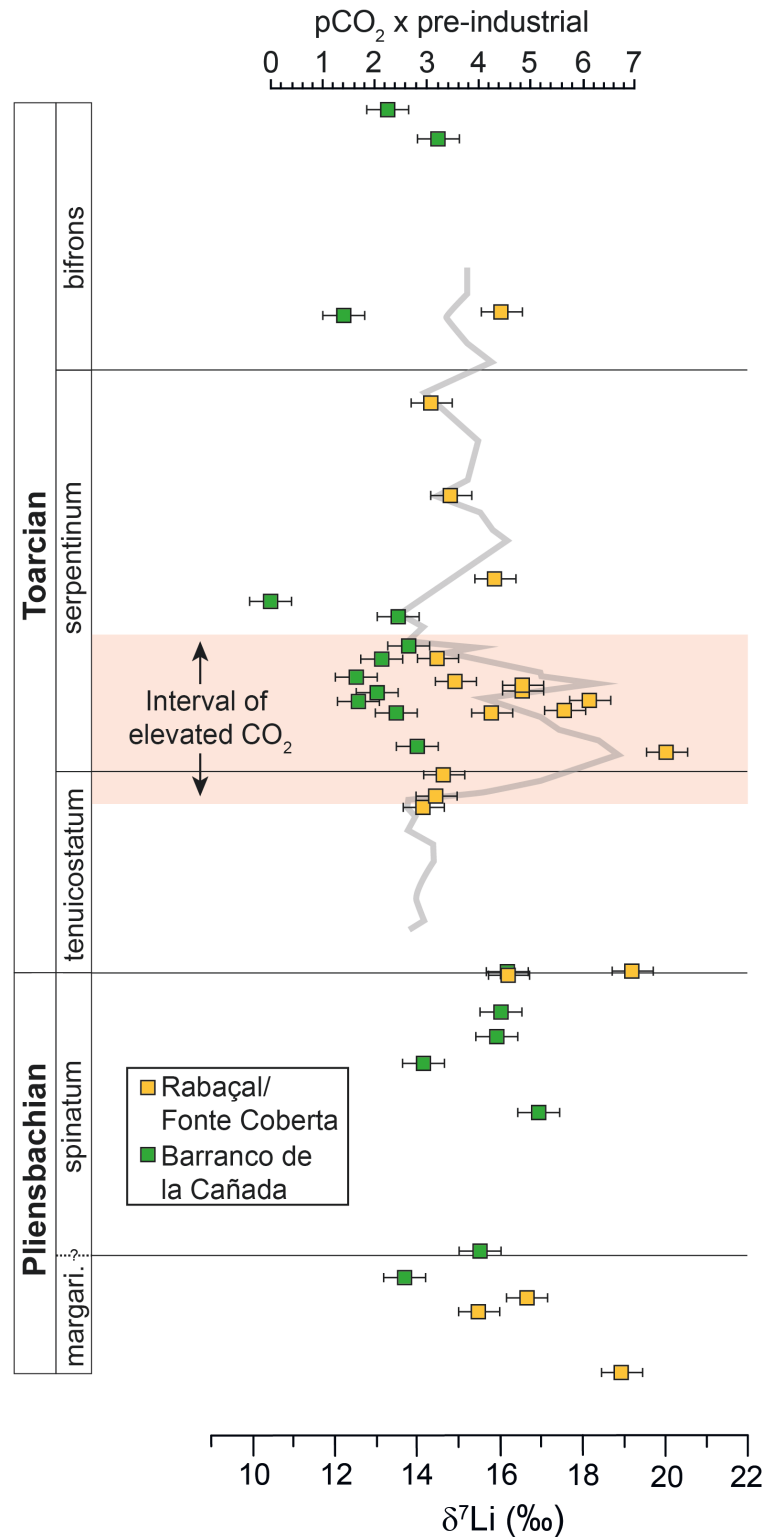
Figure 13. Plot of δ^7Li from R/FC versus BdC. The red shaded area marks the time interval with increased CO_2 concentrations, which are also separately shown with the grey line (after Ullmann et al., 2020). Margari. = margaritatus. *[High-resolution image on attached CD]*

used for the reconstruction of the weathering fluxes for both discussed events, together with the already published and above described isotope data following the example from earlier studies (Lechler et al., 2015; Pogge von Strandmann et al., 2013). Our incongruent weathering signal, recorded in the Lusitanian Basin, is therefore especially well suited because weathering rates in these regimes respond to changes in the kinetics (thus temperature, CO_2 supply and runoff) and display a global response, in contrast to congruent weathering regimes where the silicate weathering rates are dependent solely on erosion rates (West et al., 2005). In any case, a modelling effort is beyond the scope of this study and envisaged for future studies.

4.5.4. Basin restrictions during Pliensbachian–Toarcian times

The Toarcian Oceanic Anoxic Event

To say in advance, a trend to lighter Li values, if not a true seawater signal, can also derive from diagenesis and the leaching of clays during sample preparation. A possible diagenetic overprint was thoroughly checked and no indications were found for the analysed samples (see supplement/ section 2.7). Leaching procedures were also refined for our sample material, in order to avoid the leaching of clays (see supplement/ section 2.6.5) and falsification of the original matrix signal. Besides, recording the same δ^7Li values at both sections for pre- and post-T-OAE times reduces the probability that just the samples during the T-OAE at BdC should be affected by improper leaching. Accordingly, regional differences must be accounted for the different Li isotopic signatures observed in the Lusitanian basin (LB, Rabaçal/Fonte Coberta section) and Iberian basin (IB, Barranco de la Cañada section)(Fig. 14). A possible explanation for the opposing trends could be that either one basin was restricted during this time interval, and therefore not representing the global δ^7Li$_{SW}$ signature, or both basins were. There are several points that might speak for a temporary restriction of the LB, which are therefore discussed in the following.

First, a striking feature are the contrasting lithologies of both basins during the T-OAE interval (Fig. 12), although both basins should record the same facies. While the deposits prior and after the crisis interval are comparable, the LB reveals calcarenitic depositions with the onset of the T-OAE, which also prevail for the majority of the OAE interval. In fact, this calcarenitic facies represents storm deposits that are found throughout the LB (Duarte, 1997, 2007; Duarte and Soares, 2002; Pittet et al., 2014; Rodrigues et al., 2016; Suan et al., 2010; Wright and Wilson, 1984) and can also be found in several basins in the NW Tethys (Krencker et al., 2015). The Peniche section located in the LB, representing the outer ramp to basin facies, equivalently deposited turbidites during the T-OAE that were probably sourced by the Berlenga-Farilhões block (Fig. 16 E)(Hesselbo et al., 2007). This change in facies is thought to be caused by a rapid tectonically-driven sea level fall that concluded in a lowstand for the LB, which in turn was triggered by the uplift of the Berlenga-Farilhões block (Duarte, 1997, 2007; Duarte et al., 2004; Kullberg et al., 2001; Wright and Wilson,

1984). This sealevel lowstand terminated concurrently with the end of the calcarenitic deposition
and a subsequent transgressive phase in the mid-*levisoni* AZ (Fig. 16 F) (Duarte, 2007; Duarte
et al., 2004; Miguez-Salas et al., 2018).

This stands in stark contrast to the sequence stratigraphy reconstructed for the IB. Here, The
T-OAE was accompanied by a maximum flooding surface (phase between maximum rate of relative
sea level rise and maximum relative sea level fall) at the late *tenuicostatum* AZ (equals *polymor-
phum* AZ), which changes to a regressive phase at the transition of *tenuicostatum/serpentinum* AZ
(Gómez and Goy, 2005). The IB therefore did not experience an abrupt sea level fall as seen in
the LB basin during the T-OAE, showing important differences in the deposition environment in
both basins. The R/FC section deposits calcarenites that represent conditions above storm wave
base (SWB), while BdC probably stayed below the storm wave base (Gahr, 2005) (Fig. 16 F). As
already mentioned, storm derived deposits are found in several basins throughout the NW Tethys
realm during the T-OAE. Krencker et al., 2015 argued that these storm deposits are a result of
intensified storms, and hence the reason for the lowering of the SWB. As the overall trend during
the T-OAE was a rise in sea level, they generally excluded the possibility of a decreased sea level
stand as an argument for a lower SWB. However, the LB does in fact record a rapid tectonic driven
sea level fall during the T-OAE, which in turn can be accounted for the lowered SWB, although
this is just a regional circumstance.

A second argument for a LB restriction can be drawn with the occurrence of the crisis intervals
of the brachiopod species *Soaresirhynchia bouchardi*. This species appearance is typical during
the Toarcian OAE and is recorded in wide areas of the NW Tethys (e.g. Baeza-Carratalá et al.,
2011; Danise et al., 2019; Gahr, 2005; García Joral et al., 2011; Piazza et al., 2019, 2020; Ullmann
et al., 2020). The opportunistic brachiopod takes over the ecological niches that were previously
inhabited by brachiopods that got extinct at the crisis interval. It seems like for the LB the first
appearance of *S. bouchardi*, in comparison to other basins in the tethyan realm, has a somewhat
delayed first occurrence in the crisis interval, and only appears in the upper parts of the calcarenitic
facies (Comas-Rengifo et al., 2014; Comas-Rengifo et al., 2013; Gahr, 2002; Piazza et al., 2019;
Pittet et al., 2014), when the sea level was probably rising again (Fig. 16 F). This would imply that
a colonialization during the T-OAE with *S. bourchardi* was hindered in the LB owing to the basin
restriction. Nevertheless, we do not know how much time was required to deposit the calcarenites
and a relatively fast deposition could lead to a falsification of this observation. Thus, more research
on this matter is recommended.

A third point to draw is that basin restrictions during the T-OAE are not unlikely and happened
in several basins in the NE Tethys (McArthur et al., 2008). The basin restrictions in this part of the
Tethys (Paris, Cleveland and German basins) were accompanied with the typical anoxic or euxinic
conditions seen in the Early Toarcian and the deposits of organic-rich black shales (McArthur et al.,

2008 and references therein). From this it follows that if the LB really was restricted, why does it lack the development of anoxic conditions? The reason for this are the occurring strong storms (Krencker et al., 2015) together with the relative low sea level that enabled the mixing of even deep water masses and prevented their stratification (Fig. 16 E) (Suan et al., 2008). Similar conditions have once been recorded during the early Pliensbachian in the LB (Plancq et al., 2016) (Fig. 15 C), making it also a possible scenario for the Early Toarcian.

The Pliensbachian–Toarcian Boundary Event

The Pl–To boundary event experienced similar transgressive and regressive phases, with a low sea level stand during the boundary event comparable to the records during the T-OAE. While the late Pliensbachian *margaritatus* AZ experienced a transgressive phase with a maximum flooding surface, the *spinatum* AZ was dominated by a regressive phase that led to the maximum lowstand at the Pl–To boundary (Fig. 15 B), and a subsequent transgression during the *polymorphum* AZ (Fig. 15 C, D). The latest Pliensbachian and Pl–To boundary event (before the eruption of the Karoo-Ferrar LIP and the subsequent rise in temperatures) were accompanied by a severe drop in seawater temperatures (Bailey et al., 2003; Dera et al., 2009; McArthur et al., 2000; Rosales et al., 2004; Suan et al., 2008; van de Schootbrugge et al., 2005a) and probable icehouse conditions, suggesting a glacio-eustatic control on the low sea level (Guex et al., 2001; McElwain et al., 2005; Morard et al., 2003; Suan et al., 2008; van de Schootbrugge et al., 2005b).

Contrary to the T-OAE interval, the LB and IB seem to be similar in their depositional environment during the Pl–To boundary with similar sea level stands. Nevertheless, a Pl–To boundary lowstand could still have led to a short-term restriction of the LB similar to the T-OAE *levisoni* AZ depositions, although no lithological evidence exists in the LB. Numerous siliciclastic turbidites deposited in the Dades-Thodra valley in Morocco at the earliest *polymorphum* AZ indicate a storm influence (Fig. 15 C) (Brazier et al., 2015; Krencker et al., 2015) and hence again a sea level that was below the SWB in this part of the NW Tethys. Although such low levels were not reached

---

Figure 14 *(following page).* Compilation plot of published calcium, strontium and osmium isotopes together with in this study generated lithium isotopes during Pliensbachian–Toarcian times. Ca isotopes are from Brazier et al., 2015, representing the basin facies in the Lusitanian Basin (section: Peniche, Portugal). Os isotopes are from Percival et al., 2016 from a section in the Cardigan Bay Basin (Wales), covering the northern part of the NW Tethys region (white squares), and from Them et al., 2017b from a section in western North America (Western Canada Sedimentary Basin, today in Alberta), covering the Panthalassa Ocean (black squares) and thus a different realm as all other publications during the studied time interval. Strontium isotopes are from McArthur et al., 2000, B isotopes from Klein et al., in preparation (see chapter 3) and Li isotopes generated on the same sample material for this study. The red shaded interval marks the time span in which elevated CO_2 concentrations prevailed (red line, from Ullmann et al., 2020). The grey dashed line is a silicate weathering model from Ullmann et al., 2020. *[High-resolution image on attached CD]*
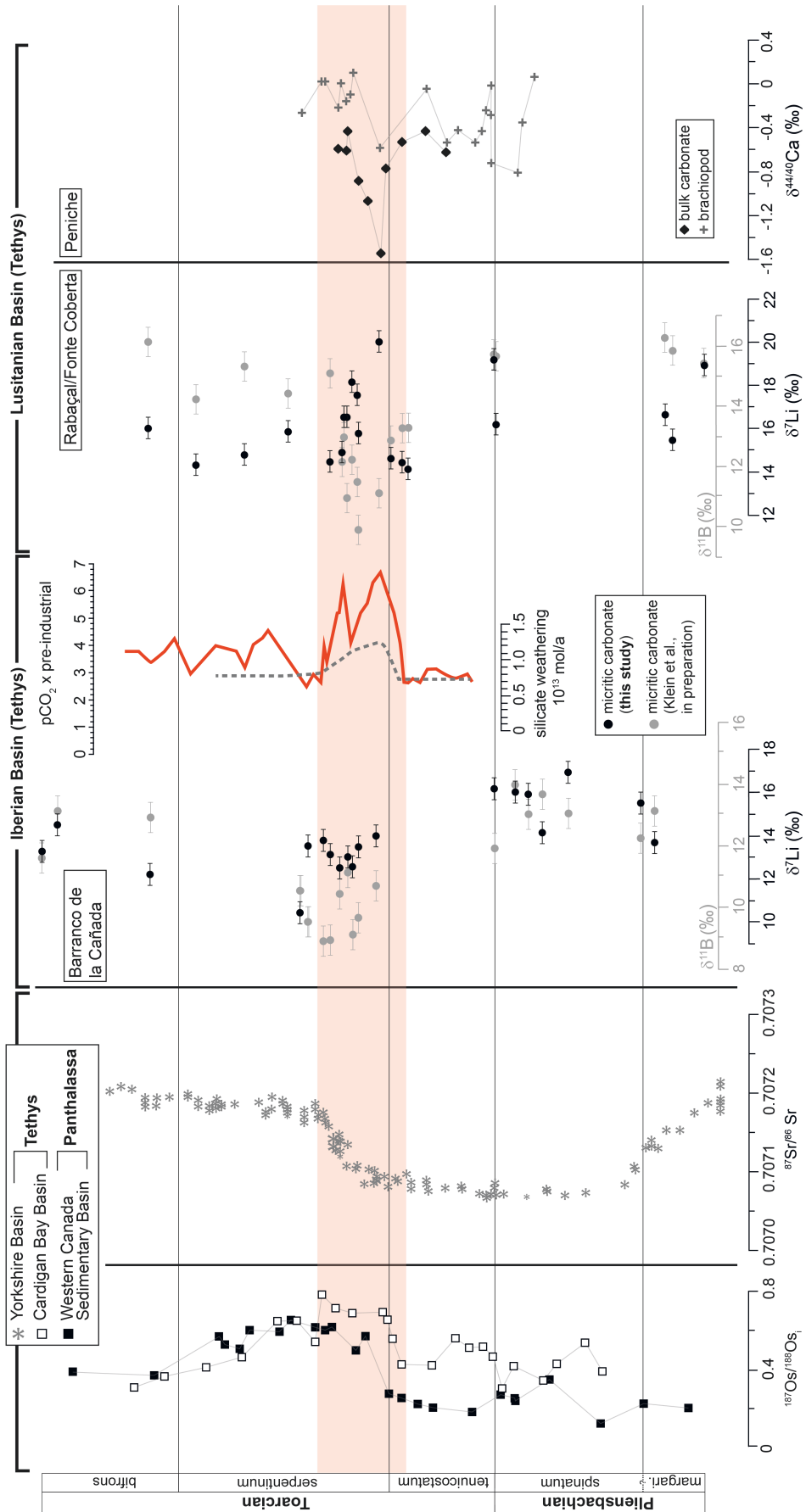
in the LB and IB, they still could have been generally low. Also, in contrast to the conditions in the LB during the T-OAE, where a strong structural control is assumed (Pittet et al., 2014), for the Pl–To boundary no such control was noticed by lithofacies (Duarte et al., 2010). Pittet et al., 2014 suggested that the tectonic structure of the LB during the earliest Toarcian was either formed during this time interval or, if it already existed, simply enhanced, and was probably not present during the Pl–To boundary. Nevertheless, a hint for a basin restriction of the LB is described by a calcareous nannofossil evolution study from Reggiani et al., 2010, who suggested that the connection of the LB basin could indeed have been restricted during the Pl–To boundary.

4.5.5. Interpretation of the Li isotopic trends

In the light of a temporary basin restriction for the LB during the T-OAE, we are able to explain our generated δ^7Li and other isotopic signals recorded for this interval, also further supporting the idea of a basin restriction.

Pre-T-OAE interval (Fig. 15 D). The early Toarcian mid-*polymorphum* AZ was dominated by low CO_2 concentrations in the atmosphere with a tendency to a rise, low bottom water temperatures (Suan et al., 2008), and a rise in the δ^{13}C signature, recording conditions of enhanced carbon burial (e.g. Hesselbo et al., 2007; Pittet et al., 2014; Ullmann et al., 2020)(Fig. 15 D). The LB and IB were connected to the open ocean and the sea level was relatively low but continuously rising. Unfortunately, our Li profile does not cover this pre-T-OAE interval, however, we assume that probably the same level as during the very onset of the T-OAE prevailed (δ^7Li = ~14.4 ‰) or a gradual declining trend from higher Pl–To boundary conditions from about 16 ‰ occurred.

T-OAE interval (Fig. 16 E, F). The onset of the T-OAE (*levisoni* AZ) marks abrupt environmental changes. The again active Karoo-Ferrar LIP volcanism lead to high atmospheric CO_2 concentrations and global warming, plus a CIE with a drop in the δ^{13}C signatures, which characterises the commencement of the global oceanic anoxic event. The lithological log in the LB indicates an abrupt sea level fall with the onset of the calcarenite horizons that record a storm influence, and go along with a pulse to a higher δ^7Li signature, and hence incongruent weathering conditions. Causes for a low sea level during the T-OAE in the LB are assumed by marked changes

Figure 15 *(following page).* Sketch displaying the paleoceanographic evolution of the Lusitanian (LB) and Iberian Basins (IB) with respect to environmental conditions. (A) Schematic outline of LB and IB with respective locations of studied sections (R/FC = Rabaçal/Fonte Coberta, BdC = Barranco de la Cañada) on the carbonate platform. For the LB the Peniche section, which is not part of this study, is additionally shown for reference. BF = Berlenga-Farilhões horst, IM = Iberian Massif, SL = sea level, MFS = maximum flooding surface, temp. = temperature. The sketches are modified after Suan et al., 2008. For detailed explanation see discussion. *[High-resolution image on attached CD]*
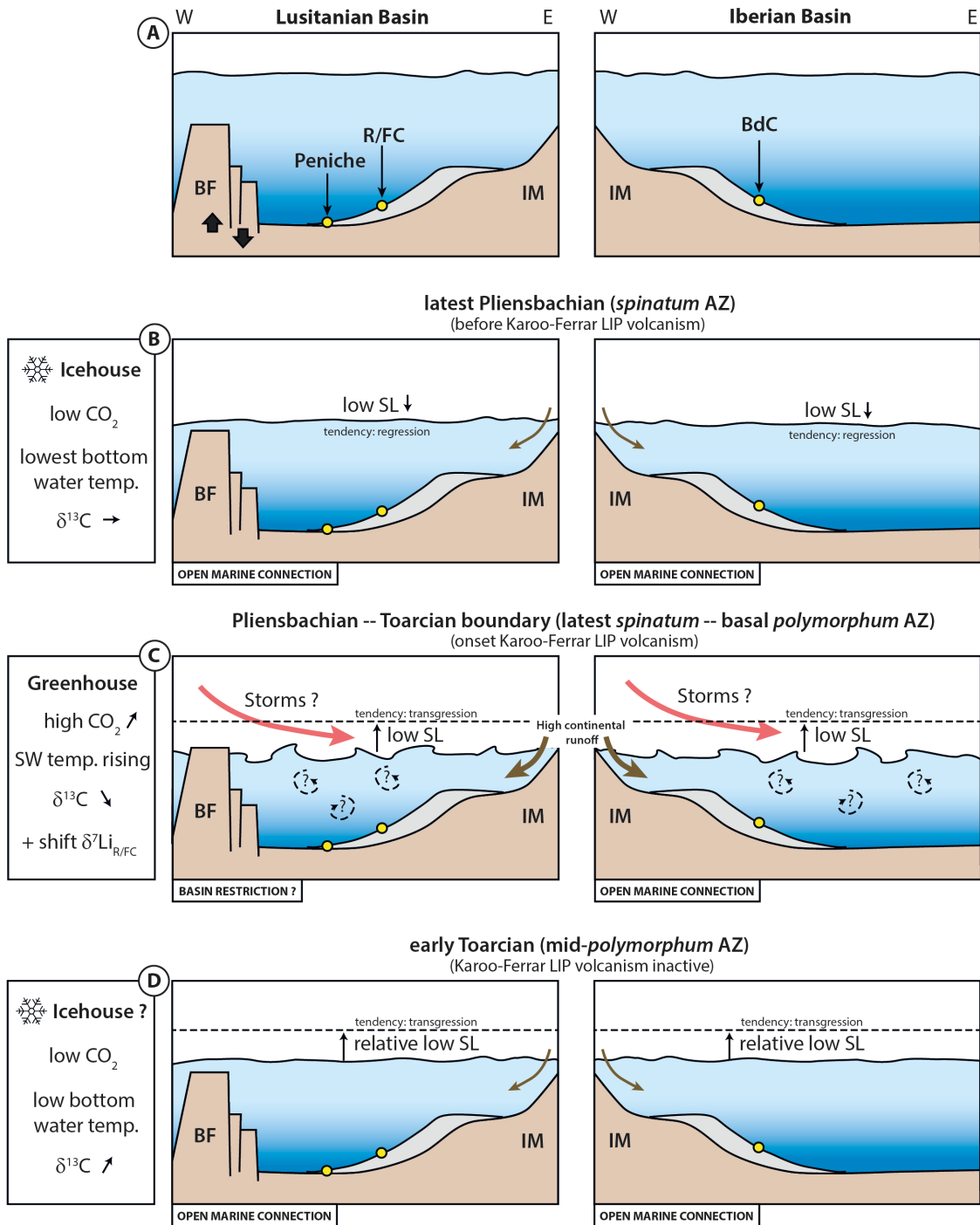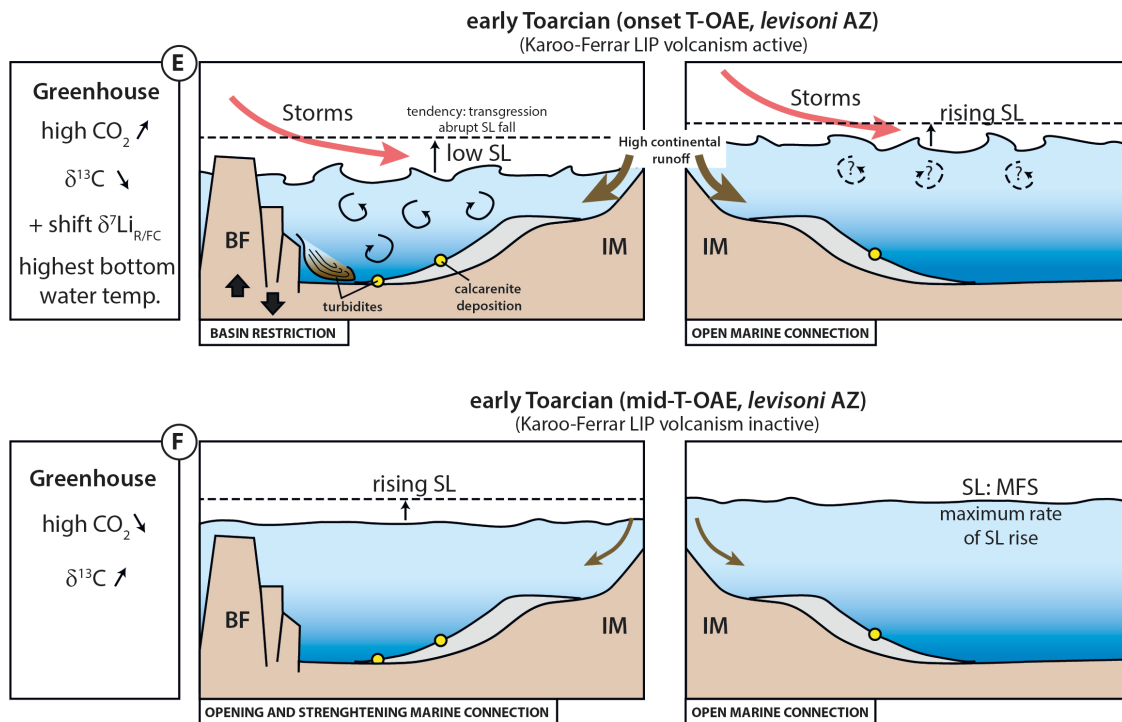
Figure 16. Continued from previous figure *[High-resolution image on attached CD]*

in the paleotopography and paleogeography, when new structural heights were formed that deeply influenced and controlled the water mass exchange (Pittet et al., 2014) through a basin restriction (see previous section). This led to changes in the equilibrium profile of rivers, which in turn drove higher erosion rates of continental blocks, as well as more siliciclastic input as observed in Peniche (Fig. 16 E) (Suan et al., 2008). This abrupt enhance in erosion rate, coupled with the sea level fall, would have led to the development of floodplain areas that have the potential to fractionate the Li isotopes through the formation of secondary clay minerals, and lead to an incongruent weathering signal (R/FC, Fig. 12, 16 E) (Pogge von Strandmann and Henderson, 2014). This change occurred concurrently with the onset of the calcarenite deposition. This pulse of incongruent weathering ($\sim$150 kyr) is subsequently replaced by a more efficient CO_2 removal mechanism when weathering became more congruent and Li values gradually decreased.

The IB, on the contrary, recorded a congruent weathering signal (thus a decreased δ^7Li signal) with the onset of the T-OAE (Fig. 13). These contrary Li isotope signatures in both basins further support the idea of a restriction of the LB basin, and hence a local signal that is recorded in R/FC. The IB probably records open ocean conditions, whereas additional basins must be examined to support this idea. The IB reaches δ^7Li values that fall into line with the values recorded in the LB at the end of the CO_2 sequestration and the end of the calcarenitic facies, indicating that both basins now record open ocean conditions. This speaks for a now again once more open ocean

connected LB, due to a rise in sea level and the overcoming of the structural barrieres (Fig. 16
F). This specifically limits the LB restriction only during the deposition of the calcarenitic facies,
when the sea level was especially low (Fig. 16 E).

Another interesting point, and further support of our ideas, comes from additional isotopic
systems of calcium (Ca) and boron (B) (Fig. 14). The study by Brazier et al., 2015 revealed
a negative peak in $\delta^{44/40}$Ca values (Peniche section, LB) derived from massive discharges from
continents. This mechanism delivered many ions to the oceans and hence raised alkalinity, and
in turn helped the seawater to recover from its acidic state through precipitation of carbonate
minerals. These massive continental discharges are also interpreted for our Li isotope signal, and
both isotopic excursions also occur simultaneously. Evidence for a drop in seawater pH during the
T-OAE are obtained by δ^{11}B isotopes (Klein et al., in preparation) that interestingly reveal the
same pattern as the Ca isotopes from Peniche. The increase in seawater pH (and likewise in δ^{11}B)
coincided with the increase in Ca isotopes, and decrease in Li isotopes, speaking for a connection
of all three isotopic systems and their reactions to same changes in environmental conditions. Yet,
the recovery from decreased pH conditions in the IB is somewhat delayed in comparison to the LB
(Fig. 14) and exceeds the interval of raised atmospheric CO_2. This observation could be due to
limited supply of silicate material and thus globally more inefficient drawdown of CO_2 (Ullmann
et al., 2020). For the carbon system to restore its equilibrium it takes several 100,000 years (e.g.
Lenton and Britton, 2006; Uchikawa and Zeebe, 2008), and hence the faster recovery from the
decreased pH conditions seen in the LB is simply owing to its restriction.

Pliensbachian–Toarcian Boundary Event (Fig. 15 C). A likewise positive shift in δ^7Li is recorded
as a pulse of silicate weathering ($\sim$7 kyrs) at the Pl–To boundary (*spinatum/tenuicosatum* AZ)
(Fig. 12, 13), which is also triggered by a relative short volcanic activity of the Karoo-Ferrar
LIP. Unfortunately, we are not able to record this shift in the IB due to lack of sample material.
However, a similar basin configuration as during the T-OAE is assumed to explain the Li signature:
a short temporal basin restriction with a high continental runoff and the development of floodpain
areas to fractionate the Li isotopes. Also, a coincident drop in Ca isotopes (from the Peniche
area) with the rise in Li isotopes is recorded (Fig. 14, Brazier et al., 2015), again mirroring the
same conditions as during the T-OAE. Nonetheless, with our study we can also simply add to the
suggestions for a basin restriction of the LB at the Pl–To boundary, because the abrupt shift in
silicate weathering could only be recorded for one basin, and also only relies on one data point.
To clarify this hypothesis more studies in different basins are advocated with a higher sampling
interval, as the Pl–To boundary event was relatively short in comparison to the Toarcian event.

4.5.6. Comparison to other OAE events

Oceanic anoxic events happened several times during the geological past and were always marked by environmental perturbations, most probably triggered by introducing huge amounts of CO_2 into the ocean–atmosphere system from enormous volcanic eruptions (Jenkyns, 2003, 2010; Larson, 1991; Larson and Erba, 1999; Weissert and Erba, 2004; Weissert et al., 1998). Two studies already reconstructed the weathering conditions and fluxes with Li isotopes during two OAE events in the Cretaceous: OAE 2/ C-T OAE at the Cenomanian–Turonian boundary ~93 Ma ago (Pogge von Strandmann et al., 2013) and OAE 1a/ Selli event during the early Aptian ~120 Ma ago (Lechler et al., 2015). Both found remarkably same trends in isotopic systems with a decrease in $^{187}Os/^{188}Os$ and $^{87}Sr/^{86}Sr$ (becoming more radiogenic), and negative shifts in $\delta^{44/40}Ca$ and δ^7Li (Lechler et al., 2015; Pogge von Strandmann et al., 2013 and respectively references therein). The trends point in equal measure to higher silicate weathering of mafic minerals derived from LIP basaltic eruptions, that simultaneously were deposited when the observed isotope shifts set in.

Interestingly, the isotope trends seen for the T-OAE are different for $^{187}Os/^{188}Os$, where more unradiogenic values were recorded with the eruption of Karoo–Ferrar and the subsequent T-OAE and Pl–To boundary events (Fig. 14). This is probably owing to the difference in location of the LIP basalts during both epochs (Percival et al., 2016), since low-latitude submarine LIPs as the Ontong-Java and Caribbean plateaus, which are both associated with the above mentioned OAEs, are more prone to weathering and hence increase the radiogenic Os flux (Cohen and Coe, 2007). In contrast, the Karoo–Ferrar LIP was located in the high latitudes and thus experienced less intense weathering, resulting in the enhanced continental Os flux dominating the seawater Os signature (Percival et al., 2016).

The likewise distinct different $^{87}Sr/^{86}Sr$ isotope trends between the T-OAE and the Cretaceous OAEs have firstly been noticed by Jones and Jenkyns, 2001. They observed that the T-OAE occurred at the end of the major decrease in $^{87}Sr/^{86}Sr$, while the C-T OAE and Selli event OAE record it more or less at the onset of each event. While enhanced hydrothermal activity was postulated as a cause for all three negative $^{87}Sr/^{86}Sr$ signatures, the decoupled onset with the beginning of the OAEs implies independent triggers for each anoxic event (Jones and Jenkyns, 2001). However, as the continental weathering Sr signature is expected to be more radiogenic (although this is also strongly depends on the weathered silicate minerals, see Raymo and Ruddiman, 1992) and this trend is not observed for the Cretaceous OAEs, it could also well be that the weathering pulse was too short to be captured by the Sr isotopes, or the amount added by the continents was not sufficient enough to overprint the seawater hydrothermal signature (Bralower et al., 1997; Jones and Jenkyns, 2001; Lechler et al., 2015; Pogge von Strandmann et al., 2013). This could also be the case for the T-OAE and Pl–To events, since no abrupt shifts in the Sr isotopes is observed.

4.6. Conclusions and outlook

Our study shows short-term pulses of silicate weathering for the Toarcian OAE and the Pl–To boundary event from the δ^7Li signature. The distinct differences in the Li isotope signature for the Lusitanian (LB) and Iberian basin (IB) leads to the conclusion that the LB was probably restricted temporarily during both events, due to a drastic drop in sea level, coupled with tectonic activity and formation of effective water mass barriers. The exposure of more continental surface and the development of floodplain areas would have led to higher physical weathering rates, and together with the generally elevated temperatures and CO_2 concentrations, also to higher runoff that led to a faster recovery of an evident seawater pH drop in the LB than in the IB. However, to confirm the nature of the open ocean seawater δ^7Li signature in the IB, more sections even in other realms like the Panthalassa ocean should be analysed and compared. Also, silicate weathering rates could be reconstructed, due to the unique incongruent weathering signal observed in the LB, to verify the different weathering rates so far published from Os and Ca isotopes.

Another finding of this study is the rather low δ^7Li seawater for the signature prior and after the T-OAE, which is recorded in the LB and IB when both were probably connected to the open ocean. Here we record for the Early Jurassic values that are comparable to the minimum δ^7Li values observed during the Paleogene ($\sim$20‰), which are distinctly different from the Cretaceous ($\sim$26‰) and nowadays ($\sim$31‰), implying major changes in the weathering realms over time.

4.7. Acknowledgements

References

Aarnes, I., H. Svensen, S. Polteau, and S. Planke (2011). "Contact metamorphic devolatilization of shales in the Karoo Basin, South Africa, and the effects of multiple sill intrusions". *Chemical Geology* 281.3-4, pp. 181–194. DOI: 10.1016/j.chemgeo.2010.12.007.

Anderson, J. M., J. Proctor, and H. W. Vallack (1983). "Ecological Studies in Four Contrasting Lowland Rain Forests in Gunung Mulu National Park, Sarawak: III. Decomposition Processes and Nutrient Losses from Leaf Litter". *The Journal of Ecology* 71.2, p. 503. DOI: 10.2307/2259731.

Baeza-Carratalá, J. F., F. García Joral, and J. E. Tent-Manclús (2011). "Biostratigraphy and paleobiogeographic affinities of the Jurassic brachiopod assemblages from Sierra Espuña (Maláguide Complex, Internal Betic Zones, Spain)". *Journal of Iberian Geology* 37.2. DOI: 10.5209/rev{\textunderscore}JIGE.2011.v37.n2.3.

Bailey, T. R., Y. Rosenthal, J. M. McArthur, B. van de Schootbrugge, and M. F. Thirlwall (2003). "Paleoceanographic changes of the Late Pliensbachian–Early Toarcian interval: A possible link to the genesis of an Oceanic Anoxic Event". *Earth and Planetary Science Letters* 212.3-4, pp. 307–320. DOI: 10.1016/S0012-821X(03)00278-4.

Bassoullet, J.-P. and F. Baudin (1994). "Le toarcien inférieur: Une période de crise dans les bassins et sur les plate-formes carbonatées de l'Europe du Nord-Ouest et de la Téthys". *Geobios* 27, pp. 645–654. DOI: 10.1016/S0016-6995(94)80227-0.

Bastian, L., N. Vigier, S. Reynaud, M.-E. Kerros, M. Revel, and G. Bayon (2018). "Lithium Isotope Composition of Marine Biogenic Carbonates and Related Reference Materials". *Geostandards and Geoanalytical Research* 42.3, pp. 403–415. DOI: 10.1111/ggr.12218.

Berglund, M. and M. E. Wieser (2011). "Isotopic compositions of the elements 2009: IUPAC Technical Report". *Pure Application Chemistry* 83, pp. 397–410.

Berner, R. A. (2003). "The long-term carbon cycle, fossil fuels and atmospheric composition". *Nature* 426.6964, pp. 323–326. DOI: 10.1038/nature02131.

Bi, E. B. B., N. Vigier, A. Poszwa, and A. Bernot (2007). "Compared Mg isotope compositions of plants, rocks and waters". *Geochimica et Cosmochimica Acta* 71.A106.

Black, J. R., Q.-z. Yin, and W. H. Casey (2006). "An experimental study of magnesium-isotope fractionation in chlorophyll-a photosynthesis". *Geochimica et Cosmochimica Acta* 70.16, pp. 4072–4079. DOI: 10.1016/j.gca.2006.06.010.

Boulila, S., B. Galbrun, E. Huret, L. A. Hinnov, I. Rouget, S. Gardin, and A. Bartolini (2014). "Astronomical calibration of the Toarcian Stage: Implications for sequence stratigraphy and duration of the early Toarcian OAE". *Earth and Planetary Science Letters* 386, pp. 98–111. DOI: 10.1016/j.epsl.2013.10.047.

Bralower, T. J., P. D. Fullagar, C. K. Paull, G. S. Dwyer, and R. M. Leckie (1997). "Mid-Cretaceous strontium-isotope stratigraphy of deep-sea sections". *Geological Society of America Bulletin* 109.11, p. 1421. DOI: 10.1130/0016-7606(1997)109{\textless}1421:MCSISO{\textgreater}2.3.CO;2.

Brazier, J.-M., G. Suan, T. Tacail, L. Simon, J. E. Martin, E. Mattioli, and V. Balter (2015). "Calcium isotope evidence for dramatic increase of continental weathering during the Toarcian oceanic anoxic event (Early Jurassic)". *Earth and Planetary Science Letters* 411, pp. 164–176. DOI: 10.1016/j.epsl.2014.11.028.

Brenot, A., C. Cloquet, N. Vigier, J. Carignan, and C. France-Lanord (2008). "Magnesium isotope systematics of the lithologically varied Moselle river basin, France". *Geochimica et Cosmochimica Acta* 72.20, pp. 5070–5089. DOI: 10.1016/j.gca.2008.07.027.

Broecker, W. S. and T. H. Peng (1982). *Tracers in the Sea*. Palisades, New York: Eldigio Pr.

Burgess, S. D., S. A. Bowring, T. H. Fleming, and D. H. Elliot (2015). "High-precision geochronology links the Ferrar large igneous province with early-Jurassic ocean anoxia and biotic crisis". *Earth and Planetary Science Letters* 415, pp. 90–99. DOI: 10.1016/j.epsl.2015.01.037.

Burton, K. W. and N. Vigier (2012). "Lithium isotopes as tracers in marine and terrestrial environments". *Handbook of Environmental Isotope Geochemistry*. Ed. by M. Baskaran.

Berlin, Heidelberg: Springer Berlin Heidelberg, pp. 41–59.

Cecca, F. and F. Macchioni (2004). "The two Early Toarcian (Early Jurassic) extinction events in ammonoids". *Lethaia* 37.1, pp. 35–56. DOI: 10.1080/00241160310008257.

Chakrabarti, R. and S. B. Jacobsen (2010). "The isotopic composition of magnesium in the inner Solar System". *Earth and Planetary Science Letters* 293.3-4, pp. 349–358. DOI: 10.1016/j.epsl.2010.03.001.

Chan, L., J. Edmond, G. Thompson, and K. Gillis (1992). "Lithium isotopic composition of submarine basalts: Implications for the lithium cycle in the oceans". *Earth and Planetary Science Letters* 108.1-3, pp. 151–160. DOI: 10.1016/0012-821X(92)90067-6.

Chan, L.-H., W. P. Leeman, and T. Plank (2006). "Lithium isotopic composition of marine sediments". *Geochemistry, Geophysics, Geosystems* 7.6, pp. 1–25. DOI: 10.1029/2005GC001202.

Clarkson, M. O., S. A. Kasemann, R. A. Wood, T. M. Lenton, S. J. Daines, S. Richoz, F. Ohnemueller, A. Meixner, S. W. Poulton, and E. T. Tipper (2015). "Ocean acidification and the Permo-Triassic mass extinction". *Science (New York, N.Y.)* 348.6231, pp. 229–232. DOI: 10.1126/science.aaa0193.

Cohen, A. S. and A. L. Coe (2007). "The impact of the Central Atlantic Magmatic Province on climate and on the Sr- and Os-isotope evolution of seawater". *Palaeogeography, Palaeoclimatology, Palaeoecology* 244.1-4, pp. 374–390. DOI: 10.1016/j.palaeo.2006.06.036.

Cohen, A. S., A. L. Coe, S. M. Harding, and L. Schwark (2004). "Osmium isotope evidence for the regulation of atmospheric CO_2 by continental weathering". *Geology* 32.2, p. 157. DOI: 10.1130/G20158.1.

Comas-Rengifo, M. J., L. V. Duarte, F. F. Felix, F. G. Joral, A. Goy, and R. B. Rocha (2014). "Latest Pliensbachian-Early Toarcian brachiopod assemblages from the Peniche section (Portugal) and their correlation". *Episodes - Journal of International Geosciences* 38.1, pp. 2–8.

Comas-Rengifo, M. J., L. V. Duarte, F. García Joral, and A. Goy (2013). "Los braquiópodos del Toarciense Inferior (Jurásico) en el área de Rabaçal-Condeixa (Portugal): distribución estratigráfica y paleobiogeografía". *Comunicações geológicas* 100.Esp. I, pp. 37–42.

Correia, V. F., J. B. Riding, L. V. Duarte, P. Fernandes, and Z. Pereira (2018). "The Early Jurassic palynostratigraphy of the Lusitanian Basin, western Portugal". *Geobios* 51.6, pp. 537–557. DOI: 10.1016/j.geobios.2018.03.001.

Danise, S., M.-E. Clémence, G. D. Price, D. P. Murphy, J. J. Gómez, and R. J. Twitchett (2019). "Stratigraphic and environmental control on marine benthic community change through the early Toarcian extinction event (Iberian Range, Spain)". *Palaeogeography, Palaeoclimatology, Palaeoecology* 524, pp. 183–200. DOI: 10.1016/j.palaeo.2019.03.039.

Dellinger, M., J. Gaillardet, J. Bouchez, D. Calmels, P. Louvat, A. Dosseto, C. Gorge, L. Alanoca, and L. Maurice (2015). "Riverine Li isotope fractionation in the Amazon River basin controlled by the weathering regimes". *Geochimica et Cosmochimica Acta* 164, pp. 71–93. DOI: 10.1016/j.gca.2015.04.042.

Dera, G. and Y. Donnadieu (2012). "Modeling evidences for global warming, Arctic seawater freshening, and sluggish oceanic circulation during the Early Toarcian anoxic event". *Paleoceanography* 27.2, pp. 1–15. DOI: 10.1029/2012PA002283.

Dera, G., P. Neige, J.-L. Dommergues, and A. Brayard (2011). "Ammonite paleobiogeography during the Pliensbachian–Toarcian crisis (Early Jurassic) reflecting paleoclimate, eustasy, and extinctions". *Global and Planetary Change* 78.3-4, pp. 92–105. DOI: 10.1016/j.gloplacha.2011.05.009.

Dera, G., E. Pucéat, P. Pellenard, P. Neige, D. Delsate, M. M. Joachimski, L. Reisberg, and M. Martinez (2009). "Water mass exchange and variations in seawater temperature in the NW Tethys during the Early Jurassic: Evidence from neodymium and oxygen isotopes of fish teeth and belemnites". *Earth and Planetary Science Letters* 286.1-2, pp. 198–207. DOI: 10.1016/j.epsl.2009.06.027.

Duarte, L. V. (1995). *O Toarciano da Bacia Lusitaniana. Estratigrafia e evolução sedimentogénica: Ph.D. thesis*. Coimbra, Portugal.

Duarte, L. V. (1997). "Facies analysis and sequential evolution of the Toarcian-Lower Aalenian series in the Lusitanian Basin (Portugal)". *Comunicações do Instituto Geológico e Mineiro* 83, pp. 65–94.

– (1998). "Clay minerals and geochemical evolution in the Toarcian Lower Aalenian of the Lusitanian Basin". *Cuadernos de Geologa Iberica* 24, pp. 69–98.

– (2007). "Lithostratigraphy, sequence stratigraphy and depositional setting of the Pliensbachian and Toarcian series in the Lusitanian Basin, Portugal". *Ciências da Terra (UNL)* 16, pp. 17–23.

Duarte, L. V., N. Perilli, R. Dino, R. Rodrigues, and R. Paredes (2004). "Lower to middle Toarcian from the Coimbra region (Lusitanian Basin, Portugal): Sequence stratigraphy, calcareous nannofossils and stable-isotope evolution". *Rivista Italiana di Paleontologia e Stratigrafia* 110.1, pp. 115–127.

Duarte, L. V., R. L. Silva, L. C. V. Oliviera, M. J. Comas-Rengifo, and F. Silva (2010). "Organic-Rich facies in the Sinemurian and Pliensbachian of the Lusitanian Basin, Portugal: Total organic carbon distribution and relation to transgressive-regressive facies cycles". *Geologica Acta* 8.3, pp. 325–340.

Duarte, L. V. and A. F. Soares (2002). "Litostratigrafia das séries margo-calcárias do Jurássico inferior da Bacia Lusitânica (Portugal)". *Comunicações do Instituto Geológico e Mineiro* 89, pp. 135–154.

Elderfield, H. and A. Schultz (1996). "Mid-Ocean Ridge Hydrothermal Fluxes and the Chemical Composition of the Ocean". *Annu. Rev. Earth Planet. Sci.* 24.1, pp. 191–224. DOI: 10.1146/annurev.earth.24.1.191.

Elliot, D. H. and T. H. Fleming (2008). "Physical volcanology and geological relationships of the Jurassic Ferrar Large Igneous Province, Antarctica". *Journal of Volcanology and Geothermal Research* 172.1-2, pp. 20–37. DOI: 10.1016/j.jvolgeores.2006.02.016.

Elliot, D. H. (2013). "The geological and tectonic evolution of the Transantarctic Mountains: A review". *Geological Society, London, Special Publications* 381.1, pp. 7–35. DOI: 10.1144/SP381.14.

Fantle, M. S. and J. Higgins (2014). "The effects of diagenesis and dolomitization on Ca and Mg isotopes in marine platform carbonates: Implications for the geochemical cycles of Ca and Mg". *Geochimica et Cosmochimica Acta* 142, pp. 458–481. DOI: 10.1016/j.gca.2014.07.025.

Ferreira, J., E. Mattioli, B. Pittet, M. Cachão, and J. E. Spangenberg (2015). "Palaeoecological insights on Toarcian and lower Aalenian calcareous nannofossils from the Lusitanian Basin (Portugal)". *Palaeogeography, Palaeoclimatology, Palaeoecology* 436, pp. 245–262. DOI: 10.1016/j.palaeo.2015.07.012.

Foster, G. L., P. A. E. Pogge von Strandmann, and J. W. B. Rae (2010). "Boron and magnesium isotopic composition of seawater". *Geochemistry, Geophysics, Geosystems* 11.8, n/a–n/a. DOI: 10.1029/2010GC003201.

France-Lanord, C. and L. A. Derry (1997). "Organic carbon burial forcing of the carbon cycle from Himalayan erosion". *Nature* 390.6655, pp. 65–67. DOI: 10.1038/36324.

Fu, X., J. Wang, S. Zeng, X. Feng, D. Wang, and C. Song (2017). "Continental weathering and palaeoclimatic changes through the onset of the Early Toarcian oceanic anoxic event in the Qiangtang Basin, eastern Tethys". *Palaeogeography, Palaeoclimatology, Palaeoecology* 487, pp. 241–250. DOI: 10.1016/j.palaeo.2017.09.005.

Gahr, M. E. (2002). "Palökologie des Makrobenthos aus dem Unter-Toarc SW-Europas: Dissertation". *Beringeria* 31.

– (2005). "Response of Lower Toarcian (Lower Jurassic) macrobenthos of the Iberian Peninsula to sea level changes and mass extinction". *Journal of Iberian Geology* 31.2, pp. 197–215.

Gaillardet, J., J. Viers, and B. Dupré (2003). "Trace Elements in River Waters". *Treatise on Geochemistry*. Ed. by H. D. Holland and K. K. Turekian. Elsevier, pp. 225–272.

Galy, A., M. Bar-Matthews, L. Halicz, and R. O'Nions (2002). "Mg isotopic composition of carbonate: Insight from speleothem formation". *Earth and Planetary Science Letters* 201.1, pp. 105–115. DOI: 10.1016/S0012-821X(02)00675-1.

Gao, T. (2016). *High-precision measurement of Mg isotopes and their geochemical behaviors during continental weathering*. Beijing: China University of Geosciences (in Chinese with English abstract).

Gao, T., S. Ke, S.-J. Wang, F. Li, C. Liu, J. Lei, C. Liao, and F. Wu (2018). "Contrasting Mg isotopic compositions between Fe-Mn nodules and surrounding soils: Accumulation of light Mg isotopes by Mg-depleted clay minerals and Fe oxides". *Geochimica et Cosmochimica Acta* 237, pp. 205–222. DOI: 10.1016/j.gca.2018.06.028.

García Joral, F., J. J. Gómez, and A. Goy (2011). "Mass extinction and recovery of the Early Toarcian (Early Jurassic) brachiopods linked to climate change in Northern and Central Spain". *Palaeogeography, Palaeoclimatology, Palaeoecology* 302.3-4, pp. 367–380. DOI: 10.1016/j.palaeo.2011.01.023.

Garrison, T. (2006). *Oceanography: An invitation to marine science.* 6. edition. Brook and Cole Publishers.

Gómez, J. J. and C. Arias (2010). "Rapid warming and ostracods mass extinction at the Lower Toarcian (Jurassic) of central Spain". *Marine Micropaleontology* 74.3-4, pp. 119–135. DOI: 10.1016/j.marmicro.2010.02.001.

Gómez, J. J., A. Goy, and M. L. Canales (2008). "Seawater temperature and carbon isotope variations in belemnites linked to mass extinction during the Toarcian (Early Jurassic) in Central and Northern Spain. Comparison with other European sections". *Palaeogeography, Palaeoclimatology, Palaeoecology* 258.1-2, pp. 28–58. DOI: 10.1016/j.palaeo.2007.11.005.

Gómez, J. J. and A. Goy (2005). "Late Triassic and Early Jurassic palaeogeographic evolution and depositional cycles of the Western Tethys Iberian platform system (Eastern Spain)". *Palaeogeography, Palaeoclimatology, Palaeoecology* 222.1-2, pp. 77–94. DOI: 10.1016/j.palaeo.2005.03.010.

– (2011). "Warming-driven mass extinction in the Early Toarcian (Early Jurassic) of northern and central Spain. Correlation with other time-equivalent European sections". *Palaeogeography, Palaeoclimatology, Palaeoecology* 306.3-4, pp. 176–195. DOI: 10.1016/j.palaeo.2011.04.018.

Guex, J., A. Morard, A. Bartolini, and E. Morettini (2001). "Découverte d'une importante lacune stratigraphique a' la limite Domérien-Toarcien: Implications paleooceanographiques". *Bull. Soc. Vaudoise Sci. Nat.* 345, pp. 277–284.

Hermoso, M. and P. Pellenard (2014). "Continental weathering and climatic changes inferred from clay mineralogy and paired carbon isotopes across the early to middle Toarcian in the Paris Basin". *Palaeogeography, Palaeoclimatology, Palaeoecology* 399, pp. 385–393. DOI: 10.1016/j.palaeo.2014.02.007.

Hesselbo, Grocke, Jenkyns, Bjerrum, Farrimond, B. H. S. Morgans, and Green (2000). "Massive dissociation of gas hydrate during a Jurassic oceanic anoxic event". *Nature* 406.6794, pp. 392–395. DOI: 10.1038/35019044..

Hesselbo, S. P., H. C. Jenkyns, L. V. Duarte, and L. C. Oliveira (2007). "Carbon-isotope record of the Early Jurassic (Toarcian) Oceanic Anoxic Event from fossil wood and marine carbonate (Lusitanian Basin, Portugal)". *Earth and Planetary Science Letters* 253.3-4, pp. 455–470. DOI: 10.1016/j.epsl.2006.11.009.

Higgins, J. A. and D. P. Schrag (2012). "Records of Neogene seawater chemistry and diagenesis in deep-sea carbonate sediments and pore fluids". *Earth and Planetary Science Letters* 357-358, pp. 386–396. DOI: 10.1016/j.epsl.2012.08.030.

Huang, K.-F., C.-F. You, Y.-H. Liu, R.-M. Wang, P.-Y. Lin, and C.-H. Chung (2010). "Low-memory, small sample size, accurate and high-precision determinations of lithium isotopic ratios in natural materials by MC-ICP-MS". *Journal of Analytical Atomic Spectrometry* 25.7, p. 1019. DOI: 10.1039/B926327F.

Huang, Y., J. Tong, M. L. Fraiser, and Z.-Q. Chen (2014). "Extinction patterns among bivalves in South China during the Permian–Triassic crisis". *Palaeogeography, Palaeoclimatology, Palaeoecology* 399, pp. 78–88. DOI: 10.1016/j.palaeo.2014.01.030.

Huh, Y., L.-H. Chan, and J. M. Edmond (2001). "Lithium isotopes as a probe of weathering processes: Orinoco River". *Earth and Planetary Science Letters* 194.1-2, pp. 189–199. DOI: 10.1016/S0012-821X(01)00523-4.

Huh, Y., L.-H. Chan, L. Zhang, and J. M. Edmond (1998). "Lithium and its isotopes in major world rivers: Implications for weathering and the oceanic budget". *Geochimica*

et Cosmochimica Acta 62.12, pp. 2039–2051. DOI: 10.1016/S0016-7037(98)00126-4.

Ikeda, M. and R. S. Hori (2014). "Effects of Karoo–Ferrar volcanism and astronomical cycles on the Toarcian Oceanic Anoxic Events (Early Jurassic)". *Palaeogeography, Palaeoclimatology, Palaeoecology* 410, pp. 134–142. DOI: 10.1016/j.palaeo.2014.05.026.

Immenhauser, A., D. Buhl, D. Richter, A. Niedermayr, D. Riechelmann, M. Dietzel, and U. Schulte (2010). "Magnesium-isotope fractionation during low-Mg calcite precipitation in a limestone cave – Field study and experiments". *Geochimica et Cosmochimica Acta* 74.15, pp. 4346–4364. DOI: 10.1016/j.gca.2010.05.006.

Izumi, K., T. Miyaji, and K. Tanabe (2012). "Early Toarcian (Early Jurassic) oceanic anoxic event recorded in the shelf deposits in the northwestern Panthalassa: Evidence from the Nishinakayama Formation in the Toyora area, west Japan". *Palaeogeography, Palaeoclimatology, Palaeoecology* 315-316, pp. 100–108. DOI: 10.1016/j.palaeo.2011.11.016.

James, R. H., M. D. Rudnicki, and M. R. Palmer (1999). "The alkali element and boron geochemistry of the Escanaba Trough sediment-hosted hydrothermal system". *Earth and Planetary Science Letters* 171.1, pp. 157–169. DOI: 10.1016/S0012-821X(99)00140-5.

Jenkyns, H. C. (1988). "The early Toarcian (Jurassic) anoxic event; stratigraphic, sedimentary and geochemical evidence". *American Journal of Science* 288.2, pp. 101–151. DOI: 10.2475/ajs.288.2.101.

Jenkyns, H. C. (2003). "Evidence for rapid climate change in the Mesozoic-Palaeogene greenhouse world". *Philosophical transactions. Series A, Mathematical, physical, and engineering sciences* 361.1810, 1885–916, discussion 1916. DOI: 10.1098/rsta.2003.1240.

– (2010). "Geochemistry of oceanic anoxic events". *Geochemistry, Geophysics, Geosystems* 11.3, pp. 1–30. DOI: 10.1029/2009GC002788.

Jones, C. E. and H. C. Jenkyns (2001). "Seawater strontium isotopes, oceanic anoxic events, and seafloor hydrothermal activity in the Jurassic and Cretaceous". *American Journal of Science* 301, pp. 112–149.

Jones, C. E., H. C. Jenkyns, and S. P. Hesselbo (1994). "Strontium isotopes in Early Jurassic seawater". *Geochimica et Cosmochimica Acta* 58.4, pp. 1285–1301.

Kemp, D. B., A. L. Coe, A. S. Cohen, and L. Schwark (2005). "Astronomical pacing of methane release in the Early Jurassic period". *Nature* 437.7057, pp. 396–399. DOI: 10.1038/nature04037.

Kisakurek, B., R. H. James, and N. B. Harris (2005). "Li and δ^7Li in Himalayan rivers: Proxies for silicate weathering?" *Earth and Planetary Science Letters* 237.3-4, pp. 387–401. DOI: 10.1016/j.epsl.2005.07.019.

Klein, T., A. Meixner, C. V. Ullmann, L. Duarte, and S. A. Kasemann (in preparation). "A comparative study on seawater pH changes during the T-OAE (Early Jurassic) with boron isotopes".

Korte, C., S. P. Hesselbo, C. V. Ullmann, G. Dietl, M. Ruhl, G. Schweigert, and N. Thibault (2015). "Jurassic climate mode governed by ocean gateway". *Nature communications* 6, p. 10015. DOI: 10.1038/ncomms10015.

Krencker, F.-N., S. Bodin, G. Suan, U. Heimhofer, L. Kabiri, and A. Immenhauser (2015). "Toarcian extreme warmth led to tropical cyclone intensification". *Earth and Planetary Science Letters* 425, pp. 120–130. DOI: 10.1016/j.epsl.2015.06.003.

Kullberg, J., F. Olóriz, B. Marques, P. Caetano, and R. Rocha (2001). "Flat-pebble conglomerates: A local marker for Early Jurassic seismicity related to syn-rift tectonics in the Sesimbra area (Lusitanian Basin, Portugal)". *Sedimentary Geology* 139.1, pp. 49–70. DOI: 10.1016/S0037-0738(00)00160-3.

Larson, R. L. (1991). "Latest pulse of Earth: Evidence for a mid-Cretaceous superplume". *Geology* 19.6, p. 547. DOI: 10.1130/0091-7613(1991)019{\textless}0547:LPOEEF{\textgreater}2.3.CO;2.

Larson, R. L. and E. Erba (1999). "Onset of the Mid-Cretaceous greenhouse in the Barremian-Aptian: Igneous events and the biological, sedimentary, and geochemical responses". *Paleoceanography* 14.6, pp. 663–678. DOI: 10.1029/1999PA900040.

Lechler, M., P. A. Pogge von Strandmann, H. C. Jenkyns, G. Prosser, and M. Parente (2015). "Lithium-isotope evidence for enhanced silicate weathering during OAE 1a (Early Aptian Selli event)". *Earth and Planetary Science Letters* 432, pp. 210–222. DOI: `10.1016/j.epsl.2015.09.052`.

Lenton, T. M. and C. Britton (2006). "Enhanced carbonate and silicate weathering accelerates recovery from fossil fuel CO2 perturbations". *Global Biogeochemical Cycles* 20, pp. 1–12. DOI: `10.1029/2005GB002678`.

Léonide, P., M. Floquet, C. Durlet, F. Baudin, B. Pittet, and C. Lécuyer (2012). "Drowning of a carbonate platform as a precursor stage of the Early Toarcian global anoxic event (Southern Provence sub-Basin, Southeast France)". *Sedimentology* 59.1, pp. 156–184. DOI: `10.1111/j.1365-3091.2010.01221.x`.

Lézin, C., B. Andreu, P. Pellenard, J.-L. Bouchez, L. Emmanuel, P. Fauré, and P. Landrein (2013). "Geochemical disturbance and paleoenvironmental changes during the Early Toarcian in NW Europe". *Chemical Geology* 341, pp. 1–15. DOI: `10.1016/j.chemgeo.2013.01.003`.

Li, W., S. Chakraborty, B. L. Beard, C. S. Romanek, and C. M. Johnson (2012). "Magnesium isotope fractionation during precipitation of inorganic calcite under laboratory conditions". *Earth and Planetary Science Letters* 333-334, pp. 304–316. DOI: `10.1016/j.epsl.2012.04.010`.

Li, Y.-H. (1982). "A brief discussion on the mean oceanic residence time of elements". *Geochimica et Cosmochimica Acta* 46.12, pp. 2671–2675. DOI: `10.1016/0016-7037(82)90386-6`.

Ling, M.-X., F. Sedaghatpour, F.-Z. Teng, P. D. Hays, J. Strauss, and W. Sun (2011). "Homogeneous magnesium isotopic composition of seawater: An excellent geostandard for Mg isotope analysis". *Rapid communications in mass spectrometry : RCM* 25.19, pp. 2828–2836. DOI: `10.1002/rcm.5172`.

Littler, K., S. P. Hesselbo, and H. C. Jenkyns (2010). "A carbon-isotope perturbation at the Pliensbachian–Toarcian boundary: Evidence from the Lias Group, NE England". *Geological Magazine* 147.02, p. 181. DOI: `10.1017/S0016756809990458`.

Liu, S.-A., F.-Z. Teng, Y. He, S. Ke, and S. Li (2010). "Investigation of magnesium isotope fractionation during granite differentiation: Implication for Mg isotopic composition of the continental crust". *Earth and Planetary Science Letters* 297.3-4, pp. 646–654. DOI: `10.1016/j.epsl.2010.07.019`.

Liu, X.-M., F.-Z. Teng, R. L. Rudnick, W. F. McDonough, and M. L. Cummings (2014). "Massive magnesium depletion and isotope fractionation in weathered basalts". *Geochimica et Cosmochimica Acta* 135, pp. 336–349. DOI: `10.1016/j.gca.2014.03.028`.

Liu, X.-M., C. Wanner, R. L. Rudnick, and W. F. McDonough (2015). "Processes controlling $\delta^7 Li$ in rivers illuminated by study of streams and groundwaters draining basalts". *Earth and Planetary Science Letters* 409, pp. 212–224. DOI: `10.1016/j.epsl.2014.10.032`.

Lui-Heung, C., J. M. Gieskes, Y. Chen-Feng, and J. M. Edmond (1994). "Lithium isotope geochemistry of sediments and hydrothermal fluids of the Guaymas Basin, Gulf of California". *Geochimica et Cosmochimica Acta* 58.20, pp. 4443–4454. DOI: `10.1016/0016-7037(94)90346-8`.

Macedo de Paula-Santos, G., M. Babinski, F. Wilckens, and A. Meixner (2017). "The Li and Mg isotope record of the carbonate rocks of the Bambuí Goup, Sao Francisco Basin, Brazil (Dissertation)". Sao Paulo.

Mattioli, E., B. Pittet, L. Petitpierre, and S. Mailliot (2009). "Dramatic decrease of pelagic carbonate production by nannoplankton across the Early Toarcian anoxic event (T-OAE)". *Global and Planetary Change* 65.3-4, pp. 134–145. DOI: `10.1016/j.gloplacha.2008.10.018`.

McArthur, J. M., T. J. Algeo, B. van de Schootbrugge, Q. Li, and R. J. Howarth (2008). "Basinal restriction, black shales, Re-Os dating, and the Early Toarcian (Jurassic) oceanic anoxic event". *Paleoceanography* 23.4, n/a–n/a. DOI: `10.1029/2008PA001607`.

McArthur, J. M., D. Donovan, M. F. Thirlwall, B. W. Fouke, and D. Mattey (2000). "Strontium isotope profile of the early Toarcian (Jurassic) oceanic anoxic event, the duration of ammonite biozones, and belemnite palaeotemperatures". *Earth and Planetary*

Science Letters 179.2, pp. 269–285. DOI: 10.1016/S0012-821X(00)00111-4.

McElwain, J. C., J. Wade-Murphy, and S. P. Hesselbo (2005). "Changes in carbon dioxide during an oceanic anoxic event linked to intrusion into Gondwana coals". *Nature* 435.7041, pp. 479–482. DOI: 10.1038/nature03618.

Miguez-Salas, O., F. J. Rodríguez-Tovar, and L. V. Duarte (2018). "Ichnological analysis at the Fonte Coberta section (Lusitanian Basin, Portugal): Approaching depositional environment during the Toarcian oceanic anoxic event (T-OAE)". *Spanish Journal of Palaeontology* 33.2, p. 261. DOI: 10.7203/sjp.33.2.13602.

Millot, R., N. Vigier, and J. Gaillardet (2010). "Behaviour of lithium and its isotopes during weathering in the Mackenzie Basin, Canada". *Geochimica et Cosmochimica Acta* 74.14, pp. 3897–3912. DOI: 10.1016/j.gca.2010.04.025.

Misra, S. and P. N. Froelich (2012). "Lithium isotope history of Cenozoic seawater: Changes in silicate weathering and reverse weathering". *Science (New York, N.Y.)* 335.6070, pp. 818–823. DOI: 10.1126/science.1214697.

Morard, A., J. Guex, A. Bartolini, E. Morettini, and P. de Wever (2003). "A new scenario for the Domerian - Toarcian transition". *Bulletin de la Societe Geologique de France* 174.4, pp. 351–356. DOI: 10.2113/174.4.351.

Moriguti, T. and E. Nakamura (1998). "High-yield lithium separation and the precise isotopic analysis for natural rock and aqueous samples". *Chemical Geology* 145.1-2, pp. 91–104. DOI: 10.1016/S0009-2541(97)00163-0.

Ogg, J. G., F. M. Gradstein, and G. Ogg (2016). *A concise geologic time scale 2016.* Amsterdam, Netherlands: Elsevier. URL: http://search.ebscohost.com/login.aspx?direct=true&scope=site&db=nlebk&AN=1218972.

Ohnemueller, F., A. R. Prave, A. E. Fallick, and S. A. Kasemann (2014). "Ocean acidification in the aftermath of the Marinoan glaciation". *Geology* 42.12, pp. 1103–1106. DOI: 10.1130/G35937.1.

Oliveira, L. C., R. Rodrigues, L. V. Duarte, and V. B. Lemos (2006). "Oil generation potential assessment and paleoenvironmental interpretation based on biomarkers and stable carbon isotopes of the Pliensbachian — lower Toarcian (Lower Jurassic) of the Peniche region (Lusitanian Basin, Portugal)". *B. Geoci. Petrobras* 14.2, pp. 207–234.

Pálfy, J. and P. L. Smith (2000). "Synchrony between Early Jurassic extinction, oceanic anoxic event, and the Karoo-Ferrar flood basalt volcanism". *Geology* 28.8, p. 747. DOI: 10.1130/0091-7613(2000)28{\textless}747:SBEJEO{\textgreater}2.0.CO;2.

Palliani, R. B. and J. B. Riding (2003). "Biostratigraphy, provincialism and evolution of European early Jurassic (Pliensbachian to early Toarcian) dinoflagellate cysts". *Palynology* 27.1, pp. 179–214. DOI: 10.1080/01916122.2003.9989586.

Paredes, R., M. J. Comas-Rengifo, and L. V. Duarte (2016). "Passagem Pliensbaquiano-Toarciano: a diversidade de macroinvertebrados antes da extinção". *O Jurássico da região de Penela: novos avanços no conhecimento estratigráfico.* Ed. by L. V. Duarte and S. Sêco, pp. 30–40.

Percival, L., A. S. Cohen, M. K. Davies, A. J. Dickson, S. P. Hesselbo, H. C. Jenkyns, M. J. Leng, T. A. Mather, M. S. Storm, and W. Xu (2016). "Osmium isotope evidence for two pulses of increased continental weathering linked to Early Jurassic volcanism and climate change". *Geology* 44.9, pp. 759–762. DOI: 10.1130/G37997.1.

Percival, L., M. Witt, T. A. Mather, M. Hermoso, H. C. Jenkyns, S. P. Hesselbo, A. H. Al-Suwaidi, M. S. Storm, W. Xu, and M. Ruhl (2015). "Globally enhanced mercury deposition during the end-Pliensbachian extinction and Toarcian OAE: A link to the Karoo–Ferrar Large Igneous Province". *Earth and Planetary Science Letters* 428, pp. 267–280. DOI: 10.1016/j.epsl.2015.06.064.

Peucker-Ehrenbrink, B. and G. Ravizza (2000). "The marine osmium isotope record". *Terra Nova* 12.5, pp. 205–219. DOI: 10.1046/j.1365-3121.2000.00295.x.

Piazza, V., L. V. Duarte, J. Renaudie, and M. Aberhan (2019). "Reductions in body size of benthic macroinvertebrates as a precursor of the early Toarcian (Early Jurassic) extinction event in the Lusitanian Basin, Portu-

gal". *Paleobiology* 45.02, pp. 296–316. DOI: 10.1017/pab.2019.11.

Piazza, V., C. V. Ullmann, and M. Aberhan (2020). "Temperature-related body size change of marine benthic macroinvertebrates across the Early Toarcian Anoxic Event". *Scientific Reports* 10.4675, pp. 1–13. DOI: 10.1038/s41598-020-61393-5.

Pistiner, J. S. and G. M. Henderson (2003). "Lithium-isotope fractionation during continental weathering processes". *Earth and Planetary Science Letters* 214.1-2, pp. 327–339. DOI: 10.1016/S0012-821X(03)00348-0.

Pittet, B., G. Suan, F. Lenoir, L. V. Duarte, and E. Mattioli (2014). "Carbon isotope evidence for sedimentary discontinuities in the lower Toarcian of the Lusitanian Basin (Portugal): Sea level change at the onset of the Oceanic Anoxic Event". *Sedimentary Geology* 303, pp. 1–14. DOI: 10.1016/j.sedgeo.2014.01.001.

Plancq, J., E. Mattioli, B. Pittet, F. Baudin, L. V. Duarte, M. Boussaha, and V. Grossi (2016). "A calcareous nannofossil and organic geochemical study of marine palaeoenvironmental changes across the Sinemurian/Pliensbachian (early Jurassic, 191 Ma) in Portugal". *Palaeogeography, Palaeoclimatology, Palaeoecology* 449, pp. 1–12. DOI: 10.1016/j.palaeo.2016.02.009.

Pogge von Strandmann, P. A. E., K. W. Burton, R. H. James, P. van Calsteren, and S. R. Gislason (2010). "Assessing the role of climate on uranium and lithium isotope behaviour in rivers draining a basaltic terrain". *Chemical Geology* 270.1-4, pp. 227–239. DOI: 10.1016/j.chemgeo.2009.12.002.

Pogge von Strandmann, P. A. E. and G. M. Henderson (2014). "The Li isotope response to mountain uplift". *Geology* 43.1, pp. 67–70. DOI: 10.1130/G36162.1.

Pogge von Strandmann, P. A. E., H. C. Jenkyns, and R. G. Woodfine (2013). "Lithium isotope evidence for enhanced weathering during Oceanic Anoxic Event 2". *Nature Geoscience* 6.8, pp. 668–672. DOI: 10.1038/NGEO1875.

Pogge von Strandmann, P. A., W. T. Fraser, S. J. Hammond, G. Tarbuck, I. G. Wood, E. H. Oelkers, and M. J. Murphy (2019). "Experimental determination of Li isotope behaviour during basalt weathering". *Chem-*

ical Geology. DOI: 10.1016/j.chemgeo.2019.04.020.

Raymo, M. E. and W. F. Ruddiman (1992). "Tectonic forcing of late Cenozoic climate". *Nature* 359.6391, pp. 117–122. DOI: 10.1038/359117a0.

Reggiani, L., E. Mattioli, B. Pittet, L. V. Duarte, L. C. Veiga de Oliveira, and M. J. Comas-Rengifo (2010). "Pliensbachian (Early Jurassic) calcareous nannofossils from the Peniche section (Lusitanian Basin, Portugal): A clue for palaeoenvironmental reconstructions". *Marine Micropaleontology* 75.1-4, pp. 1–16. DOI: 10.1016/j.marmicro.2010.02.002.

Rodrigues, B., L. V. Duarte, J. G. Mendonça Filho, L. G. Santos, and A. Donizeti de Oliveira (2016). "Evidence of terrestrial organic matter deposition across the early Toarcian recorded in the northern Lusitanian Basin, Portugal". *International Journal of Coal Geology* 168, pp. 35–45. DOI: 10.1016/j.coal.2016.06.016.

Rosales, I., S. Quesada, and S. Robles (2004). "Paleotemperature variations of Early Jurassic seawater recorded in geochemical trends of belemnites from the Basque–Cantabrian basin, northern Spain". *Palaeogeography, Palaeoclimatology, Palaeoecology* 203.3-4, pp. 253–275. DOI: 10.1016/S0031-0182(03)00686-2.

Rudnick, R. L. and S. Gao (2003). "Composition of the Continental Crust". *Treatise on Geochemistry.* Ed. by H. D. Holland and K. K. Turekian. Elsevier, pp. 1–64.

Ruebsam, W., T. Müller, J. Kovács, J. Pálfy, and L. Schwark (2018). "Environmental response to the early Toarcian carbon cycle and climate perturbations in the northeastern part of the West Tethys shelf". *Gondwana Research* 59, pp. 144–158. DOI: 10.1016/j.gr.2018.03.013.

Saenger, C. and Z. Wang (2014). "Magnesium isotope fractionation in biogenic and abiogenic carbonates: Implications for paleoenvironmental proxies". *Quaternary Science Reviews* 90, pp. 1–21. DOI: 10.1016/j.quascirev.2014.01.014.

Schauble, E. A. (2011). "First-principles estimates of equilibrium magnesium isotope fractionation in silicate, oxide, carbonate and hexaaquamagnesium^{2+} crystals". *Geochimica et Cosmochimica Acta* 75.3,

pp. 844–869. DOI: 10.1016/j.gca.2010.09.044.

Seyfried, W. E., X. Chen, and L.-H. Chan (1998). "Trace Element Mobility and Lithium Isotope Exchange During Hydrothermal Alteration of Seafloor Weathered Basalt: An Experimental Study at 350C, 500 Bars". *Geochimica et Cosmochimica Acta* 62.6, pp. 949–960. DOI: 10.1016/S0016-7037(98)00045-3.

Stoffynegli, P. and F. T. Mackenzie (1984). "Mass balance of dissolved lithium in the oceans". *Geochimica et Cosmochimica Acta* 48.4, pp. 859–872. DOI: 10.1016/0016-7037(84)90107-8.

Strelow, F. W. E. (1960). "An Ion Exchange Selectivity Scale of Cations Based on Equilibrium Distribution Coefficients". *Analytical Chemistry* 32.9, pp. 1185–1188. DOI: 10.1021/ac60165a042.

Strelow, F. W. E., R. Rethemeyer, and C. J. C. Bothma (1965). "Ion Exchange Selectivity Scales for Cations in Nitric Acid and Sulfuric Acid Media with a Sulfonated Polystyrene Resin". *Analytical Chemistry* 37.1, pp. 106–111. DOI: 10.1021/ac60220a027.

Suan, G., E. Mattioli, B. Pittet, C. Lécuyer, B. Suchéras-Marx, L. V. Duarte, M. Philippe, L. Reggiani, and F. Martineau (2010). "Secular environmental precursors to Early Toarcian (Jurassic) extreme climate changes". *Earth and Planetary Science Letters* 290.3-4, pp. 448–458. DOI: 10.1016/j.epsl.2009.12.047.

Suan, G., E. Mattioli, B. Pittet, S. Mailliot, and C. Lécuyer (2008). "Evidence for major environmental perturbation prior to and during the Toarcian (Early Jurassic) oceanic anoxic event from the Lusitanian Basin, Portugal". *Paleoceanography* 23.1. DOI: 10.1029/2007PA001459.

Suan, G., B. L. Nikitenko, M. A. Rogov, F. Baudin, J. E. Spangenberg, V. G. Knyazev, L. A. Glinskikh, A. A. Goryacheva, T. Adatte, J. B. Riding, K. B. Föllmi, B. Pittet, E. Mattioli, and C. Lécuyer (2011). "Polar record of Early Jurassic massive carbon injection". *Earth and Planetary Science Letters* 312.1-2, pp. 102–113. DOI: 10.1016/j.epsl.2011.09.050.

Svensen, H., F. Corfu, S. Polteau, Ø. Hammer, and S. Planke (2012). "Rapid magma emplacement in the Karoo Large Igneous Province". *Earth and Planetary Science Letters* 325-326, pp. 1–9. DOI: 10.1016/j.epsl.2012.01.015.

Teng, F.-Z. (2017). "Magnesium Isotope Geochemistry". *Reviews in Mineralogy and Geochemistry* 82.1, pp. 219–287. DOI: 10.2138/rmg.2017.82.7.

Teng, F.-Z., W.-Y. Li, S. Ke, B. Marty, N. Dauphas, S. Huang, F.-Y. Wu, and A. Pourmand (2010a). "Magnesium isotopic composition of the Earth and chondrites". *Geochimica et Cosmochimica Acta* 74.14, pp. 4150–4166. DOI: 10.1016/j.gca.2010.04.019.

Teng, F.-Z., W.-Y. Li, R. L. Rudnick, and L. R. Gardner (2010b). "Contrasting lithium and magnesium isotope fractionation during continental weathering". *Earth and Planetary Science Letters* 300.1-2, pp. 63–71. DOI: 10.1016/j.epsl.2010.09.036.

Them, T. R., B. C. Gill, A. H. Caruthers, D. R. Gröcke, E. T. Tulsky, R. C. Martindale, T. P. Poulton, and P. L. Smith (2017a). "High-resolution carbon isotope records of the Toarcian Oceanic Anoxic Event (Early Jurassic) from North America and implications for the global drivers of the Toarcian carbon cycle". *Earth and Planetary Science Letters* 459, pp. 118–126. DOI: 10.1016/j.epsl.2016.11.021.

Them, T. R., B. C. Gill, D. Selby, D. R. Gröcke, R. M. Friedman, and J. D. Owens (2017b). "Evidence for rapid weathering response to climatic warming during the Toarcian Oceanic Anoxic Event". *Scientific reports* 7.1, p. 5003. DOI: 10.1038/s41598-017-05307-y.

Tipper, E. T., A. Galy, J. Gaillardet, M. Bickle, H. Elderfield, and E. Carder (2006). "The magnesium isotope budget of the modern ocean: Constraints from riverine magnesium isotope ratios". *Earth and Planetary Science Letters* 250.1-2, pp. 241–253. DOI: 10.1016/j.epsl.2006.07.037.

Tipper, E. T., J. Gaillardet, P. Louvat, F. Capmas, and A. F. White (2010). "Mg isotope constraints on soil pore-fluid chemistry: Evidence from Santa Cruz, California". *Geochimica et Cosmochimica Acta* 74.14, pp. 3883–3896. DOI: 10.1016/j.gca.2010.04.021.

Tomascak, P. B., C. H. Langmuir, P. J. Le Roux, and S. B. Shirey (2008). "Lithium

isotopes in global mid-ocean ridge basalts". *Geochimica et Cosmochimica Acta* 72.6, pp. 1626–1637. DOI: 10.1016/j.gca.2007.12.021.

Uchikawa, J. and R. E. Zeebe (2008). "Influence of terrestrial weathering on ocean acidification and the next glacial inception". *Geophysical Research Letters* 35, pp. 1–5. DOI: 10.1029/2008GL035963.

Ullmann, C. V., R. Boyle, L. V. Duarte, S. P. Hesselbo, S. A. Kasemann, T. Klein, T. M. Lenton, V. Piazza, and M. Aberhan (2020). "Warm afterglow from the Toarcian Oceanic Anoxic Event drives the success of deep-adapted brachiopods". *Scientific reports* 10.6549. DOI: 10.1038/s41598-020-63487-6.

Ullmann, C. V., H. J. Campbell, R. Frei, S. P. Hesselbo, P. A. Pogge von Strandmann, and C. Korte (2013). "Partial diagenetic overprint of Late Jurassic belemnites from New Zealand: Implications for the preservation potential of δ^7Li values in calcite fossils". *Geochimica et Cosmochimica Acta* 120, pp. 80–96. DOI: 10.1016/j.gca.2013.06.029.

van de Schootbrugge, B., J. M. McArthur, T. R. Bailey, Y. Rosenthal, J. D. Wright, and K. G. Miller (2005a). "Toarcian oceanic anoxic event: An assessment of global causes using belemnite C isotope records". *Paleoceanography* 20.3. DOI: 10.1029/2004PA001102.

van de Schootbrugge, B., T. R. Bailey, Y. Rosenthal, M. E. Katz, J. D. Wright, K. G. Miller, S. Feist-Burkhardt, and P. G. Falkowski (2005b). "Early Jurassic climate change and the radiation of organic-walled phytoplankton in the Tethys Ocean". *Paleobiology* 31.1, pp. 73–97. DOI: 10.1666/0094-8373(2005)031{\textless}0073:EJCCAT{\textgreater}2.0.CO;2.

Verney-Carron, A., N. Vigier, and R. Millot (2011). "Experimental determination of the role of diffusion on Li isotope fractionation during basaltic glass weathering". *Geochimica et Cosmochimica Acta* 75.12, pp. 3452–3468. DOI: 10.1016/j.gca.2011.03.019.

Vigier, N., A. Decarreau, R. Millot, J. Carignan, S. Petit, and C. France-Lanord (2008). "Quantifying Li isotope fractionation during smectite formation and implications for the Li cycle". *Geochimica et Cosmochimica Acta*

72.3, pp. 780–792. DOI: 10.1016/j.gca.2007.11.011.

Wang, W., T. Qin, C. Zhou, S. Huang, Z. Wu, and F. Huang (2017). "Concentration effect on equilibrium fractionation of Mg-Ca isotopes in carbonate minerals: Insights from first-principles calculations". *Geochimica et Cosmochimica Acta* 208, pp. 185–197. DOI: 10.1016/j.gca.2017.03.023.

Wang, W., C. Zhou, Y. Liu, Z. Wu, and F. Huang (2019). "Equilibrium Mg isotope fractionation among aqueous Mg^{2+}, carbonates, brucite and lizardite: Insights from first-principles molecular dynamics simulations". *Geochimica et Cosmochimica Acta* 250, pp. 117–129. DOI: 10.1016/j.gca.2019.01.042.

Weissert, H. and E. Erba (2004). "Volcanism, CO 2 and palaeoclimate: a Late Jurassic–Early Cretaceous carbon and oxygen isotope record". *Journal of the Geological Society* 161.4, pp. 695–702. DOI: 10.1144/0016-764903-087.

Weissert, H., A. Lini, K. B. Föllmi, and O. Kuhn (1998). "Correlation of Early Cretaceous carbon isotope stratigraphy and platform drowning events: A possible link?" *Palaeogeography, Palaeoclimatology, Palaeoecology* 137.3-4, pp. 189–203. DOI: 10.1016/S0031-0182(97)00109-0.

West, A., A. Galy, and M. Bickle (2005). "Tectonic and climatic controls on silicate weathering". *Earth and Planetary Science Letters* 235.1-2, pp. 211–228. DOI: 10.1016/j.epsl.2005.03.020.

Wignall, P. B. and D. P. Bond (2008). "The end-Triassic and Early Jurassic mass extinction records in the British Isles". *Proceedings of the Geologists' Association* 119.1, pp. 73–84. DOI: 10.1016/S0016-7878(08)80259-3.

Williams, L. B. and R. L. Hervig (2005). "Lithium and boron isotopes in illite-smectite: The importance of crystal size". *Geochimica et Cosmochimica Acta* 69.24, pp. 5705–5716. DOI: 10.1016/j.gca.2005.08.005.

Wimpenny, J., C. A. Colla, P. Yu, Q.-z. Yin, J. R. Rustad, and W. H. Casey (2015). "Lithium isotope fractionation during uptake by gibbsite". *Geochimica et Cosmochimica Acta* 168, pp. 133–150. DOI: 10.1016/j.gca.2015.07.011.

Wimpenny, J., R. H. James, K. W. Burton, A. Gannoun, F. Mokadem, and S. R. Gíslason (2010). "Glacial effects on weathering processes: New insights from the elemental and lithium isotopic composition of West Greenland rivers". *Earth and Planetary Science Letters* 290.3-4, pp. 427–437. DOI: 10.1016/j.epsl.2009.12.042.

Wright, P. V. and R. C. L. Wilson (1984). "A carbonate submarine-fan sequence from the Jurassic of Portugal". *Journal of Sedimentary Petrology* 54.2, pp. 394–412.

Wunder, B., F. Deschamps, A. Watenphul, S. Guillot, A. Meixner, R. L. Romer, and R. Wirth (2010). "The effect of chrysotile nanotubes on the serpentine-fluid Li-isotopic fractionation". *Contributions to Mineralogy and Petrology* 159.6, pp. 781–790. DOI: 10.1007/s00410-009-0454-x.

Wunder, B., A. Meixner, R. L. Romer, A. Feenstra, G. Schettler, and W. Heinrich (2007). "Lithium isotope fractionation between Li-bearing staurolite, Li-mica and aqueous fluids: An experimental study". *Chemical Geology* 238.3-4, pp. 277–290. DOI: 10.1016/j.chemgeo.2006.12.001.

Wunder, B., A. Meixner, R. L. Romer, and W. Heinrich (2006). "Temperature-dependent isotopic fractionation of lithium between clinopyroxene and high-pressure hydrous fluids". *Contributions to Mineralogy and Petrology* 151.1, pp. 112–120. DOI: 10.1007/s00410-005-0049-0.

Young, E. D. and A. Galy (2004). "The Isotope Geochemistry and Cosmochemistry of Magnesium". *Reviews in Mineralogy and Geochemistry* 55.1, pp. 197–230. DOI: 10.2138/gsrmg.55.1.197.

Chapter 5

Conclusions and Outlook

5. Conclusions and Outlook

The Early Jurassic T-OAE was a time of extreme environmental perturbations, with a massive input of volcanogenic CO_2 that lead to a seawater pH drop, as evidenced with $\delta^{11}B$ isotopes on marine inorganic carbonates for two basins in this study. The magnitude of the pH drop is a matter of current models and will clarify if we can ultimately speak of an acidification event. First simple approaches to reconstruct the seawater pH showed that firstly, the boron isotopic composition of seawater ($\delta^{11}B_{SW}$) during the Early Jurassic could not exceed a value of 36 ‰, because this would cause several of our measured boron values to be not calculated for a pH value. Still, this leaves a large range of possible pH drops from 0.9 units to 0.4 (with $\delta^{11}B_{SW} = 33$ ‰).

Another finding is that the B isotope excursion preserved in the inorganic carbonates is not recorded in brachiopod or bivalve shells, leaving the question of their liability as pH recorders. However, if we assume that they record the pH value only of their internal fluid, we could reconstruct the $\delta^{11}B_{SW}$ ($\sim$35 ‰) because pre- and post T-OAE inorganic carbonate $\delta^{11}B$ have the same range as the brachiopod signature. This would lead to a pH drop of 0.6 units during the T-OAE. Nevertheless, this is an assumption no studies support so far, only the suggestion of a mixed signal of internal fluid and ambient seawater has been pronounced. This further stresses the point for more research on brachiopods as possible pH recorders.

Our second study shows short-term pulses of silicate weathering for the Toarcian OAE and the Pl–To boundary event from the δ^7Li signature. Nevertheless, as we record distinct differences in the Li isotope signature for the Lusitanian (LB) and Iberian basin (IB), with only the LB recording two incongruent weathering pulses (heavier δ^7Li) at the onset of each event. The IB, in contrast, only recorded a congruent weathering signature (lighter δ^7Li) during the T-OAE. This led to the conclusion that the LB was probably temporarily restricted during both events, due to a drastic drop in sea level, coupled with tectonic activity and the formation of effective water mass barriers. The exposure of more continental surface would have led to higher physical weathering rates (and thus incongruent weathering), and together with the generally elevated temperatures and CO_2 concentrations, also to higher runoff that additionally led to a faster recovery of an evident seawater pH drop in the LB. The IB is hence thought to record more open ocean conditions. But, to support this theory more δ^7Li sections in different basins should be analysed and compared.

Also, silicate weathering rates could possibly be reconstructed due to the unique incongruent weathering signal observed in the LB to verify the different weathering rates so far published from Os and Ca isotopes. However, this is beyond the scope of our study and should be conducted for future studies.

Another finding of this study is the rather low δ^7Li seawater for the signature prior and after

the T-OAE, which is recorded in the LB and IB when both were probably connected to the open ocean. Here we record for the Early Jurassic values that are comparable to the minimum δ^7Li values observed during the Paleogene ($\sim$20 ‰), which are distinctly different from the Cretaceous ($\sim$26 ‰) and nowadays ($\sim$31 ‰), implying major changes in the weathering realms over time.

Despite all this, following a few questions and suggestions that future studies can focus on to clarify the points made in this thesis:

1. What does brachiopod shell δ^{11}B signature really record — Is it solely internal fluid or a mixture, or even something wholly different?

2. Compilation of the environmental reconstructions of the T-OAE with paleontological findings to find a link between the stressors (acidification, deoxygenation, warming) and the extinction

3. Conduct Li isotope analyses on brachiopods to see if they retrace the signature seen in BdC inorganic carbonates

4. Investigate more sections and basins for their Li isotopic signature to clarify if the IB really records open marine conditions

5. Conduct box modelling with the Li isotopes generated in this thesis to reconstruct silicate weathering fluxes during T-OAE, and compare them with the different flux rates that already exist and hopefully support one of those studies

6. Higher sampling intervals at Pl–To boundary at different sections than in this study (because the sample material here during this time interval was badly preserved) to unravel the weathering history and support the ideas stated in this study

Acknowledgements

First and foremost, I would like to thank my supervisor Prof. Dr. Simone Kasemann for enabling me to conduct this PhD project. I am deeply grateful for you always being available for any minor and major issues. Also, I am especially grateful for the help you provided in disentangling the different boron fractionation curves (they still haunt me in my dreams). Also, thank you for the constructive discussions about my data and your immense patience!

Moreover, a very big thank you goes to our lab manager Anette Meixner. Thank you for introducing me into the deeper mysteries of stable isotopes and always helping me out with any lab and Neptune problems. Also thank you for your patience with me and answering every dumb question of mine.

Also, I would like to give another big thank you to Dr. Friedrich Lucassen – you were a huge help in the field. I would have never accomplished the sampling without all your pickaxe expertise. Further, thank you for being available as our Sr isotope and TIMS consultant.

Another thank you goes to Dr. Martin Aberhan and Dr. Dieter Korn from the Naturkundemuseum in Berlin, also for the help and especially the fun during our field trips.

I would also like to thank my second supervisor Prof. Dr. Rachel Wood (University Edinburgh, UK) for the short but intensive discussions about my data.

A special thanks goes to Barbara Muntz for the administrative help and pleasant conversations. Also thank you Frederike Wilckens for handling Mg isotope separation problems and being my backup help for Neptune.

A big and special thank you goes out to my dear V.! I am so happy that I met you during the course of my PhD and finding a new friend in you. The dopey memories of our field trips will always stay in my mind and make me laugh forever. Also, thank you so much for introducing me into the magic tricks of italian cooking and all the dinners with "Pasta mit Meeresfrüchten"! Moreover, thank you for the interminable skype and phone sessions for unraveling our lithological profiles! You will always have a free place on my couch.

And now to my dear Lucy-Li :P I am so deeply happy to have found even another friend in you! Thank you for showing me different corners of Bremen and all the coffee and lunch breaks. I am so grateful for you always being there for me and listening to everything that was on my mind. You definitely made my stay in Bremen enjoyable :) Simply thank you for being such a good friend, you will always be in my heart.

I am also grateful for you Tam(ara). Although there are now several hundred kilometers that separate us we still stayed connected. Thanks for listening to all my wailing and bringing me back

down to earth (because, there are still people who have it worse than me). I deeply admire your endurance and hope you get out of your PhD with still a bit of sanity. Looking forward to our all so long postponed stay in Erding to hopefully regain our zen status.

Ein ganz besonderer Dank geht an meine Familie: Danke, Mama und Papa, dass ihr mich immer unterstützt und ermutigt habt meinen eigenen Weg zu gehen. Danke Mama, für die ganze Essensversorgung und die emotionale Untersützung und danke Papa, dass du wenigstens ein bisschen von dem verstehst was ich hier zum Henker eigentlich mache. Und natürlich mein liebes sistaaaspack aka Pravda Sistaaas! Danke ihr drei für all die verrückten Wochenenden, ihr seid die besten. Ich hab euch alle unglaublich lieb!!

Last but not least, I would like to thank Simo (the one and only, of course) — thank you for always and always supporting me! Especially in my hard decision to move many hundred kilometers away from you to make my PhD. And even more so to follow me later although you knew it would be hard for you up here in northern Germany, due to the lack of any mountain you could climb with your bike. Thank you for enduring all my bad moods and the extra love you gave me on those days. Rakastan sinua.

Appendices

A. Isotope and element plots
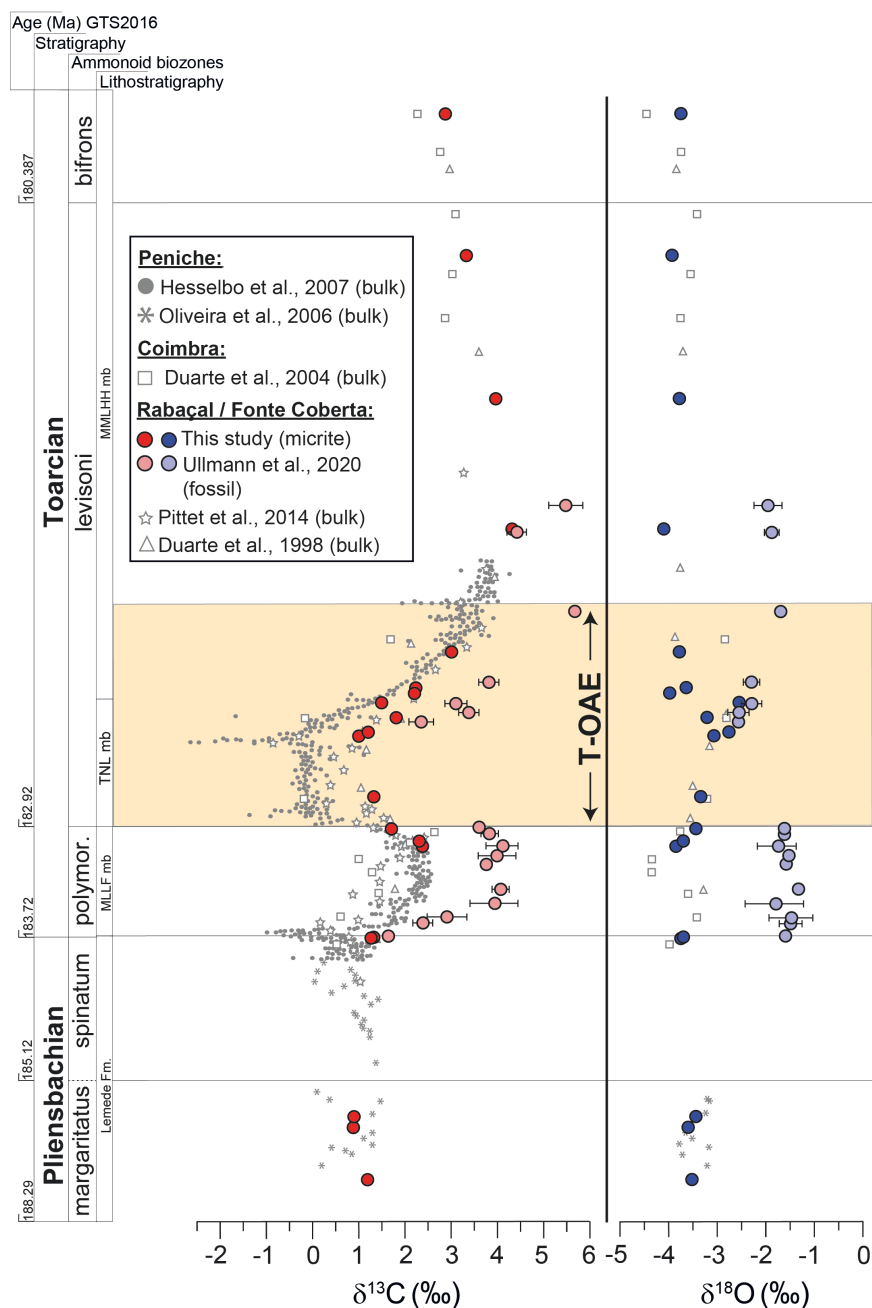
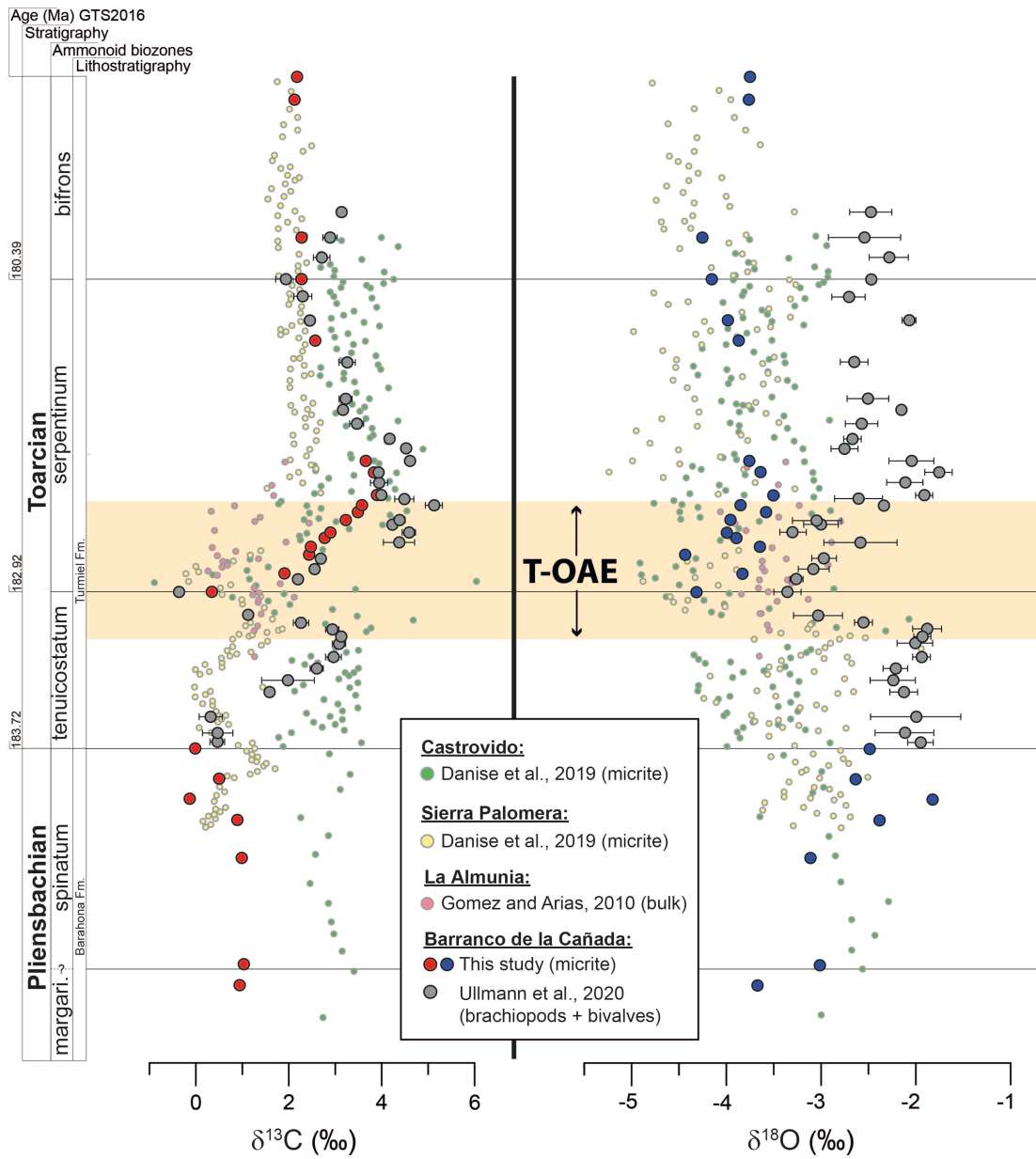**Figure 17.** Compilation of published micritic carbonate $\delta^{13}C$ and $\delta^{18}O$ data of the Lusitanian Basin with the micrite data generated for this study for the Pliensbachian–Toarcian in Rabaçal/Fonte Coberta. Additionally the $\delta^{13}C_{fossil}$ and $\delta^{18}O_{fossil}$ (brachiopods and bivalves) from Ullmann et al., 2020, from the same section as our micrites are plotted. Polymor. = polymorphum. *[High-resolution image on attached CD]*

Figure 18. Compilation of published micrite and bulk carbonate $\delta^{13}C$ and $\delta^{18}O$ data of the Iberian Basin with the micrite data generated for this study for the Pliensbachian–Toarcian in Barranco de la Cañada. Also compiled are the bivalve and brachiopod $\delta^{13}C$ and $\delta^{18}O$ data from Ullmann et al., 2020 originating from the same transect as the micrite data. Margari. = margaritatus. *[High-resolution image on attached CD]*
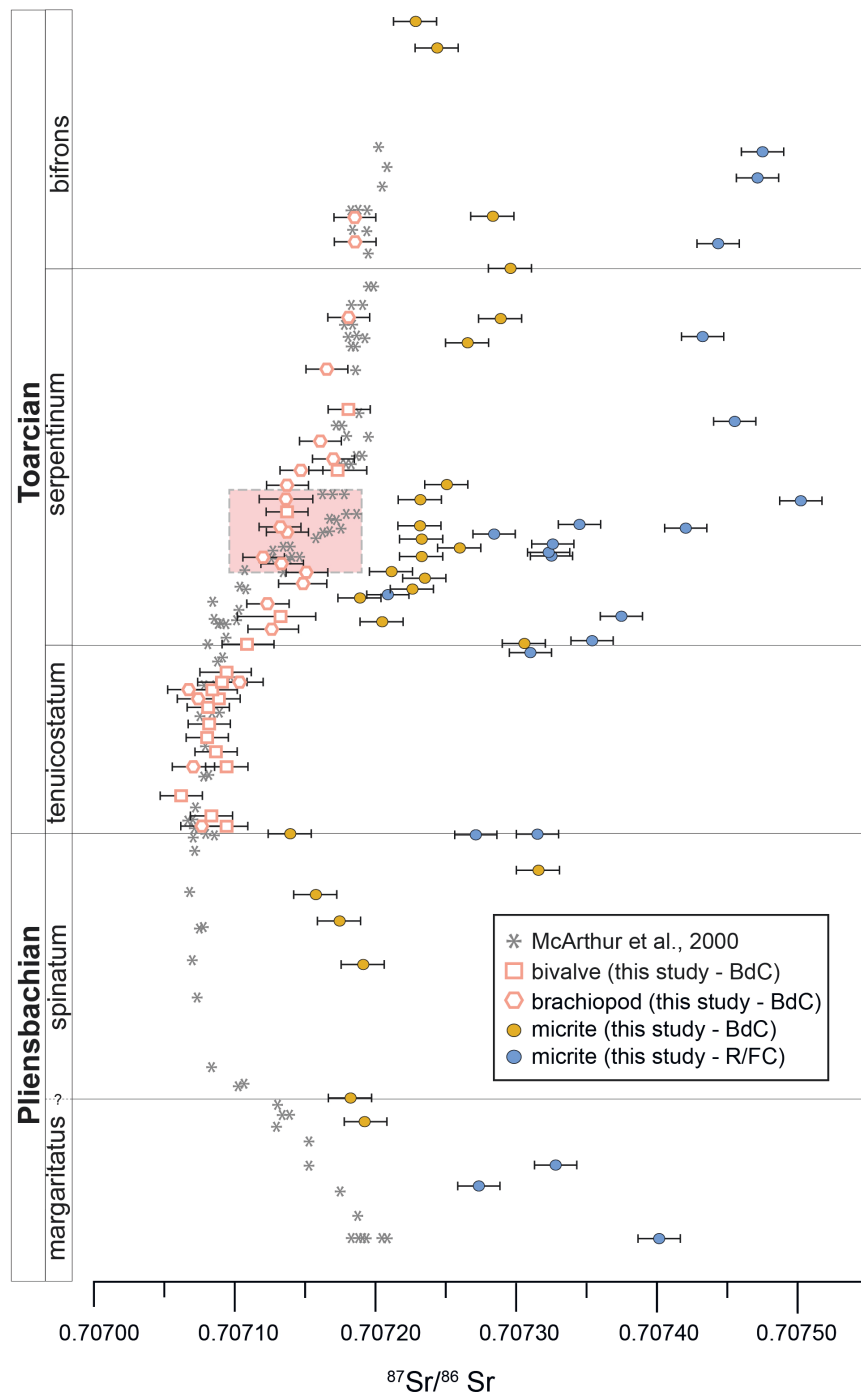
Figure 19. Comparison of published seawater ^{87}Sr/^{86}Sr curve by McArthur et al., 2000 with micrite data generated for both sections in this study, and fossil data analysed on brachiopods and bivalves published by Ullmann et al., 2020 and originating from Barranco de la Cañada. All values are normed to the value NIST987 = 0.710248 given by McArthur et al., 2001 for correcting interlabotary bias and thus better correlation. The light red box marks the sudden increase to more radiogenic Sr isotopic values in the McArthur-curve. For discussion see text. *[High-resolution image on attached CD]*

P5 (Pliensbachian/*spinatum*, R/FC)
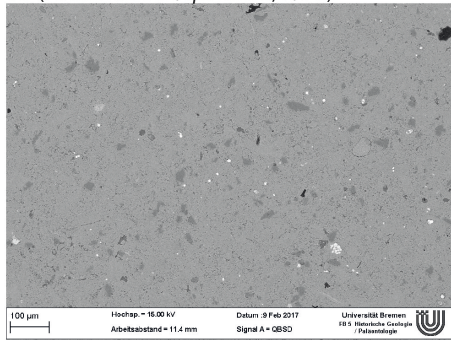
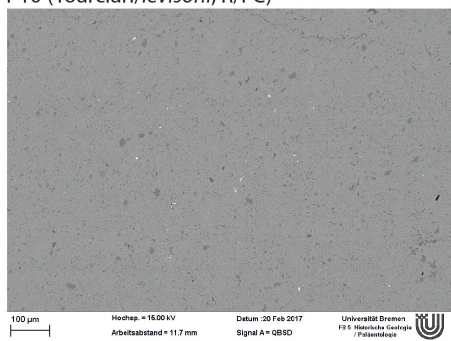S4 (Pliensbachian/*spinatum*, BdC)
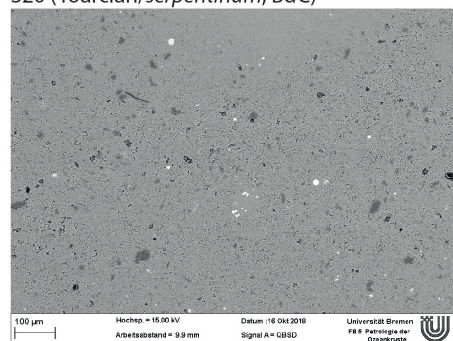
P8 (Toarcian/*polymorphum*, R/FC)
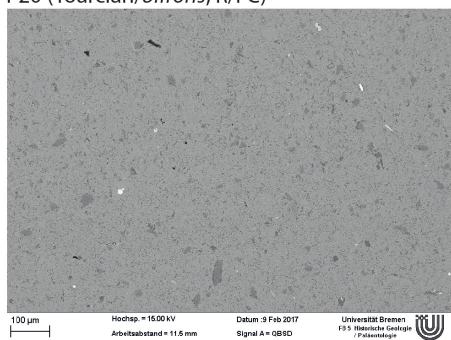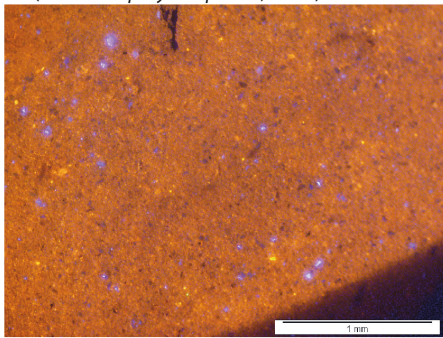
S13 (Toarcian/*serpentinum*, BdC)
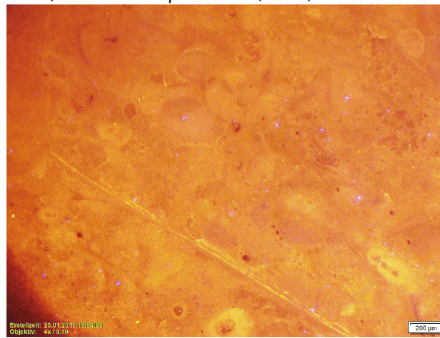
P10 (Toarcian/*levisoni*, R/FC)
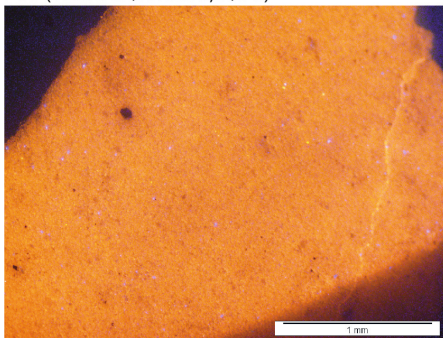
S20 (Toarcian/*serpentinum*, BdC)
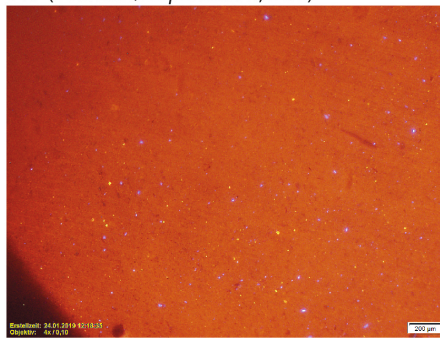
P20 (Toarcian/*bifrons*, R/FC)
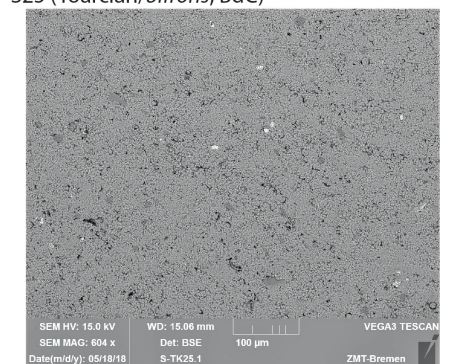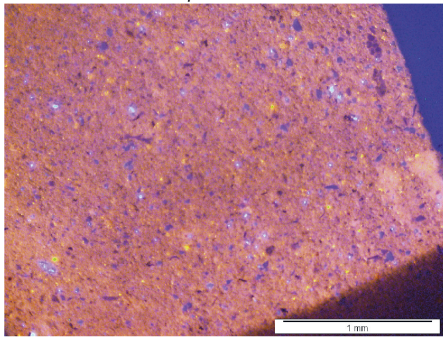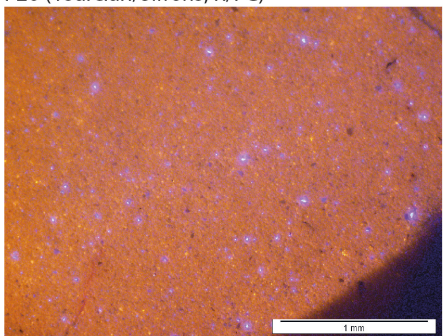
S25 (Toarcian/*bifrons*, BdC)

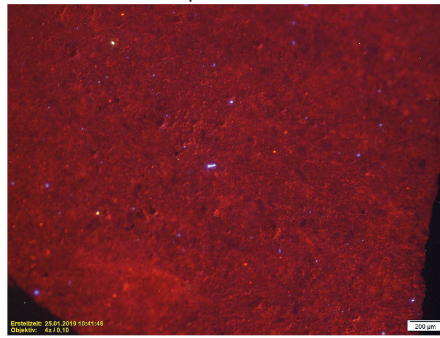**Figure 20.** Example SEM images from micrites in this study. *[High-resolution images of all samples on attached CD]*

Figure 21. Example CL images from micrites in this study. *[High-resolution images of all samples on attached CD]*

B. Data tables

Listed in this printed section are only an extract of the totality of the generated data for this thesis. The complete digital lists can be found on the attached CD.

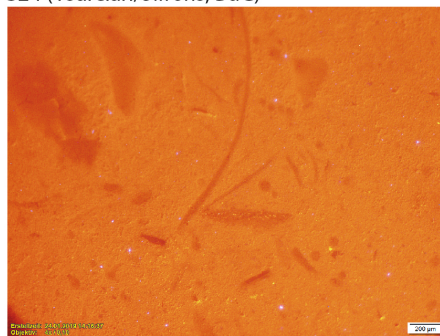| Sample name	Sample code	Height (m)	Detritus (wt%)	B (µg/g)	Mn (µg/g)	Sr (µg/g)	Ba (µg/g)	Fe (µg/g)	P (µg/g)	S (µg/g)	Al (µg/g)	Si (µg/g)	Mn/Sr
FC - Z10	P1	-15.25	9	1.9	98	380	5.7	1070	63	549	107	404	0.3
FC - Z23	P2	-11.84	16	2.9	73	638	6.6	836	37	1293	79	348	0.1
FC - Z29	P3	-11.14	13	2.2	78	464	10.9	803	147	967	39	213	0.2
FC - Z06 Top - 85	P4	0.00	14	3.7	117	535	6.8	1467	16	1237	116	401	0.2
FC - Z44 + 375	P5	0.07	11	2.5	119	409	4.6	1274	30	762	63	280	0.3
FC - Z13 Top -35	P6	5.96	15	2.5	140	440	11.1	2223	19	728	98	367	0.3
FC - Z13 Top	P7	6.32	22	2.9	146	486	7.2	1792	8.3	826	99	383	0.3
FC - Z14	P8	7.12	16	1.9	171	430	15.0	2253	29	348	84	353	0.4
FC - Z14 + 9	P9	9.23	8	1.1	117	466	2.0	2923	3.3	226	76	304	0.3
FC - V - Z14 + 425	P10	13.19	13	1.1	149	312	2.4	1667	4.5	288	15	150	0.5
FC - V - Z14 + 455	P11	13.44	10	1.3	166	337	2.3	2189	17	253	90	347	0.5
FC - V - Z14 + 730	P12	14.39	11	1.5	170	392	3.4	3167	15	355	112	436	0.4
FC - Z14 + 19	P13	15.38	8	1.2	207	360	2.3	3269	11	290	83	350	0.6
FC - Z17	P14	16.01	16	1.6	176	320	3.2	3109	4.3	450	80	384	0.6
FC - V - Z17	P15	16.34	12	1.3	195	388	3.6	3376	16	459	56	266	0.5
FC - V - Z17 + 235	P16	18.69	16	1.8	183	301	5.4	3001	2.7	497	65	382	0.6
R - Z23 Top	P17	26.74	13	1.6	145	317	3.0	2609	18	473	116	379	0.5
R - Z30	P18	35.21	16	1.9	167	370	4.0	2452	5.9	533	49	284	0.5
R - Z30 + 10m	P19	44.58	15	1.7	176	375	4.7	2890	170	590	49	246	0.5
R - Z40 + 1	P20	53.87	17	1.8	137	334	3.5	2070	6.1	539	88	426	0.4

Table 5. Element concentration and detritus content data from Rabaçal/Fonte Coberta. Heights are given relative to the Pl–To boundary, negative values thus are from the Pliensbachian.

Sample name	Smpl code	Height (m)	Detritus (wt%)	B (µg/g)	Mn (µg/g)	Sr (µg/g)	Ba (µg/g)	Fe (µg/g)	Al (µg/g)	Si (µg/g)	Mn/Sr
C3 Top -1180	S1°	-11.8	4	1.9	41	279	1.5	851	66	86	0.1
C3 Top -1080	S2	-10.8	5	1.1	36	274	1.6	543	36	65	0.1
C3 Top -540	S3°	-5.4	2	1.9	47	251	44.0	693	20	40	0.2
C3 Top -354	S4°	-3.54	4	1.4	43	224	1.4	488	28	46	0.2
C3 Top -250	S5°	-2.5	4	1.2	44	217	1.1	506	20	31	0.2
C3 Top -150	S6°	-1.5	3	1.8	54	210	1.6	600	24	42	0.3
C3 Top	S7°	0	6	1.3	118	338	6.3	1003	23	36	0.3
C21+22/C25+26	S8*	7.79	20	0.7	475	260	2.1	2725	50	179	1.8
C25/26 + 30	S9°	8.72	9	0.8	231	311	3.1	2057	35	53	0.7
C30-T	S10°*	9.66	2	0.5	255	318	10.0	3046	24	62	0.8
C28/C31_32	S11°	10.05	12	0.8	215	353	9.9	2011	47	54	0.6
C31/C32	S12°	10.48	14	0.8	209	394	9.1	2047	50	55	0.5
C33	S13	10.75	11	0.7	204	396	6.8	2170	37	32	0.5
C37	S14°	11.38	14	0.7	211	385	7.7	2060	33	88	0.5
C37/BC1 (C37 + 50)	S15°	11.78	17	0.8	207	389	6.5	1531	70	211	0.5
BC1	S16°	12.12	14	0.7	224	390	7.6	2105	48	97	0.6
BC2	S17	12.62	13	0.8	205	375	5.2	2094	37	86	0.5
BC4	S18	13.74	10	0.8	239	372	7.0	2123	26	51	0.6
BC5	S19	14.32	13	0.6	269	350	8.9	2692	39	85	0.8
BC16	S20°*	20.21	10	0.7	312	353	5.5	2931	46	133	0.9

BC17	S21*	21.21	16	0.9	305	366	8.8	2302	57	201	0.8
BC19	S22*	23.26	15	0.9	336	367	9.9	2149	46	172	0.9
BC21	S23	25.35	13	0.9	263	383	7.3	2245	40	75	0.7
BC26	S24°	32.24	5	0.5	118	428	2.5	465	19	42	0.3
BC27	S25	33.38	5	0.5	99	427	2.3	374	34	60	0.2

Table 6. Element concentration and detritus content data from Barranco de la Cañada. Heights are given relative to the Pl–To boundary, negative values thus are from the Pliensbachian. Samples marked with (°) are mixed samples containing not only matrix but also shell material. Samples with (*) indicate altered samples.

C. Isotope separation procedures

Sr-spec column separation procedure (modified after Pin and Bassin, 1992):

1. Add 500 µl – 1500 µl 2M HNO_3 to the sample
2. Load the Sr-spec (~70 µl) in the PE column with Milli-Q
3. Clean the resin:
    i. 4 x Milli-Q (full reservoir)
    ii. 2 x 500 µl 2M HNO3
4. Add the sample in 100 µl steps
5. Remove the unwanted elements from the matrix:
    i. 12 x 100 µl 2M HNO_3
6. Remove barium (only if Ba concentrations are several 100 ppm):
    i. 2 x 500 µl 7M HNO_3
    ii. 3 x 100 µl 2M HNO_3
7. Dispose the eluate
8. Collect the Sr fraction:
    i. 5 x 200 µl 0.05M HNO_3
    ii. Add 20 µl 0.1M H_3PO_4 in the beaker
9. Dry the Sr fraction at 80 – 100°C
10. Removal of resin (organic matter) from the sample:
    i. 70 µl concentrated HNO_3 and dry at 80 – 100°C
    ii. Add 40 µl of H_2O_2 into the warm beaker and dry at 100°C
11. Clean the columns and discard the resin

Figure 22. Sr-spec column separation procedure (modified after Pin and Bassin, 1992).

Boron cation exchange using Biorad Resin AG 50WX8 200 – 400 mesh:

1. Add 1 ml 0.02M HCl to the sample
2. Stir up the resin
3. Clean the resin:
   i.   2 x 6.2M HCl (full reservoir)
4. Conditioning:
   i.   4 x 1 ml 0.02M HCl
5. From here collect the main boron fraction in 15 ml Savillex beaker
6. Add the sample solution in 4 x 250 μl steps
7. Elution:
   i.   2 x 250 μl 0.02M HCl (wash the sample beaker with the first 500 μl)
   ii.   7 x 500 μl 0.02M HCl
   iii. 4 x 1 ml 0.02M HCl
8. Collect the B tail fraction (in 7 ml Savillex beaker):
   i.   2 x 1 ml 0.02M HCl
9. Purification of resin and columns:
   i.   2 x 6.2M HCl (full reservoir)
10. Dry the B main and tail fraction at <67 °C

Figure 23. Boron cation exchange using Biorad Resin AG 50WX8 200 – 400 mesh

First Lithium ion exchange chromatography using Biorad Resin AG 50WX8 200 – 400 mesh:

1. Add 2 ml 0.15M HCl to the sample
2. Stir up the resin
3. Clean the resin:
   i. 2 x 6M HCl (full reservoir)
   ii. 1 x ultrapure water (Milli-Q – full reservoir)
4. Conditioning:
   i. 2 x 1 ml 0.15M HCl
5. From here collect the head Li fraction in 7 ml Savillex beaker
6. Add the sample solution in 8 x 250 µl steps
7. Head fraction (with 0.15M HCl):
   i. 1 x 0.5 ml (wash the sample beaker)
   ii. 1 x 0.5 ml
   iii. 1 x 1 ml
8. Elution (collect Li main fraction in 30 ml Savillex beaker):
   i. 4 x 5 ml 0.15M HCl
   ii. 2 x 4 ml 0.15M HCl
9. Collect the Li tail fraction (in 7 ml Savillex beaker):
   i. 1 x 2 ml 0.15M HCl
10. Purification of resin and columns:
    i. 2 x 6M HCl (full reservoir)
    ii. 2 x ultrapure water (Milli-Q – full reservoir)
11. Dry the all Li fractions at 90 °C

Figure 24. First Lithium ion exchange chromatography using Biorad Resin AG 50WX8 200–400 mesh

Second Lithium ion exchange chromatography using Biorad Resin AG 50WX8 200 – 400 mesh:

1. Add 1 ml 0.15M HCl to the sample
2. Stir up the resin
3. Clean the resin:
    i. 6 x 6M HCl (full reservoir)
    ii. 2 x ultrapure water (Milli-Q – full reservoir)
4. Conditioning:
    i. 1 x 1 ml 0.15M HCl
5. From here collect the head Li fraction in 7 ml Savillex beaker
6. Add the sample solution in 4 x 250 µl steps
7. Head fraction (with 0.5M HCl in 50% ethanol):
    i. 1 x 0.5 ml (wash the sample beaker)
    ii. 1 x 0.5 ml
8. Elution (collect Li main fraction in 15 ml Savillex beaker):
    i. 1 x 0.5 ml 0.5M HCl in 50% ethanol
    ii. 12 x 1 ml 0.5M HCl in 50% ethanol
9. Collect the Li tail fraction (in 7 ml Savillex beaker):
    i. 2 x 1 ml 0.5M HCl in 50% ethanol
10. Purification of resin and columns:
    i. 3 x ultrapure water (Milli-Q – full reservoir)
    ii. 6 x 6M HCl (full reservoir)
11. Dry the all Li fractions at 90 °C

Figure 25. Second Lithium ion exchange chromatography using Biorad Resin AG 50WX8 200–400 mesh

Magnesium ion exchange chromatography using Biorad Resin AG 50WX8 200 – 400 mesh:

1. Add 0.5 ml 0.8M HCl to the sample
2. Stir up the resin
3. Clean the resin:
    i. 6 x 6M HCl (full reservoir)
    ii. 3 x ultrapure water (Milli-Q – full reservoir)
4. Conditioning:
    i. 1 x 1 ml 0.8M HCl
5. From here collect the head Mg fraction in 15 ml Savillex beaker
6. Add the sample solution in 1 x 500 μl steps
7. Head fraction (with 0.8M HCl):
    i. 1 x 0.5 ml (wash the sample beaker)
    ii. 8 x 1 ml
8. Elution (collect Mg main fraction in 15 ml Savillex beaker):
    i. 13 x 1 ml 0.8M HCl
9. Collect the Mg tail fraction (in 7 ml Savillex beaker):
    i. 2 x 1 ml 0.8M HCl
10. Purification of resin and columns:
    i. 6 x 6M HCl (full reservoir)
    ii. 3 x ultrapure water (Milli-Q – full reservoir)
11. Dry the all Mg fractions at 90 ℃
12. If there is no visible residue, add 15 μl H_2O_2 in the hot beaker and dry at 90 ℃

Figure 26. Magnesium ion exchange chromatography using Biorad Resin AG 50WX8 200–400 mesh

D. Contents of attached CD

The attached CD contains the following data:

- All figures shown in this thesis in high-resolution

- Tables of all generated isotope and element data shown in this thesis

- Tables of all measured standard materials during the course of this project

- SEM and CL images produced for all samples